

High-resolution Ground-magnetic (HRGM) and Radiometric Surveys for Hydrocarbon Exploration: Six Case Histories in Western Canada

Leonard A. LeSchack

Hectori Inc.

Calgary, Alberta, Canada

David R. Van Alstine

Applied Paleomagnetism, Inc.

Redmond, Washington, U.S.A.

ABSTRACT

In Western Canada, and probably elsewhere around the world, “magnetically enhanced zones” above microseeping hydrocarbon reservoirs can exhibit distinctive magnetic signatures that are characteristic of the reservoir. These distinctive magnetic signatures have proven to be invaluable for hydrocarbon exploration, and we have achieved 85% exploration success using ground-based magnetic and radiometric techniques in Western Canada. Differences in timing and duration of microseepage and differences in composition and pressure of the microseeping hydrocarbon gases from separate petroleum systems probably control the magnetic mineralogy, magnetic grain-size distributions, magnetic susceptibility, and natural remanent magnetization (NRM) directions in the magnetically enhanced zones. Together, these differences can yield diagnostic “residual” (remanent + induced) short-spatial-wavelength magnetic anomalies above different reservoirs.

Whereas our magnetic surveys are measuring *fossil* anomalies at depths of about 150 m, our radiometric surveys are measuring *modern* geochemical alterations at depths <25 cm. Thus, finding both magnetic and radiometric anomalies at the same location implies not only that a microseeping hydrocarbon reservoir once existed below, but also that it is still there and still leaking. In this study, we present six case histories from Western Canada in which our combined magnetic and radiometric surveys were effective for hydrocarbon exploration.

Our high-resolution ground-magnetic (HRGM) surveys have sufficiently high resolution that residual magnetic anomalies commonly appear to be dipolar in Western Canada. Nearly equal intensities for the positive and negative lobes of the anomalies, and major departure of the dipole axes from present magnetic north, imply that (1) about half the intensity of the residual anomalies represents remanent, rather than induced, magnetization; and (2) a significant proportion of the remanent magnetization is “reversed polarity” and hence is older than the most recent geomagnetic reversal at 0.78 Ma.

In the prolific Devonian reservoirs of Western Canada, much of the reversed-polarity magnetization probably dates from a strong “reversed-polarity-bias interval” that prevailed during the early Tertiary, from 63 to 41 Ma. At that time, generation of hydrocarbons, rapid subsidence, and the regional topographic hydrodynamic drive created high pore pressures that facilitated regional vertical fracturing of the Laramide foreland. Above reservoirs where oil was trapped during early Tertiary migration, buoyant hydrocarbon microbubbles began to rise along the regional, vertical microfractures. At higher structural levels, the microseeping hydrocarbons caused magnetic minerals to precipitate (by inorganic and/or biogenic processes) in magnetically enhanced zones, thereby recording early Tertiary, reversed-polarity remanent magnetization. Later in the Tertiary, a second generation of magnetically enhanced zones probably was created after maximum burial, at peak overpressure, and when methane began to exsolve by pressure reduction during isostatic uplift.

In Western Canada, the strongest HRGM anomalies occur above the deepest, most prolific reservoirs at the highest pressures, and the weakest HRGM anomalies occur above shallower, less-productive reservoirs at lower pressures. In the Alberta Basin, the HRGM anomaly intensity decreases monotonically, from highest values over prolific Leduc Formation (Upper Devonian) pinnacle-reef reservoirs, to somewhat lower values over Nisku Formation (Upper Devonian) biostrome reservoirs, to still lower values over less-productive Cretaceous blanket/channel-sand reservoirs, to lowest values over dry and abandoned (D&A) wells. In the Williston Basin, strong HRGM anomalies occur above Mission Canyon Formation (Mississippian) limestone cuesta reservoirs, whereas no HRGM anomalies (only radiometric anomalies) occur above shallower lower Amaranth Formation (Triassic?) channel-sand reservoirs. The stronger HRGM anomalies above the deeper Devonian and Mississippian reservoirs may reflect (1) *higher concentrations* of authigenic magnetic minerals in the magnetically enhanced zones; (2) *more focusing* of vertically ascending microbubbles by the more nearly point-source pinnacle reef and cuesta reservoirs, compared with more spatially diffuse blanket/channel-sand reservoirs; and (3) *shallower depths* of magnetically enhanced zones as a result of higher pressure within the deeper reservoirs.

For hydrocarbon exploration, the distinctive magnetic signatures revealed by high-resolution ground-magnetic surveys have an important practical application: We find that the HRGM anomaly intensity and the residual magnetic-anomaly azimuth can identify the reservoir that is causing the anomaly. We illustrate this principle in three case histories in the Williston Basin and three case histories in the Alberta Basin. Although all six of these case histories are from Western Canada, ground-magnetic surveys would probably be equally successful worldwide, especially where hydrocarbon microseepage has occurred during the Tertiary (65 to 1.8 Ma), when the geomagnetic field exhibited reversed-polarity bias.

Case histories 1 and 2 document three new oil-field discoveries, based on magnetic and/or radiometric anomalies over lower Amaranth and Mission Canyon reservoirs near Pierson, Manitoba. Case history 3, at the Waskada field, Manitoba, is an after-drilling study, in which the HRGM survey delineates Mission Canyon limestone reservoirs and the radiometric survey delineates productive channels in the overlying lower Amaranth sand. Case history 4, another after-drilling study, documents that an HRGM survey and a 3-D seismic survey are equally effective in targeting a Leduc pinnacle reef at the Rumsey field, Alberta. Case histories 5 and 6 cover 10⁴ ha in central Alberta, including 55 Cretaceous producers, 15 Nisku producers, and 22 abandoned wells. After-drilling comparison of the magnetic data with the production data reveals that the HRGM surveys could have been used to predict the producers and to avoid the dry holes.

Statistical comparisons of high-resolution ground-magnetic (HRGM) with high-resolution aeromagnetic (HRAM) data and verification with ground data of a specific HRAM

anomaly in central Alberta reveal that airborne and ground-magnetic surveys can be used together, cost-effectively, for hydrocarbon exploration. Reconnaissance HRAM surveys are especially useful in targeting prospects for further, more-detailed evaluation by HRGM/radiometric surveys. In Western Canada, combined HRGM and concurrent radiometric surveys have been highly successful in finding hydrocarbons, and the total cost, including permitting, is about 20% the cost of a 3-D seismic survey over the same area. These surveys complement traditional exploration methods, substantially reduce finding costs, and significantly increase the probability of exploration success.

INTRODUCTION

Aeromagnetic surveys over sedimentary basins have been used for decades for mapping basement structure and depth. Only relatively recently, however, have such surveys been used for *directly* locating hydrocarbon reservoirs by identifying shallow, diagenetic magnetic anomalies produced by upward-leaking hydrocarbon gases. For example, Donovan et al. (1984), Foote (1986a, b, 1992, 1996), Andrew et al. (1991), Foote et al. (1997), and Wolleben and Greenlee (2002) have shown, in a variety of ways, the applicability of *high-resolution aeromagnetic* (HRAM) surveys for mapping such anomalies.

Based on the encouraging results of the early airborne magnetic studies, author LeSchack developed a *high-resolution ground-magnetic* (HRGM) survey technology (LeSchack, 1994, 1997) that reveals excellent correlation between hydrocarbon reservoirs and small (1–12-nT) near-surface magnetic anomalies in Western Canada. Concurrently with the development of the magnetic survey technology, a ground-based radiometric survey technique, adapted largely from Saunders et al. (1993a), was also developed to complement the ground-based magnetic surveys. The magnetic and radiometric surveys detect, by geophysical methods, geochemical alterations caused by vertical microseepage of hydrocarbons.

In this paper, we present six case histories in which HRGM and radiometric surveys were used, cost-effectively, for hydrocarbon exploration in Western Canada. Generally, our ground-based magnetic/radiometric surveys were being used in conjunction with more traditional geologic and seismic methods for evaluating prospective areas, verifying seismic anomalies, and inexpensively targeting areas for conducting expensive 3-D seismic surveys. Occasionally, as in two of the case histories in which seismic exploration is not effective, our magnetic/radiometric surveys were used successfully as a stand-alone exploration method. Of the six case histories, three are examples in which our surveys were conducted prior to drilling. These before-drilling surveys resulted in discovery of three new oil fields, based on subsequent drilling of magnetic and/or radiometric anomalies.

In addition to presenting the six case histories, we verify that the subtle, shallow, short-spatial-wavelength magnetic anomalies that are mapped by our HRGM sur-

veys are commonly also present in HRAM surveys. To illustrate this, we present a comparison of an HRGM survey with an HRAM survey flown over nearly the same area in central Alberta. Although this comparison reveals some of the limitations of using HRAM data alone for mapping shallow anomalies, it demonstrates how airborne surveys can be used to target higher-resolution, ground-based surveys to better define prospects.

THEORETICAL BACKGROUND

The case histories discussed in this paper are part of a growing body of evidence that relates surface and near-surface anomalies in magnetics, topography, potassium, uranium, and seismic velocities to microseepage from underlying hydrocarbon reservoirs. Microseepage from hydrocarbon reservoirs is thought to occur by nearly vertical ascent of colloid-size microbubbles of light hydrocarbons (methane through the butanes) through a network of interconnected groundwater-filled joints, fractures, and bedding planes (Saunders et al., 1993a, b, 1999, 2002; Thompson et al., 1994). Chemical and/or bacterial degradation of microseeping hydrocarbons instigates diagenetic changes that alter the near-surface magnetic mineralogy, the concentration of uranium and potassium minerals, and the seismic properties of lithologies overlying the microseeping reservoirs. Machel and Burton (1991a) concluded that in hydrocarbon microseepage environments, bacterial and chemical processes most commonly produce magnetite or pyrrhotite and destroy hematite.

Hydrocarbon microseepage has been reported to enhance the magnetic mineralogy over a wide range in *depth*, from surface soils to strata as deep as 1500 m (~5000 ft). Hydrocarbon microseepage can also affect the magnetic mineralogy over a wide range in *time*, from fossil paleomagnetic directions recording the initiation of microseepage to modern magnetic enhancement resulting from presently thriving bacteria.

In surface soils, Saunders et al. (1991) documented that anomalously high concentrations of authigenic magnetic minerals occur just below the grass roots in 89% of cases over 19 oil and gas fields. They identified magnetite spherules, octahedral crystals of magnetite,

and highly magnetic “hematite” (probably maghemite) as having been produced by microseepage into the surface-soil diagenetic environment. Ellwood and Burkart (1996) documented significant increases in magnetic susceptibility that were caused by microseepage of methane through the cover of a landfill in a time as short as 20 years.

Most magnetically enhanced zones detected in HRGM and HRAM surveys over hydrocarbon reservoirs are thought to occur at depths of 60–600 m (200–2000 ft), significantly above the microseeping reservoirs themselves (Foote, 1992). Hereafter, we refer to hydrocarbon-microseepage-related enhanced concentrations of magnetic minerals, over the depth range of 60–600 m, as “magnetically enhanced zones,” or MEZ. Over this depth range, it is difficult to investigate the source of the magnetic anomalies because strata in these nonproductive intervals are generally of little interest to the petroleum industry, and hence they have not been cored. Coring is the most direct way to evaluate the magnetic mineralogy and grain size, and coring will ultimately be necessary to achieve a thorough understanding of the origin of magnetically enhanced zones.

Some understanding of the magnetic mineralogy in this 60- to 600-m-depth range has been achieved by analyzing drill cuttings rather than cores. Foote (1986a) reported powder X-ray diffraction analyses (subsequently corroborated by Mossbauer spectroscopy; Foote, 1992) of drill cuttings from many boreholes in oil and gas fields over which short-spatial-wavelength aeromagnetic HRAM anomalies have been observed. He reported that the predominant magnetic mineral in the magnetically enhanced zones is maghemite ($\gamma\text{Fe}_2\text{O}_3$), although greigite (Fe_3S_4) is present in cuttings from some wells. Based on his magnetic-susceptibility measurements of drill cuttings from hundreds of wells, Foote (1992) observed zones of enhanced magnetic susceptibility only in producing wells located on HRAM anomalies. Foote (1996) concluded that in survey areas in Oklahoma, Colorado, Utah, and Alabama, the combination of short-spatial-wavelength HRAM anomalies and high magnetic susceptibility in drill cuttings could be used to predict hydrocarbon discoveries with 78–90% success.

Relying on drill cuttings alone can be misleading, unless great care is taken to minimize contamination from steel and magnetic iron oxides introduced during drilling. For example, at the Cement field, Oklahoma, where it was first proposed that aeromagnetic detection of oil and gas fields might be possible, Donovan et al. (1979) reported that as much as 1 wt. % of authigenic magnetite had formed by hydrocarbon microseepage into hematitic clastics, based on their analyses of drill cuttings from depths to 300 m. However, more-detailed analysis of drill cuttings from the Cement field by Reynolds et al. (1990a) revealed that most of the iron oxides in the cuttings had been introduced as an artifact of

drilling. In these cuttings, they identified magnetite occurring as sharp angular blades and spheres, commonly with metallographic textures and associated with steel from drilling. They concluded that steel particles in the cuttings had been partially oxidized and replaced by magnetite, maghemite, and hematite.

Not *all* magnetite at the Cement field can be dismissed as reflecting industrial contamination, however, as demonstrated in a paleomagnetic study by Elmore and Leach (1990). They extracted spherical authigenic magnetite from bleached, carbonate-cemented sandstone samples from surface outcrops on the Cement anticline. The authigenic magnetite in the bleached sandstone records a Late Permian–Early Triassic secondary chemical remanent magnetization (CRM) direction, probably reflecting the initiation of microseepage into the red beds. Other paleomagnetic studies have also identified authigenic magnetite associated with hydrocarbons (McCabe et al., 1987; Elmore and Crawford, 1990; Banerjee et al., 1997).

At the Cement field, Elmore and Leach (1990) found that only trace quantities of authigenic magnetite had been produced in the altered (bleached) sandstones. Consequently, the unaltered red beds and the bleached sandstones have similar magnetization intensities, and the average magnetic susceptibility in the bleached samples is slightly *lower* than that in the unaltered red beds. This would be insufficient to produce the magnetic contrast required to explain aeromagnetic anomalies over the Cement field. Moreover, the remanent magnetization residing in the authigenic magnetite in the bleached samples exhibits “dual polarity” (nearly equal normal and reversed polarities), and the remanent component was assumed to “self-cancel” when modeling aeromagnetic anomalies at Cement (Reynolds et al., 1990b).

Despite finding unambiguous evidence of industrial contamination of magnetic iron *oxides* at the Cement field, Reynolds et al. (1990a) demonstrated that the magnetic iron *monosulfide*, Fe_7S_8 (monoclinic pyrrhotite), occurs naturally at Cement, not only in cuttings but also in quarries and cores. The highest pyrrhotite concentrations occur at depths of 200–500 m beneath the surface. Magnetic forward models by Reynolds et al. (1990b) indicate that the pyrrhotite is capable of producing aeromagnetic anomalies as high as 7 nT at 120-m flight altitudes over the Cement field. Other occurrences of pyrrhotite associated with near-surface bacterial activity are increasingly being reported and may be capable of producing magnetic anomalies (Sassen, 1987; Kyle et al., 1987; Gose and Kyle, 1988; Ellwood and Crick, 1988; Sommer and Jain, 1990; Kyle and Gose, 1991).

Paleomagnetic studies by Fishman et al. (1989), Hudson et al. (1989), Kilgore and Elmore (1989), and Elmore and Leach (1990) have now thoroughly discredited Donovan et al.’s (1979) prediction of enhanced magnetization arising from hematite reduction to form authi-

genic magnetite upon hydrocarbon seepage into red sandstones. On the other hand, numerous paleomagnetic studies have revealed secondary magnetization arising from authigenic magnetite and pyrrhotite in *limestones* and *dolomites* (Wisniowiecki et al., 1983; Hornafius, 1984; Van Alstine, 1986, 1987; Elmore et al., 1987; Hart and Fuller, 1988; Elmore et al., 1993; Van Alstine and Butterworth, 1994; Fruit et al., 1995; Banerjee et al., 1997; Van Alstine et al., 1997; Lewchuk et al., 1998; Gillen et al., 1999). In carbonates, magnetite authigenesis has been attributed to a variety of mechanisms: oxidation of early-diagenetic pyrite, by-products of the smectite-to-illite clay-mineral transformation, dolomitization, and organic maturation. Although numerous paleomagnetic studies have been conducted on subsurface cores and surface outcrops of Devonian and Mississippian carbonate reservoir rocks in Western Canada (Hamilton et al., 1995; Symons et al., 1993; Van Alstine et al., 1997; Lewchuk et al., 1998; Gillen et al., 1999), magnetic-intensity and magnetic-susceptibility values are generally too low to be capable of producing detectable magnetic anomalies originating within the reservoirs.

In most aeromagnetic surveys for petroleum exploration, it has been assumed that a magnetically enhanced zone over a microseeping reservoir will produce a detectable HRAM anomaly merely because of its high magnetic susceptibility. Yet high magnetic susceptibility merely indicates that a magnetically enhanced zone is capable of producing a detectable *induced* magnetization, and this induced magnetization will be aligned with the earth's present magnetic field.

In the six case histories discussed below, we document that in Western Canada, the short-spatial-wavelength magnetic anomalies that we observe over producing oil and gas fields are generally *dipolar*, with positive and negative lobes. Azimuths and dip angles estimated from the dipolar anomalies are at high angles to the present magnetic field, indicating that the dipolar anomalies probably contain a significant component of *reversed-polarity remanent* magnetization. This reversed-polarity magnetization is older than the most recent geomagnetic polarity reversal (0.78 Ma), and probably records the dominant reversed-polarity bias that prevailed during most of the Tertiary, from 63 to 1.8 Ma.

In Western Canada, the intensities and azimuths inferred from the dipolar HRGM anomalies appear to be diagnostic of the microseeping reservoirs causing the anomalies. Besides having valuable predictive power in hydrocarbon exploration, this observation suggests that the magnetic mineralogy and grain-size distributions in the magnetically enhanced zones are intimately related to the history of microseepage from a particular reservoir.

For a broader understanding of the hydrocarbon microseepage phenomenon and its effects in the lithologic column, including the development of shallow magnetic anomalies, the reader is referred to AAPG Mem-

oir 66, *Hydrocarbon Migration and its Near-surface Expression* (Schumacher and Abrams, 1996). A more-detailed treatment of the thermodynamic stabilities of magnetic mineral assemblages in hydrocarbon microseepage environments is given in Machel and Burton (1991a, b) and Machel (1995, 1996).

SURVEY METHODS

Our magnetic HRGM and radiometric surveys are conducted concurrently, to maximize the geophysical information obtained at each survey station. Below, we describe our magnetic and radiometric survey procedures, and we then discuss how magnetic and radiometric surveys complement one another in hydrocarbon exploration. A glossary of terminology is included in Appendix A.

High-resolution Ground-magnetic (HRGM) Survey Methods

Our high-resolution ground-magnetic surveys are designed to yield two kinds of maps. The first map is of the residual (remanent + induced) magnetic anomalies (in nanoteslas, or nT), after subtracting the regional background magnetization, as discussed below. The second map is of the absolute value of the *second horizontal derivative* of the residual anomalies (proportional to nT/m²); hereafter, we refer to second-horizontal-derivative maps as HG' maps, because the second horizontal derivative is the derivative of the horizontal gradient (HG). Second-horizontal-derivative maps are commonly used for sharpening and enhancing near-surface anomalies that are revealed in magnetic and gravity surveys (e.g., Robinson, 1982; Telford et al., 1990). In Western Canada, we found that the *shape* of an HRGM anomaly, as revealed on an HG' map rather than on a residual-anomaly map, conforms more closely to the *shape* of the microseeping reservoir.

In our ground-magnetic surveys, we measure the total field directly, then compute residual magnetic anomalies, and then calculate the second horizontal derivative (HG') from the residual-anomaly map. At first, we constructed second-horizontal-derivative maps purely for the advantage that reservoir shapes, and hence drilling locations, are better defined on contour maps of HG' values, rather than on contour maps of residual anomaly intensities (in nT). It later became apparent that the HG' values, as well as the *azimuths* of the residual anomalies, have diagnostic value for identifying the microseeping reservoir, as discussed below.

In conducting our HRGM surveys, we use two Scintrex OMNI IV proton-precession magnetometers. One magnetometer is used for surveying and the other is used as a base station to allow correcting for diurnal varia-

tions. Although these magnetometers have a precision of 0.1 nT, we find that diurnally corrected readings are repeatable to 1 nT. Total-field magnetic data are recorded at intervals of 50 m along linear profiles nominally 400 m apart. An all-terrain vehicle (ATV) is used as a survey vehicle. The magnetometer operator, on foot, trails 50 m behind the vehicle, away from its magnetic influence. The magnetometer sensor, mounted on the end of an aluminum pole, is 2 m above the ground. The ATV driver operates the onboard gamma-ray spectrometer and sensor, the global positioning system (GPS) navigator, and the data-acquisition computer. The preliminary survey covers 6 to 8 linear mi (9.6 to 13 km)/section. Fill-in data are recorded later, as needed, to verify specific anomalies.

During the data recording process, the magnetometer operator scans the terrain at each station and checks the data to avoid obvious cultural interference. Any data point that is more than a few nanoteslas different from the last point is reread at a slightly different location. Experience in examining the raw total-field profiles suggests that in Western Canada, the shallow diagenetic magnetic anomalies probably originate between 100 and 200 m below the surface. This is further suggested by Andrew et al.'s (1991) spectral analysis of HRAM data recorded in Sheridan County, Montana, just south of the Canadian border, on the northwest side of the Williston Basin. Using the method of Spector and Grant (1970), Andrew et al. (1991) calculated an average subsurface depth to anomaly of 120 m.

For magnetic anomalies at this depth, there should be no significant change in reading if the magnetometer is moved a few meters horizontally. If there are changes, the observed anomaly must be very shallow and is probably man-made. In this case, a new location for the reading is chosen. Forearmed with pipeline and well plats, the magnetometer operator can either avoid major cultural anomalies or empirically model them and learn the exact boundaries of the corrupted data. The data profiles are examined daily to ensure data quality. Buried pipelines and invisible surface casing of dry and abandoned (D&A) wells create unmistakable signatures, and associated erroneous data points can easily be identified and removed.

The diurnally corrected data are then gridded using a kriging algorithm. Kriging, named after mining engineer D. G. Krige, refers to a collection of generalized linear regression techniques for the estimation of spatial phenomena. The advantages and methodology of kriging are well described by Olea (1992), who discusses reasons why, of the numerous computerized gridding methods currently used, "kriging is best." As part of the kriging process, a semivariogram is derived to estimate spatial coherence of the data. Semivariograms computed for data of this study indicate coherence of both the magnetic and radiometric data, up to about 500 m. Accordingly, profile line spacing of 400 m appears to be adequate and is logistically practicable for constructing

an equispaced grid for both magnetic and radiometric survey data. We have found that computing a 100-m kriged grid, in conjunction with subsequent mathematical analysis, works well in Western Canada to resolve anomalies at 100- to 200-m depths and to attenuate surface magnetic influences.

A map-convolution filter (Nettleton, 1971; Sheriff, 1973), designed to focus on the short-spatial-wavelength anomalies presumed to have originated in the near-surface magnetically enhanced zones, then operates on the gridded data matrix to remove the longer-wavelength, regional magnetic effects of the Precambrian basement. This filter uses the "center point and one ring system" (Nettleton, 1971, p. 25), whereby the filtered value at each 100-m-spaced gridpoint represents the difference between the unfiltered value (i.e., the kriged gridpoint value) and the average value at the eight surrounding grid points on a circle of 447-m diameter. These difference values, which range from about 1 to 12 nT, are contoured directly to produce the residual anomaly map, and the absolute value of their second horizontal derivative is contoured to produce the HG' anomaly map.

Radiometric Survey Methods

In the case histories at the Pierson (Manitoba) and the Rumsey reef (Alberta) fields, a Scintrex GIS-4 gamma-radiation spectrometer with a 43-cm³ sodium iodide crystal detector enriched with thallium was either hand-carried or mounted forward of the ATV. A GPS navigation system was also hand-carried or mounted on the ATV. For the Waskada (Manitoba) and the two multisection case histories in Alberta, a Scintrex GAD-6 with a GSP-4S 360-cm³ sodium iodide crystal enriched with thallium was used. This instrument and the GPS navigation system were both mounted on an ATV.

The GIS-4 can record, separately, counts in any of four individual channels: total count (0.05-MeV threshold), potassium + uranium + thorium (1.38-MeV threshold), uranium + thorium (1.66-MeV threshold), and thorium (2.44-MeV threshold). Prior to the Rumsey survey (i.e., for the North and South Pierson, Manitoba, surveys), only total-count radiation was used for mapping. At Rumsey, all four channels were used to evaluate the thorium-normalization techniques described by Saunders et al. (1993a).

The GAD-6 spectrometer is capable of recording simultaneously in all four discrete energy windows: total count, potassium (measured by ⁴⁰K radiation), uranium (measured by ²¹⁴Pb daughter radiation), and thorium (measured by ²⁰⁸Tl daughter radiation). The data are automatically spectral-stripped to remove any contributions to lower-energy windows from higher-energy peaks or cosmic radiation.

A dwell time of 100 s was used with both spectrometers, representing a compromise between counting statis-

tics (which require longer counts) and survey logistical requirements (which favor rapid data acquisition). Currently, we use a GSA-61 1.8-L crystal, which permits recording the same number of counts with a dwell time of only 30 s.

Gamma-radiation measurements in the uranium window must be corrected for diurnal variations in near-surface atmospheric radon concentrations as well as for day-to-day variations caused by changing atmospheric conditions. This is accomplished by making measurements at four separate control points at the beginning and end of each day's operations. Measurements are taken only between 1100-hr solar time and sunset, when diurnal variations are at a minimum (Morse, 1989). During this period, diurnal variations are usually statistically insignificant compared with the variability in microseepage-related anomalies.

Measurements are not made on rainy days, and no further measurements are made on a survey day after rain begins to fall, because for several hours after rain, significant increases occur in the number of counts recorded in the uranium window. This reflects rainfall washout of the radon daughter, ^{214}Bi , from the atmosphere. Beginning and ending measurements in each channel for all control points are averaged, and these averages are used to normalize individual measurements from one day to the next.

As with HRGM survey data, the radiometric survey data, corrected for diurnal and atmospheric conditions as above, are gridded for contouring using a kriging algorithm. The gridded data are expressed either directly (as counts/100 s) or as Z-scores (in terms of standard deviations, or s , about the mean). The difference between each grid value and the average value at the eight surrounding grid points on a circle of 447-m diameter is then computed, as described above for the magnetic data. These difference values are then contoured to map the radiometric anomalies.

This procedure of mapping the differences is an analytical attempt to account for surface-soil variations, such as transitions from clayey to sandy soils. Although such soil variations will clearly affect potassium, the observed spatial wavelength of the soil variations is typically several times larger than 447 m, so the circular averaging process attenuates their effects in our radiometric survey.

The thorium-normalized uranium and potassium measurements discussed by Saunders et al. (1993a, b) are more robust than the total-count measurements used for the surveys in Pierson, Manitoba, in terms of terrain, meteorological, and diurnal variations. Because thorium does not appear to be affected by microseeping hydrocarbons, thorium can be used to normalize the potassium and uranium measurements, which are affected by microseeping hydrocarbons. The thorium-normalization process helps to suppress variations in surface lithology, soil moisture content, vegetative shielding, and counting

geometry, all of which can interfere with accurate radiometric measurements. We now routinely map both thorium-normalized potassium and what Saunders calls the DRAD, which is the difference between thorium-normalized uranium and thorium-normalized potassium.

Sikka (1959) and Sikka and Shives (2002) have reported that faults can be detected at the surface by mapping anomalously high thorium concentrations. We also create thorium-distribution maps for evaluating faulting in our prospect areas. At one prospect where we also have 3-D seismic coverage, we saw good correlation between faulting as interpreted from the seismic data and faulting as interpreted from the thorium-concentration map. We have found "thorium-faulting maps" to be useful in geologic interpretation of our prospect areas. Thus, our DRAD anomaly maps must be evaluated with respect to the thorium-faulting maps to ensure that mapped DRAD values are not biased by anomalous thorium concentrations along faults.

How Magnetic and Radiometric Surveys Are Complementary

Contour maps of radiometric anomalies, unlike contour maps of magnetic HG' values, do not necessarily conform to the shape of the reservoir except in the case of channel sands, such as at the South Pierson and Wasakada fields. Generally, radiometric anomalies occur either as halo (edge-leakage) anomalies around the margins of the reservoir or as apical anomalies located more centrally over the reservoir (Saunders et al., 1999). We usually use radiometric surveys and now more specifically DRAD surveys to complement and verify the more location-specific anomalies revealed by HG' maps.

Although in a survey there are numerous reasons why either magnetic or radiometric anomalies may be unrelated to the presence of hydrocarbons, it is less likely that radiometric and HRGM anomalies would both occur at roughly the same location without hydrocarbon microseepage being the common cause. In case histories 5 and 6, which cover 39 sections (10^4 ha), we observed that every significant magnetic HRGM anomaly was accompanied by a radiometric DRAD anomaly.

Whereas our magnetic surveys are measuring *fossil* anomalies at depths of about 150 m, our radiometric surveys are measuring *modern* geochemical alterations at depths <25 cm. Thus, finding both magnetic and radiometric anomalies at the same location implies not only that a microseeping hydrocarbon reservoir once existed below, but also that it is still there and still leaking. Our gamma-ray spectrometer measures radiation emanating from the surface to a depth of about 25 cm (gamma rays are absorbed by greater thicknesses of soil). Because our study areas in Western Canada are covered by glacial till, the top 25 cm is demonstrably younger than 2.6 Ma (Cioppa et al., 1995). However, this top 25 cm generally

has been disturbed by human activity during the past 100 years because of timber harvesting, cultivating, and cattle grazing. Hence, in our surveys, the radiometric anomalies that we measure at the surface are probably <100 years old.

Because radiometric alterations caused by hydrocarbon microseepage can be found throughout the lithologic column above reservoirs (Pirson, 1969) as well as at the surface, the geochemical changes detected by our surveys in Western Canada probably began at the initiation of microseepage (the early Tertiary?) and continue to this day. Whereas magnetic HRGM anomalies (sourced at ~150 m) probably record the initiation of microseepage, the surface radiometric anomalies (sourced at <25 cm) probably reflect modern microseepage.

SIX CASE HISTORIES IN WESTERN CANADA

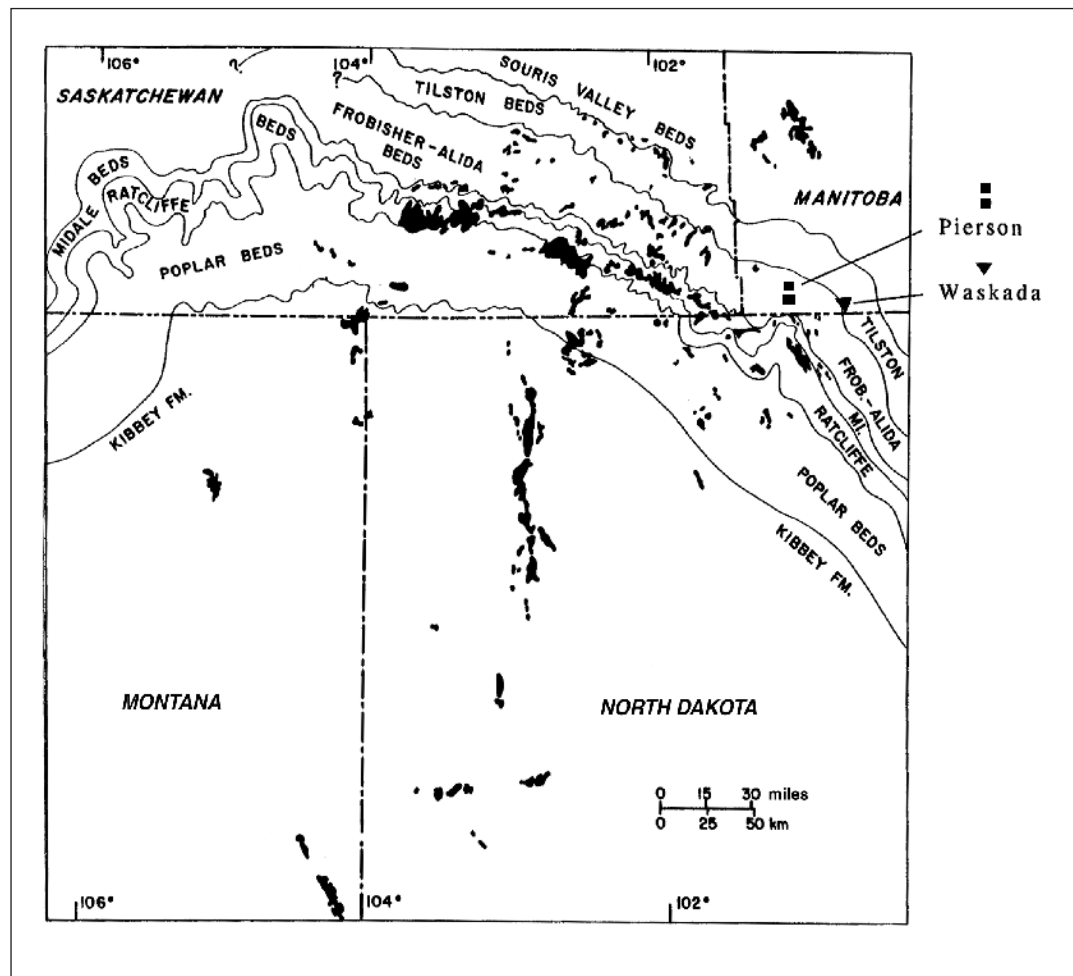
Three Case Histories in Manitoba

Case histories 1, 2, and 3 are from southwestern Manitoba, on the northeastern margin of the Williston

Basin (Figure 1). In this region, oil production is mostly from Mission Canyon Formation (Mississippian) limestones but partly from unconformably overlying lower Amaranth (Triassic?) sand (Figure 2). At the North Pierson field (case history 1), production is from the Mission Canyon limestone; at the South Pierson field (case history 2), production is from the lower Amaranth sand; and at the Waskada field, production is from both formations. At both the North and South Pierson fields, our HRGM and radiometric surveys were conducted *prior to* drilling. At the Waskada field, our surveys were conducted *after* drilling and where well logs and extensive production histories were available for comparison and verification of predictions.

In 1993, we conducted a magnetic HRGM and total-count radiometric survey over what was called the North Pierson prospect (case history 1). The goal was to investigate a downdip seismic "nose" contoured from old seismic data of the erosion surface on the top of the Mississippian limestones. At the time we conducted our survey, there were no wells in the study area. Also in 1993, we conducted a total-count radiometric survey over part of the South Pierson lower Amaranth field (case history 2). The goal was to determine whether the existing pro-

FIGURE 1. Location map showing the Waskada field (triangle) and Pierson fields (squares) relative to oil pools in Mississippian reservoirs (black-filled shapes). Modified from Kent (1984).



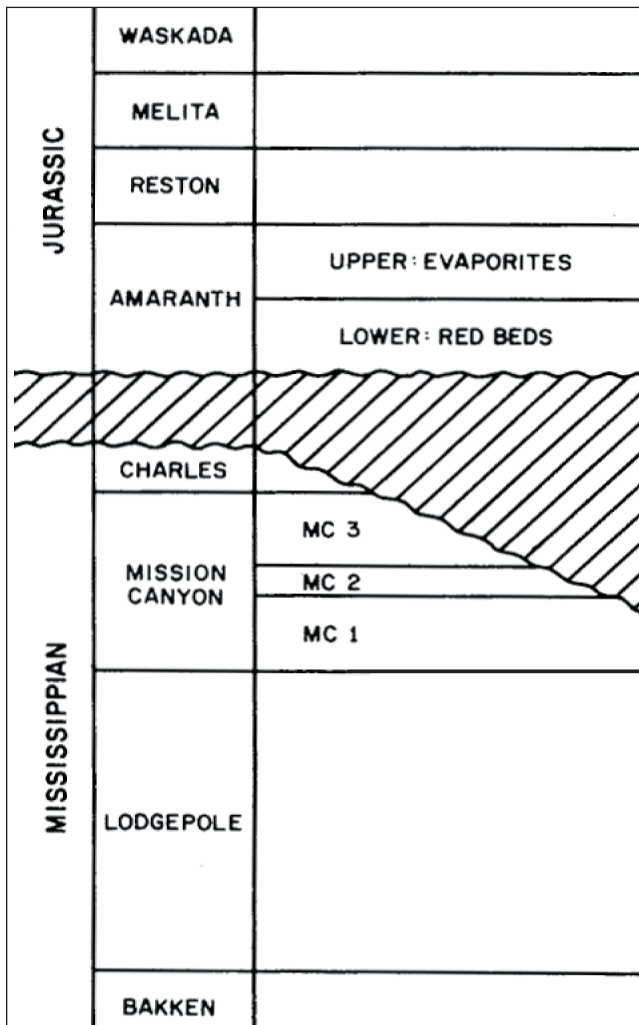


FIGURE 2. Stratigraphic column at Waskada showing lower Amaranth sands unconformably overlying Mississippian limestones. MC-3 is known locally as the Fro-bisher-Alida beds, and MC-1 and MC-2 are the Tilston beds. After Barchyn (1984).

ducting field could be extended or whether a new field could be discovered on offsetting land. Subsequent drilling on the mapped anomalies yielded two new field discoveries in North Pierson and a new field discovery at South Pierson. These discoveries were briefly discussed in LeSchack (1994, 1997).

Our 1995 survey at the Waskada field (case history 3) was motivated by the success of the HRGM and radiometric surveys at the nearby Pierson fields and by the fact that seismic surveys are ineffective in mapping lower Amaranth stratigraphic traps at all three of these fields. These traps have little structural relief, and they are usually too thin to be resolved seismically. Moreover, the lower Amaranth sand is seismically within 10 ms of the Mississippian unconformity, which often produces a strong reflection interfering with any possible lower Amaranth reflection.

The Geology of North Pierson, South Pierson, and Waskada Fields

At the Pierson and Waskada fields, the sedimentary section represents a basinward thickening of Paleozoic and Mesozoic rocks, which are separated by a significant angular unconformity. Beneath the unconformity are limestones of the Mission Canyon Formation (Mississippian), and above the unconformity are sandstones and siltstones of the lower member of the Amaranth Formation (Figure 2). Although the poorly dated lower Amaranth Formation is shown in Figure 2 as being Jurassic, Edwards et al. (1994) consider it to be Triassic (?) and correlative with the lower Watrous Formation in Saskatchewan and the upper Spearfish Formation in North Dakota. At the sub-Mesozoic unconformity is a zone characterized by secondary infilling by anhydrite, chert, or dolomite (Podruski et al., 1987). This "zone of anhydritization" generally forms an effective seal between the Mississippian and lower Amaranth reservoirs.

In the Mission Canyon reservoirs at the North Pierson and Waskada fields, oil pools occur primarily in unconformity-related traps, referred to as "paleogeomorphic traps" (Martin, 1966; Miller, 1972), which reflect late Paleozoic erosion of the Mississippian limestones to form cuestas. The oil is thought to have migrated into the Mission Canyon limestones and subsequently into the lower Amaranth sands by updip migration from basinal oil sources, probably during the late Mesozoic or early Tertiary (Podruski et al., 1987).

At the Pierson and Waskada fields, Mission Canyon inner-shelf carbonates consist predominantly of burrowed, peloidal, and skeletal lime mudstones and wackestones, with local accumulations of skeletal packstones and grainstones (Kent, 1984). Stromatolites, desiccation features, storm-layered sequences, and displacive and layered anhydrite characterize the peritidal deposits. The entire Mississippian succession, of which the described inner shelf is the northeasternmost edge of the Williston Basin, represents a prograding, shallowing-upward megasequence.

The Waskada field produces light-gravity oil, mostly from the lower Amaranth sand. The lower Amaranth consists predominantly of dolomitic siltstones and sandstones interbedded with argillaceous siltstones and shales. These strata have a mottled red to maroon color, and they are commonly referred to as "red beds." The depositional environment was probably intermittently shallow-marine. Sand beds in the lower Amaranth have been interpreted as being either fluvial deposits on a periodically emergent mud flat or sediment that has been winnowed by wave action in shallow-marine conditions (Barchyn, 1984).

The reservoir characteristics of the lower Amaranth Formation are highly variable. Based on numerous wells in the Waskada field, specific channels of higher productivity occur locally within the lower Amaranth sand. Al-

though the entire lower Amaranth may show oil staining, only the more porous sandy beds have adequate permeability to be good reservoirs, and most of the net pay is found in these siltstones and sandstones.

**Case History 1:
North Pierson Field, Mission Canyon
(Mississippian) Limestone**

Case history 1, at the North Pierson field, Manitoba, is a predrilling example in which our ground-based magnetic and radiometric surveys were successfully used in targeting productive wells in Mississippian limestones. The reservoirs occur just below the zone of anhydritization, which is at the erosion surface developed on Frobisher-Alida (MC-3) limestones of the Mission Canyon Formation.

The magnetic HG' map at the North Pierson field (Figure 3a) reveals shapes similar to those expected for the erosional limestone cuestas in this part of the Williston Basin (Martin, 1966). Comparison of the magnetic survey (Figure 3a) with the concurrent total-count radiometric survey (Figure 3b) reveals that apical as well as halo radiometric anomalies are associated with the magnetic anomalies at the North Pierson field.

At North Pierson, our magnetic/radiometric survey was completed prior to any drilling. Well A was subsequently drilled on the edge of an HG' anomaly (Figure 3a), and this well made 1550 bbl of oil in its first month on production. The company that drilled well A had chosen its location based on a seismic line and had ignored the HRGM survey, which would have predicted that even more successful wells could have been drilled to the south or east, closer to the heart of the HG' anomaly. This was confirmed by the subsequent drilling of horizontal well C, which was drilled through the heart of the anomaly and which produced 1680 bbl of oil in its first month.

Wells B, F, and G were drilled at locations based solely on the magnetic/radiometric survey. Wells F and G were cored, and these cores showed oil saturation. Wells B and G were put on production but were later suspended. Well F, although completed, was never put on production. As suggested by the HG' map, well G discovered a different pool from the others shown in Figure 3a, and oil from this pool well has a different gravity than oil from the other wells.

In summary, five wells were drilled *after* our magnetic/radiometric surveys at the North Pierson field, and all five found oil in two new pool discoveries. All five wells clearly lie on HG' anomalies (Figure 3a).

Of these five wells, horizontal well C provides the most compelling evidence of the accuracy of magnetic HG' maps. Not only did the HG' map predict that hydrocarbons would be encountered at the beginning of the horizontal leg of well C, it also predicted a breach or pinch-out of effective reservoir, seen as the erosional

embayment at the southern end of the lateral. This, in fact, was encountered during the horizontal drilling of the lateral section. Foote (1986a) and Tompkins (1990) have also noted this general congruence of near-surface magnetic anomalies with the underlying microseeping reservoirs that caused them.

**Case History 2:
South Pierson Field, Lower Amaranth
(Triassic?) Sand**

In some cases, such as above channel sands, radiometric surveys alone can be used to delineate hydrocarbon reservoirs. For example, Saunders (personal communication, 1995) observed that radiometric surveys reveal productive sand channels in the Paluxy Formation (Lower Cretaceous) in Texas. Similarly, radiometric surveys in the northeastern Williston Basin can be used to explore for hydrocarbons in lower Amaranth sand channels, as demonstrated in this case history.

Our radiometric survey resulted in a new discovery at the South Pierson field, where microseepage above productive lower Amaranth sand channels caused the typical ⁴⁰K depletion over hydrocarbon reservoirs (Figure 4). This type of potassium depletion produces negative total-count anomalies with respect to the mean background count for a survey area. Based solely on this map, an exploratory well was drilled at D and made 1000 bbl of oil in its first month on production.

While we were conducting the radiometric survey used for locating vertical well D, another company spudded horizontal well E southwest of well D. Unknown to us at that time, well E penetrated the axis of the channel shown in the southwestern quadrant of Figure 4. The location of well E had been chosen solely by interpretation of the subsurface geology from nearby wells. Well E produced 3800 bbl of oil in its first month on production.

**Case History 3:
Waskada Field, Amaranth and
Mission Canyon Stacked Reservoirs**

A question often asked of proponents of surface exploration methods is: In the case of vertically stacked reservoirs (a common occurrence in Western Canada), can you distinguish between anomalies caused by one reservoir and those caused by an underlying reservoir? For surface exploration methods based on geochemical alterations resulting from microseeping hydrocarbons, the answer has essentially been "no." However, case history 3, at the Waskada field, demonstrates that our magnetic/radiometric surveys can distinguish between anomalies in fields where the reservoirs are stacked. In particular, this case history provided our first indication that magnetic versus radiometric surveys might be detecting

microseepage from different reservoirs at different pressures and depths. Thus, we present this case history in detail, and we expand on these findings in the “Discussion” section.

The original goal of our magnetic/radiometric survey at the Waskada field, where seven wells had been drilled prior to our survey, was to determine whether the two economic producers (wells V and S in Figure 5) are located in the *same* lower Amaranth sand-channel “sweet

spot.” The other five wells included two dry holes and three marginal producers. Contrary to expectations, the radiometric survey revealed that the two economic producers, despite their proximity to each other, were producing from two different lower Amaranth channels.

Figure 5 shows the locations of the seven wells and their cumulative oil production at the 130-ha (320-ac) case-history area in the Waskada field. Because all five producers had been drilled within a 13-month period

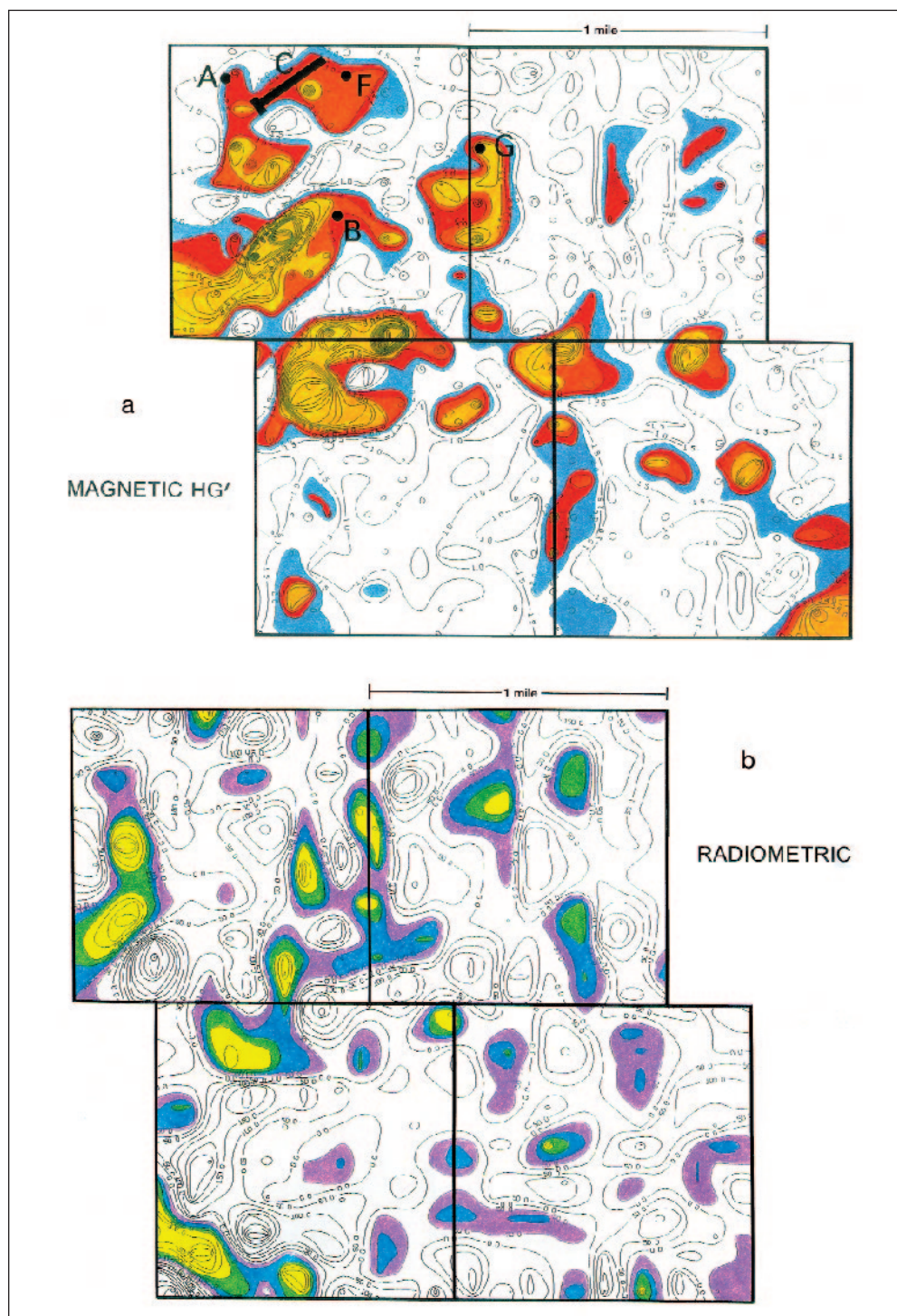


FIGURE 3. (a) Magnetic HG' map of a four-section (10³-ha) part of the Alida (Mississippian limestone) field at North Pierson. The survey was completed prior to drilling of the wells shown. All five wells were drilled on HG' anomalies and all encountered oil. Note the northwest-southeast subcrop trend of erosional Mississippian cuesta reservoirs, seen also in Figure 1. HG' contour values (proportional to nT/m²) greater than 2 were considered significant and are colored. (b) A map of the total-count radiometric survey conducted concurrently with the magnetic survey shown in Figure 3a. The colored negative anomalies indicate typical removal of ⁴⁰K over hydrocarbon reservoirs. The contoured values are in units of counts/100 s. After LeSchack (1997), courtesy of *Oil & Gas Journal*.

and had been on production for more than 5 years at the time of our survey, we assume that production from all wells commenced simultaneously, so comparison of the cumulative production totals is valid for this study.

At the Waskada field, the data points in our magnetic/radiometric survey were nominally spaced at 50-m increments along traverses 400 m apart (Figure 5). We find this to be the optimum data-point spacing—far

enough from the wells to avoid magnetic contamination, yet close enough to exhibit adequate data coherence as determined from kriging-process semivariograms. Small irregularities in the 50-m data-point spacing reflect individual errors in the GPS navigation system; larger deviations reflect obstacle avoidance. In this area, there are no pipelines that could introduce other magnetic contamination; the oil is transported away by truck.

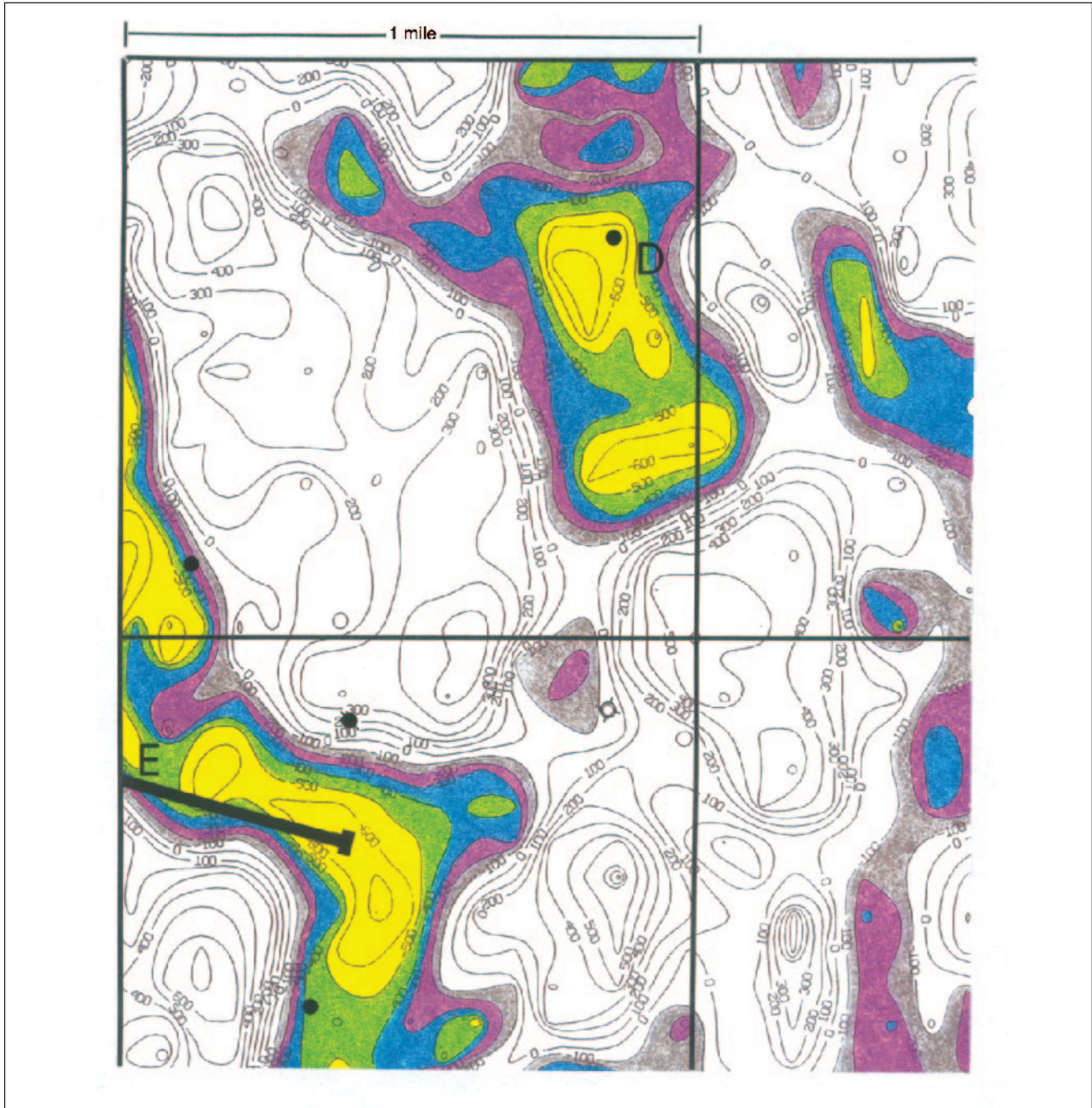


FIGURE 4. Total-count radiometric anomaly map over lower Amaranth sand channels in the South Pierson field. The colored negative anomalies indicate typical removal of ^{40}K over hydrocarbon reservoirs. The contoured values are in units of counts/100 s. The mean background count level is nominally zero. After LeSchack (1997), courtesy of *Oil & Gas Journal*.

Induction and sonic logs covering the lower Amaranth sand and the underlying Tilston limestone (MC-1 of the Mission Canyon Formation) are shown in Figure 5. The log suite for well W, which has been enlarged in Figure 6, shows both the lower Amaranth sand and the Tilston porosity beneath the anhydrite cap. Based on the good correlation between cumulative production from the lower Amaranth and the sand quality as depicted on the logs, it is not surprising that wells S and V, the two best lower Amaranth producers, were originally assumed to have been drilled into the same channel-sand body.

Figure 7 shows the results of our magnetic and concurrent radiometric surveys at the Waskada field. Comparison of production data from the lower Amaranth (Figure 5) with results of our radiometric survey (Figure 7b) demonstrates that radiometric surveys provide a valuable tool for targeting good drilling locations in lower Amaranth sand channels. In our Waskada radiometric survey, we mapped DRAD anomalies rather than total-count radiometric anomalies as in case histories 1 and 2. DRAD anomalies are expressed as positive numbers, and the more positive, the more anomalous. The contour map of DRAD anomalies in the Waskada field (Figure 7b) not only defines a coherent pattern of fluvial channels but also reveals that the most productive wells, S and V, had been drilled in distinctly different channel-sand bodies. Moreover, the cumulative lower Amaranth production from the well nearest each major anomaly exhibits a good correlation with the DRAD anomaly value. For example, well S, which had the greatest lower Amaranth production, is located on the highest DRAD contour of any of the wells. Well V, with the second-largest production, is on the edge of the second-largest anomaly on the map. Wells R and T, both dry holes, are located on wide, contiguous nonanomalous regions. Wells Q, U, and W are only marginal producers.

At the Waskada field, the pattern and trend of the contours on the magnetic HG' map (Figure 7a) are qualitatively different from the radiometric DRAD map (Figure 7b). This was surprising, based on the observed similarity between maps produced by these two exploration techniques in other areas.

The most important revelation in Figure 7a is the unmistakable paleogeomorphic pattern of erosional Mississippian limestone cuestas, which are also revealed in the HG' map from the North Pierson field (Figure 3a). Figure 8 shows an idealized representation of the Mississippian cuesta reservoirs that are delineated by the HG' map and illustrates some of the nomenclature used for discussing cuesta reservoirs (e.g., “consequent slope,” “subsequent slope,” and “subsequent valley”). This representation is consistent with the description of paleogeomorphic traps in the Williston Basin by Martin (1966; see his Figure 18 of Mississippian Frobisher-Alida fields) and Miller (1972; see his Figure 5 of the Mississippian Tilston reservoir in the Parkman field). Both the northwest-

southeast subcrop trend and the essentially perpendicular consequent/subsequent slope trends are observed at the Waskada field (Figure 7a) and at the North Pierson field (Figure 3a). Author LeSchack, who has developed economically successful plays on the same cuesta subcrop trend by mapping the Tilston limestone (MC-1) in the Parkman field in Saskatchewan, is familiar with these erosional patterns and recognized them at the Waskada field.

Examination of the well logs (Figure 5) supports our contention that the magnetic survey (Figure 7a) is essentially mapping the Mississippian cuesta reservoirs, whereas the radiometric survey (Figure 7b) is essentially mapping the lower Amaranth channel-sand reservoirs. In particular, the well logs indicate that oil is present in Mississippian strata beneath high HG' contour values, whereas oil is *not* present in Mississippian strata beneath low HG' contour values.

Of the seven wells, only wells W and Q had some Mississippian production. Well W produced 538 bbl of oil from a Mississippian (Tilston) porosity zone approximately 2 m thick, just beneath the tight anhydrite cap typical of Tilston reservoirs. Well Q produced 918 bbl of oil from a similar Tilston porosity zone approximately 1 m thick. These Mississippian reservoirs have a strong natural water drive, and wells with a resistivity of 5 ohm-m or more in the porosity zone commonly produce economic quantities of oil, if the pay zone is thick enough (usually 3 m or thicker). Resistivities of 1–2 ohm-m indicate porosity zones that are completely wet. Wells Q and W, which have resistivities of 9.0 and 4.5 ohm-m, respectively, proved to be marginally productive, mostly because their Tilston pay zones are so thin (<2 m).

Well V, closer to the strongest HG' anomaly thought to be associated with microseepage out of a Mississippian reservoir, has a thicker Tilston porosity zone, with a resistivity of 3.5 ohm-m. Although it has a low resistivity, well V might have produced Mississippian oil if it had been perforated in that zone. On the HG' anomaly map (Figure 7a), well V appears to be on the edge of an erosional embayment (“obsequent valley”). Hence, we expect that if well V had been drilled 200 m to the south (i.e., at the maximum HG' value), it would have been structurally nearer the top of the cuesta reservoir and likely would have produced from the Mississippian strata.

Well T is located near the second-highest HG' anomaly on the map and has a Tilston porosity zone with 5.5 ohm-m resistivity, suggesting that oil is there. However, the Mississippian porosity zone is only ~1 m thick, which was considered too thin to be worth perforating. Well T probably would have produced oil if it had been perforated in the Tilston, like wells Q and W, which were perforated in and produced from the Mississippian.

Well S is shown as being on the *idealized* cuesta reservoir in Figure 8, and hence might have been expected to produce from the Mississippian strata. However, well S

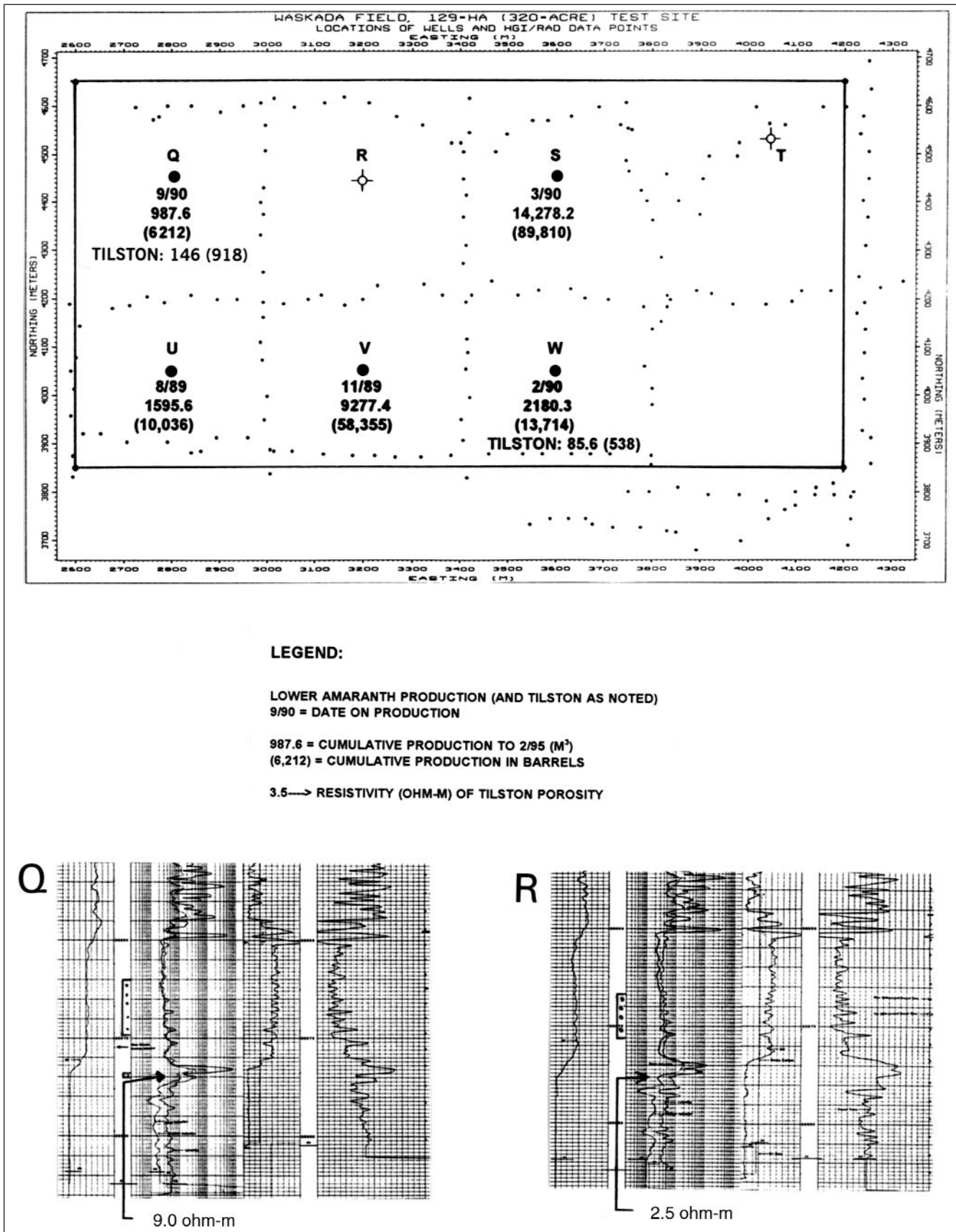


FIGURE 5. The half-section (130-ha) survey area at the Waskada field. Data-point locations for the magnetic/radiometric survey are shown as small dots, and well locations are shown as large dots. For producers, dates placed on production and cumulative production to February 1995 are shown.

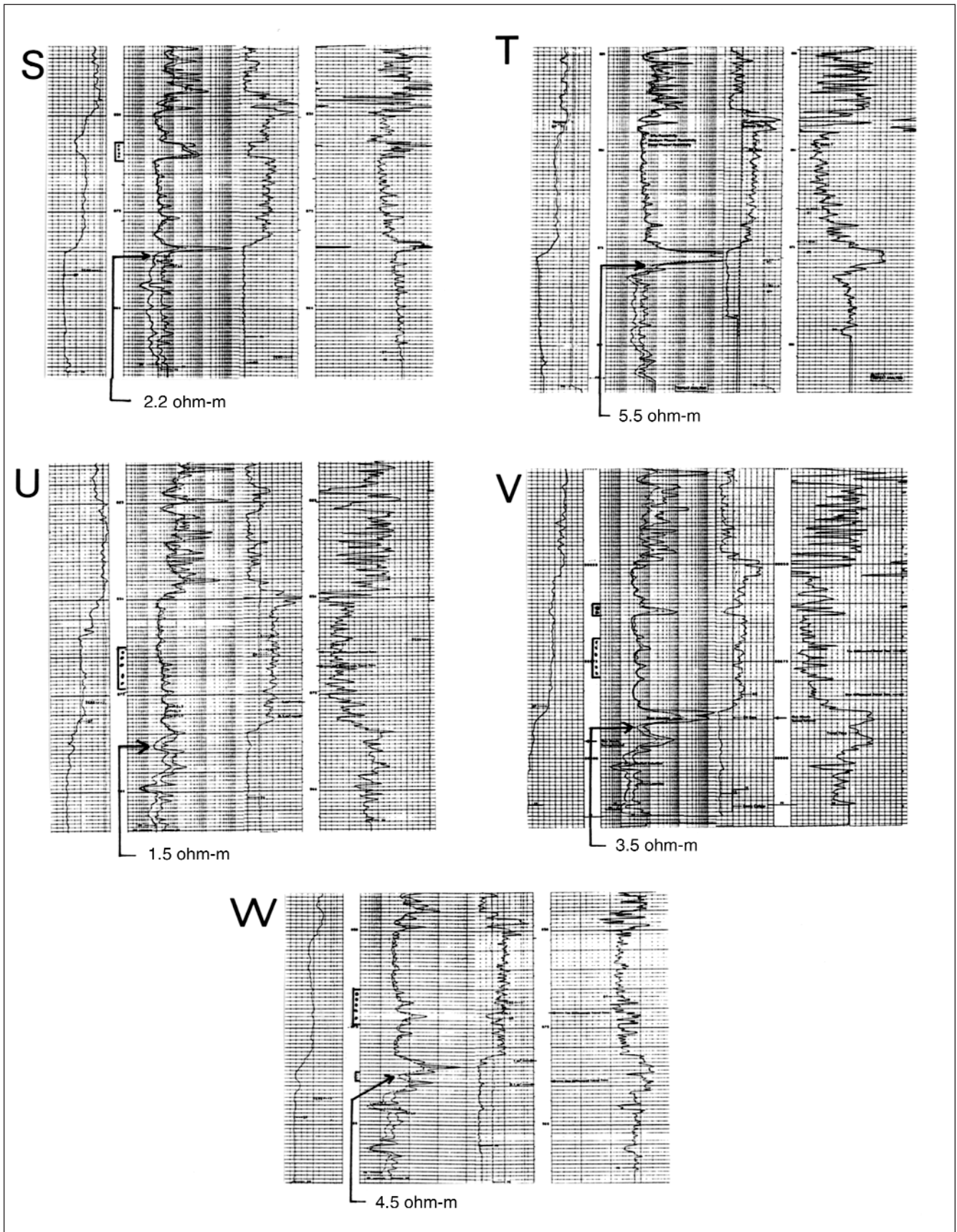


FIGURE 5 (cont.). The induction and sonic logs covering the lower Amaranth and the underlying Tilston beds are illustrated for each well, and the resistivity in the Tilston porosity zone is indicated.

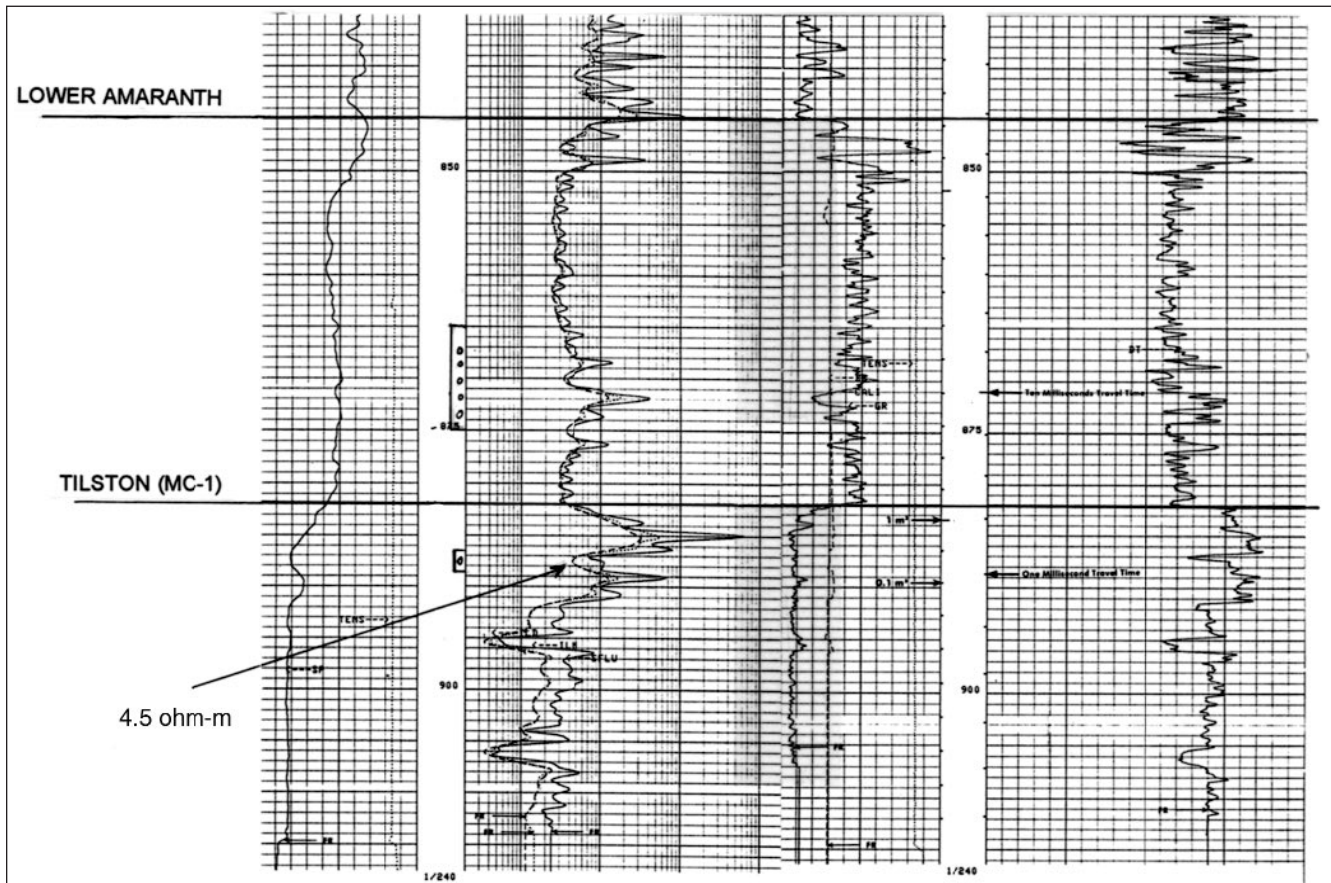


FIGURE 6. The induction and sonic logs for well W illustrate the lower Amaranth sand and the underlying Tilston limestone. The tops of the lower Amaranth and Tilston are picked, and the productive pay zones in the sand are perforated where shown. The Tilston porosity zone and its resistivity are also identified.

exhibits low resistivity (2.2 ohm-m) in its Tilston porosity zone, indicating that it is wet. Moreover, judging from the very low HG' value (0.4) nearest well S and the well's proximity to an erosional embayment on the HG' map (Figure 7a), the failure of well S to produce from the Mississippian probably reflects erosion of reservoir rock in the cuesta (i.e., similar to the erosional embayment at the southern end of horizontal well C in case history 1).

Based on HG' contour morphology, wells U and R are off the Tilston cuesta structure and therefore are wet. This is confirmed by their low resistivities of 1.5 and 2.5 ohm-m, respectively.

Comparison of Figures 7a and 7b suggests a rough, *inverse* spatial correlation between the radiometric anomalies created by microseeping lower Amaranth channel-sand reservoirs and the magnetic HG' anomalies created by microseeping Mississippian limestone cuesta reservoirs. This is geologically reasonable, because lower Amaranth sands that were deposited on the erosion surface would have first filled the topographic lows (e.g., subsequent valleys), thereby leading to thicker pay sands and stronger radiometric anomalies above these channels. Later-formed lower Amaranth channels would be in contact with a leaky sub-Mesozoic unconformity higher up

the consequent slopes (as depicted in Figure 8), perhaps explaining the strong radiometric anomalies west of wells V and T. By this reasoning, the radiometric anomalies are essentially recording places where the anhydritic seal along the sub-Mesozoic unconformity has failed locally, allowing oil to migrate from high-pressure Mississippian limestone reservoirs into low-pressure lower Amaranth channel-sand reservoirs.

Further implications of the apparent inverse spatial correlation between magnetic and radiometric anomalies at the Waskada field are explored in the "Discussion" section.

Three Case Histories in Alberta

Just as the Waskada field (case history 3) is an example of Mesozoic clastic reservoirs stacked over Paleozoic carbonate reservoirs, in our Alberta case-history areas, similar stacked reservoirs are the norm. In central Alberta, shallower, less-productive Cretaceous clastic reservoirs are commonly stacked over deeper, more-productive Devonian carbonate reservoirs. In these cases, differences in the magnetic signatures above Devonian and Cretaceous reservoirs have proved to be valuable guides for identify-

ing the microseeping reservoir that caused each magnetic anomaly. In case histories 4, 5, and 6, we illustrate this principle by comparing HRGM data with oil-production data from 110 wells in central Alberta. These 110 wells are at latitudes between Edmonton and Calgary, on the east limb of the Alberta syncline.

Case History 4: Rumsey Field, Leduc (Upper Devonian) Pinnacle Reef

Case history 4, which is a postdrilling example at the Rumsey field, central Alberta, is especially important for three reasons. (1) It documents the occurrence of the *strongest HRGM anomaly directly over the most prolific oil producer* of any of the 124 wells where we could compare HRGM data with production data in Western Canada. (2) It shows that a magnetic HG' map is as effective as a 3-D seismic survey in delineating the boundaries of a pinnacle-reef reservoir. (3) It is the "type example" of a *dipolar residual magnetic anomaly* revealed in our HRGM surveys in Western Canada.

The Rumsey reef is on the Fenn–Big Valley Shoal near Stettler, Alberta (Figure 9). At the Rumsey field, the reservoir is a dolomitized Leduc Formation (Upper Devonian) pinnacle reef (Figure 10). This reef is 100 m high, and its top is at a depth of 1750 m. Andrichuk (1958) observed that Leduc coral reefs occur preferentially on a 30-m-thick dolomitized platform immediately overlying the Cooking Lake Formation and underlying the Erskine, Stettler, Fenn, and Big Valley Leduc reef fields on the shoal. He further suggested that because this dolomitic trend extends about 12 km (7 mi) southwest of the Big Valley field, the area to the southwest may well contain productive reef buildups as yet undiscovered (in 1958). The Rumsey reef, discovered in that southwestern extension in 1982, is the most significant productive Leduc buildup discovered on the shoal since the publication of Andrichuk's paper in 1958.

The Rumsey reef is a drowned reef, the drowning having resulted from subsidence of the Cooking Lake carbonate platform, thereby arresting development of a full-grown Leduc reef. Although these Leduc drowned reefs are typically of small areal extent, they are filled to the spill point with light-gravity oil and, where found, are prolific producers. These small pinnacle reefs are particularly difficult to find by 2-D seismic exploration, unless the seismic line passes directly over the apex of the reef. A geologic and seismic description of the Rumsey reef is presented in Anderson et al. (1989, p. 114–117), and a general discussion of seismic and geologic characteristics of drowning events on carbonate platforms is presented in Erlich et al. (1990).

The Rumsey reef was discovered by Gulf Canada in 1982, after a single seismic line encouraged Gulf to lease the land. Subsequently, two additional seismic lines were used to define a 30-ms seismic anomaly revealed by iso-

chronal thinning between the Viking Formation (Lower Cretaceous) and the Ireton Formation (Upper Devonian). No clear seismic anomaly was seen at the Leduc/Cooking Lake target level—just a defocusing of the seismic energy. Upon drilling, a well flowing as much as 4000 BOPD for 3 years produced from this pinnacle-reef reservoir, which covers an area of only 16 ha (40 ac). To date, 3.8 million bbl have been recovered from this well, which is the only well that drains this Leduc pinnacle reef (Lemon and Taylor, 1993). Lemon (personal communication, 1993) acknowledged that this discovery was based as much on serendipity as on science.

After the Rumsey discovery, Gulf commissioned a 3-D seismic survey to determine the full extent of the reef. In 1994, Gulf participated in a joint project with author LeSchack to share and make public this 3-D seismic survey, in exchange for his magnetic HG' and radiometric DRAD maps of the same area. Gulf provided the 3-D seismic survey only *after* LeSchack presented his magnetic/radiometric survey.

Comparison of the magnetic HG' map (Figure 11a) and the 3-D seismic survey (Figure 11b) reveals that the magnetic and seismic surveys delineate the reef equally well. In Figure 11a, the "8" contour appears to outline the base of the pinnacle. At the Rumsey field, we measured the magnetic contamination from well casing, pipes, infrastructure, and pipelines, and we removed this cultural interference before preparing the HG' map. Magnetic data were recorded every 10 m, moving away from one of the other wells on the reef. The data showed that moving either north-south or east-west from this well, the magnetic effect of the well was no longer detectable at a distance of 80 m. Magnetic interference from pipelines was undetectable at a distance of 20 m. Accordingly, total-field magnetic data within 80 m of wells and within 20 m of pipelines were replaced by regional averages derived from values outside the affected zone, prior to computing the HG'.

The radiometric DRAD survey (Figure 11c) was conducted as described by Saunders et al. (1993a, b). The DRAD values mapped in Figure 11c reveal an apparent halo anomaly around the periphery of the Rumsey reef, reinforcing indications from the HRGM survey that there are hydrocarbons below. We interpret the DRAD anomalies to the east of the Rumsey reef as halo anomalies on the western flank of the Big Valley reef field, shown in Figure 9. Sikka (1959) and Sikka and Shives (2002) presented airborne radiometric data over the major Leduc reef field at Redwater, Alberta, and they observed similar halo anomalies around that Leduc reef. We have also observed radiometric halo anomalies around the Morinville and Golden Spike Leduc reef fields. Saunders (personal communication, 1994) suggested that reef fields are more likely to exhibit halo rather than apical radiometric anomalies because of differential-compaction-related faulting around reefs.

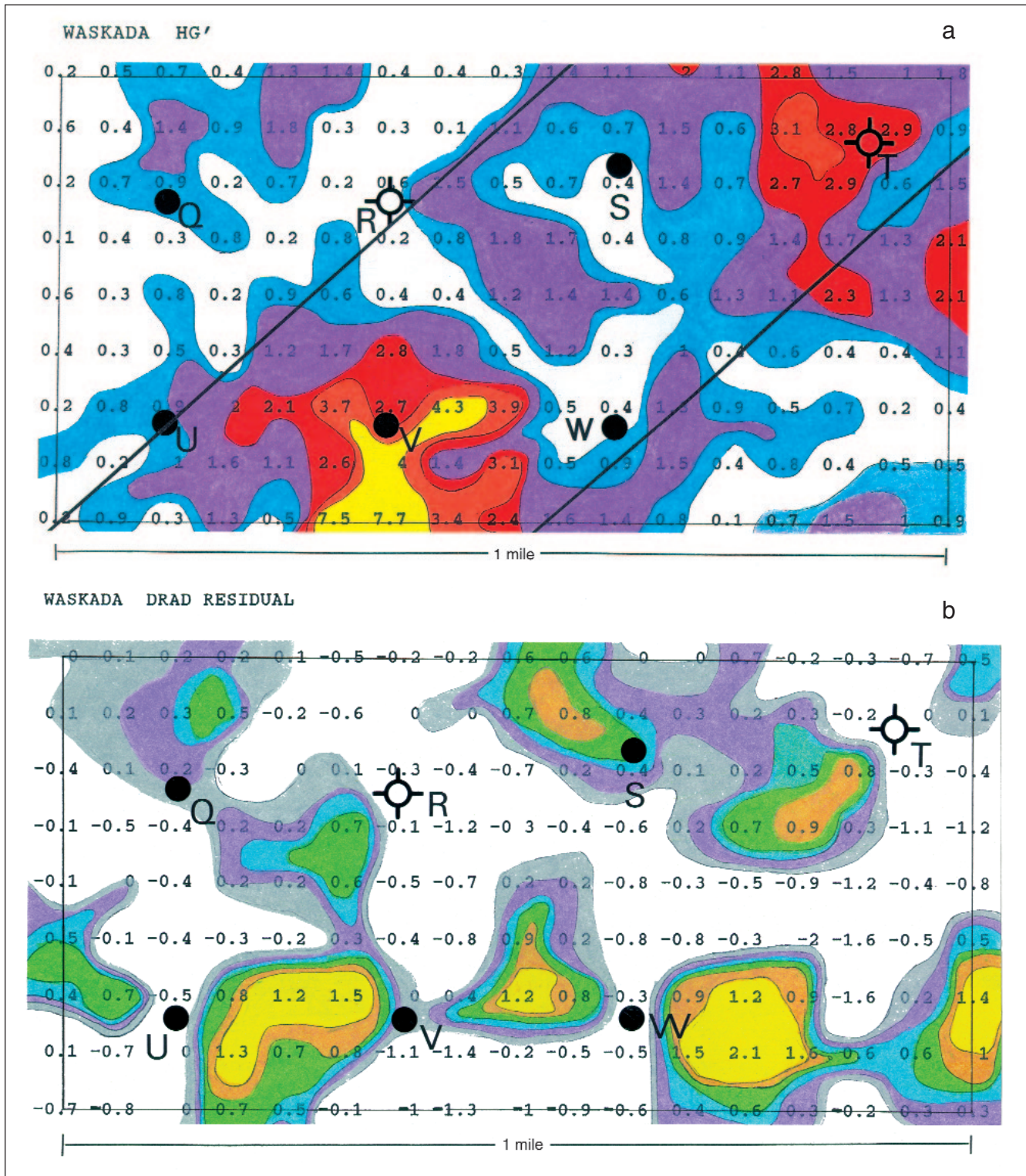


FIGURE 7. (a) Waskada HG' map, showing magnetic anomalies taking the shape and trend of typical Mississippian erosional (cuesta) features that form paleogeomorphic traps. HG' contour values (proportional to nT/m²) greater than 2 were considered significant and are colored. The two northeast-southwest-trending lines have been added to emphasize the northeast subsequent slope and southwest consequent slope trends of the Mississippian cuesta reservoirs. Most production is from the lower Amaranth; only wells Q and W produced from the Mississippian. (b) Waskada DRAD anomaly map (the difference between thorium-normalized uranium and thorium-normalized potassium). Anomalous values are expressed as positive numbers, the more positive, the more anomalous. Values greater than 0 were considered significant and are colored. The radiometric anomalies are located over lower Amaranth sand-channel reservoirs with known lower Amaranth production. After LeSchack (1997), courtesy of *Oil & Gas Journal*.

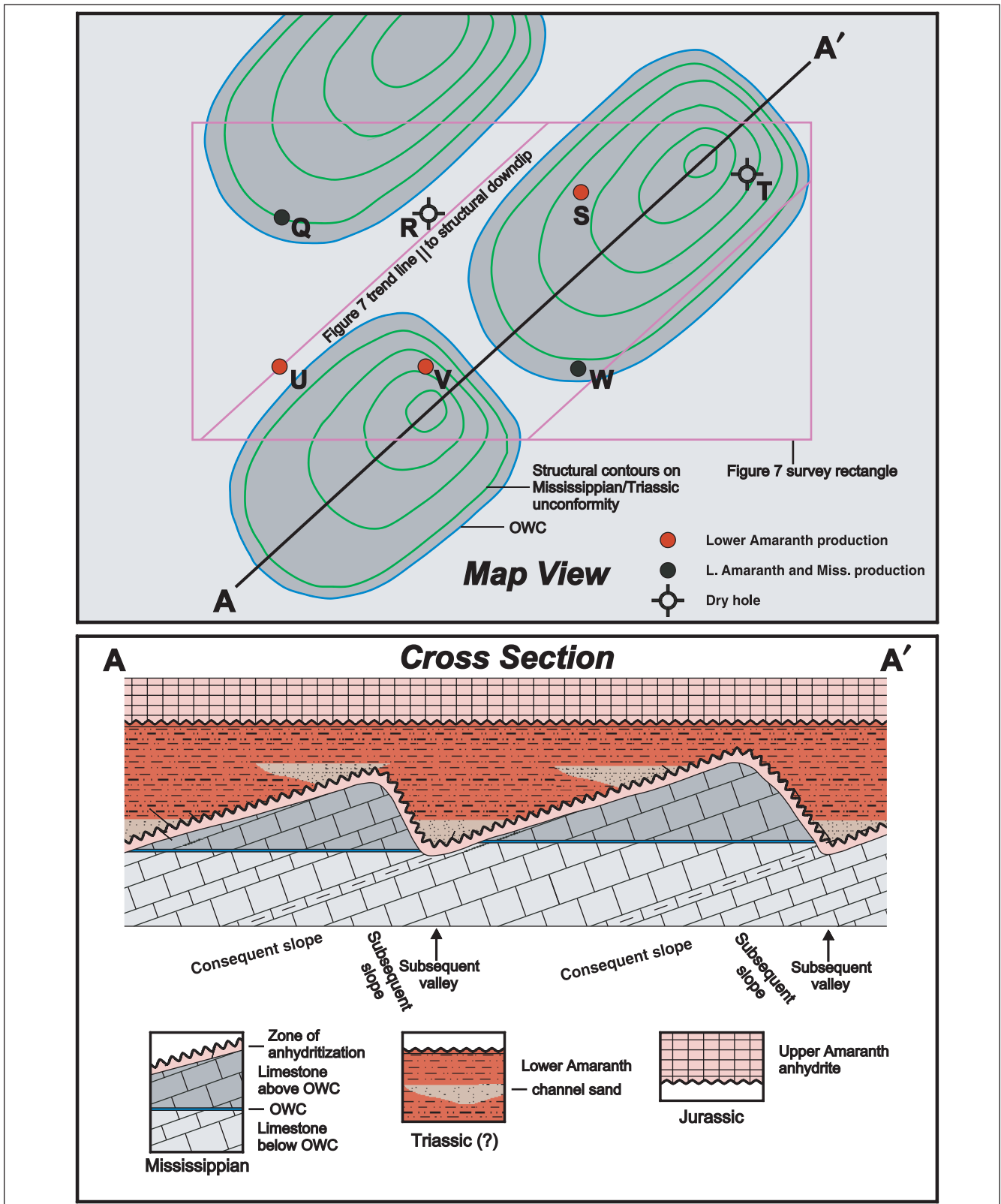


FIGURE 8. An idealized representation of the erosional Mississippian cuesta reservoirs depicted on the HG' map (Figure 7a). The map view shows the idealized Tilston paleogeomorphic traps and the location of the seven wells. The cross section shows the cuesta nomenclature used in this study and the inferred oil-water contacts (OWC). The north-east-southwest-trending lines in the map view (also shown in Figure 7a) indicate the basinward structural down-dip direction and the downslope directions of the subsequent/consequent slopes of the cuestas. Also shown are the locations of the lower Amaranth sand channels mapped in Figure 7b.

FIGURE 9. Generalized dolomitization pattern of the 30-m-thick unit directly above the Cooking Lake Formation in the Stettler–Fenn–Big Valley area of Alberta (after Andrichuk, 1958). The location of the Rumsey reef is shown. The scale is in miles. Courtesy of AAPG.

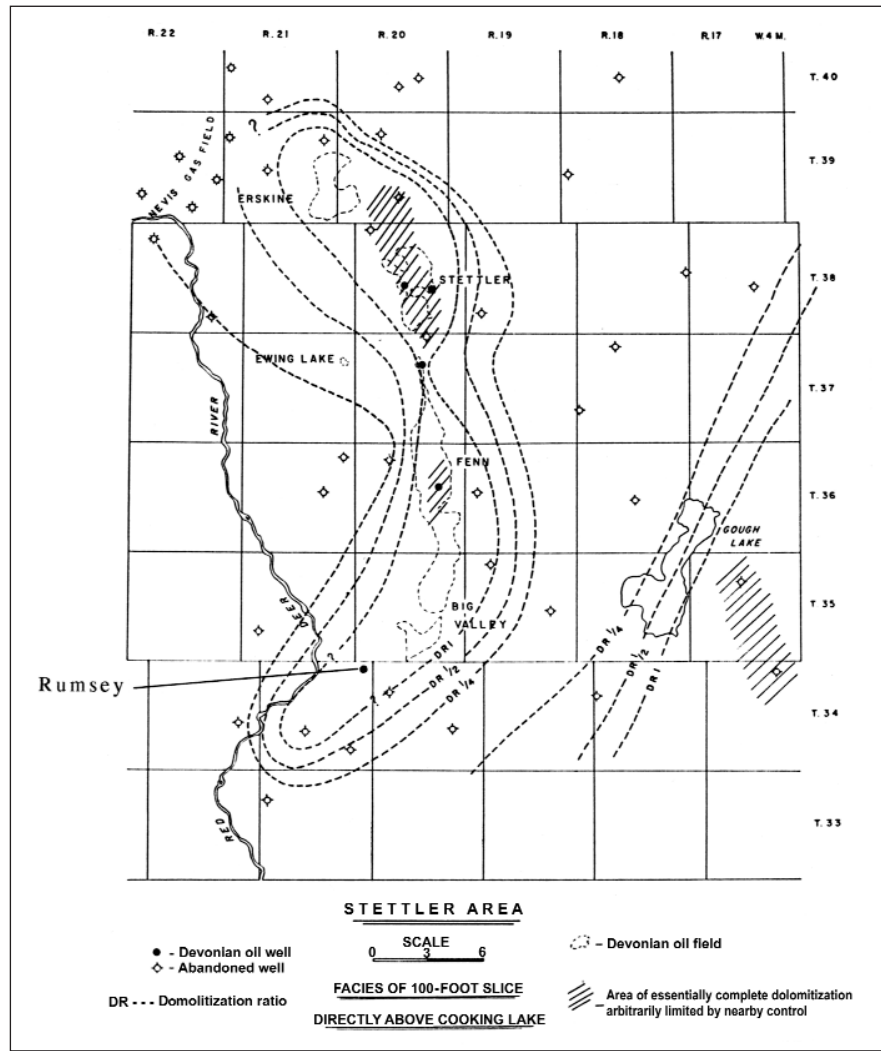
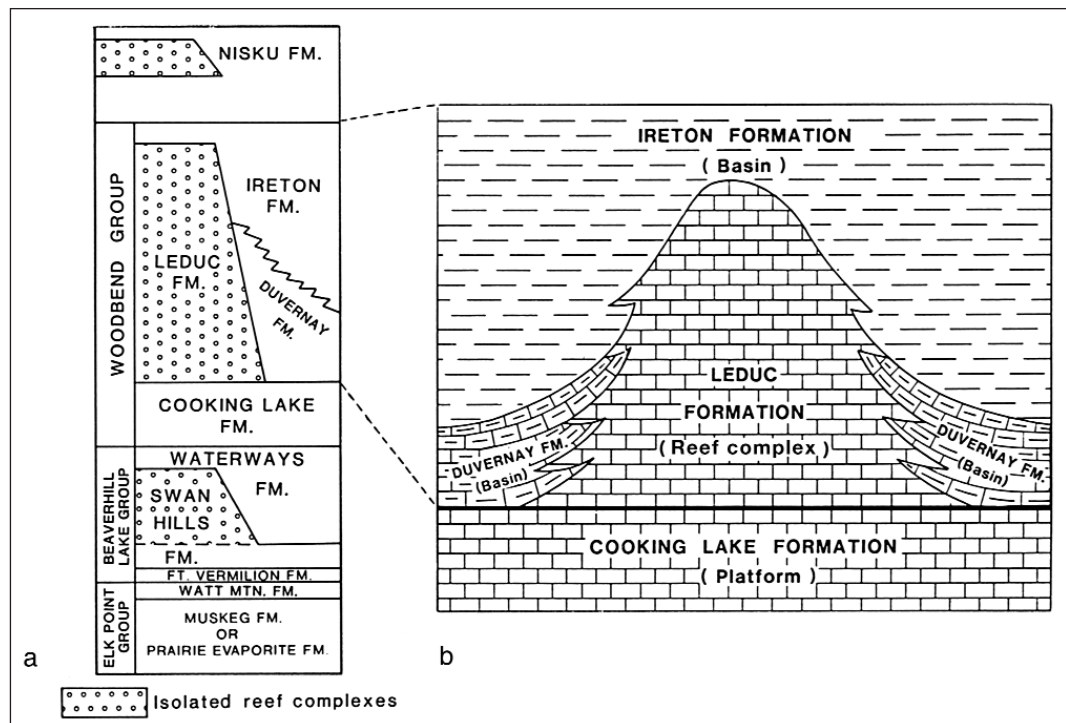


FIGURE 10. The Devonian stratigraphic section showing Leduc reef buildup (modified from Wendte, 1994). Courtesy of CSPG.



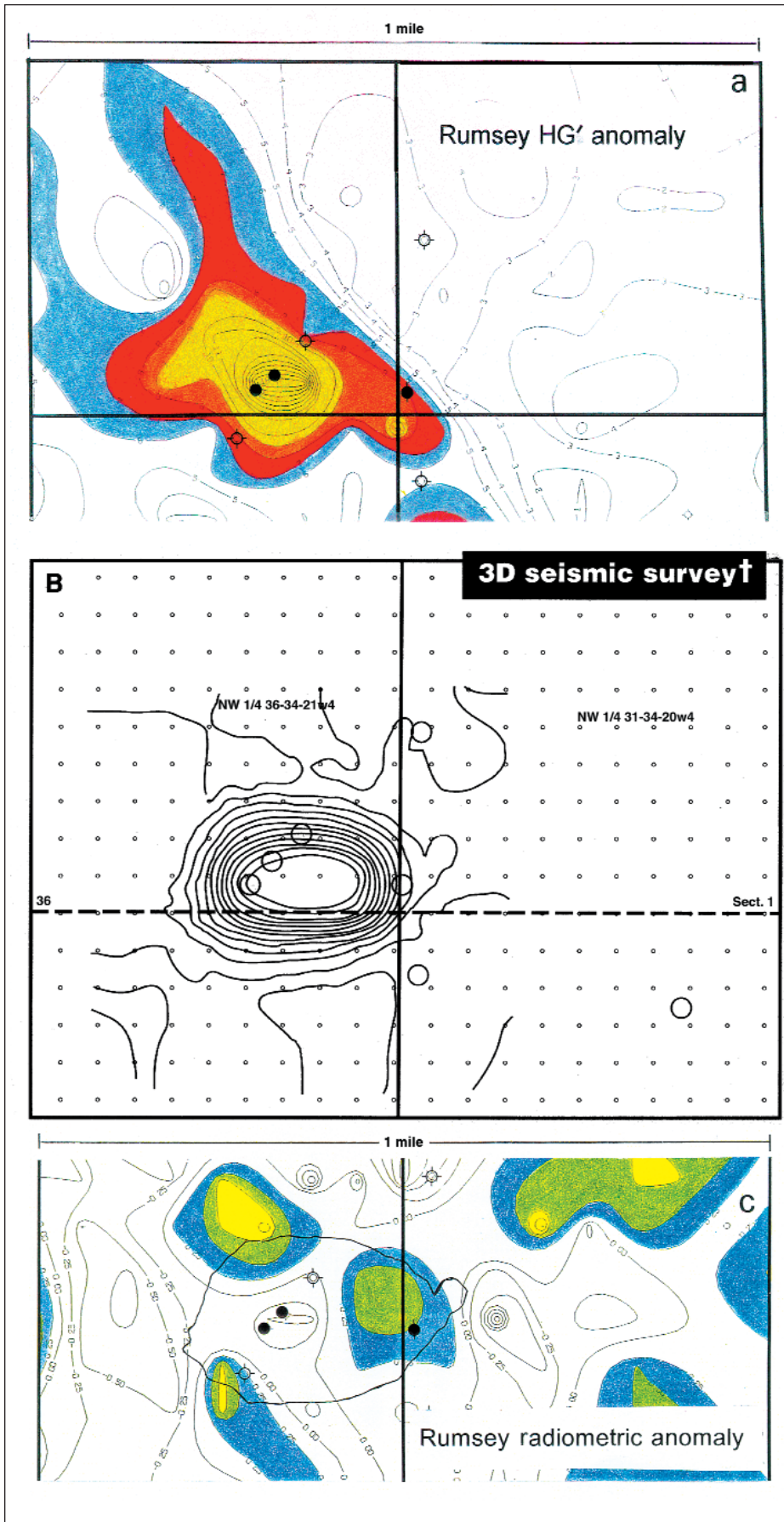


FIGURE 11. (a) HG' anomaly map of the Rumsey pinnacle reef, Alberta. HG' contour values (proportional to nT/m^2) greater than 4 are colored. After LeSchack (1997), courtesy of *Oil & Gas Journal*. (b) The Gulf Canada Resources Ltd. 3-D seismic survey. Contours are in meters below sea level. The base of the pinnacle is at -1020 m and the top is at -920 m. The top of the Cooking Lake platform starts at -1030 m. The contour interval is 10 m. (c) A DRAD anomaly map showing typical halo anomalies around the Rumsey reef. The contour interval is 0.25 s (i.e., 0.25 standard deviations about the mean). The base of the reef, as determined from 11b, is outlined. Anomalies to the east are halo anomalies on the western flank of the Big Valley reef field shown in Figure 9.

Case History 5: Nisku (Upper Devonian) Biostrome

Case histories 5 and 6 are both based on proprietary surveys that we conducted at two survey locations in central Alberta. The oil company that commissioned these surveys allowed us to use them only for the statistical purposes outlined in this paper. Hence, we are not at liberty to discuss details of the geology and geographic locations for these two case histories.

The main value of case histories 5 and 6 is in providing a large number of wells (105) with known hydrocarbon production data in areas of Nisku Formation (Upper Devonian) and Cretaceous production. We used the HG' values associated with the first 92 wells in the case-history 5 and 6 survey areas as a "learning set." By statistically analyzing HRGM data associated with different classes of well (i.e., 15 Nisku producers, 55 Cretaceous producers, and 22 D&A wells), we calculated HG' threshold values for different classes of wells. These values allowed us to "postdict" the producers and dry holes and, more important, to *predict where* hydrocarbons will be encountered by future drilling in these and adjacent areas. Subsequent HRGM and production data continue to support the validity of these HG' threshold values, not only in the case-history 5 and 6 survey areas but elsewhere in the Alberta Basin.

We emphasize that none of the 105 wells in these two case histories was drilled on the basis of our HRGM/radiometric surveys, which were conducted after 90% of the wells had already been drilled. Moreover, our surveys were never made available to the drillers of the 10% of wells that were drilled after our surveys were complete. Thus, all well locations were chosen on the basis of seismic or other geologic data, totally independently of magnetic methods.

The magnetic HG' anomaly map (Figure 12) for case history 5 covers a 19-section (4.9×10^3 -ha) area in Alberta. The entire map area is overlain by Cretaceous clastics, which include several producing horizons. The southern part of this map area includes a Nisku biostrome that is a prolific producer. The Nisku biostrome play was defined by a 3-D seismic survey that was not revealed to the authors.

Prior to our magnetic survey, 37 wells had been drilled in the case-history 5 map area at the locations shown in Figure 12. Based on the known production (or lack thereof) from these wells, we calculated an HG' threshold value of 1.1 for use in predicting whether a well in this area would produce hydrocarbons from Nisku reservoirs. Computational details and the significance of this Nisku threshold value are explained more fully in the "Discussion" section. In Figure 12, the $HG' = 1$ contour is the minimum contour level shown; wells located inside this contour ($HG' > 1$) would be expected to produce hydrocarbons from Nisku reservoirs, and wells out-

side this contour ($HG' < 1$) would be expected to be dry. Prediction statistics for case history 5 (Table 1 and Figure 12) demonstrate the value of HG' maps for predicting both the producers and the dry holes in this area.

Comparison of the HG' anomaly locations with the seismically defined well locations for this case history (Figure 12) reveals that our HG' map could have been used to target these wells nearly as effectively as the 3-D seismic survey. However, the total cost for our HRGM survey of this 19-section study area was only about 20% of the cost of the 3-D seismic survey.

Case History 6: Cretaceous Clastic Reservoirs

Case history 6 is essentially an after-drilling case history, because all but one well had already been drilled when we conducted our HRGM survey. The magnetic HG' anomaly map (Figure 13) for case history 6 covers a 20-section (5.2×10^3 -ha) area in Alberta. This area contains oil and gas fields producing from shallow reservoirs in Cretaceous clastics, including sandy units in the Mannville Group (Ellerslie Formation and Glauconitic Sandstone), Colorado Group (Viking Formation), and Belly River Formation. In most wells in this area, only Cretaceous horizons were tested.

Prior to our magnetic survey, 58 wells had been drilled in the case-history 6 mapped area, at the locations shown in Figure 13. Based on the known production (or lack thereof) from these wells, we calculated an HG' threshold value of 0.5 for use in predicting whether a well in this area would produce hydrocarbons from Cretaceous reservoirs. In Figure 13, the $HG' = 0.5$ contour is the minimum contour level shown; wells located inside this contour ($HG' > 0.5$) would be expected to produce hydrocarbons from Cretaceous reservoirs, and wells outside this contour ($HG' < 0.5$) would be expected to be dry. As with case history 5, prediction statistics for case history 6 (Table 1 and Figure 13) demonstrate the value of HG' maps for predicting both the producers and the dry holes in this area.

In summary, case histories 5 and 6 show how HRGM surveys can be calibrated against well production data to yield HG' threshold values that can be used to predict exploration success. Such predictions, of course, relate only to encountering hydrocarbons upon drilling, not to whether any given well will be economically successful. Note that if the HG' threshold is set high, this minimizes the chance of false positives but leaves some good prospects undrilled. In contrast, if the HG' threshold is set low, this minimizes the chance of false negatives but increases the risk of dry holes. In either case, setting thresholds derived from HRGM surveys allows us to rank and drill prospects in the order of decreasing probability of encountering hydrocarbons.

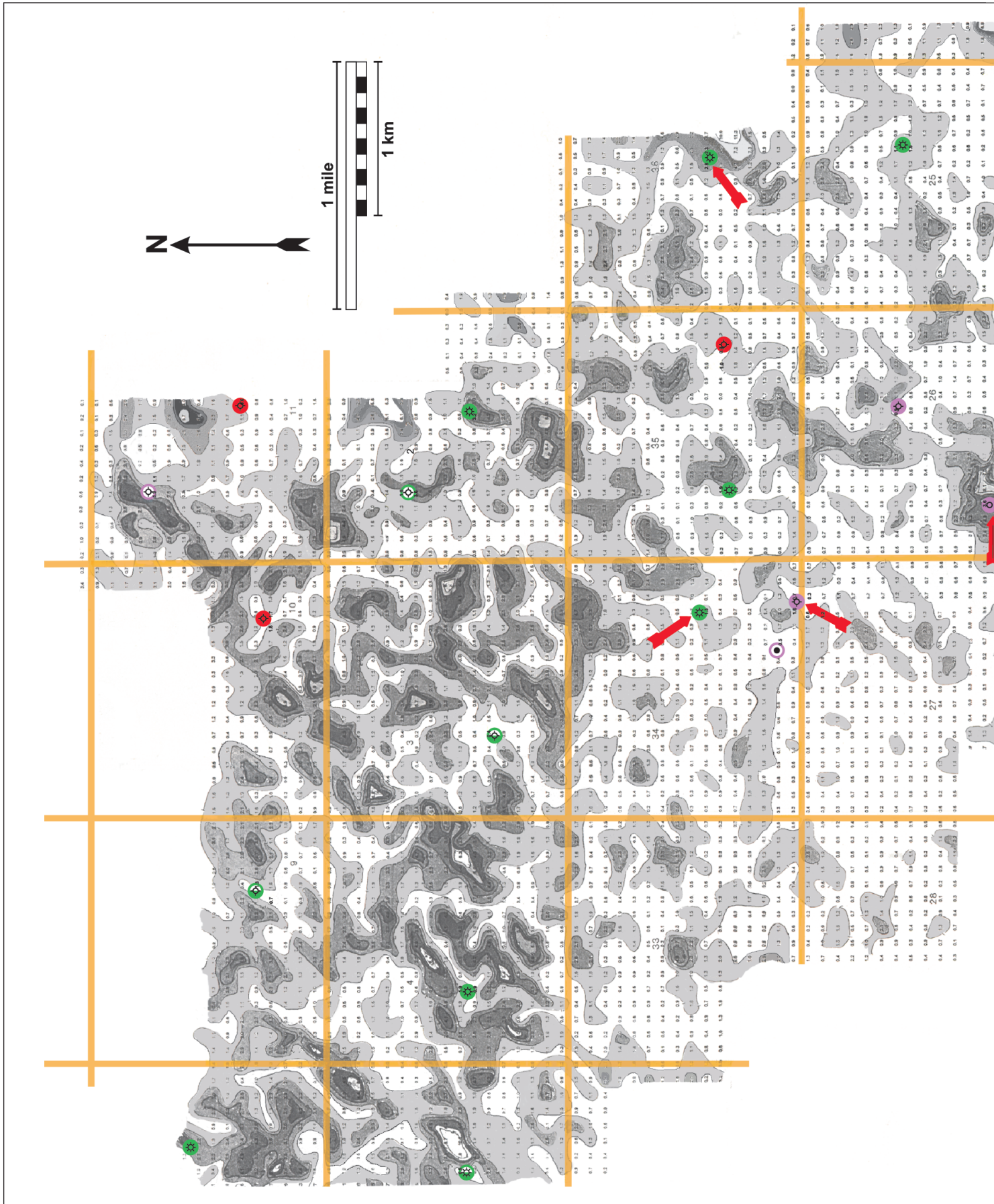
TABLE 1. Prediction statistics for case histories 4, 5, and 6.

Reservoir HG' threshold*	Case history 5				Case history 6				Case histories 4, 5, 6 combined†			
	Wells drilled before survey		Wells drilled after survey		Wells drilled before survey		Wells drilled after survey		Wells drilled before survey		Wells drilled after survey	
	Producers	D&A	Producers	D&A	Producers	D&A	Producers	D&A	Producers	D&A	Producers	D&A
Cretaceous HG' threshold = 0.5												
Predicted	9	0	4	0	33	2	1	0	42	2	5	0
Not predicted	0	1	0	0	2	2	0	0	2	3	0	0
Too close to call‡	2	2	0	0	9	2	0	0	11	4	0	0
Predicted Cret. producers	10/11 = 91%		4/4 = 100%		37.5/44 = 85%		1/1 = 100%		47.5/55 = 86%		5/5 = 100%	
Predicted Cret. D&A	1/3 = 33%		N/A		3/6 = 50%		N/A		4/9 = 44%		N/A	
Devonian – Nisku HG' threshold = 1.1												
Predicted	13	1	3	2	0	2	0	0	13	3	3	2
Not predicted	1	1	0	0	0	0	0	0	1	1	0	0
Too close to call‡	2	1	0	0	0	0	0	0	2	1	0	0
Predicted Nisku producers	14/16 = 88%		3/3 = 100%		N/A		N/A		14/16 = 88%		3/3 = 100%	
Predicted Nisku D&A	1.5/3 = 50%		2/2 = 100%		2/2 = 100%		N/A		3.5/5 = 70%		2/2 = 100%	
Devonian – Leduc HG' threshold = 6.9												
Predicted	0	4	0	0	0	6	0	0	0	10	4	0
Not predicted	0	0	0	0	0	0	0	0	0	0	1	0
Too close to call‡	0	0	0	0	0	0	0	0	0	0	0	0
Predicted Leduc producers	N/A		N/A		N/A		N/A		N/A		4/5 = 80%	
Predicted Leduc D&A	4/4 = 100%		N/A		6/6 = 100%		N/A		10/10 = 100%		N/A	

* HG' threshold values used for predictions are based on the geometric mean divided by geometric standard deviation values listed in Table 2.

† Includes data from case histories 5 and 6, as well as 5 Leduc producers from case history 4 and vicinity.

‡ Wells straddling the threshold contour values (Figures 12 and 13) were considered “too close to call” in making predictions; these wells were given half weight in calculating the prediction success (%) values.



Legend and Prediction Statistics for Case History 5

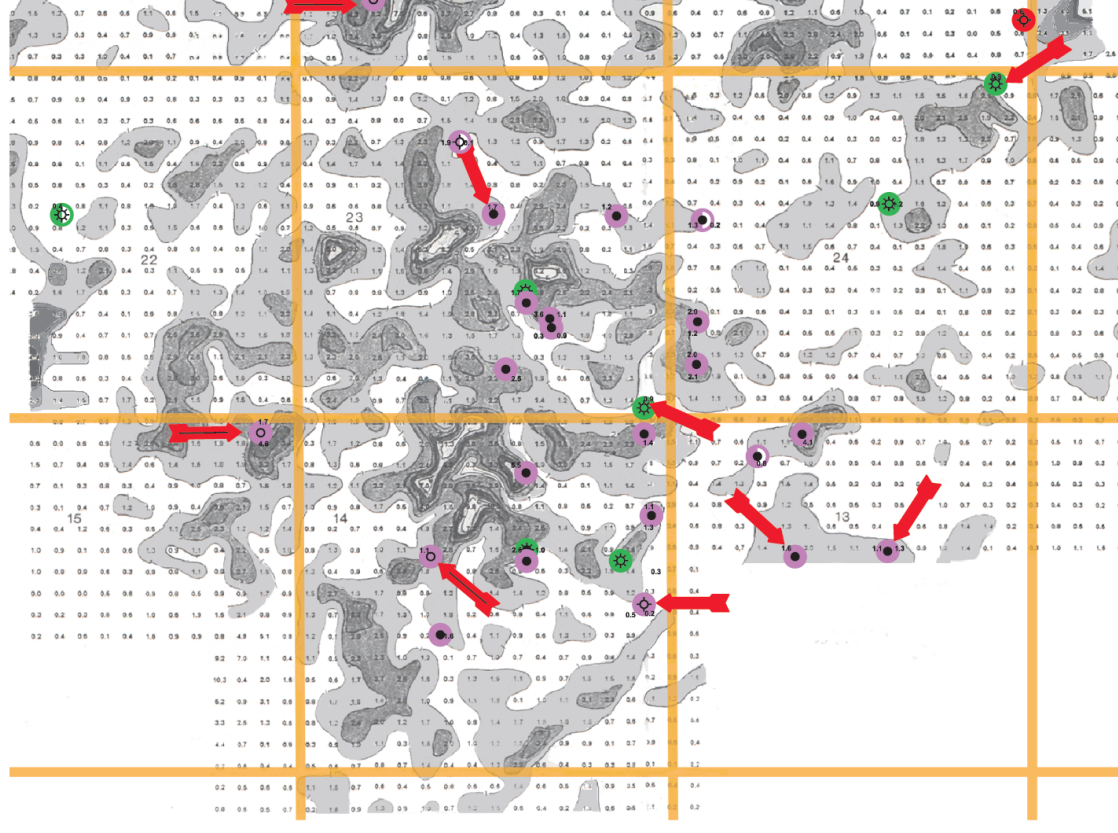
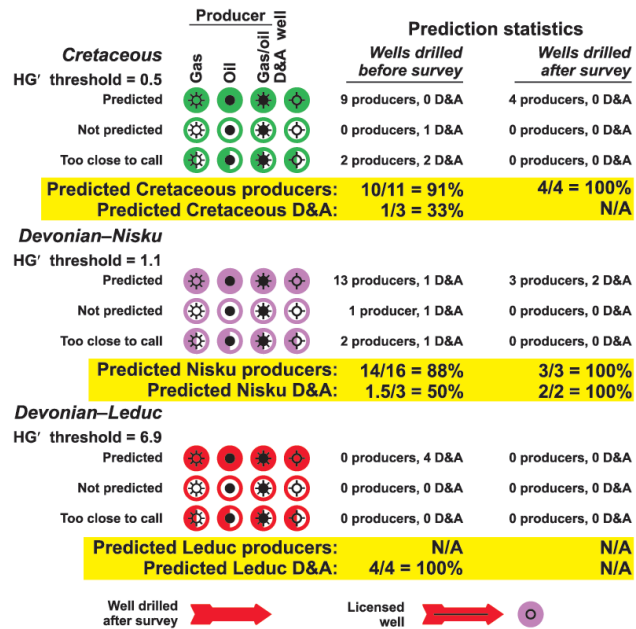


FIGURE 12. Magnetic HG' anomaly map of case history 5, a 19-section (4.9×10^3 -ha) area in Alberta. The HG' map was used to predict success or failure for 37 wells drilled prior to our survey, 9 wells drilled after our survey, and 3 wells planned to be drilled. Prediction statistics are shown in the map legend and in Table 1. Probability density functions (Figure 14 and Table 2) indicate that Nisku anomalies will likely have an HG' value >1 (i.e., the geometric mean divided by the geometric standard deviation), the minimum contour level shown and colored light gray. Other contours are at HG' = 2, 3, 4, 5, 6, 7.

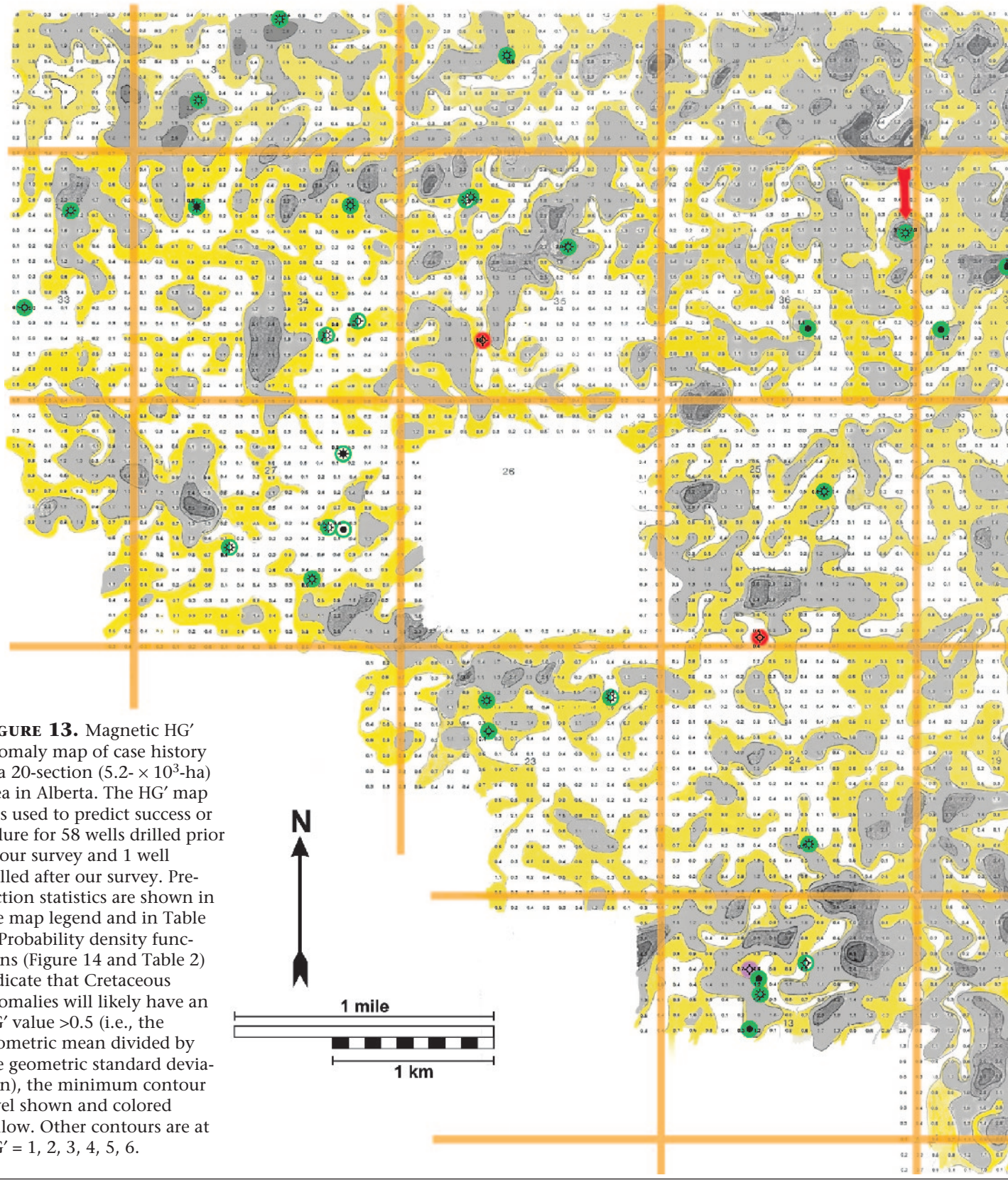
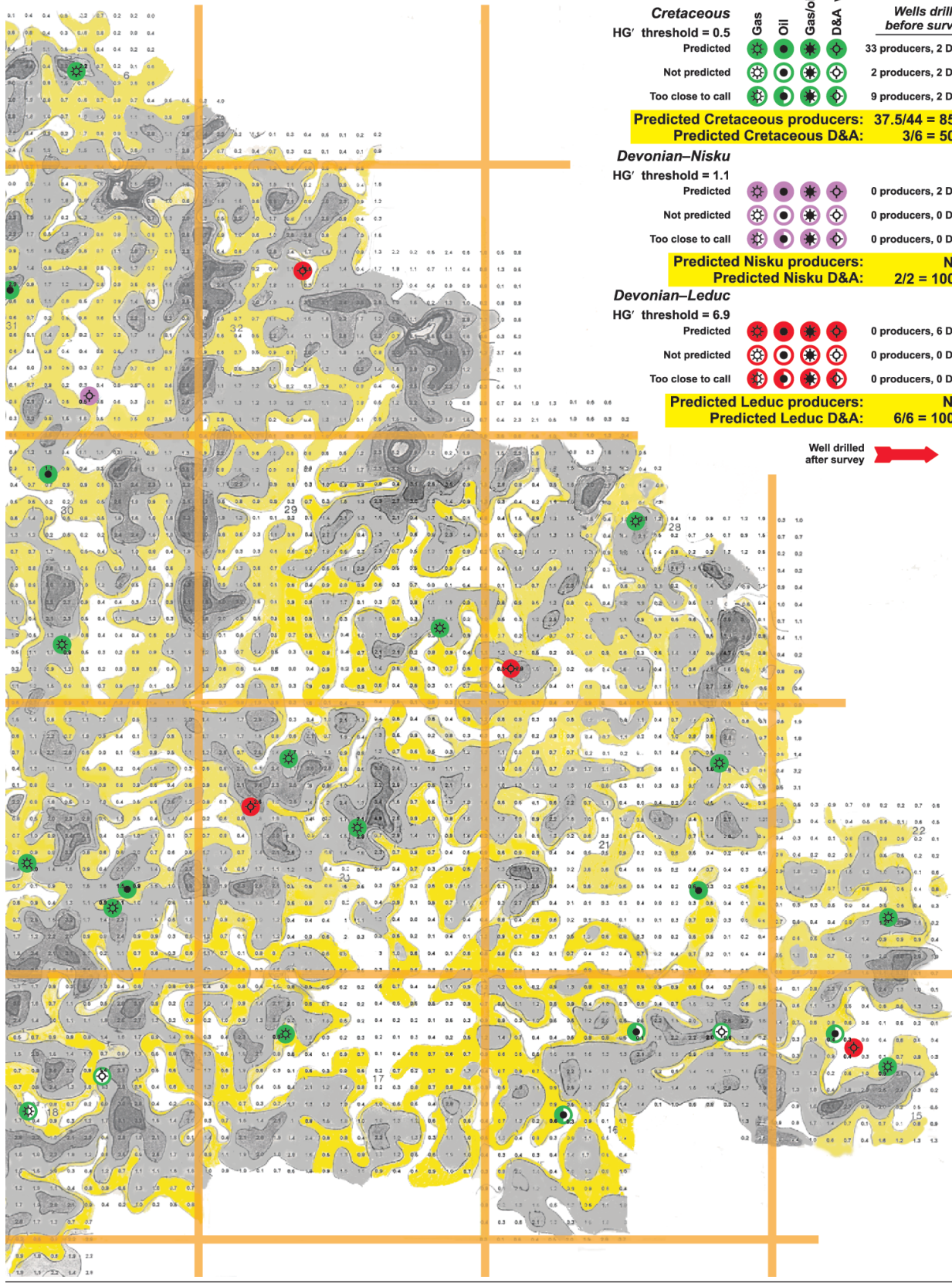


FIGURE 13. Magnetic HG' anomaly map of case history 6, a 20-section (5.2×10^3 -ha) area in Alberta. The HG' map was used to predict success or failure for 58 wells drilled prior to our survey and 1 well drilled after our survey. Prediction statistics are shown in the map legend and in Table 1. Probability density functions (Figure 14 and Table 2) indicate that Cretaceous anomalies will likely have an HG' value >0.5 (i.e., the geometric mean divided by the geometric standard deviation), the minimum contour level shown and colored yellow. Other contours are at $HG' = 1, 2, 3, 4, 5, 6$.

Legend and Prediction Statistics for Case History 6



	Producer well				Prediction statistics	
	Gas	Oil	Gas/oil	D&A	Wells drilled before survey	Wells drilled after survey
Cretaceous						
HG' threshold = 0.5						
Predicted					33 producers, 2 D&A	1 producer, 0 D&A
Not predicted					2 producers, 2 D&A	0 producers, 0 D&A
Too close to call					9 producers, 2 D&A	0 producers, 0 D&A
Predicted Cretaceous producers:					37.5/44 = 85%	1/1 = 100%
Predicted Cretaceous D&A:					3/6 = 50%	N/A
Devonian-Nisku						
HG' threshold = 1.1						
Predicted					0 producers, 2 D&A	0 producers, 0 D&A
Not predicted					0 producers, 0 D&A	0 producers, 0 D&A
Too close to call					0 producers, 0 D&A	0 producers, 0 D&A
Predicted Nisku producers:					N/A	N/A
Predicted Nisku D&A:					2/2 = 100%	N/A
Devonian-Leduc						
HG' threshold = 6.9						
Predicted					0 producers, 6 D&A	0 producers, 0 D&A
Not predicted					0 producers, 0 D&A	0 producers, 0 D&A
Too close to call					0 producers, 0 D&A	0 producers, 0 D&A
Predicted Leduc producers:					N/A	N/A
Predicted Leduc D&A:					6/6 = 100%	N/A

Well drilled after survey

DISCUSSION

The six case histories provide a large database of high-resolution, ground-based magnetic and radiometric data from above both producing reservoirs and dry holes over a wide region. Author LeSchack acquired these magnetic and radiometric data from Western Canada during the past 10 years. Working independently, author Van Alstine has 25 years of experience conducting paleomagnetic studies on surface outcrops and subsurface cores from many of these same reservoir rocks in Western Canada. Thus, we can now begin to synthesize these disparate databases into a coherent pattern with important implications for *direct detection of hydrocarbon reservoirs* by magnetic and radiometric methods.

In this section, we first discuss indications that in Western Canada, the intensity of HRGM anomalies appears to correlate positively with reservoir pressure. Next, we discuss the diagnostic value of HRGM anomaly intensities and directions for identifying the microseeping reservoir formation. We then discuss how depth constraints, paleomagnetic constraints, hydrocarbon generation/migration constraints, and regional fracture/pore-pressure constraints all converge on the early Tertiary as the most important time for the initiation of microseepage-related dipolar HRGM anomalies in Western Canada. We incorporate these constraints into a model for sequential development of HRGM anomalies over the Devonian and Cretaceous reservoirs of the Alberta Basin. This is followed by a postmortem for three unsuccessful wells that were drilled after we had completed our survey but before we understood the diagnostic value of residual magnetic anomaly directions. We then compare a ground-based HRGM survey with an airborne HRAM survey over the same area to demonstrate the valuable synergy between ground-based and aeromagnetic methods when applied to an exploration program. Finally, we discuss the implications of being able to detect distinctive magnetic signatures over microseeping reservoirs for hydrocarbon exploration throughout the world.

Apparent Correlation between HRGM Anomaly Intensity and Reservoir Pressure

An important clue to the origin and implications of magnetic/radiometric anomalies above microseeping hydrocarbon reservoirs is provided from the three case histories in Manitoba. These case histories not only yielded three new field discoveries using only magnetic and/or radiometric surveys for locating the discovery wells but also helped us develop a technique for associating HRGM anomalies with the specific reservoirs that caused them.

In the Waskada field (case history 3), where lower Amaranth reservoirs are stacked vertically above Mission Canyon reservoirs, magnetic HRGM anomalies appear to be *inversely* spatially correlated with radiometric anomalies. This was an unexpected result, because in our other survey areas, the magnetic and radiometric anomalies generally are *positively* correlated (i.e., occur at roughly the same locations).

To explain case history 3, we hypothesized that the reservoir pressure may control the intensity of an HRGM anomaly. We formulated this hypothesis based on our observation at the Waskada field that strong HRGM anomalies occur over Mississippian reservoirs with a strong *natural* water drive, indicating high reservoir pressure. In contrast, essentially no HRGM anomalies occur over lower Amaranth reservoirs, which have such low pressures that they require *artificial* pressure maintenance through water and gas injection to produce (Barchyn, 1984). Presumably, the zone of anhydritization (Figure 8) along the sub-Mesozoic unconformity acts as an effective seal between the high-pressure Mississippian reservoirs and the low-pressure lower Amaranth reservoirs. Vertical migration of colloid-size hydrocarbon gas bubbles is the proposed mechanism for instigating the diagenetic changes measured in the HRGM and radiometric surveys. Apparently, pressure in the Mississippian reservoirs below the unconformity was high enough to cause HRGM anomalies above microseeping Mississippian reservoirs. In contrast, pressure in the lower Amaranth reservoirs above the unconformity has probably always been low, so there may never have been enough microseepage from lower Amaranth reservoirs to cause discernible HRGM anomalies. However, there apparently has been enough microseepage from lower Amaranth reservoirs to alter the potassium and uranium ratios at the surface, as measured by the radiometric survey.

Although case history 3, in the Williston Basin, provided our first indication that magnetic HRGM anomaly intensity may ultimately be controlled by reservoir pressure, this was further confirmed by case histories 4, 5, and 6, in the Alberta Basin. The strongest HRGM anomalies in the Alberta Basin occur over deep, productive reservoirs in Leduc pinnacle reefs. These reservoirs have the highest inferred pressure, because Leduc producers commonly flow spontaneously. Weaker HRGM anomalies in the Alberta Basin occur above shallower, less-productive reservoirs in Cretaceous blanket/channel sands. These have lower inferred pressure, because Cretaceous wells commonly need to be pumped to produce oil. The weakest HRGM anomalies in the Alberta Basin occur over nonproductive areas associated with D&A wells. Presumably, there was never enough hydrocarbon microseepage at D&A well locations to produce detectable magnetically enhanced zones.

Diagnostic Value of HRGM Anomaly Intensity for Identifying the Microseeping Hydrocarbon Reservoir Formation

For a more rigorous test of the hypothesis that reservoir pressure controls the intensity of HRGM anomalies, we now statistically analyze the distribution of HG' values from our three case-history areas in central Alberta. Although in this analysis we used HG' values (proportional to nT/m²) as a proxy for HRGM anomaly intensity, we probably would have achieved the same result by using nanotesla values of the residual magnetic anomalies (e.g., the highest HG' value, at the Rumsey reef, also exhibits the highest residual anomaly intensity). Statistically analyzing distributions of HG' values is easier, because each well can be associated with only *one HG' value*, whereas each well is generally associated with *two nanotesla values* (one positive and one negative value) for each of the *dipolar* residual anomalies we generally observe in Western Canada.

In the following analysis, we pooled HG' values from our three case histories in Alberta. We compared HG' values with well production data from a total of 97 wells over a 50-section (1.3- × 10⁴-ha) survey area in central Alberta where the geology is relatively similar. The first 97 wells in these areas can be subdivided into four classes: 55 wells produce from Cretaceous reservoirs, 15 wells produce from Nisku (Devonian) reservoirs, 5 wells produce (or exhibit significant shows) from Leduc (Devonian) reservoirs, and 22 wells were D&A. HG' values associated with each well were tabulated and plotted on histograms (Figure 14). These first 97 wells had all been drilled before we conducted our HRGM survey. An additional 10 wells were drilled in these survey areas after our HRGM surveys, but they were excluded from the statistical analysis. We also excluded data from Mississippian reservoirs in Figure 14 because all of our Mississippian data are from the Williston Basin, where the geology and tectonic history are different. However, we note here that our five Mississippian (Alida) HG' values from the Williston Basin plot between the HG' values from the Leduc and Nisku reservoirs of the Alberta Basin.

A histogram of HG' values representing the 97-well data set exhibits a much better fit to a lognormal probability distribution (Figure 14b) than to a normal probability distribution (Figure 14a). In a lognormal distribution, it is the *logarithms* of the values, rather than the values themselves, that conform to the familiar bell curve. We only recently recognized the lognormal pattern, after we had enough data to distinguish between normal and lognormal distributions. In fact, a lognormal distribution of magnetic anomaly (HRGM and HRAM) values is more to be expected, because it is widely known in paleomagnetism that distributions of magnetic-intensity and mag-

netic-susceptibility values both follow lognormal distributions (Tarling, 1983; Harding et al., 1988). As discussed by Tarling (1983, p. 109):

Both magnetic intensity and susceptibility depend ultimately on the size and number of magnetic grains and are thus influenced by the grain-size distribution within a rock. Such distributions can be complex as more than one generation of grains may be present. . . . However, virtually all such natural distributions have a log normal (geometric) distribution in which a normal histogram of their frequency is skewed with a long "tail" of high values, but if the frequency of the logarithmic values is graphed, then these distributions have a symmetrical Gaussian distribution and their mean and standard deviations can be calculated using the log values as the variable. Both low-field susceptibility and intensity of remanence of igneous and sedimentary rocks show this distribution function. Where more than one distribution is present, the total distribution is still dominantly geometric.

Another reason why lognormal (rather than normal) distributions of magnetic anomalies might be expected is that free-gas measurements (i.e., measurements of methane through the butanes, which are thought to produce the magnetic anomalies we are measuring) also appear to be lognormally distributed (H. von der Dick, personal communication, 1999).

Because we initially performed prediction statistics assuming a normal rather than a lognormal distribution of HG' values, we present both normal and lognormal statistics in Figure 14 and Table 2. However, the clear demonstration that the HG' values are distributed according to the *lognormal* probability density functions (Figure 14, right side) underscores that the differences in HG' values and the distinctly different magnetic anomaly directions (discussed below) ultimately have the same cause—differences in magnetic mineralogy and grain size in the magnetically enhanced zones above the microseeping reservoirs. In contrast, if the HG' values were distributed according to the *normal* probability density functions (Figure 14, left side), the distribution of HG' values could be more easily dismissed as reflecting experimental errors or artifacts of the statistical processing.

Perhaps the most important trend revealed in Figure 14b and 14d is that the highest HG' values, which are associated with the most prolific (Leduc) wells, all lie near the right tip of the tail of the lognormal distribution representing all 97 wells. Besides their having enormous predictive power in magnetic exploration for Leduc pinnacle reefs, we speculate that the statistically distinct population of high Leduc HG' values may have a geo-

logic explanation: These higher HG' values may reflect focusing of hydrocarbon microseepage above the more nearly point-source pinnacle reefs, rather than the more diffuse hydrocarbon microseepage above reservoirs in more areally extensive carbonate (Nisku biostrome) or Cretaceous blanket and channel sands. Figure 14b and 14d suggests that a better statistical model of the total 97-well HG' data set comprises one lognormal distribution of HG' values representing the 92 non-Leduc wells (Nisku producers, Cretaceous producers, and D&A wells) and a second lognormal distribution of HG' values representing the five Leduc producers.

Just as Tarling (1983) mentions that multiple lognormal distributions of magnetic data may be hidden within a single, parent lognormal distribution, we illustrate in Figure 14f and 14h how even the 92 non-Leduc HG' values can be subdivided into three separate lognormal distributions: Nisku producers, Cretaceous producers, and D&A wells. Thus, the combined distribution of 97 HG' values included in Figure 14b probably reflects superposition of four distinctly different lognormal distributions, one for each class of well. We emphasize that the class subdivisions illustrated by different colors in Figure 14 were determined solely on the basis of *known hydrocarbon production* from the nearest associated well, and not by where any given HG' value falls relative to the overall probability distribution.

Table 2 lists the statistical parameters derived from each class of well and used to define the probability density functions illustrated in Figure 14. Although both nor-

mal and lognormal statistics are listed, we consider only the lognormal statistics to be valid because the overall distribution of 92 HG' values, as well as subsets of the four classes, exhibits a much better fit to lognormal probability density functions (Figure 14, right side) than to normal probability density functions (Figure 14, left side).

For lognormal distributions, the mean and standard deviation are calculated using the logarithms of the HG' values. The peak of the bell curve of the log values is the "logarithmic mean" (\bar{x}), and the antilog of the logarithmic mean is the "geometric mean" (\bar{x}^*). The range of variation about the mean is reported either as the "logarithmic standard deviation" (s) or as the "geometric standard deviation" (s^*). Just as in a normal distribution, 68.3% of the log values lie between $\bar{x} \pm s$. After making the antilog transformation, 68.3% of the original data values lie between \bar{x}^*/s^* and $\bar{x}^* \times s^*$ (Limpert et al., 2001). Note that this "one-sigma" range is asymmetric about the geometric mean because of the antilog transformation.

In case histories 5 and 6, we used the probability density functions shown in Figure 14 to derive HG' threshold values for predicting the likelihood of encountering hydrocarbons. In the Nisku biostrome area (case history 5), a value of 1.1 was chosen as the threshold for a possible Nisku reservoir (i.e., the Nisku geometric mean of 1.8 divided by the Nisku geometric standard deviation of 1.6). In the Cretaceous area (case history 6), a value of 0.5 was chosen as the threshold for a possible Cretaceous reservoir (i.e., the Cretaceous geometric mean of 1.0 divided by the

FIGURE 14. The frequency of occurrence of 97 HG' values recorded in central Alberta near known producing and D&A wells. These 97 values can be segregated into four classes: 55 Cretaceous producers, 15 Nisku producers, 5 Leduc producers, and 22 dry and abandoned (D&A) wells. The highest HG' values are associated with the Leduc wells. The statistical parameters used in constructing these figures are listed in Table 2.

(a) All 97 undifferentiated HG' values plotted in normal HG' space. In this coordinate system, the HG' values (proportional to nT/m²) are plotted on a linear abscissa, and the histogram is overlain by a probability density curve (a bell curve) calculated for a normal probability distribution. Note the poor fit of the actual HG' values to the bell curve. Note also that the five highest HG' values (all associated with Leduc producers) are on or to the right of the tail of the bell curve.

(b) All 97 undifferentiated HG' values plotted in lognormal HG' space. In this coordinate system, the logarithms (logs) of the HG' values are plotted on a linear abscissa, and the histogram is overlain by a probability density curve calculated for a lognormal distribution. Note the much better fit of the logs of the actual HG' values to the curve. Note also that the five highest HG' values (all associated with Leduc producers) are on or to the right of the tail of the bell curve.

(c) All 97 HG' values plotted in normal HG' space, segregated into the four classes on a stacked-bar histogram. The histogram is overlain by a probability density curve calculated from all 92 non-Leduc HG' values, assuming normal probability density. Note the poor fit of the actual HG' values to the bell curve.

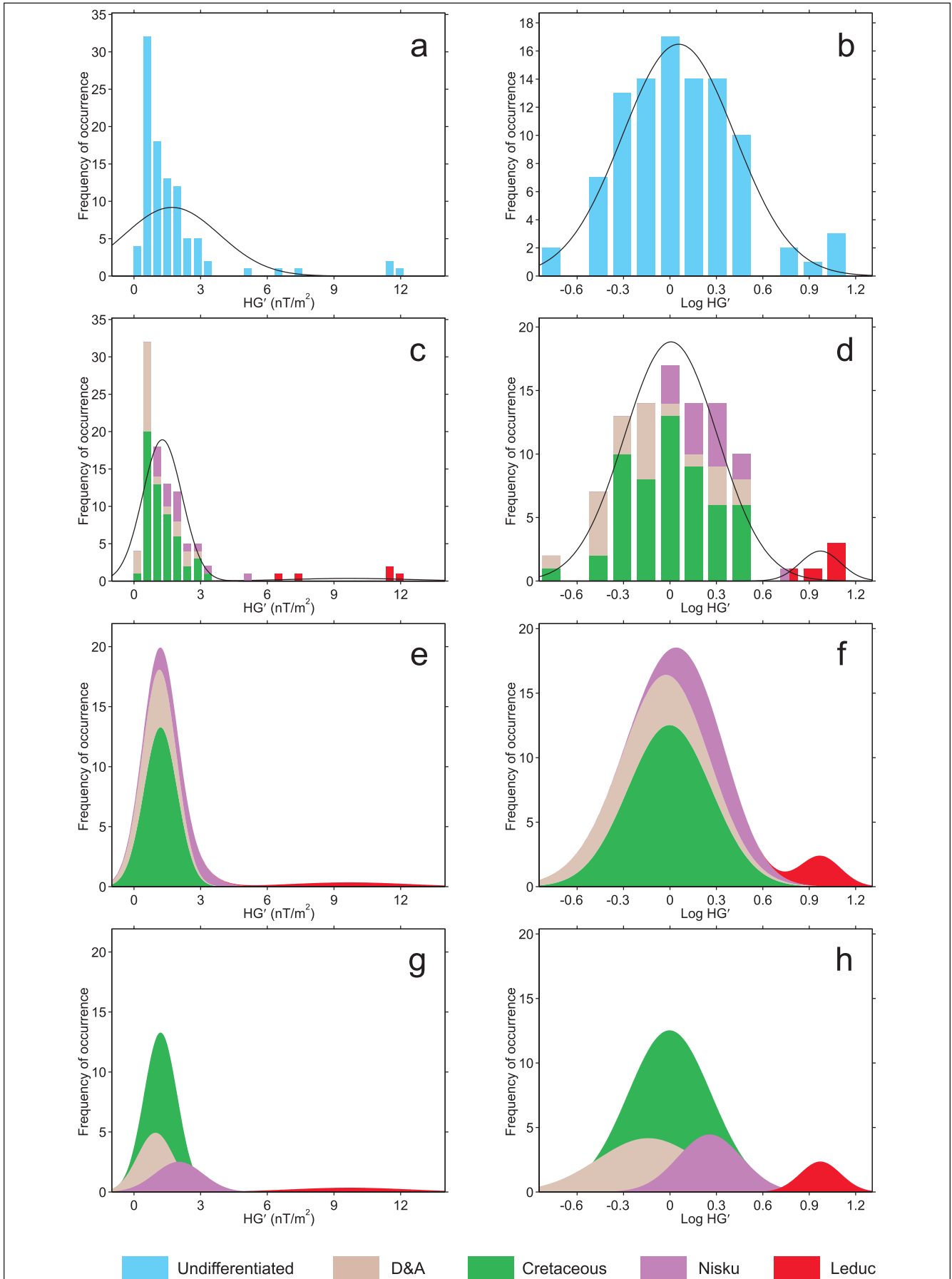
(d) All 97 HG' values plotted in lognormal HG' space, segregated into the four classes on a stacked-bar histogram. The histogram is overlain by a bell curve calculated from all 92 non-Leduc HG' values, assuming lognormal probability density. Note the much better fit of the logs of the 92 HG' values to the bell curve, and the indications that the five Leduc values are from a separate lognormal distribution.

(e) Stacked normal probability density curves in normal HG' space, derived from the four classes.

(f) Stacked lognormal probability density curves in lognormal HG' space, derived from the four classes.

(g) Unstacked normal probability density curves in normal HG' space, derived from the four classes.

(h) Unstacked lognormal probability density curves in lognormal HG' space, derived from the four classes. Each well class can be represented by a separate lognormal distribution of HG' values, which, when stacked together (14f), form the lognormal distribution of the combined data set.



Cretaceous geometric standard deviation of 1.9). In the combined areas for case histories 4, 5, and 6, a value of 6.9 was chosen as the threshold for a possible Leduc reservoir (i.e., the Leduc geometric mean of 9.4 divided by the Leduc geometric standard deviation of 1.3). We realize that these HG' threshold values are based on statistics from small data sets, especially for Leduc wells. However, we continue to find that these threshold values provide excellent predictive guides for hydrocarbon exploration in this part of the Alberta Basin.

In summary, the statistical correlations among HRGM anomaly intensity (as measured by HG' values), hydrocarbon reservoir formation, and production data further suggest that the HRGM anomaly intensity is ultimately being controlled by reservoir pressure or reservoir geometry. In the Alberta Basin, HG' values and inferred reservoir pressure appear to be monotonically related. The average HG' values range from 9.4 above prolific Leduc pinnacle reefs that flow spontaneously, to 1.8 above less-prolific Nisku biostrome reservoirs, to 1.0 above still-less-prolific Cretaceous clastic reservoirs, to 0.7 above the least-productive and D&A wells. This suggests that the HG' value may provide a useful parameter for estimating which microseeping reservoir has caused a specific HRGM anomaly and for determining where not to drill.

Diagnostic Value of HRGM Anomaly Directions for Identifying the Microseeping Hydrocarbon Reservoir Formation

The previous discussion focused on interpreting second-horizontal-derivative (HG') maps, which have the useful properties that (1) HG' contours conform most closely to the shapes of the microseeping reservoirs, and (2) HG' values have predictive power in helping to identify the microseeping reservoir causing a magnetic anomaly.

We now turn our attention to the equally important information contained in residual-magnetic-anomaly

maps, which are derived from the same kriged magnetic data used to generate the HG' maps. By "residual magnetic anomaly," we mean the total magnetization (remanent + induced) of the short-spatial-wavelength (shallow-depth) anomaly, after subtracting the long-spatial-wavelength, background magnetization that largely reflects the Precambrian basement.

When residual-magnetic-anomaly maps are created from the kriged total-field magnetic data, the HRGM anomalies in Western Canada generally appear to be *dipolar*, with positive and negative lobes of nearly equal intensity. From these dipolar residual anomalies, the total magnetization *direction* can be estimated using the method of Zietz and Andreasen (1967). A magnetization direction has an *azimuth* (= declination) measured on a horizontal plane and a *dip* (= inclination) measured on a vertical plane. By the method of Zietz and Andreasen (1967), the total magnetization azimuth can be estimated from the line connecting the maximum positive value to the minimum negative value of a dipolar anomaly. The total magnetization dip angle can be estimated from the ratio between the maximum and minimum anomaly values. In this study, we estimated dip angles by interpolating from Table 2 of Zietz and Andreasen (1967), who emphasized that these estimates are essentially independent of the size (areal extent and thickness) and remanent magnetization azimuth of the magnetic prism used in their model. In this study, we are equating the magnetically enhanced zones that are the source of the HRGM anomalies with the magnetic prisms used in the models of Zietz and Andreasen (1967).

Applying Zietz and Andreasen's (1967) method to our study area (where the present geomagnetic field inclination is the same +75° value used in their calculations) yields several important empirical relationships, as follows:

- When the dip (inclination) of the total magnetization direction is steeper than 75°, the residual magnetic anomalies are essentially unipolar (not dipolar),

TABLE 2. Probability distribution statistics for different classes of 97 HG' values from case histories 4, 5, and 6.

Class	Normal probability distribution					Lognormal probability distribution							
	N	Arith. mean	Arith. std. dev.(s)	Arith. mean + 1s	Arith. mean - 1s	Log mean	Log std. dev.(s)	Log mean + 1s	Log mean - 1s	Geom. mean	Geom. std. dev.(s*)	Geom. mean × s*	Geom. mean ÷ s*
All	97	1.70	2.10	3.80	-0.40	0.06	0.36	0.42	-0.31	1.14	2.31	2.63	0.49
All but Leduc	92	1.28	0.89	2.17	0.39	0.01	0.30	0.31	-0.29	1.02	2.00	2.03	0.51
Leduc	5	9.70	2.69	12.39	7.01	0.97	0.13	1.10	0.84	9.37	1.35	12.66	6.94
Nisku	15	2.02	1.08	3.10	0.94	0.26	0.21	0.46	0.05	1.81	1.61	2.90	1.12
Cretaceous	55	1.20	0.75	1.95	0.44	-0.00	0.27	0.27	-0.27	0.99	1.86	1.85	0.53
D&A	22	0.97	0.81	1.78	0.15	-0.14	0.33	0.19	-0.47	0.72	2.14	1.54	0.34

because the ratio between the maximum and minimum lobes is greater than 10, and hence the weaker lobe is too weak to detect (<1 nT in our study).

- When the dip of the total magnetization direction is 60°, the ratio of the maximum and minimum lobes is about 6, so the strongest anomalies would begin to appear to be dipolar.
- When the dip of the total magnetization direction is 30°, the ratio of the maximum and minimum lobes is about 2, so most anomalies would be dipolar.
- When the dip of the total magnetization direction is 0° (i.e., is horizontal), the ratio of the maximum and minimum lobes is about 1, so all anomalies would be dipolar.
- For dipolar residual anomalies, the maximum/minimum values are centered over the edges of the magnetically enhanced prism used in the models of Zietz and Andreasen (1967), implying that the reservoir that caused the anomaly is located halfway between the center of the positive and negative lobes.

Figure 15 illustrates how we estimate the azimuth of an HRGM anomaly, using the type example of a dipolar residual anomaly at the Rumsey reef (case history 4). In this paper, we employ azimuthal conventions used in paleomagnetism, such that all magnetic azimuths (i.e., paleomagnetic declinations) in the text and figures are measured clockwise-positive from *geographic* north (i.e., true north, or TN). At the Rumsey reef, connecting the maximum positive lobe (+11.2 nT) to the minimum negative lobe (-13.8 nT) of the anomaly yields an azimuth of 117°. This azimuth is nearly perpendicular to present magnetic north (MN), indicating that the residual anomaly has a major contribution from *remanent* magnetization, not merely *induced* magnetization (which would be along the +18° MN azimuth). At the Rumsey reef, the *dip* of the total magnetization direction can be estimated from the maximum/minimum ratio ($11.2/13.8 = 0.8$), from which we estimate a slightly upward-pointing dip of -5°.

We emphasize that it is the *combination* of dipolar residual anomalies and azimuths at a high angle to the present magnetic field that indicates a significant remanent contribution, not just dipolarity alone. This is demonstrated by results of Reynolds et al.'s (1990b) magnetic forward models at the Cement oil field in Oklahoma. Based on magnetic properties of pyrrhotite-bearing strata at depths of 200–500 m at the Cement field, Reynolds et al. (1990b) calculated that aeromagnetic anomalies (at 120-m flight altitude) with amplitudes as high as 7 nT are possible. In their forward models, the total magnetization reflects only induced magnetization, because they assumed that the remanent magnetization would self-cancel (by equal contributions from normal and reversed polarity). Self-cancellation of remanent magnetization is reasonable at the Cement field, based

on Elmore and Leach's (1990) observation of dual polarity (i.e., mixed normal and reversed polarity), Late Permian/Early Triassic chemical remagnetization directions in Rush Springs Formation red beds on the crest of the Cement anticline. Although Reynolds et al.'s (1990b) magnetic forward models at Cement reveal dipolar anomalies with nearly equal positive and negative lobes, the azimuths connecting the positive to negative lobes are within about 10° of being parallel to present magnetic north, as would be expected for a purely induced magnetization. In contrast, the azimuths of the dipolar HRGM anomalies we observe in Western Canada are significantly different from present magnetic north, indicating that the remanent magnetization is *not* self-canceling, as at Cement.

For hydrocarbon exploration in Western Canada, the importance of measuring the azimuths of the dipolar HRGM anomalies stems from LeSchack's (1997) observation, which continues to be supported by new data, that the anomaly's azimuth is apparently diagnostic of the microseeping reservoir formation. This is demonstrated in Figure 16, where the residual-anomaly azimuths for Leduc (Upper Devonian), Nisku (Upper Devonian), and Alida (Mississippian) producers were estimated, as discussed for the Rumsey reef. The anomalies were classified by the production (or significant show) of the nearest associated well. All five of the Leduc-associated anomalies exhibit essentially one azimuth (Figure 16a), all 15 of the Nisku anomalies exhibit another azimuth (Figure 16b), and all five of the Alida anomalies exhibit yet a third azimuth (Figure 16c). Most of these azimuths are different from azimuths associated with the numerous Cretaceous producers. In interpreting Figure 16, we emphasize that only the Figure 16c well locations were selected on the basis of our HRGM surveys; wells in Figures 16a and 16b had been drilled prior to our survey. We recognize that matching positive with negative lobes (and hence determining anomaly azimuths) can be subjective, especially where the reservoirs are stacked. However, the consistent HRGM anomaly azimuths from areas where all production is essentially from one formation (e.g., Figures 16b and 16c) suggests that our method of linking positive to negative lobes is valid.

As illustrated in Figure 17, plotting the HG' values together with the residual-anomaly directions reveals distinctive HRGM anomaly clusters that are diagnostic of the microseeping reservoir formation. Figure 17a reveals that HG' values decrease in the order Leduc > Alida > Nisku > Cretaceous. Figure 17b reveals that the residual anomaly dips/inclinations are typically shallow (between ±35°), and the residual anomaly azimuths/declinations (for all but some Cretaceous producers) are biased toward the eastern hemisphere.

What do the shallow-inclination, eastern-hemisphere magnetization directions we infer from the dipolar HRGM anomalies imply about magnetically enhanced

zones and hydrocarbon microseepage in Western Canada? To answer this question, we must combine knowledge concerning the probable depth of the magnetically enhanced zones, the stratigraphic column above the microseeping reservoirs, the hydrocarbon generation and migration history, the paleostress and present-day in-situ stress fields, and the behavior of the geomagnetic field over both geologically short (<2000-yr) and geologically long (100-m.y.) time scales.

Depth Constraints on the Age of HRGM Anomalies in Western Canada

Little is known about either the geologic age of enhanced magnetization above microseeping reservoirs or about the precise depths over which the phenomenon occurs. Foote (1992) reported that the authigenic magnetic minerals responsible for the magnetic anomalies are concentrated over the depth range of 60 to 600 m (200 to

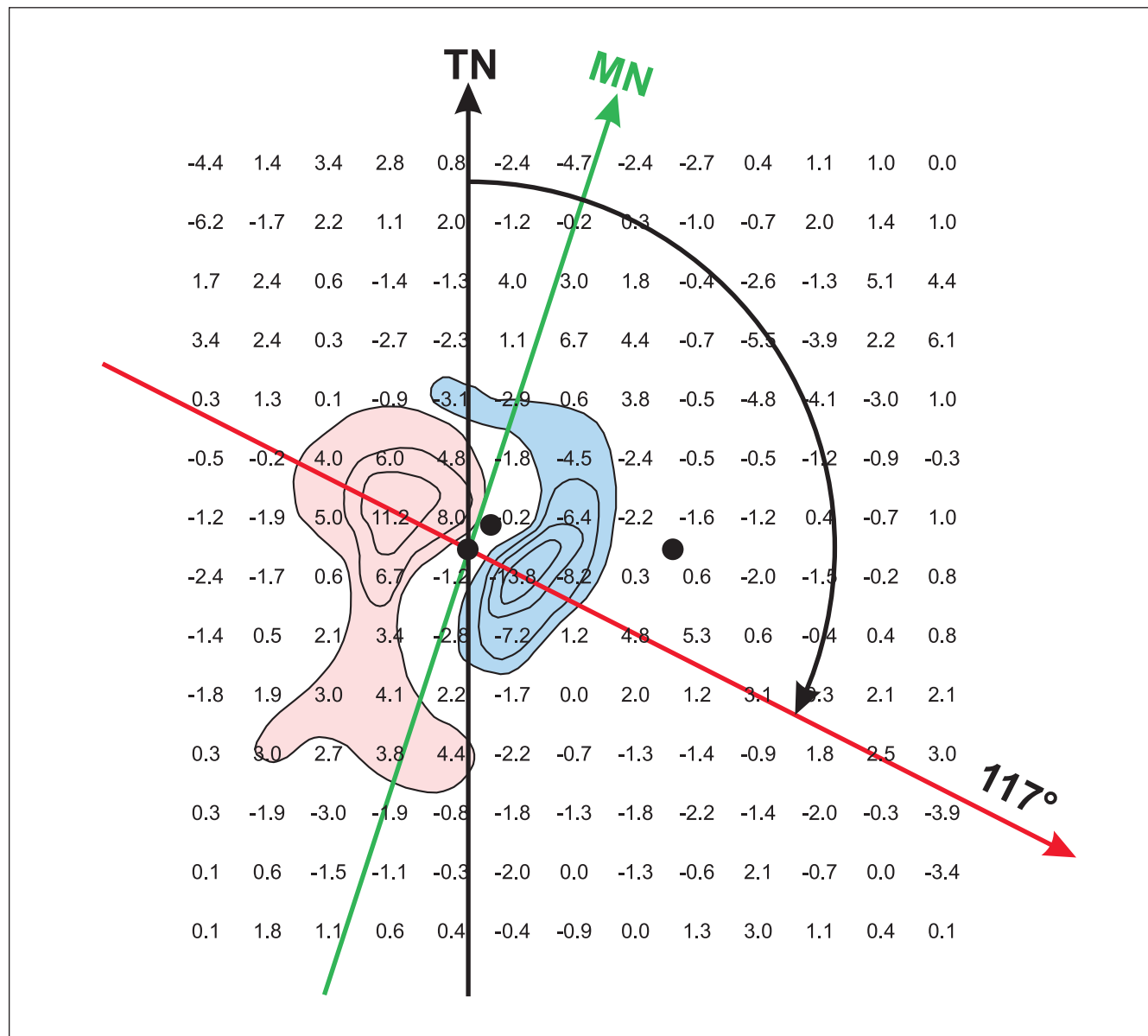


FIGURE 15. Illustration of how we compute the azimuth of a dipolar HRGM anomaly, using the type example at the Rumsey reef, Alberta. A vector (red arrow) is first drawn from the maximum positive value to the minimum negative value of the residual magnetic anomaly. The azimuth (= paleomagnetic declination) of this vector is then measured clockwise from true north (TN = 0°, black arrow). The Rumsey HRGM anomaly azimuth of 117° is nearly perpendicular to present magnetic north (MN = 18°, green arrow), indicating a significant contribution from remanent (rather than induced) magnetization. Of the three producing wells (also shown in Figure 11), the prolific Leduc producer (as much as 4000 BOPD for 3 yr) is the southwest well. Grid spacing is 100 m. Values are in nT. Pink areas = positive nT values; blue areas = negative nT values.

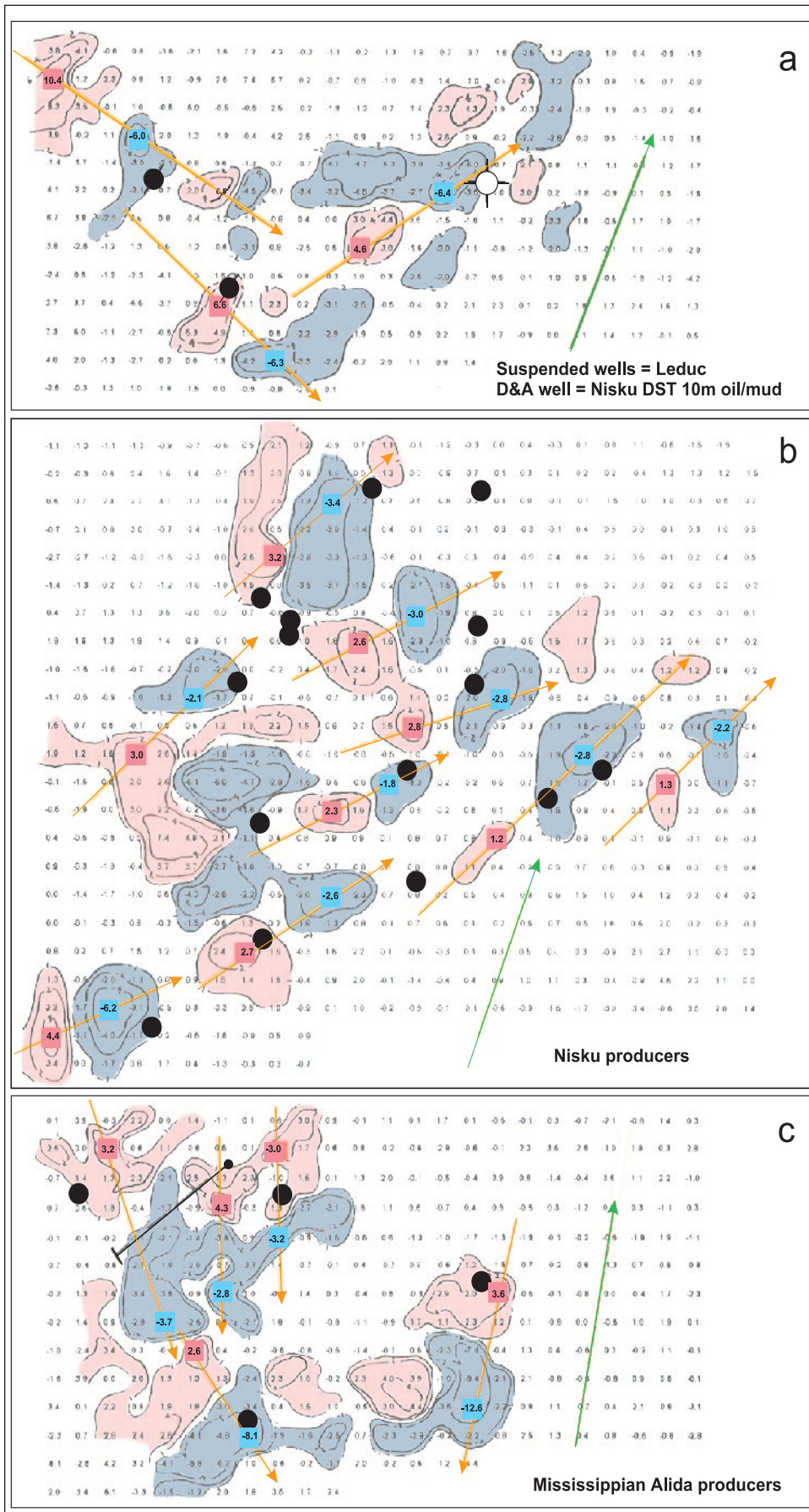


FIGURE 16. Examples of dipolar HRGM anomalies with distinctive azimuths (orange arrows) diagnostic of the micro-seeping reservoir formation. Green arrows point to magnetic north. Computed grid points are 100 m apart and are oriented with respect to true north. Values are in nT. Pink areas = positive nT values; blue areas = negative nT values. Each anomaly azimuth is derived from the vector (orange) connecting the maximum positive value (highlighted in pink) with the minimum negative value (highlighted in blue) of the anomaly. Arrows are drawn only for those anomalies where there is a nearby producing well to verify that the magnetic anomalies are related to hydrocarbon micro-seepage. (a) Two Leduc HRGM anomalies with east-southeast azimuths similar to the Leduc anomaly at the Rumsey reef (Figure 15) and one Nisku HRGM anomaly with an east-northeast azimuth similar to those at the Nisku biostrome field (16b). These anomalies are on the northwestern part of the Stettler reef (Figure 9). The three wells were drilled prior to our HRGM survey. (b) Nisku HRGM anomalies with east-northeast azimuths in the Nisku biostrome field at the south end of Figure 12 (case history 5). All 15 producers were drilled prior to our HRGM survey. (c) Five HRGM anomalies with south azimuths from an Alida (Mississippian) field in the Williston Basin (case history 1). The five wells, which were drilled after our survey, are the same wells in the northwest corner of Figure 3a. These Alida HRGM anomaly azimuths are similar to one another but clearly differ from Leduc and Nisku HRGM anomaly azimuths in the Alberta Basin. The Alida HRGM anomaly azimuths point nearly opposite to the present magnetic-field direction, indicating a major component of *reversed-polarity remanent* magnetization.

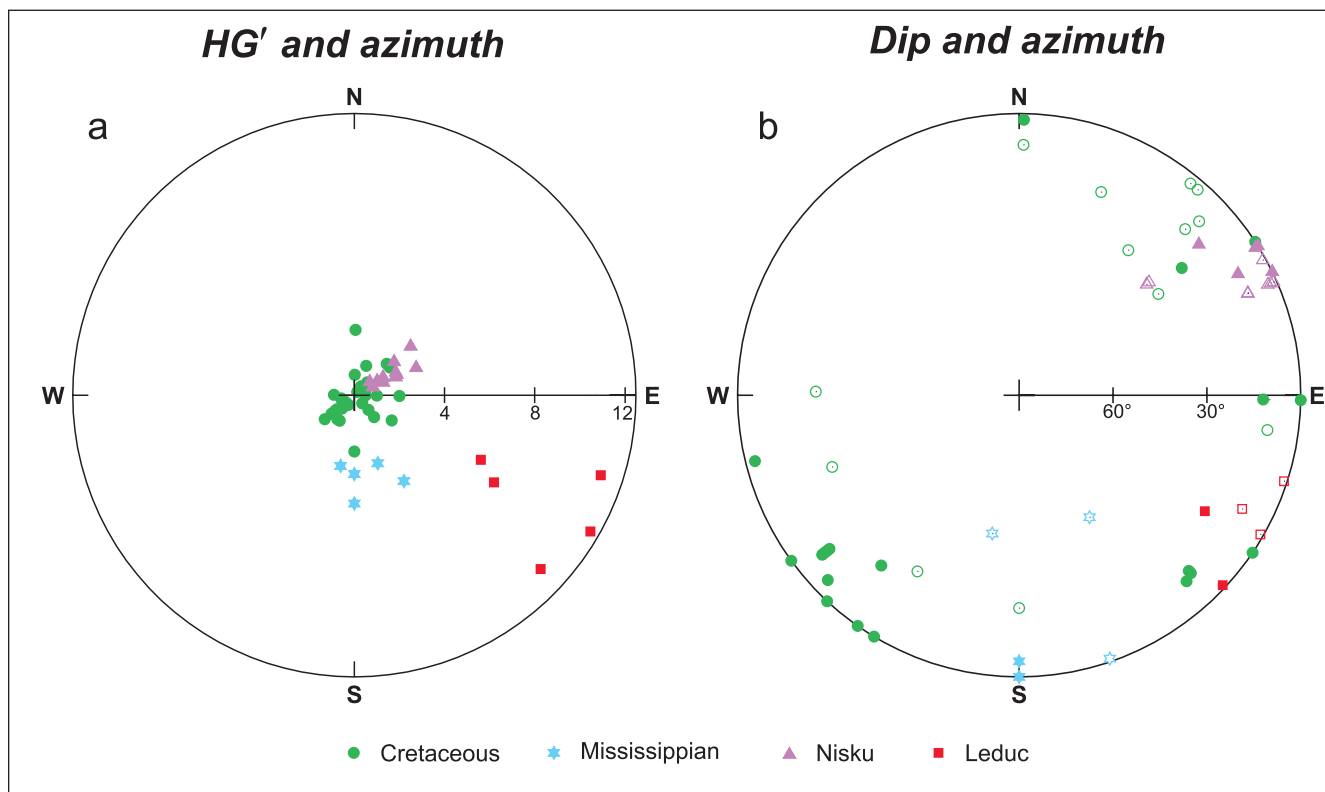


FIGURE 17. Distinctive clusters of HRGM anomaly data can be used to identify the microseeping reservoir formation that caused the anomaly. (a) Polar coordinate plot of the magnitude of the HG' value (proportional to nT/m^2) on the radius against the azimuth (= declination) of the anomaly, as defined in Figure 15. HG' values increase with distance from the center; the strongest anomalies occur over Leduc reservoirs, and the weakest anomalies occur over Cretaceous reservoirs. (b) Stereographic projection (like that used in paleomagnetism) of the magnetization direction of the residual anomaly, with azimuth (= declination) defined as in Figure 15 and dip (= inclination) interpolated from Table 2 of Zietz and Andreasen (1967). Solid symbols have positive inclinations, point downward, and are on the lower hemisphere. Open symbols have negative inclinations, point upward, and are on the upper hemisphere.

2000 ft). At the Cement field, Oklahoma, the predominant authigenic magnetic mineral, Fe_7S_8 pyrrhotite, achieves its highest concentration at depths of 200 to 400 m (~650–1300 ft) (see Figure 5 of Reynolds et al., 1990a, and Figure 10 of Foote, 1992). However, Foote (1992) also reported anomalously high concentrations of authigenic maghemite at 1000–1300 m (3300–4300 ft), based on high magnetic susceptibility of Selma chalk in the discovery well at the Vocation oil field, Alabama. Author Van Alstine has found anomalously high concentrations of authigenic magnetic minerals in subsurface cores at depths of 2600 m (8500 ft) in sandstones from Alaska and 4600 m (15,000 ft) in limestones from Oklahoma.

Perhaps most relevant to our present study in Western Canada is the work of Andrew et al. (1991), who estimated the depth to anomalies from spectral analysis of the wavelengths of aeromagnetic HRAM anomalies in Sheridan County, Montana. They calculated that the source of the anomalies is at an average depth of 120 m, in the Fort Union Formation (Paleocene). Similar calculations based on our ground magnetic surveys place the

source of the anomalies in Western Canada at depths of 100 to 200 m.

The 100-m minimum depth has important age implications, because the thickness of glacial drift is no more than 50 m over our study area in central Alberta and no more than 100 m over our study area in Manitoba (see Figure 26.3 of Fenton et al., 1994). This means that in Western Canada, the magnetically enhanced zones occur beneath the glacial drift, which could be as old as 2.6 Ma (Cioppa et al., 1995).

At 100- to 200-m depths beneath our central Alberta study area are continental sediments of the Paskapoo Formation (Paleocene) and the underlying Scollard Formation (upper Maastrichtian to lower Paleocene). Stratigraphic equivalents of these formations occur at 100- to 200-m depths beneath our Manitoba study area. Thus, remanent magnetization recorded in the magnetically enhanced zones could be no older than 63 Ma if in the Paskapoo Formation or 67 Ma if in the Scollard Formation (see Figure 4 of Lerbekmo et al., 1995, using the polarity time scale of Ogg, 1995; see also Lerbekmo and Sweet, 2000).

Although microseepage-related authigenesis of magnetic minerals in magnetically enhanced zones of Western Canada probably began in the early Tertiary, it is important to remember that over much of our study area in central Alberta, 1000 to 3000 m of Paleogene sediments had been deposited and subsequently removed by erosion as a result of post-Laramide isostatic uplift before deposition of the Pliocene-Pleistocene tills (see Figure 24.23 of Dawson et al., 1994, and Figure 33.15 of Smith et al., 1994). Of this total, 500 m of uplift may have occurred in the past 2 m.y. (Tóth and Corbet, 1987). Thus, as we discuss more fully below, the magnetic anomalies we measured in Western Canada probably originate in old, eroded or exhumed vertical conduits (fracture zones or chimneys) rather than in young, sub-horizontal accumulations, as may be more typical in regions that have not experienced recent uplift.

Paleomagnetic Constraints on the Age of HRGM Anomalies in Western Canada

We next discuss the key paleomagnetic constraints on the age and origin of the dipolar HRGM anomalies we observe in Western Canada. We minimize the use of paleomagnetic terminology, and we present a guide to paleomagnetic nomenclature and basic concepts in Appendix B. Although we summarize the key paleomagnetic constraints below, we present more details in Appendixes C and D. In this discussion, we refer to geologic time using the following convention: 1 million years = 10^6 yr = 1 m.y. (time) = 1 Ma (age). This allows us to distinguish between durations of temporal processes (m.y.) and geologic or absolute ages (Ma).

The dipolar HRGM anomalies we observe in Western Canada almost certainly reflect a significant contribution from reversed-polarity remanent magnetization for the following reasons.

- 1) A consideration of recent geomagnetic field behavior indicates that for the past 2000 yr, remanent magnetization directions in central Alberta would record inclinations (dips) steeper than $+55^\circ$ (red triangles in Figure 18a). This is too steep to produce dipolar HRGM anomalies in the present magnetic field inclination of $+75^\circ$ (Zietz and Andreasen, 1967).
- 2) More than 90% of the dipolar HRGM anomalies we observe in Western Canada exhibit declinations (azimuths) that are well outside the expected 342° to 19° declination range (red triangles in Figure 18a) for the past 2000 yr in this region. Figure 18a approximates the expected remanent magnetization directions over most of the Brunhes normal-polarity chron, which is the time since the last geomagnetic reversal at 0.78 Ma (Ogg, 1995).
- 3) The depth-to-source estimates (100–200 m) indicate that the host rocks for the magnetically enhanced zones are bracketed in age between the Paskapoo

Formation (Paleocene) and the Scollard Formation (Maastrichtian/Paleocene), implying that the HRGM anomalies are no older than 67 Ma.

- 4) Assuming a maximum age of 67 Ma for the HRGM anomalies and assuming that their remanent magnetization averages the geomagnetic field for at least 10^4 yr, the expected remanent magnetization inclinations would be $+69^\circ \pm 2^\circ$ (normal polarity) and $-69^\circ \pm 2^\circ$ (reversed polarity), and the expected declinations would be $353^\circ \pm 7^\circ$ (normal polarity) and $173^\circ \pm 7^\circ$ (reversed polarity). These magnetization directions (indicated by red circles in Figure 18b) are inconsistent with >90% of the magnetization directions we infer from the observed dipolar HRGM anomalies (Figure 17b).
- 5) Given that the HRGM anomaly directions correspond to no known magnetic-field directions recorded in Western Canada during the past 67 m.y., *the HRGM anomalies almost certainly record "intermediate" directions representing vector sums of normal-polarity and reversed-polarity magnetizations in nearly equal balance.*
- 6) If each HRGM anomaly time-averages the geomagnetic field during a 10-m.y. pulse of enhanced microseepage, the most likely times to record reversed-polarity remanent magnetization are during the early Tertiary, 63–41 Ma, or during the middle Tertiary, 35–25 Ma (Appendix B).
- 7) If each HRGM anomaly time-averages the geomagnetic field during constant-flux microseepage over tens of millions of years (i.e., from the initiation of microseepage to the present), the reversed-polarity remanent magnetization in the magnetically enhanced zones could be recording the reversed-polarity bias that prevailed over the entire interval from 89.7 to 1.8 Ma (Appendix B).

Vector-sum, Remagnetization-circle Model for Dipolar HRGM Anomalies in Western Canada

The key to understanding the origin of the dipolar HRGM anomalies in Western Canada is to realize that *they probably record vector sums of reversed-polarity remanent + normal-polarity magnetizations in nearly equal balance.* In Appendix D, we demonstrate how each of the distinctive HRGM anomaly clusters (Nisku, Leduc, Cretaceous, and Alida) shown in Figure 17b can be explained by four geologically and paleomagnetically plausible models. In the four models, the *reversed-polarity magnetization* is inferred to be *chemical remanent magnetization* (CRM), acquired either during an approximately 10-m.y. pulse near the initiation of microseepage from a particular reservoir or over the tens of millions of years from the initiation of microseepage to the present. In the four models, the *normal-polarity magnetization* is inferred to be either *viscous remanent magnetization* (VRM) residing in

“multidomain” magnetic grains $>10\ \mu\text{m}$, or *induced magnetization* aligned with the present magnetic field.

In paleomagnetism, distributions of natural remanent magnetization (NRM) directions representing vector sums of normal- and reversed-polarity magnetizations are commonly encountered when analyzing rocks older than 0.78 Ma, which is when the last geomagnetic reversal occurred. These “great-circle” distributions of paleomagnetic directions are referred to as “remagnetization circles” (Halls, 1976, 1978; Kirschvink, 1980; Schmidt, 1985).

Examples of remagnetization circles derived from our paleomagnetic studies of Devonian and Mississippian reservoir rocks from the Alberta and Williston Basins are included in Appendix C. These reservoir rocks all contain early Tertiary reversed-polarity CRM probably associated with the reversed-polarity CRM we infer in magnetically enhanced zones above at least some (e.g., Nisku) microseeping reservoirs of Western Canada. The reversed-polarity magnetization in these reservoir rocks probably was acquired during a regional early Tertiary chemical remagnetization event (Van Alstine and Butterworth, 1994; Van Alstine et al., 1997). This event was closely associated with hydrocarbon generation; with late-Laramide thrusting; and with the fluid-migration event that filled traps in the Laramide orogenic foreland, led to emplacement of the Alberta tar sands (Garven, 1989), and involved fluid flow as far east as the Williston Basin (Bethke and Marshak, 1990).

In Appendix D, we include age-dated “reference remagnetization circles” calculated from the reference North American apparent-polar-wander (APW) path. Based on comparison of the reference and observed remagnetization circles, we infer a 57-Ma age for the reversed-polarity CRM in the Devonian and Mississippian reservoir rocks from the Alberta Basin, and we infer a 45-Ma age for the reversed-polarity CRM in the Devonian reservoir rocks from the Williston Basin. The 12-m.y.-older age for the reversed-polarity CRM in the Alberta Basin is geologically reasonable, given that the Alberta Basin cores are from reservoirs close to their hydrocarbon source rocks, whereas the Williston Basin cores are from reservoirs thought to be filled by long-distance hydrocarbon migration.

In both the Alberta and Williston Basins, the midpoints of the reference remagnetization circles exhibit increasingly more clockwise azimuths with decreasing age. These remagnetization-circle midpoints correspond to nearly horizontal magnetization directions, which are intermediate between normal and reversed polarity. The horizontal magnetization is a resultant vector (vector sum) of normal- and reversed-polarity components in nearly equal balance.

It is our contention that the distinctive clusters of HRGM anomaly directions we observe above microseeping reservoirs in Western Canada (Figure 17b) represent

midpoints on remagnetization circles connecting reversed-polarity CRM with normal-polarity VRM and induced magnetization directions. The shallow-inclination, eastern-hemisphere directions (Figure 17b) resemble paleomagnetic NRM directions we have measured in surface-outcrop and subsurface-core samples over a wide region extending from the McConnell thrust west of Calgary to the Williston Basin in Montana, North Dakota, and Saskatchewan. As shown in Appendix C, NRM directions from the northeastern limb of the fold at Moose Mountain, Alberta, provide a real example of an eastern-hemisphere (declination = 89°), shallow-inclination ($+4^\circ$) average NRM direction capable of causing a dipolar HRGM anomaly with an easterly azimuth if this direction had been recorded in a near-surface magnetically enhanced zone.

We should emphasize that initial recognition of the distinctive HRGM anomaly clusters (Figure 17) and specifically the determination of HRGM anomaly azimuths were made by author LeSchack before he was aware of their paleomagnetic implications. The fact that the HRGM anomaly azimuths make perfect paleomagnetic sense if interpreted as midpoints on remagnetization circles further implies that these dipolar magnetic anomalies are physically real rather than being artifacts of the mathematical filters used in our computations. It also seems unlikely that artifacts of the mathematical filters would have yielded the observed lognormal distribution of HG' values.

The different magnetization directions we infer from the HRGM anomaly clusters probably reflect differences in grain-size distributions and magnetic mineralogy of the authigenic magnetic minerals in the magnetically enhanced zones. It is well known in paleomagnetism that magnetic grain size exerts profound controls on magnetic properties and magnetic stability over geologic time scales (Dankers, 1978; Dunlop, 1983; Dekkers, 1988). Specifically, the ratio of “single-domain” ($0.05\text{--}1\ \mu\text{m}$) + “pseudosingle-domain” ($1\text{--}10\ \mu\text{m}$) to “multidomain” ($>10\ \mu\text{m}$) authigenic magnetite will determine the R/N-polarity ratio (i.e., the ratio of *reversed-polarity* CRM to *normal-polarity* VRM + induced magnetization). In turn, the R/N-polarity ratio determines the relative magnitudes of the positive and negative lobes of the observed dipolar HRGM anomalies. Differences in composition and pressure of the hydrocarbon gases leaking from different reservoirs in different petroleum systems could easily affect the magnetic mineralogy and grain-size distributions, yielding distinctive NRM directions and hence *diagnostic HRGM anomaly directions above different reservoirs*.

Further work will be needed to substantiate this vector-sum, remagnetization-circle model for explaining the distinctive clusters of dipolar HRGM anomalies we observe in Western Canada. It is especially important that oriented cores be obtained from magnetically enhanced

zones, so that complete paleomagnetic laboratory and directional analyses can be performed. The cores could be oriented either by conventional multishot or by paleomagnetic core-orientation techniques (Bleakly et al., 1985a, b; Van Alstine et al., 1991; Van Alstine and Butterworth, 1993; Hamilton et al., 1995, 1996; Corbett et al., 1997). This would allow separation and age-dating of the normal- and reversed-polarity magnetizations, as well as determination of the magnetic mineralogy and grain-size distribution.

Hydrocarbon Generation and Migration Constraints on the Age of HRGM Anomalies in Western Canada

If vertical microseepage of hydrocarbon microbubbles is the mechanism responsible for causing short-spatial-wavelength magnetic anomalies detected in HRGM surveys, then these magnetic anomalies must postdate the generation of oil. In the Western Canada Sedimentary Basin, burial/maturation profiles indicate that oil did

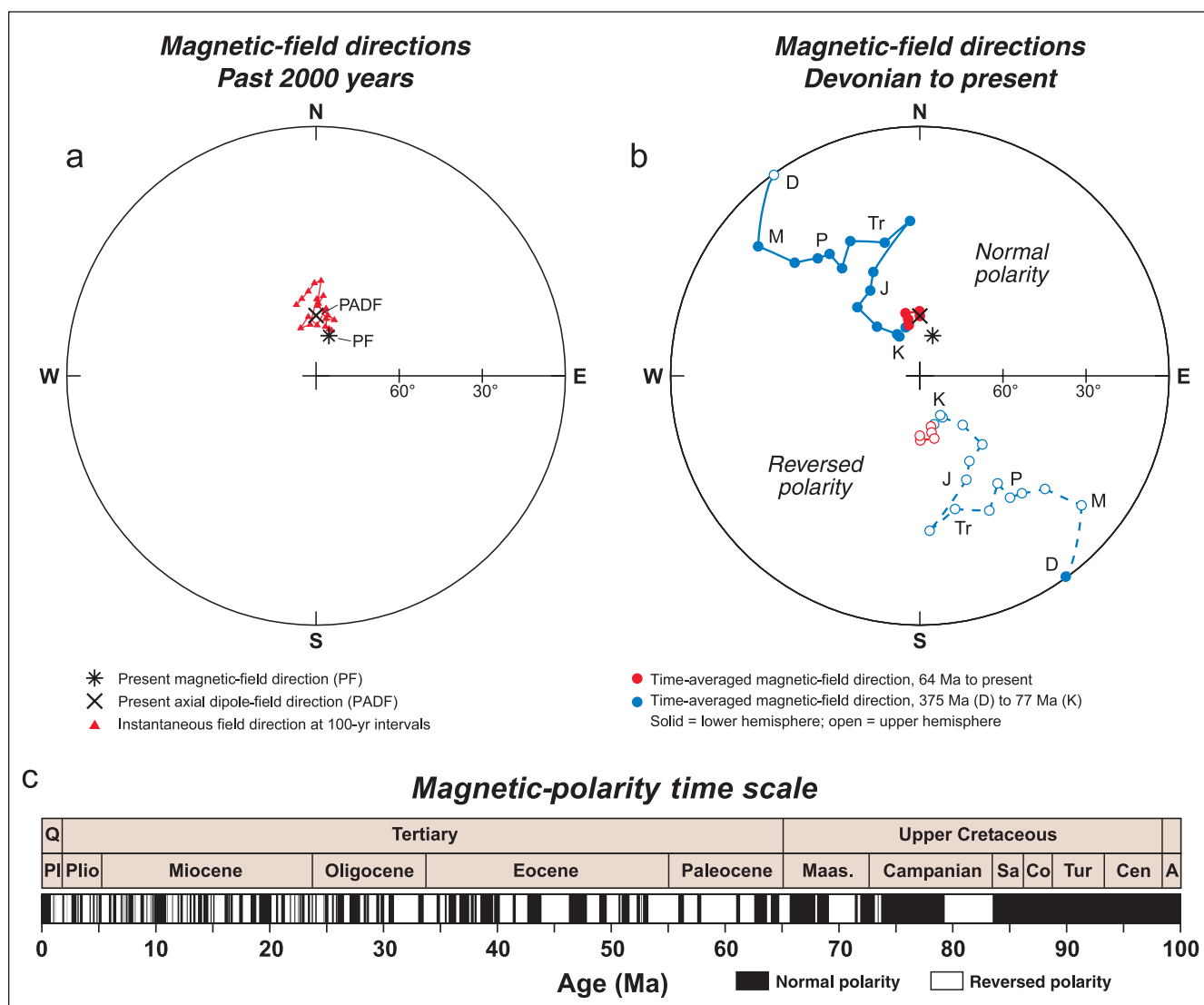


FIGURE 18. (a) Instantaneous magnetic-field directions (red triangles) calculated at 100-yr intervals for the past 2000 yr for a location near Rumsey reef, Alberta. These directions were calculated from the instantaneous magnetic poles (VGPs) from Holocene lavas of the western United States, listed in Champion (1980). All points are on the lower hemisphere and exhibit normal polarity. (b) Time-averaged magnetic-field directions calculated from the present back to 64 Ma (red circles) and from 77 Ma back to the Devonian (blue circles). These directions were calculated from the North American reference apparent-polar-wander (APW) path, for a location near Rumsey reef, Alberta. Solid symbols connecting solid lines are on the lower hemisphere. Open symbols connecting dashed lines are on the upper hemisphere. Normal-polarity directions are in the northwest quadrant; reversed-polarity directions are in the southeast quadrant. Because the source of the dipolar HRGM anomalies is at about 150-m depth in Paleocene/Maastrichtian strata, only the <77-Ma magnetization directions (i.e., the red circles) can contribute to the anomalies. (c) The magnetic-polarity time scale (Ogg, 1995) from 100 Ma to the present.

not begin to be generated prior to ~110 Ma in Devonian source rocks, ~65 Ma in Jurassic source rocks, and ~50 Ma in Cretaceous source rocks (Figure 19). (Note that the burial-history curves in Figure 19 include what we presume to be a drafting error in linear tick marks on the time scale in the original Figure 31.27 of Creaney et al. [1994]. Our references to maturation ages are based on a linear interpolation between the 0- and 100-Ma ticks on their figure.)

Oil and gas pools underlying HRGM anomalies in our Alberta Basin study areas belong to three petroleum systems: the Duvernay Petroleum System (Leduc and Nisku reservoirs) and the Mannville Group and Colorado Group Petroleum Systems (Cretaceous reservoirs). Using the terminology of Magoon (1988), Creaney et al. (1994) described the complete petroleum system as including source rock, maturation, migration path, reservoir rock, trap, and seal. The petroleum systems of Western Canada are named after their source rock. The Duvernay Petroleum System is named for the Duvernay Formation (Upper Devonian), which consists of bituminous carbonates and calcareous shales and which is the basal equivalent of the Leduc Formation. The Duvernay Formation is the source rock for oil in the Leduc and Nisku reservoirs in our case-history 4 and 5 study areas (Figure 31.11 of Creaney et al., 1994), and Duvernay source rocks are in contact with lower Leduc pinnacle reefs (Figure 10).

For an HRGM anomaly sourced at ~150-m depth to reflect microseepage from a Leduc oil reservoir now at 1900-m depth, the Duvernay Petroleum System must have been open to *microseepage of gaseous* hydrocarbons but closed to *migration of liquid* hydrocarbons. The hydrocarbon microseepage phenomenon is thought to reflect the vertical, buoyant rise of colloid-size hydrocarbon gas microbubbles through a network of vertical microfractures. Hydrocarbon microbubbles emanating from different petroleum systems can be expected to have different chemistries (e.g., H₂S content), different microseepage initiation times (depending on when their source rocks matured), and different buoyancies and pressures as they rise from different depths (Sahagian and Proussevitch, 1992; Osborne and Swarbrick, 1997).

Hydrocarbon generation itself can cause reservoir overpressuring (Spencer, 1987; Yassir and Bell, 1994; Osborne and Swarbrick, 1997; Payne et al., 2000). Primary migration, or expulsion of oil from source rocks, is thought to occur by “hydrocarbon-phase pressure-migration” involving microfracturing of the source rock (Tissot and Welte, 1984, p. 336–340). In Austin Chalk reservoirs in south-central Texas, Berg and Gangi (1999) demonstrated that primary migration of oil generated in low-permeability source rock (Eagleford Shale) was sufficient to fracture the source rocks, thereby increasing permeability and providing hydrocarbon migration pathways. In a paleomagnetic study on a subsurface core transecting the contact between the Austin Chalk and the Eagleford Shale, Corbett et al. (1997) found highest fracture density and strongest *reversed-polarity* CRM remagnetization in Austin Chalk cores directly overlying the contact with the Eagleford Shale source rocks. If similar fracturing caused by primary migration of oil occurred at the contact between Duvernay source rocks and Leduc dolomite low on the Rumsey reef flank (compare Figure 10), this could help explain the concordance of HG’ contours with the reef margin as defined by the 3-D seismic survey (Figure 11).

Moreover, the much higher HG’ values overlying the five Leduc pinnacle-reef reservoirs, compared with the separate lognormal distribution of 92 non-Leduc wells (Figure 14d), may partly reflect reservoir pressurization by primary migration of oil expelled from Duvernay source rocks directly into Leduc reefs. All five of the Leduc high HG’ values are from locations where the Duvernay source rocks are mature (Figure 31.7 of Creaney et al., 1994). The small size (16 ha) of

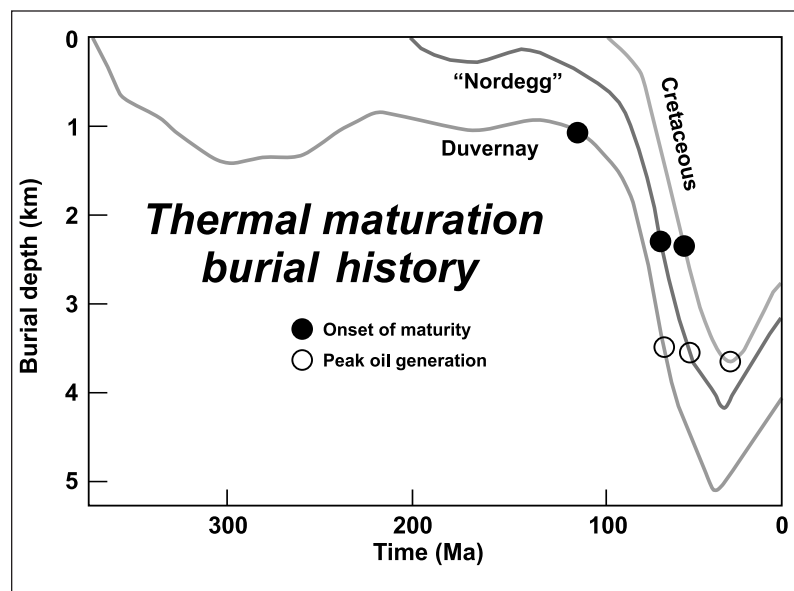


FIGURE 19. Generalized burial history and organic maturation curves for different petroleum systems of the Western Canada Sedimentary Basin. Redrawn exactly from Figure 31.27 of Creaney et al. (1994), courtesy of CSPG. Note the progressively younger maturation ages proceeding from the Duvernay (Devonian) to the “Nordegg” (Jurassic) to the Cretaceous petroleum systems. Note also that peak oil generation occurred well before maximum burial in the Duvernay Petroleum System, but peak oil generation was barely achieved in the Cretaceous petroleum systems. Thus, the strong HRGM anomalies above Devonian reservoirs and the weak HRGM anomalies above Cretaceous reservoirs may partly reflect increased generation of hydrocarbon gases in the deeper petroleum systems.

the Rumsey reef, its isolation from the rest of the Stettler reef complex, and its being surrounded by impermeable Ireton Formation shale would all contribute to a high pressure buildup, episodic microfracturing of seal/cap rocks, and the highest HRGM anomaly intensity we observed in this study.

Within the Duvernay Petroleum System, the highest pore pressure may have been achieved between ~67 Ma (peak oil generation) and ~38 Ma (maximum burial). These ages coincide almost exactly with the 63- to 41-Ma age range for the early Tertiary reversed-polarity-bias interval (Figure 20c). Moreover, the Cooking Lake Formation, which was a regional aquifer during petroleum migration (Switzer et al., 1994; Márquez and Mountjoy, 1996), lies directly above carbonates of the Beaverhill Lake Group (Figure 10), which is also part of the Duvernay Petroleum System. Creaney et al. (1994) discuss how oil migrated out of Leduc reservoirs into underlying Beaverhill Lake/Swan Hills reservoirs. Paleomagnetic studies of subsurface Beaverhill Lake/Swan Hills cores by us (Appendix C) and by Gillen et al. (1999) reveal that these Devonian carbonates have been pervasively chemically remagnetized by early Tertiary, reversed-polarity CRM within the hydrocarbon reservoirs.

Paleomagnetic studies of chemically remagnetized carbonates are increasingly finding a link between the timing of CRM acquisition in authigenic magnetite and the timing of hydrocarbon maturation (Banerjee et al., 1997). In these chemically remagnetized carbonates, pyrite-to-magnetite transformations (Reynolds, 1990; Suk et al., 1990) may occur when organically complexed ferric iron acts as an oxidizing agent at temperatures of ~90°C (Brothers et al., 1996). Leduc reservoirs occur within the same (Duvernay) petroleum system as Beaverhill Lake/Swan Hills reservoirs in which fluids were precipitating authigenic magnetite recording reversed-polarity CRM during the early Tertiary at ~57 Ma. This is after the ~67-Ma time when Duvernay source rocks reached peak oil generation but before the ~38-Ma time of maximum burial (Figure 20b). Between 67 and 38 Ma, large quantities of methane and other light hydrocarbons were probably dissolved in the liquid phase within Leduc pinnacle-reef reservoirs as they approached maximum burial. The highest intensity of HRGM anomalies above microseeping Leduc reservoirs probably reflects the highest methane storage capacity, highest overpressure, and closest proximity to source rocks for Leduc reservoirs, compared with overlying Nisku and Cretaceous reservoirs.

In the Alberta Basin, the next strongest HRGM anomalies occur above Nisku reservoirs, which, in our study area, are ~1800 m deep and are also considered to be part of the Duvernay Petroleum System (Creaney et al., 1994). In our case-history 5 area, on the Nisku shelf, Nisku reservoirs are thought to reflect drape traps over Leduc reefs (Figures 15 and 31 of Podruski et al., 1987). Podruski et al.

(1987, p. 50) state, "The oil was probably sourced originally from the Duvernay Formation and migrated from Leduc complexes through fractures in the Ireton into the Nisku shelf." Thus, the somewhat lower HRGM anomaly intensity above Nisku reservoirs probably reflects their being connected less directly with regional aquifers (e.g., Cooking Lake Formation) and farther from Duvernay source rocks (Figure 10) than Leduc reservoirs are. Moreover, less differential compaction probably occurred around Nisku shelf reservoirs than around Leduc pinnacle-reef reservoirs, so vertical microfractures may be less well developed above Nisku (case-history 5) than above Leduc (case-history 4) reservoirs.

Still weaker HRGM anomalies occur above shallower (600- to 1500-m-deep) Cretaceous reservoirs in the Mannville Group (Lower Cretaceous) and Colorado Group (Upper Cretaceous) Petroleum Systems. As discussed by Creaney et al. (1994), the Mannville Group Petroleum System contains a mixture of oils derived from Mississippian through Lower Cretaceous source rocks, whereas oil in the Colorado Group Petroleum System is sourced entirely within the Colorado Group. Neither the Mannville nor the Colorado Group Petroleum System contains Duvernay-sourced oil, which testifies to the effectiveness of the seals between the Upper Devonian and Cretaceous petroleum systems. This also helps explain why HRGM anomalies above Cretaceous reservoirs (which are microseeping Mississippian through Cretaceous-sourced hydrocarbons) have different magnetic signatures than do HRGM anomalies above Nisku or Leduc reservoirs (which are microseeping Duvernay-sourced hydrocarbons). One reason why HRGM anomalies may be so weak above the Cretaceous reservoirs is that Mannville and Colorado Group source rocks were in the petroleum-generation kitchen for less time, at lower temperatures, at shallower depths, at lower pressures, and at younger ages than were Duvernay source rocks (Figure 20b). Before the Cretaceous source rocks had reached peak oil generation, the early Tertiary reversed-polarity-bias interval had ended (~41 Ma; Figure 20c). This implies that remanent magnetization in the magnetically enhanced zones above Cretaceous reservoirs would more nearly self-cancel, as inferred at the Cement field (Reynolds et al., 1990b).

In Manitoba, on the northeast flank of the Williston Basin, the strongest HRGM anomalies occur above Mission Canyon (Mississippian) reservoirs, into which oil is thought to have migrated from Bakken/Lodgepole Formation (Devonian/Mississippian) source rocks in the United States (Figure 31.14 of Creaney et al., 1994). In our Manitoba case-history areas, Mississippian and younger possible source rocks are considered to be thermally immature, so any localized primary-migration pressurization mechanisms would not be expected to contribute to HRGM anomaly intensity. Long-distance migration from deeper, mature Devonian/Mississippian source rocks into Mission Canyon reservoirs on the basin

margin is thought to have occurred in the early Tertiary (Podruski et al., 1987). This coincides with the ~55-Ma time of maximum burial (Figure 3.10 of Wright et al., 1994), with the early Tertiary reversed-polarity-bias interval (Figure 20c), and with our observation of early Tertiary reversed-polarity CRM in cores from Mission Canyon, Bakken, and Three Forks reservoirs in the Williston Basin (Appendix C). Thus, reversed polarity CRM in magnetically enhanced zones (causing dipolar HRGM anomalies) above Mission Canyon reservoirs is entirely reasonable in our Manitoba study areas (case histories 1 and 3). The strong natural water drive in these Mississippian reservoirs probably forced hydrocarbon microbubbles through weak points and fractures in the zone of anhydritization seal along the sub-Mesozoic unconformity. Above the unconformity, low reservoir pressure and thermal immaturity of Mesozoic source rocks combined to yield *no* HRGM anomalies (only radiometric anomalies) above lower Amaranth reservoirs.

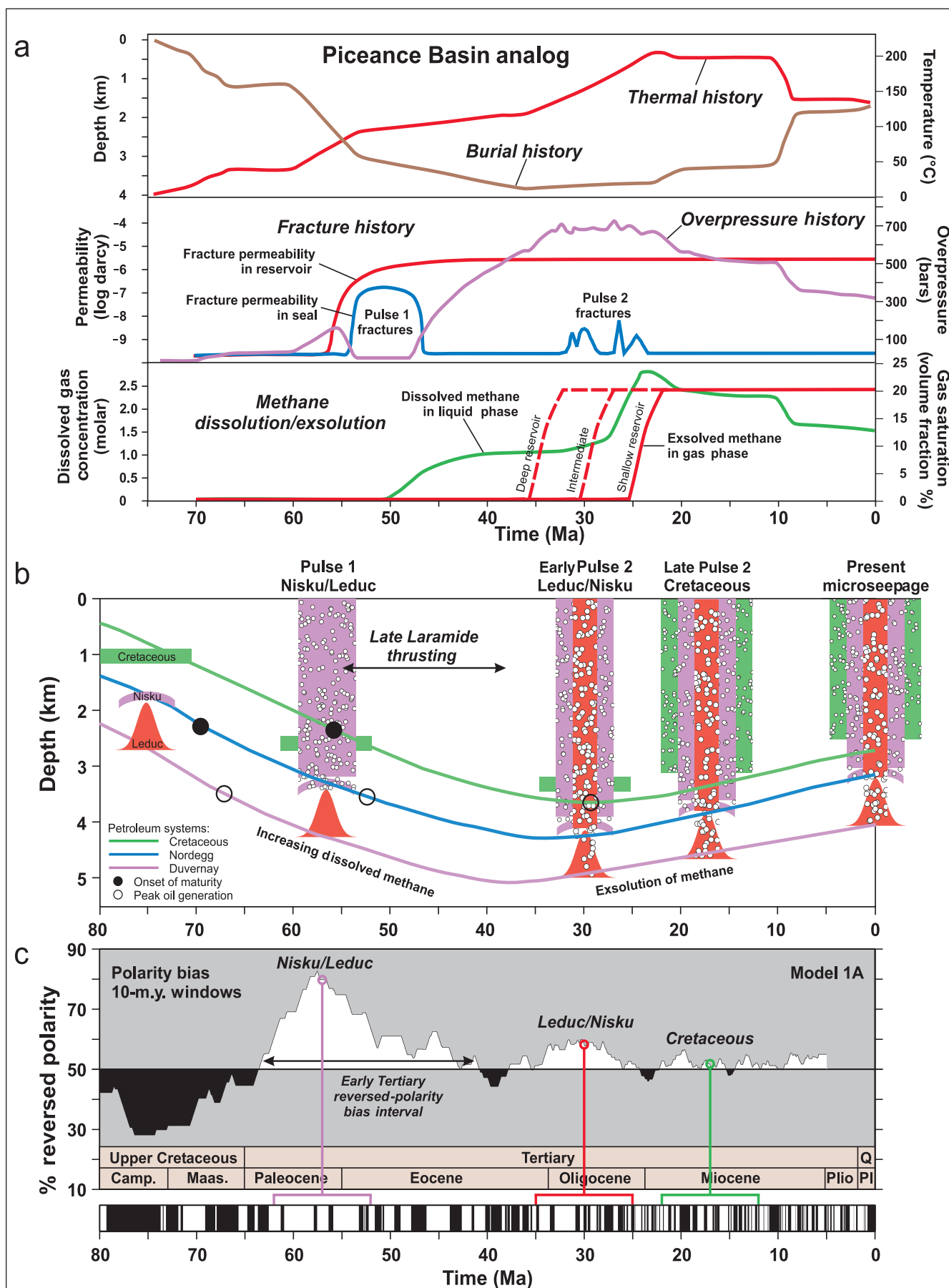
Regional Fracture and Pore-pressure Constraints on the Age of HRGM Anomalies in Western Canada

In both the Alberta and Williston Basins, we observe that HRGM anomalies sourced at ~150-m depths consistently lie *directly above* microseeping hydrocarbon reservoirs as deep as 1900 m. This inferred vertical microseepage might at first seem remarkable, given that (1) the strongest HRGM anomalies occur over reservoirs in the deepest (Duvernay) petroleum system; (2) no Duvernay-sourced oil is present in the Cretaceous (Mannville and Colorado Group) petroleum systems; and (3) the giant oil-sand deposits in eastern Alberta are considered a “type example” of long-distance lateral migration reflecting “a gravity-driven groundwater flow system that operated throughout Tertiary time as a result of foreland basin uplift” (Garven, 1989). Moreover, Machel and Burton (1991a) essentially regarded vertical seepage of hydrocarbons as a “special case” and suggested that in general,

FIGURE 20. (a) Reaction-transport-mechanical (RTM) modeling of the interrelationships among gas generation, overpressuring, and fracturing in the Mesaverde Group, Piceance Basin, Colorado. Selected curves have been redrawn from Payne et al. (2000), courtesy of AAPG.

(b) Conceptual model of sequential development of microseepage-related HRGM anomalies of the Alberta Basin, with paleomagnetic age control according to Model 1A (Appendix D) and generalized Alberta Basin burial/maturation curves from Figure 19 (Creaney et al., 1994). According to this model, reversed-polarity chemical remanent magnetization (CRM) above different reservoir classes (Leduc, Nisku, Cretaceous) is acquired during different 10-m.y. pulses of enhanced microseepage at times of reversed-polarity bias >50%. Above microseeping reservoirs, hydrocarbon microbubbles buoyantly rise along vertical microfractures that facilitate development of geochemical chimneys (colored). The microbubbles transport Fe leached from the reservoirs and wall rocks to near-surface levels, where the Fe is reprecipitated as authigenic magnetic minerals (magnetite, maghemite, pyrrhotite, greigite) in magnetically enhanced zones. The authigenic magnetic minerals record reversed-polarity-biased CRM (20c), which causes dipolar magnetic anomalies detectable in HRGM surveys. Microseepage pulses at different times produce HRGM anomalies with different azimuths. A microseepage pulse at 57 Ma, which produces HRGM anomalies with east-northeast azimuths above Nisku reservoirs, probably reflects late Laramide fracturing of the seal of the Duvernay Petroleum System, analogous to “Pulse 1 fractures” of the Piceance Basin (20a). A microseepage pulse at 30 Ma, which produces HRGM anomalies with east-southeast azimuths above Leduc reservoirs, may reflect methane exsolution (“degassing”) of the Duvernay Petroleum System, triggered by pressure reduction upon isostatic uplift after maximum burial; this corresponds to the onset of “Pulse 2 fractures” in the Piceance Basin, when methane exsolution first occurred in the “deep reservoir” (Leduc analog). The youngest Pulse 2 fractures are associated with methane exsolution from the “shallow reservoir” (= coastal sandstone) in the Piceance Basin; this probably explains the 17-Ma pulse of enhanced microseepage and HRGM anomalies above Cretaceous reservoirs in the Alberta Basin.

(c) Polarity-bias time-averaging of the magnetic-polarity time scale of Ogg (1995) if CRM is acquired during 10-m.y. pulses as in Model 1A (above). Black = normal polarity; white = reversed polarity. Polarity bias has been calculated by sliding-window averages with a constant window width of 10 m.y. centered at 2000 equally spaced points between 80 Ma and the present. Note that CRM acquired during 10-m.y. microseepage pulses centered at any time between 63 and 5 Ma has an 88% probability of recording reversed-polarity bias. This partly explains why all of the more than 100 HRGM anomalies we observed in Western Canada apparently record reversed-polarity CRM. Note that the reversed-polarity bias is particularly strong (80% and 58%, respectively) during microseepage pulses at 57 Ma and 30 Ma. This partly explains the high intensity and good clustering of HRGM anomaly azimuths above Nisku and Leduc reservoirs. In contrast, the reversed-polarity bias is only 51% during a microseepage pulse at 17 Ma. This partly explains why HRGM anomalies above Cretaceous reservoirs have scattered azimuths and are much weaker than the anomalies above Leduc and Nisku reservoirs.



magnetically enhanced zones would *not* occur directly above the reservoirs, because the seepage-related “geochemical plumes” would be deflected or distorted by the lateral groundwater flow.

For vertical microseepage to be occurring in Western Canada, without violating the integrity of the petroleum systems and without being significantly deflected by the groundwater flow, two conditions are almost certainly being met. (1) Microseepage of gas, rather than oil, is occurring, because buoyant force increases with density contrast, which is much higher for gas than for oil (Tissot and Welte, 1984, p. 341–347). (2) The gas microbubbles must be rising along vertical pathways, which almost certainly implies a network of closely spaced vertical fractures and microfractures. Saunders et al. (1999) cite examples of colloid-size light-hydrocarbon gas bubbles migrating vertically upward at rates of 0.2 to 91 m/day, in contrast to lateral groundwater movement at 0.003 to 0.012 m/day. Yet for these high vertical-migration rates to be achieved, vertical microfractures almost certainly need to be present to permit vertical migration through the numerous shale beds and seals separating the many petroleum systems from the near-surface environment. Fractures and microfractures can enhance permeability by orders of magnitude in rocks with low matrix permeability (Lorenz and Finley, 1991).

The existence and importance of regional vertical microfractures is increasingly recognized by the petroleum industry, especially in foreland-basin structural settings. Lorenz et al. (1991) describe how such regional, vertical extension fractures can form at depth, parallel to the regional maximum horizontal stress (S_{Hmax}) direction. They also discuss how the regional compressive stress can be “amplified by sedimentary architecture,” such as in a sandstone lens embedded in a mudstone matrix. Similar stress amplification may have promoted microfracturing (and hence microseepage) out of pinnacle-reef, biostrome, and channel-sand reservoirs in our Western Canada case-history areas. Laubach (1997) described regional (“Category I”), dilatant, subvertical microfractures with widths $<0.5 \mu\text{m}$ and width/length ratios of 10^{-3} to 10^{-4} in cores from hydrocarbon reservoirs in nearly flat-lying sandstones in Wyoming and Texas.

Lorenz et al. (1991), Lorenz and Finley (1991), and Laubach (1997) emphasized that these regional fractures and microfractures propagate at times of basinwide dilatancy and high pore pressure at depth. As discussed by Lorenz et al. (1991), fractures initiate in three ways: (1) by an increase in the maximum stress (S_{Hmax}), such as by regional compression; (2) by a decrease in the minimum stress (S_{Hmin}), such as by regional extension; or (3) by an increase in pore pressure, which lowers all three principal effective stresses.

A combination of the first and third [ways] is perhaps the most common near tectonically

active areas, where pulses of increased horizontal compression from a thrust belt can create an anisotropy in the horizontal stresses in the adjacent foreland basin, as well as concurrent pulses of increased formation pore pressure due to reduction of pore volume in the strata, enhancing the susceptibility of the strata to fracturing (Lorenz et al., 1991).

This combination of mechanisms (1) and (3) is especially pertinent to our case histories in the Laramide foreland in Alberta.

Orogenic compressive stress, which promotes regional vertical microfractures striking perpendicular to the mountain front, can be transmitted hundreds of kilometers into forelands (Lorenz et al., 1991). The HRGM anomalies we observed above microseeping Leduc, Nisku, and Cretaceous reservoirs are located 125 to 175 km east of the Laramide fold-thrust belt. Because fractures propagate in a plane perpendicular to the least principal stress, vertical microfractures are expected in cases where the vertical stress (S_V) is *not* the least principal stress (i.e., as long as the least principal stress is horizontal). Regional vertical fractures propagate when the stress regime is either extensional ($S_V > S_{Hmax} > S_{Hmin}$) or strike-slip ($S_{Hmax} > S_V > S_{Hmin}$), and these are the stress regimes in our Alberta and Manitoba case-history areas (Bell et al., 1994). In contrast, subhorizontal microfractures and associated thrust faults, which could inhibit the formation of HRGM anomalies directly above deep reservoirs, propagate in the thrust stress regime ($S_{Hmax} > S_{Hmin} > S_V$). This stress regime would be expected only within or immediately ahead of fold-thrust belts. Márquez and Mountjoy (1996) described subhorizontal microfractures, in Leduc cores from the Strachan buildup, that formed during thermal cracking of crude oil to gas. Although this is an excellent example of fracturing that was facilitated by high pore pressure resulting from thermal maturation of hydrocarbons, the Strachan gas field is only ~15 km east of the fold-thrust belt, where the thrust stress regime is far more likely than in any of our case-history areas.

Recent apatite fission-track data were interpreted by Stockmal et al. (1997) as indicating early to middle Eocene (~55 to 38 Ma) late Laramide thrusting in the outer Foothills belt in southern Alberta. Thus, as emphasized in Figure 20b, three events occurred during the 63- to 41-Ma early Tertiary reversed-polarity-bias interval, to begin recording *reversed-polarity chemical remanent magnetization* in magnetically enhanced zones above the deepest reservoirs. (1) The Laramide fold-thrust belt made its closest approach to our study area, implying maximum horizontal compressive stress. (2) Hydrocarbons were generated (exceeding peak oil generation in the Duvernay Petroleum System), contributing to high pore pressure, thereby lowering effective stresses and promoting

fracturing. (3) Rapid subsidence and maximum burial further increased pore pressure. These are the same conditions that promoted regional fracturing, which enhanced permeability in Mesaverde Group (Upper Cretaceous) tight-gas sandstone reservoirs in the Piceance Basin, Colorado, as discussed by Lorenz and Finley (1991, p. 1754):

The fractures in Mesaverde reservoirs that create significant and highly anisotropic permeability were probably formed at about 36–40 Ma at maximum depth of burial, with high pore pressure due to organic maturation, and during enhanced west-northwest tectonic compression. The fractures are an example of basinwide dilatancy producing regional, basinwide, systematic fractures in the absence of flexure.

As Bell et al. (1994) discussed, present-day in-situ stress (S_{Hmax}) directions in central Alberta are essentially parallel to the Laramide S_{Hmax} direction (i.e., perpendicular to the fold-thrust belt). This implies that regional, vertical microfractures that formed in the foreland during the waning stages (55 to 38 Ma) of the Laramide orogeny can be expected to remain partially open in the present-day in-situ stress field. These Laramide microfractures would continue to provide vertical conduits for hydrocarbon microseepage, which explains how modern radiometric anomalies can continue to form over fossil magnetic anomalies directly above microseeping reservoirs.

Interpretation of Paleomagnetically Dated HRGM Anomalies in the Context of Alberta Basin and Piceance Basin Histories

In Figure 20, we summarize our current understanding of the timing and origin of HRGM anomalies in Western Canada in the context of reaction-transport-mechanical (RTM) modeling by Payne et al. (2000) at the Multiwell Experiment (MWX) site in the Piceance Basin, Colorado. The BasinRTM simulator discussed by Payne et al. (2000) is a finite-element, forward-modeling approach designed to simulate effects of compaction, fracturing, hydrocarbon generation, and multiphase flow. Figure 20a illustrates the thermal, burial, overpressure, fracture, and methane dissolution/exsolution histories inferred for the Piceance Basin. The similarities between the Alberta and Piceance Basins include maximum burial at about 35 Ma, fracturing during the late stages of the Laramide orogeny, and early to middle Tertiary hydrocarbon generation followed by methane exsolution upon later Tertiary uplift.

In Figure 20b and 20c, we illustrate one of four possible models (Model 1A, Appendix D) for explaining the origin of the reversed-polarity remanent magnetization

required for formation of the dipolar HRGM anomalies we observe in Western Canada. These models differ as to whether (1) the reversed-polarity magnetization is acquired in a 10-m.y. pulse of enhanced microseepage or reflects constant flux from the initiation of microseepage to the present, and (2) whether the superimposed normal-polarity magnetization records PADF (present-axial-dipole-field) VRM over the past 10^4 to 10^6 yr or records PF (present-field) VRM over the past $<10^2$ yr. Of the four models discussed in Appendix D, Model 1A is the only one that can explain HRGM anomaly azimuths associated with all three well classes in the Alberta Basin (i.e., Nisku, Leduc, and Cretaceous producers).

According to Model 1A, the reversed-polarity chemical remanent magnetization (CRM) within a magnetically enhanced zone above a particular microseeping reservoir is acquired during a 10-m.y. pulse of enhanced microseepage. In a foreland-basin structural setting, HRGM anomalies above reservoirs in the same formation (e.g., Nisku) and the same petroleum system can be expected to form during the same 10-m.y. pulse. In contrast, HRGM anomalies above reservoirs in different formations and different petroleum systems (e.g., Nisku versus Cretaceous) can be expected to form during microseepage pulses at different times, depending on differences in their hydrocarbon-generation, fracturing, overpressure, and methane-exsolution histories.

In the Piceance Basin simulation (Figure 20a), two different 10-m.y. enhanced microseepage pulses can be inferred from the blue curve, labeled “fracture permeability in seal.” Acquisition of CRM in magnetically enhanced zones (and hence the paleomagnetically determined HRGM anomaly ages) will primarily reflect magnetic mineral authigenesis at these times of high fracture permeability in the seals. In the Piceance Basin, “Pulse 1 fractures” are shown as propagating during the early Tertiary (57 to 47 Ma), and “Pulse 2 fractures” are shown as propagating during the middle Tertiary (32 to 22 Ma). (Note: Although structural geologists generally refer to different fracture “phases,” we refer in this discussion to fracture “pulses” to minimize confusion with methane in a liquid versus a gas phase.) In Figure 20a, the Pulse 1 fractures, which create significant fracture permeability in the sandstone reservoir (Leduc analog), are associated with an initial peak in overpressure (purple curve) at about 55 Ma. These early Tertiary Pulse 1 fractures form even in this 1-D RTM simulation by Payne et al. (2000), which ignores lateral stresses associated with tectonic activity. The apatite fission-track evidence for late Laramide thrusting (about 55 to 38 Ma) in the Alberta Foothills means that early Tertiary Pulse 1 fractures (and associated microseepage) are even more likely in the Alberta Basin than in the Piceance Basin. The Pulse 2 fractures in the Piceance Basin simulation propagate at the time of maximum overpressure and methane exsolution just after maximum burial. Similar Pulse 2 fractures

probably propagated in the Alberta Basin by this same mechanism.

As indicated in Figure 20b, “Nisku” HRGM anomalies (i.e., those with east-northeast azimuths) were the first to form, promoted by Pulse 1 fractures in the early Tertiary at about 57 Ma. The Pulse 1 fractures accomplished two necessary conditions for vertical microseepage. (1) They cut through Ireton Formation shale, allowing oil to migrate from Leduc into Nisku reservoirs. (2) They broke the seal of the Duvernay Petroleum System at the time of the closest approach of the Laramide structural front to our Alberta Basin study area (early to middle Eocene time, ~55–38 Ma; Stockmal et al., 1997). Within the Duvernay Petroleum System, Pulse 1 fractures probably began to propagate after significant methane had been generated (i.e., beyond the “peak oil generation” open-circle symbol in Figure 20b), so it is geologically reasonable that microseepage of light-hydrocarbon gases began at 57 Ma above Nisku (and Leduc) reservoirs. Moreover, as discussed in Appendix D, east-northeast-trending remagnetization circles and HRGM anomalies with east-northeast azimuths indicate that the reversed-polarity CRM above microseeping Nisku reservoirs is about 57 Ma, the same age as the reversed-polarity CRM in subsurface cores from the Duvernay Petroleum System (Appendix C).

As indicated in Table 3 (and Appendix D), “Leduc” HRGM anomalies (i.e., those with east-southeast azimuths) can be interpreted as having formed either during Pulse 1 (early Tertiary) or Pulse 2 (middle Tertiary). The Pulse 1 origin for Leduc HRGM anomalies represents a coarser-grained version (Model 1B) of the same 10-m.y. pulse centered on 57 Ma that was inferred for Nisku HRGM anomalies according to Model 1A. The only difference between Models 1A and 1B is the average grain size of the authigenic magnetic minerals in the magnetically enhanced zones. In Model 1A, discussed for the Nisku above, the average magnetic grain size is about 10 μm , and the coarsest multidomain grains (>10 μm) record the PADF direction ($D/I = 0^\circ/+68^\circ$) over the past 10^4 to 10^6 yr. In Model 1B, the average grain size is >10 μm , and the coarsest multidomain grains record the PF direction ($D/I = 18^\circ/+75^\circ$) over the past $<10^2$ yr. The paleomagnetically determined 57-Ma age for the Nisku (east-northeast azimuth) HRGM anomalies according to Model 1A is the same as the 57-Ma age for the Leduc (east-southeast azimuth) HRGM anomalies according to Model 1B. This suggests that microseepage from Leduc and Nisku reservoirs may have occurred at the same time (a 10-m.y. pulse centered on 57 Ma) but that microseepage was volumetrically greater above Leduc than above Nisku reservoirs.

An alternative (Model 1A, shown in Figure 20b) origin for Leduc HRGM anomalies is that they reflect Pulse 2 (middle Tertiary) fracturing of the seal of the Duvernay Petroleum System during a 10-m.y. pulse of microseepage

centered on 30 Ma. Microseepage associated with Pulse 2 fractures may have been more intense than during Pulse 1, because Pulse 2 fractures propagated at the time of maximum overpressure in the fully charged Duvernay Petroleum System, shortly after maximum burial. This could partly explain the five-times-stronger HRGM anomaly intensity above Leduc than above Nisku reservoirs. In the Piceance Basin, Pulse 2 fractures and associated microseepage are indicated in Figure 20a by the fluctuations in the blue curve (“fracture permeability in seal”) and in the purple curve (“overpressure history”). These fluctuations reflect the dynamic and cyclic processes involved in fracturing and overpressuring, as discussed by Payne et al. (2000). In particular, the spikes in the overpressure curve (purple) and in the seal-fracture curve (blue) correlate with times when different stacked reservoirs (deep, intermediate, and shallow) successively exsolve methane by pressure reduction on uplift. Note that different reservoirs exsolve methane at different times over about a 10-m.y. interval, as indicated by the three red curves (“exsolved methane in gas phase”), labeled “deep” (analogous to Leduc), “intermediate,” and “shallow” (analogous to Cretaceous). Onset of this probably more intense Pulse 2 fracturing and microseepage occurs at about 32 Ma in the Piceance Basin simulation, which correlates well with the 30-Ma paleomagnetically inferred age for “Leduc” HRGM anomalies according to Model 1A (Appendix D).

Regardless of whether Leduc HRGM anomalies are explained by Models 1A or 1B, it seems clear that Leduc HRGM anomalies have formed at the expense of Nisku

TABLE 3. Paleomagnetically inferred HRGM anomaly ages[†] according to four models.

Reservoir	10-m.y. pulse		Constant flux	
	PADF Model 1A	PF Model 1B	PADF Model 2A	PF Model 2B
Nisku	57	X _C	64	X _C
Leduc	30	57	X _C	64
Cretaceous	17	X _C	17	X _C
Alida	X _A	7	X _A	7

[†]Ages (Ma) represent either the centers of 10-m.y. pulses (Models 1A and 1B) or microseepage initiation ages for the constant-flux models (Models 2A and 2B).

X_C = Model cannot explain HRGM anomalies, either because no Tertiary reference remagnetization circles pass through the HRGM anomaly clusters (for Nisku or Leduc) or because model fails to predict the observed girdle distribution of HRGM anomaly directions (for Cretaceous).

X_A = Model cannot explain HRGM anomalies (for Alida), because the Δ antiparallel angle for the late Tertiary reference remagnetization circles is $<3^\circ$ and hence would preclude the good clustering of HRGM anomaly azimuths observed above Alida reservoirs.

HRGM anomalies. Nisku and Leduc HRGM anomalies both reflect microseepage from the same (Duvernay) petroleum system, but microseepage from Leduc pinnacle reefs was more intense and volumetrically greater, resulting from both higher overpressure and higher storage capacity in Leduc pinnacle reefs compared with Nisku biostrome reservoirs. Because Nisku reservoirs of this study are drape traps over Leduc pinnacle reefs, Leduc HRGM anomalies (i.e., with east-southeast azimuths) would have been superimposed on and would have obliterated preexisting “Nisku” HRGM anomalies (i.e., in their same vertical-migration path). This interpretation has important exploration significance because it implies that Nisku HRGM anomalies (i.e., with east-northeast azimuths) would be observed only at locations where underlying Leduc reservoirs are absent. This may explain why, in the case-history 5 Nisku biostrome area, all oil production from Devonian reservoirs is from the Nisku, no Leduc reservoirs have been discovered despite numerous Leduc tests, and we observed no Leduc HRGM anomalies with east-southeast azimuths. However, in the case-history 4 area at the Rumsey reef, the prolific Leduc reservoir is overlain by a Nisku reservoir that was also prolific, but only a Leduc HRGM anomaly with east-southeast azimuth was observed, rather than a Nisku HRGM anomaly with an east-northeast azimuth.

Although Nisku HRGM anomalies must have formed during Pulse 1 and Leduc HRGM anomalies could have formed during either Pulse 1 or Pulse 2, Cretaceous HRGM anomalies must have formed during Pulse 2 (Appendix D). Microseepage above the Cretaceous reservoirs reflects degassing (i.e., methane exsolution) upon isostatic uplift after maximum burial. Payne et al. (2000, p. 560–561) described this process (see green and red methane curves in Figure 20a) as follows:

Starting at about 52 Ma, after incipient maturation of the underlying source rock, gas is initially transported into the sandstone dissolved in pore fluids. Aqueous methane concentration increases as more gas is generated by maturing source rocks, and as pore fluid migrates upward into the sandstone from compacting and overpressuring source rocks below. Aqueous methane concentration continues to increase until its peak at about 25 Ma. At this time, aqueous methane concentration begins to decrease and the free gas phase forms. The gas phase is exsolving from the aqueous phase because uplift and erosion are decreasing the confining stresses and decreasing the solubility of the gas in the aqueous phase. Aqueous methane continues to decline for the remainder of the simulation, and gas saturation is maintained at about 20%.

Methane exsolution upon postorogenic uplift almost

certainly explains the initiation of microseepage-related dipolar HRGM anomalies above Cretaceous reservoirs of the Alberta Basin. In fact, most of the 55 HRGM anomalies associated with Cretaceous producers (Figure 14 and Table 2) are from reservoirs in the Colorado Group and Upper Mannville Group. These reservoirs are part of the “Colorado Aquitard” (hydrogeologic group) and “Erosional Rebound System” (fluid-dynamic system) of Tóth and Corbet (1987), who discussed the evolution of groundwater flow systems in the Taber and Cypress Hills region of southeast Alberta. Within the Colorado Aquitard and Erosional Rebound System, “elastic rebound [in] its shales in response to erosional unloading . . . reduced pressures in the aquitard . . . [and] induced gas to exsolve and accumulate in the sands” (Tóth and Corbet, 1987). As illustrated in Figure 21, Tóth and Corbet (1987) attributed gas exsolution in the Erosional Rebound System to 700 m of uplift that occurred in the past 10 m.y.; of this total, 500 m of uplift may have occurred in the past 2 m.y. This renewed uplift marks the end of the Cypress Plain, which is thought to have existed for 30 m.y. and which was described by Tóth and Corbet (1987, p. 62–63) as follows:

The Cypress Plain, which represents the first recorded major break in uplift since the Rocky Mountains formed, probably developed by late Eocene or Oligocene time and existed at least until early Miocene time, and possibly until a major uplift occurred near the end of Miocene time roughly 5 Ma. . . . This surface lasted for a much longer time than other post-Palaeocene surfaces and thus was able to exert a dominant influence on the distribution of coal rank.

In Figure 21, the dashed line marking the end of the Cypress Plain begins at 17 Ma, which is remarkably close to the paleomagnetically inferred 17-Ma age for HRGM anomalies above Cretaceous reservoirs, as discussed in Appendix D. Our Alberta Basin study area is on the same uplift contour (2500 m of eroded overburden; Figure 33.15 of Smith et al., 1994) as the Taber area studied by Tóth and Corbet (1987), so the uplift history in the Taber area should be applicable to our central Alberta study area. It is beyond the scope of this paper to resolve the discrepancies among the 700 m of post-Cypress Plain uplift discussed by Tóth and Corbet (1987), the 1200 m of uplift indicated near Drumheller in Figure 24.23 of Dawson et al. (1994), and the 2500 m of uplift in our area indicated in Figure 33.15 of Smith et al. (1994). We merely note that at least 700 m of uplift almost certainly occurred after microseepage was initiated from Nisku and Leduc reservoirs, and probably also from Cretaceous reservoirs. This 700 m of uplift, together with our 150-m depth-to-source estimate for the HRGM anomalies and preservation of 57 Ma CRM above Nisku reservoirs,

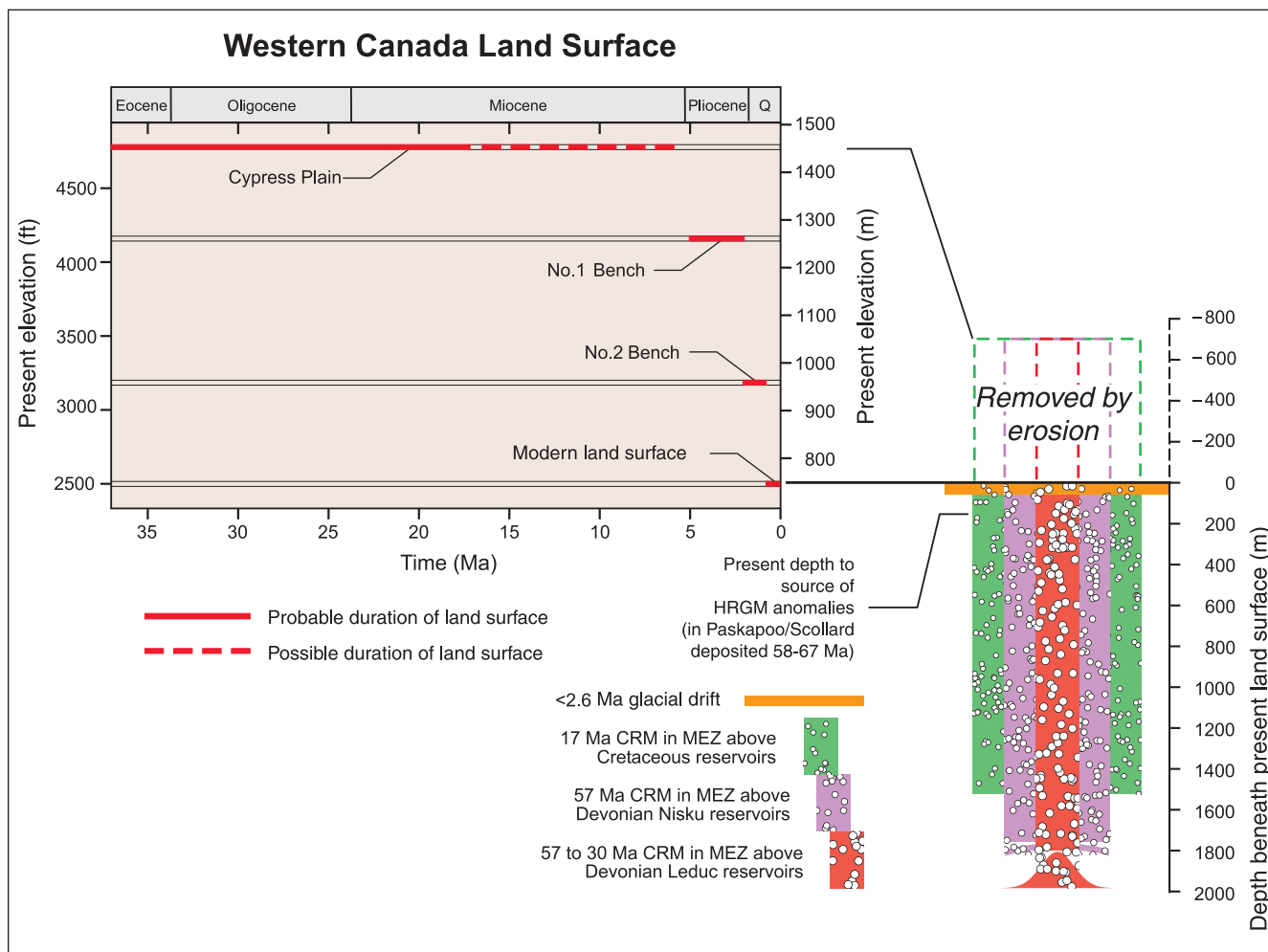


FIGURE 21. Left = duration and elevation of post-Paleocene land surfaces (modified from Tóth and Corbet, 1987). Right = relative timing and depth relationships inferred for HRGM anomalies in the vicinity of a 200-m-diameter Leduc pinnacle reef at a depth similar to the Rumsey reef (case history 4). Note that 500 m of the geochemical chimney has been eroded probably in the past 2 m.y., and 700 m has been eroded since the end of the Cypress Plain. MEZ = magnetically enhanced zone; CRM = chemical remanent magnetization.

strongly suggests that the HRGM anomalies we measured in Western Canada are sourced in vertical geochemical chimneys along which hydrocarbon gases promoting chemical remagnetization have migrated.

In summary, interpretation of the HRGM anomaly azimuths in the context of the Alberta and Piceance Basin histories yields the following conclusions:

- 1) Nisku HRGM anomalies exhibiting east-northeast azimuths probably reflect acquisition of reversed-polarity CRM during a 10-m.y. microseepage pulse centered on 57 Ma (early Tertiary), when late-Laramide fractures broke the seal of the Duvernay Petroleum System hosting Nisku and Leduc reservoirs.
- 2) The strong Leduc HRGM anomalies exhibiting east-southeast azimuths may also reflect acquisition of this same reversed-polarity CRM during this same 10-m.y. pulse centered on 57 Ma. However, higher
- 3) Alternatively, the strong Leduc anomalies could be interpreted as reflecting the acquisition of reversed-polarity CRM during rapid methane exsolution in the Duvernay Petroleum System, triggered by post-orogenic isostatic uplift. Dipolar HRGM anomalies with east-southeast azimuths could have formed during a 10-m.y. microseepage pulse centered on 30 Ma (middle Tertiary).
- 4) The Cretaceous HRGM anomalies were the last to form, and their weakness partly reflects lower-pressure, less-voluminous microseepage driven by meth-

methane flux from more voluminous Leduc pinnacle-reef reservoirs may have increased the average grain diameter of authigenic magnetic minerals in magnetically enhanced zones above Leduc reservoirs. This increase in magnetic grain size can explain the 59° difference between Nisku HRGM anomaly azimuths (averaging 61°) and Leduc HRGM anomaly azimuths (averaging 120°).

ane exsolution upon uplift at about 17 Ma. The Cretaceous reservoirs beneath most of the Cretaceous HRGM anomalies of this study are part of the Erosional Rebound System (Tóth and Corbet, 1987), in which methane exsolution upon uplift is thought to have occurred. The paleomagnetically inferred 17-Ma age of Cretaceous HRGM anomalies may be recording the renewed late Tertiary uplift marking the end of the Cypress Plain.

- 5) At least 700 m of late Tertiary to Quaternary uplift occurred over our Alberta Basin study area, 500 m of which may have occurred in the past 2 m.y. This, in conjunction with preservation of a 57-Ma reversed-polarity CRM above Nisku reservoirs and a 150-m average depth to source of the HRGM anomalies, strongly suggests that the HRGM anomalies are sourced in erosionally truncated geochemical chimneys along which chemical remagnetization has occurred during hydrocarbon microseepage.

Possible Relationships among HG' Values, Reservoir Geometry, and HRGM Anomaly Depths

In this study, we used the second horizontal derivative (HG') as a proxy for HRGM anomaly intensity, mostly for statistical convenience in being able to relate each well to a single HG' value rather than to two intensity (nanotesla, or nT) values for the dipolar anomalies. Strictly speaking, however, HG', because it is the *second horizontal derivative of the residual magnetic anomaly*, is related to curvature of the residual anomaly in map view. As discussed below, the decreasing trend in HG' values above Leduc > Alida > Nisku > Cretaceous reservoirs could be interpreted as reflecting decreasing curvature or increasing depth to source of the magnetically enhanced zones.

If vertical microseepage truly has occurred, we would expect the boundaries of a magnetically enhanced zone to approximate the boundaries of a microseeping reservoir, in map view. Thus, the decrease in HG' values from Leduc pinnacle-reef reservoirs to Mississippian cuesta reservoirs to Nisku biostrome reservoirs to Cretaceous blanket/channel-sand reservoirs could be mimicking the decrease in 3-D or "Gaussian curvature" (Lisle, 1994) of these reservoir shapes. This HG' trend might also reflect a decrease in fracture density as the curvature of the reservoir decreases. Many workers have noted that high fracture density is associated with high curvature and high rate-of-dip change, such as on plunging folds (Narr, 1991; Lisle, 1994; Hennings et al., 2000). Around pinnacle reefs Saunders et al.'s (2002) observation of apical radiometric anomalies and Sikka and Shives' (2002) observation of thorium anomalies may reflect an increased density of differential-compaction-related faults and frac-

tures around pinnacle reefs. Thus, the association between strongest HRGM anomalies, as measured by HG', and reservoir geometry (curvature) further suggests that a vertical fracture/microfracture network is the key to formation of strong magnetic and geochemical anomalies above microseeping reservoirs.

The decrease in HG' in the order Leduc > Alida > Nisku > Cretaceous, could also be interpreted as reflecting an increase in depth to source of the HRGM anomalies (i.e., increasing depth to the magnetically enhanced zones). Second derivatives are a measure of curvature, and large curvatures are to be expected for shallow anomalies (Telford et al., 1990, p. 32). In mapping gravity or magnetic anomalies, second derivatives are commonly used to enhance near-surface anomalies at the expense of deeper anomalies. Because the magnetic field satisfies Laplace's equation, by knowing the second horizontal derivative of the residual magnetic anomaly, we also know the second vertical derivative of the residual magnetic anomaly. Thus, the monotonic decrease in HG' values might indicate that magnetically enhanced zones are shallowest above Leduc, somewhat deeper above Alida, even deeper above Nisku, and deepest above Cretaceous reservoirs. This trend might be expected regardless of whether the HRGM anomalies are sourced in magnetically enhanced vertical chimneys or in magnetically enhanced horizontal lenses or sills. Perhaps greater flow rates of more-buoyant microbubbles emanating from deeper, higher-pressure reservoirs have transported greater amounts of gaseous hydrocarbons into magnetically enhanced zones at higher, near-surface structural levels.

Any relationship between depth to source and intensity of HRGM anomalies would also be affected by the relative amounts of postremagnetization subsidence versus uplift. For example, *if post-CRM uplift is greater than post-CRM subsidence* (e.g., Figure 20b), then geochemical chimneys would all be eroded to the same present-day level. In this case, HRGM anomalies might all originate at the same present-day depth and might have nearly equal intensities, as measured at the present surface. On the other hand, *if post-CRM subsidence is greater than post-CRM uplift*, then older chimneys (e.g., above Nisku reservoirs at 57 Ma, before maximum burial) may have deeper present-day tops than younger chimneys (e.g., above Leduc reservoirs at 30 Ma, after maximum burial). In this case, the tops of chimneys above Nisku reservoirs would be farther from a magnetometer at the present surface than would the tops of chimneys above Leduc reservoirs, so Leduc HRGM anomaly nanotesla and HG' values would be much larger than the values for Nisku anomalies.

Resolving these and other mysteries of the hydrocarbon microseepage phenomenon must await direct paleomagnetic and rock-magnetic studies of cores taken along the entire plumbing system, from hydrocarbon source rock to reservoir rock to magnetically enhanced zones.

Postmortem for Three Nonproductive Wells

The importance of being able to resolve the residual anomalies into dipolar lobes from which azimuths can be determined is demonstrated by our experience with three nonproductive wells in Western Canada. These three wells had been drilled *before* we appreciated the diagnostic value of the distinctive anomaly azimuths. All three were drilled in areas that we had already surveyed.

The first two of the nonproductive wells were drilled in the Williston Basin to explore for Frobisher-Alida (Mississippian) reservoirs in the Arcola area of southeastern Saskatchewan. One of our clients drilled one of these wells, and another company that outbid our client at the land sale drilled the other well. At both locations, adequate 2-D seismic profiles were available. At our lease, a seismically defined structure seemed to be present at the Mississippian level, beneath the surface location of our magnetic and radiometric anomalies. On drilling, no Mississippian structure or hydrocarbons were found. Presumably, this was also the case for the nearby well drilled by the other company, for it also abandoned its well.

When these two wells were drilled, in 1993 and 1994, it had generally been thought that no hydrocarbons would be found by drilling below the Mississippian in this part of the Williston Basin. A few years later, some significant discoveries were made by drilling deeper, in the nearby Mississippian Midale field, into the Ordovician Yeoman Formation (Yurkovich and Sitzler, 1997). After the nearby Ordovician discoveries were made, we reexamined our magnetic survey to determine the azimuths of the dipolar residual anomalies. To our surprise, they showed azimuths distinctly different from those shown in Figure 16c and attributed to Mississippian formations. Whether these anomalies reflect microseepage from Ordovician or other reservoirs cannot be ascertained until we conduct HRGM surveys over producing wells in this area from reservoirs deeper than the Mississippian. With regard to the seismic anomaly we saw at our well, it was real, but it did not derive from structure at the Mississippian level. Presumably, this seismic anomaly and the one that the other company drilled reflect velocity increases caused by diagenetic cements produced by upward-leaking hydrocarbons from some deeper formation, as Davis (1972) and Saunders et al. (1999) have suggested.

The third unsuccessful well, drilled in 1996, was exploring for a Leduc reef reservoir in the Alberta Basin. Our magnetic HRGM anomaly coincided with a seismically defined structure of similar areal extent at the Leduc level that was defined by a 2-D seismic "swath" shoot with ~200-m line spacing. On drilling, no Leduc reef buildup was encountered. What was encountered was ~3 m of oil staining in each of the following Upper Devonian units: Stettler dolomite at 1425 m, Nisku dolomite at

1620 m, and Camrose Member dolomite at 1637 m. In a zone 70 m thick above the Stettler, unusually high concentrations of pyrite (?), suggestive of microseeping hydrocarbons, were observed in the cuttings. Although all three units are occasionally productive, in this case, they were not. Presumably, anomalous increases in seismic velocities caused by diagenetic cementation also occurred in this area and produced a seismic anomaly that had been mistaken for a Leduc anomaly. After the well was abandoned, another seismologist reexamined the original seismic data and concluded that no seismic structural anomaly is present at the Leduc level.

After we became aware of the significance of the dipolar residual anomaly azimuths (LeSchack, 1997), we reexamined our magnetic survey data at this well location. The HRGM anomaly azimuth is significantly different from anomaly azimuths at the five wells (Figure 17) that produced hydrocarbons from the Leduc. Thus, in hindsight, we would not have predicted a Leduc discovery at the location of this third unsuccessful well.

General Comments on Ground-based versus Airborne Magnetic/Radiometric Surveys

Much of the impetus for developing our ground-based HRGM survey techniques, beginning in 1990, came from earlier successes in the 1980s with airborne radiometric and magnetic surveys. After nearly a decade of conducting HRGM surveys in Western Canada, we think it would be instructive to make some general observations about the value of ground-based versus airborne surveys for hydrocarbon exploration.

Airborne and ground-based surveys each have advantages and disadvantages. The chief advantage of airborne surveys is that they cover vast areas more quickly than can be done on the ground, especially in remote or hostile locations. Moreover, the costs for an airborne survey are less than the costs for a ground-based survey *per unit area*, although mobilization costs are higher for airborne surveys. The main disadvantage of airborne surveys is their lower signal-to-noise ratio, because the magnetometers and gamma-ray spectrometers are farther from the source of the anomalies. This partly explains why airborne magnetic surveys have failed to observe the dipolar magnetic anomalies that we consistently observe in our ground-magnetic surveys in Western Canada.

The chief advantages of ground-based surveys are their higher signal-to-noise ratio and the opportunity to check for, avoid, and correct for cultural interference from buried pipelines and magnetic infrastructure. The disadvantages of ground-based surveys are the higher cost per unit area and accessibility problems in remote or hostile locations. In our case histories in Western Canada, most of the survey areas are on open farm or rangeland, so accessibility has not been a significant problem.

Based on comparison tests we have made between airborne and ground-based radiometric surveys, we conclude that airborne radiometric surveys, although useful for reconnaissance, are of marginal value for detailed hydrocarbon exploration. In Western Canada, we found that the footprint of airborne radiometric surveys is generally far too large to delineate the typically ~300-m-wide radiometric anomalies above channel-sand reservoirs and the typically ~250-m-diameter halo radiometric anomalies around pinnacle-reef reservoirs.

On the other hand, we have been more impressed by the value of high-resolution aeromagnetic (HRAM) surveys, especially when they are used to target subsequent higher-resolution ground-magnetic (HRGM) surveys. Below, we compare our HRGM surveys with HRAM surveys flown over central Alberta, including direct ground confirmation of a specific HRAM anomaly. This comparison reveals how aeromagnetic and ground-magnetic surveys can be used together, advantageously and cost-effectively, for hydrocarbon exploration.

Statistical Comparison of HRGM and HRAM Anomalies in Central Alberta

As a check on the resolution and sensitivity of our ground-based surveys versus aeromagnetic surveys, we now compare the statistical distribution of 97 HRGM anomalies we measured in central Alberta that are associated with known producing or D&A wells against an HRAM survey flown over nearly the same area and with similar geology. This HRAM survey was flown at an altitude of 120 m, used flight-line spacings of 800 and 1600 m, and covered 25 townships (2330 km²). This survey was interpreted by R. S. Foote (using the method described in Foote, 1992), who identified 315 HRAM anomalies in the survey area. Foote (1996) nicely illustrates other examples of HRAM anomalies over hydrocarbon reservoirs.

In Figure 22, we constructed histograms comparing the intensities of Foote's 315 HRAM anomalies against the 97 HRGM anomalies we measured from 50 sections (130 km²) in nearly the same area. This comparison reveals that a lognormal (Figure 22d) rather than a normal probability density function (Figure 22c) is a much better fit to the 315 HRAM anomalies, just as it is for the 97 HRGM anomalies. The similar histogram shapes and lognormal probability distributions revealed in Figure 22 strongly suggest that the aeromagnetic HRAM and ground-based HRGM surveys are both magnetically detecting geochemical changes caused by the same physical phenomenon. This in turn suggests that the lognormal distribution of 315 HRAM anomalies may also be a composite of separate lognormal distributions, like the "classes" (i.e., Leduc, Nisku, Cretaceous, D&A) we recognized in the distribution of HG' values.

In Figure 22e, we fitted the lognormal probability

density function derived from the 92 non-Leduc HG' values (Figure 22b) to the lognormal probability density function derived from Foote's 315 HRAM anomalies (Figure 22d). Figure 22e, which is a double-abscissa/double-ordinate plot, allows us to relate threshold values we previously discussed and measured in "lognormal HG' space" with threshold values we would predict in "lognormal HRAM space." For example, the HG' = 1.1 threshold value for a Nisku reservoir (Nisku geometric mean divided by geometric standard deviation; Table 2) is close to the log HG' = 0.0 value at the peak of the bell curve in lognormal HG' space. Thus, by analogy, we predict that the Nisku threshold in lognormal HRAM space would also be at the peak of the HRAM lognormal curve, which occurs at log HRAM = -0.22, corresponding to an HRAM intensity of 0.60 nT (i.e., the antilog of -0.22). This suggests that 0.6 nT is a good value to use for a Nisku HRAM threshold.

Similar calculations can be performed to derive a "Cretaceous HRAM threshold." The HG' = 0.53 threshold value for a Cretaceous reservoir (Cretaceous geometric mean divided by geometric standard deviation; Table 2) corresponds to -0.27 in lognormal HG' space, which in turn corresponds to -0.4 in lognormal HRAM space. This suggests that 0.4 nT (= antilog of -0.4) is a good value to use for a Cretaceous HRAM threshold.

The *weakest* Leduc HG' anomaly (HG' = 6.3; log[6.3] = 0.80) projects to an abscissa value of 0.4 in lognormal HRAM space, corresponding to an HRAM intensity of 2.5 nT (= antilog of 0.4). The *strongest* Nisku anomaly (HG' = 5; log[5] = 0.70) projects to an abscissa value of 0.33 in HRAM lognormal space, corresponding to an HRAM value of 2.1 nT (= antilog of 0.33). Of the 315 HRAM anomalies, the highest HRAM intensity is 2.2 nT, which is slightly higher than the HRAM value we would predict for a microseeping Nisku reservoir, but slightly lower than the HRAM value we would predict for a microseeping Leduc reservoir.

This HRGM versus HRAM comparison suggests one of two possibilities. (1) The HRAM survey may have completely missed all Leduc pinnacle-reef anomalies (because the 800- and 1600-m flight-line spacings were too large to detect 75- to 400-m-diameter pinnacle reefs). (2) Alternatively, the HRAM survey may just have begun to detect the weakest Leduc pinnacle-reef anomalies, which might have the greatest areal extent (because microseepage above large-diameter pinnacles would probably be less focused, yielding more diffuse magnetically enhanced zones).

In either case, the above example demonstrates how aeromagnetic HRAM surveys can be used to guide the more site-specific, ground-based HRGM surveys, which then can be used to better define a prospect and to estimate, by the residual anomaly azimuth, the reservoir formation responsible for the anomaly. In central Alberta, where our HRGM and Foote's HRAM surveys were con-

ducted, Nisku reservoirs invariably overlie Leduc reef buildups (Figure 12.32b of Switzer et al., 1994; Figure 15 of Podruski et al., 1987). Thus, the strong indications of Nisku anomalies in the aeromagnetic data, as indicated by numerous HRAM anomalies > 1 nT, imply that underlying Leduc pinnacle-reef reservoirs are probably also present. If the aeromagnetic survey had been flown with a flight-line spacing of 400 m, rather than the actual 800-m and 1600-m line spacings, strong (2.5 to 4 nT) HRAM anomalies presumed to be associated with Leduc reservoirs might have been observed. Most Leduc pinnacle-reef reservoirs, which can be prolific producers, are less than 800 m in diameter, and they could easily have been missed because of the wide flight-line spacing in the HRAM survey.

Investigation of an HRAM Anomaly by HRGM Survey Techniques

We conducted a proprietary HRGM survey to evaluate more definitively one of Foote's 315 HRAM anomalies in central Alberta. This HRAM anomaly's intensity (1.2 nT; $\log \text{HRAM} = 0.08$) lies near the high end of values we infer to be associated with microseeping Nisku reservoirs, based on the Figure 22e histogram. Our radiometric survey, as well as free-gas (von der Dick et al., 2002) and microbial (Hitzman et al., 2002) surveys conducted over this anomaly, also support the presence of microseeping hydrocarbons at this location.

With its higher spatial resolution, our ground-magnetic survey revealed that the single, unimodal HRAM

anomaly actually consists of two separate, *dipolar* HRGM anomalies: one large-diameter, lower-intensity, dipolar HRGM anomaly and a much-smaller-diameter, higher-intensity, dipolar HRGM anomaly. The broader, weaker anomaly has an HG' value of 4.0 ($\log HG' = 0.6$), and the sharper, stronger anomaly has an HG' value of 7.3 ($\log HG' = 0.9$). Based on the lognormal HG' probability density functions (Figures 14 and 22), the broader, weaker HRGM anomaly is inferred to reflect microseepage from a Nisku reservoir, and the sharper, stronger HRGM anomaly is inferred to reflect microseepage from a Leduc pinnacle-reef reservoir. This is further suggested by the different azimuths computed from the dipolar residual anomalies: the broader, weaker HRGM anomaly yields a Nisku azimuth, whereas the sharper, stronger HRGM anomaly yields a Leduc azimuth when compared with the "distinctive anomaly clusters" in Figure 17. For the sharper, stronger anomaly, therefore, the combination of high HG' value and distinctive anomaly azimuth both suggest that a microseeping Leduc pinnacle-reef reservoir lies beneath the stronger HRGM anomaly. Of course, this can be verified only by drilling.

This example demonstrates the synergy between airborne and ground-based magnetic exploration techniques. We probably would not have found the Leduc pinnacle-reef prospect without having first noticed the relatively strong (1.2-nT) HRAM anomaly on the aeromagnetic survey. By targeting our HRGM survey over the 1.2-nT HRAM anomaly, the higher signal-to-noise ratio and higher spatial resolution in our ground-based survey were able to resolve the unimodal HRAM anomaly into

FIGURE 22. Statistical comparisons between 97 HG' values derived from our ground-based surveys and 315 HRAM anomalies derived from aeromagnetic surveys flown over nearly the same area in central Alberta. The HG' values, which are the same data as in Figure 14, are derived from a 50-section (130-km²) area. R. S. Foote interpreted the 315 HRAM anomalies from airborne surveys over 25 townships (2330 km²) in an area near and geologically similar to the area we surveyed on the ground.

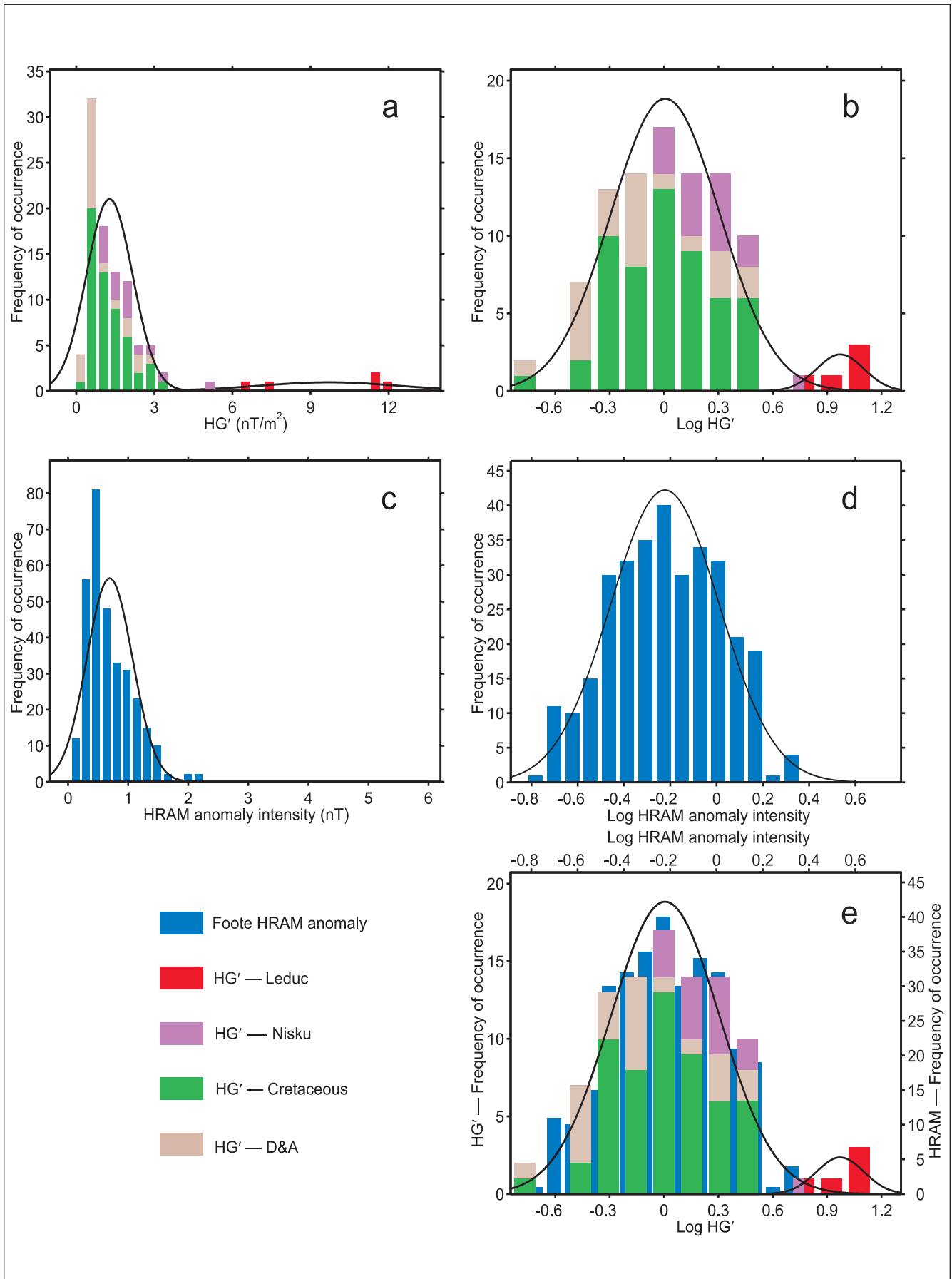
(a) All 97 HG' values plotted in normal HG' space segregated into the four well classes on a stacked-bar histogram. The histogram is overlain by two bell curves, both of which assume normal probability density. One curve is calculated from all 92 non-Leduc HG' values, and the other curve is calculated from the five Leduc HG' values. Note the poor fit of the actual HG' values to the non-Leduc bell curve.

(b) All 97 HG' values plotted in lognormal HG' space segregated into the four well classes on a stacked-bar histogram. The histogram is overlain by two bell curves, both of which assume lognormal probability density. One curve is calculated from all 92 non-Leduc HG' values, and the other curve is calculated from the five Leduc HG' values. Note the much better fit of the *logs* of the 92 HG' values to the bell curve and the indications that the five Leduc values are from a separate lognormal distribution.

(c) All 315 of Foote's aeromagnetic HRAM anomalies, plotted in normal HRAM space. The histogram is overlain by a bell curve calculated from all 315 values, assuming they are derived from a normal probability distribution. Note the poor fit of the actual HRAM values to the bell curve.

(d) All 315 of Foote's aeromagnetic HRAM anomalies plotted in lognormal HRAM space. The histogram is overlain by a bell curve calculated from all 315 values, assuming they are derived from a lognormal probability distribution. Note the much better fit of the *logs* of the HRAM values to the bell curve.

(e) Fitting the lognormal probability density curve derived from the 92 non-Leduc HG' values (22b) to the lognormal curve derived from the 315 HRAM anomalies (22d) allows us to use the HRAM data as a guide for targeting ground-based magnetic exploration for specific reservoirs. Note that the aeromagnetic HRAM survey apparently missed all the high values associated with Leduc pinnacle-reef reservoirs, probably because the 800-m and 1600-m flight-line spacings are larger than the typical diameter of Leduc pinnacle reefs.



two different dipolar HRGM anomalies. If a well location had been chosen solely on the basis of the aeromagnetic survey, it would fall *between* the two HRGM anomalies resolved on the ground and hence would miss the Leduc pinnacle reef. By resolving the HRGM anomalies into their dipolar components, we not only can target well locations more precisely, but also can determine how deep to drill (i.e., by inferring the microseeping reservoir formations, based on determining the residual anomaly azimuths connecting the positive and negative lobes of the anomalies).

In summary, hydrocarbon-microseepage-related magnetic anomalies can be detected by aeromagnetic HRAM surveys, although not with the sensitivity and spatial resolution obtainable by ground-based HRGM surveys. Aeromagnetic surveys might begin to have the spatial resolution of our HRGM surveys if the flight-line spacing is no more than 400 m, which allows pinnacle-reef reservoirs to be detected. Apparently, HRAM surveys conducted in the past did not have sufficient resolution to be able to map dipolar anomalies. R. S. Foote (personal communication, 1996), who has conducted numerous HRAM surveys, including the Alberta example discussed above, states that he has not observed positive and negative lobes of individual HRAM anomalies, only a unimodal resultant anomaly. P. Eick (personal communication, 1997) reported only hints of dipolar HRAM anomalies in aeromagnetic surveys flown over the Alaskan North Slope. Thus, the increased spatial resolution and higher signal-to-noise ratio obtainable with ground-based HRGM surveys are required to be able to resolve microseepage-related anomalies into dipoles, from which distinctive anomaly azimuths with diagnostic value can be calculated.

Implications of Dipolar HRGM Anomalies for Worldwide Hydrocarbon Exploration

At the outset of this discussion, we said that our goal was to synthesize our empirical observations derived from two disparate technologies pertaining to hydrocarbon exploration by magnetic methods: (1) high-resolution ground-magnetic (HRGM) surveys conducted over hydrocarbon reservoirs and (2) paleomagnetic studies of surface-outcrop and subsurface-core samples of hydrocarbon reservoir rocks.

In the six case histories discussed in this paper, we have presented evidence for more than 100 dipolar magnetic (HRGM) anomalies directly overlying productive hydrocarbon reservoirs in the Alberta and Williston Basins of Western Canada. These dipolar HRGM anomalies appear to originate in near-surface (about 150-m-deep) concentrations of authigenic magnetic minerals, which we refer to as magnetically enhanced zones. By connecting the positive with the negative lobes of the dipolar anomalies, we observe distinctive HRGM anom-

aly azimuths that are diagnostic of the microseeping reservoir formation. The azimuths of the dipolar HRGM anomalies are generally at high angles to the present magnetic-field direction, indicating that they record a major component of reversed-polarity chemical remanent magnetization (CRM).

Using the science of paleomagnetism, we can infer an early Tertiary (57-Ma) age for the reversed-polarity CRM in magnetically enhanced zones above Nisku (Upper Devonian) reservoirs of the Duvernay Petroleum System. We also infer a 57-Ma age for the reversed-polarity CRM we observed in our paleomagnetic studies of subsurface Devonian cores from the Duvernay Petroleum System. In cores from deep within hydrocarbon reservoirs, the CRM intensity is generally low, magnetic susceptibility commonly exhibits *negative* values, and magnetic mineral concentrations are generally in trace amounts of only a few ppm.

By combining our ground-magnetic-survey data *over* hydrocarbon reservoirs with our paleomagnetic data from reservoir rocks *within* hydrocarbon reservoirs, we are beginning to see the broad outlines of a pattern with important implications for hydrocarbon exploration. Geochemical changes recorded in magnetically *enhanced* zones in the *near surface* appear to be linked with geochemical changes recorded in magnetically *depleted* zones within hydrocarbon reservoirs *at depth*. The magnetically enhanced zones and magnetically depleted zones are probably connected by geochemical chimneys and vertical fracture networks, along which microbubbles carrying iron (Fe) have risen buoyantly. This Fe was probably leached from the reservoir and wall rocks by organic acids (Shock, 1988; Surdam et al., 1989, 1993) to be reprecipitated as authigenic magnetic iron oxides (magnetite, maghemite) or magnetic iron sulfides (pyrrhotite, greigite) in the near-surface magnetically enhanced zones. Thus, the short-spatial-wavelength magnetic anomalies detected in HRGM and HRAM surveys probably indirectly detect geochemical changes in the hydrocarbon reservoirs at depth. Moreover, we are beginning to see how the hydrocarbon generation, methane dissolution/exsolution, fracturing, overpressure, and chemical remagnetization histories are probably intimately related. As illustrated in Figure 20, this is revealed by the remarkable similarities in timing between our paleomagnetic and HRGM observations in the Alberta Basin with fracture pulses in the reservoir seal in the Piceance Basin RTM simulation (Payne et al., 2000).

Dipolar HRGM anomalies above microseeping hydrocarbon reservoirs are probably not unique to Western Canada. The ubiquity of dipolar HRGM anomalies above hydrocarbon reservoirs in the Alberta and Williston Basins strongly suggests that the following two conditions are being met within the magnetically enhanced zones.

- 1) Tertiary (65- to 1.8-Ma) reversed-polarity chemical remanent magnetization (CRM) has been recorded by the growth of authigenic magnetic minerals with a grain size in the single-domain (0.05–1 μm) and pseudo-single-domain (1–10 μm) range.
- 2) A nearly equal balance (vector sum) has been achieved between this Tertiary reversed-polarity CRM and normal-polarity magnetizations acquired during the past $<10^6$ yr and residing in multidomain grains $>10 \mu\text{m}$.

The reversed-polarity CRM probably has integrated the geomagnetic field over millions of years, whether in a single 10-m.y. pulse of enhanced microseepage or at constant flux from the initiation of microseepage to the present. Since the beginning of the Tertiary at 65 Ma, there have been 175 reversals of the geomagnetic field, which separate “normal-polarity chrons” (black) from “reversed-polarity chrons” (white) on the magnetic-polarity time scale (Ogg, 1995). For more than 88% of Tertiary time (65 to 1.8 Ma), reversed-polarity chrons have been slightly longer than normal-polarity chrons, yielding a predominant “reversed-polarity bias” (Appendix B). The magnetic-polarity time scale is applicable worldwide, implying that reversed-polarity CRM in magnetically enhanced zones can generally be expected wherever microseepage has occurred during the Tertiary. This is probably the major reason why all of the more than 100 HRGM anomalies we observed in Western Canada are inferred to record reversed-polarity CRM. Moreover, if nearly equal balances of normal- and reversed-polarity components (condition 2, above) are as easy to achieve as the more than 100 dipolar HRGM anomalies of this study suggest, similar dipolar HRGM anomalies can be expected above microseeping hydrocarbon reservoirs anywhere in the world where microseepage occurred during the Tertiary.

Achieving a thorough understanding (by direct drilling) of the HRGM anomalies in Western Canada will undoubtedly have important implications for hydrocarbon exploration throughout the world. If CRM in hydrocarbon reservoirs is truly linked to CRM in magnetically enhanced zones, as the results of this study strongly suggest, then dipolar HRGM anomalies with diagnostic azimuths can be expected wherever we have observed reversed-polarity chemical remagnetization in paleomagnetic studies of hydrocarbon reservoir rocks. We know that early Tertiary, reversed-polarity CRM is pervasive in Lisburne Group carbonates of northeastern Alaska in the foreland of the Brooks Range, from the Sadlerochit Mountains to Prudhoe Bay (Van Alstine, 1986, 1987). In the Texas Gulf of Mexico coastal plain, Corbett et al. (1997) found a reversed-polarity, probably early Tertiary CRM residing in pyrrhotite and strongest in fractured Austin Chalk reservoirs. This reversed-polarity CRM might well be present along the entire Austin Chalk

trend. As a by-product of our paleomagnetic core-orientation work in the North Sea (e.g., Van Alstine and Butterworth, 1993), we have found reversed-polarity, early Tertiary CRM in the U.K., Danish, Dutch, and Norwegian sectors. This reversed-polarity CRM probably is associated with early Tertiary basin inversion and is capable of producing dipolar magnetic anomalies like those in Western Canada. We have also found reversed-polarity CRM in subsurface cores of hydrocarbon reservoir rocks in La Luna/Cogollo carbonates and Misoa sandstones of Lake Maracaibo, Venezuela, and in carbonates from the Gulf of Campeche, offshore Mexico.

The early Tertiary was an important time for tectonism, basin inversion, maturation and migration of hydrocarbons, and development of regional fracture systems that can extend hundreds of kilometers into forelands (Lorenz et al., 1991; Lorenz and Finley, 1991; Hanks et al., 1997). In the Laramide foreland of Western Canada, these regional fractures probably provided the vertical pathways connecting hydrocarbon reservoirs with magnetically enhanced zones far above the microseeping reservoirs.

CONCLUSIONS

From the six case histories presented in this paper, we conclude that the combination of ground-based magnetic and radiometric surveys is a highly successful, relatively inexpensive way to conduct exploration for hydrocarbons in Western Canada and probably elsewhere around the world.

At North and South Pierson, Manitoba, our pre-drilling HRGM and radiometric surveys demonstrate the efficacy of this combination of surface exploration technologies in the Williston Basin. Of the six wells that were subsequently drilled on HRGM and/or radiometric anomalies, all produced oil, and three new fields were discovered.

In the Williston Basin, ground-based *radiometric* surveys are best used for mapping potential drilling locations in channel sands in the lower Amaranth Formation. At the Waskada field, Manitoba, comparison of radiometric surveys with production histories from seven wells revealed good correlation between radiometric anomalies and lower Amaranth production. At South Pierson, the radiometric map was the sole basis for a successful exploration well.

In the Williston Basin, ground-based *magnetic* (HRGM) surveys are best used for mapping potential drilling locations in cuesta reservoirs (paleogeomorphic traps) in Mission Canyon Formation limestones beneath the sub-Mesozoic unconformity. At North Pierson, Manitoba, five wells were drilled on HRGM anomalies revealed by our surveys, and all five wells found oil, resulting in two new Mission Canyon pool discoveries. At the Was-

kada field, Manitoba, production history and well logs showed good correlation between cuesta morphology, as revealed by our HG' map, and production (or lack thereof) from the Mississippian limestones.

In the Alberta Basin, at the Leduc (Upper Devonian) Rumsey pinnacle reef, a prolific well that flowed spontaneously at as much as 4000 BOPD for 3 years was drilled near the center of the strongest HRGM anomaly we measured in Western Canada. Moreover, the reef boundary, as revealed by our HG' map, is congruent with the 3-D seismic survey of the reef. The radiometric anomalies are peripheral to the reef, as has been observed at other Leduc reef fields. This demonstrates that HRGM and radiometric surveys can be an efficient combination for locating small but prolific Leduc pinnacle reefs for further definition by more expensive 3-D seismic surveys.

Also in the Alberta Basin, at the Nisku (Upper Devonian) biostrome play, our magnetic HG' map delineated the biostrome as effectively as a 3-D seismic survey did, but at only 20% of the cost. Eighteen months after we completed our survey, the operator had drilled seven new wells based on the seismic data. After plotting the well locations on our magnetic HG' map, we predicted that the operator would encounter hydrocarbons in all seven wells. In fact, all seven wells proved to be producers. Whenever we discover magnetic HG' anomalies where the reservoir trap is also revealed by seismic surveys, *the seismic and magnetic HG' anomalies are nearly congruent*, as at the Rumsey reef.

In our surveys in Western Canada, in the Alberta and Williston Basins, we observe that the *strongest HRGM anomalies occur over reservoirs with the highest pressure*. In the Williston Basin, strong HRGM anomalies (average $HG' = 3.8$) occur over Mississippian limestone cuesta reservoirs that have a strong natural water drive. In contrast, *no* HRGM anomalies (only radiometric anomalies) occur over lower Amaranth sand-channel reservoirs that need artificial pressure maintenance to produce oil.

In the Alberta Basin, reservoir-pressure control on HRGM anomaly intensity is suggested by the monotonic decrease in average HG' values as a function of reservoir formation, depth, and production history. Average HG' values systematically decrease in the order:

- $HG' = 9.4$ above prolific Leduc pinnacle-reef reservoirs that are at depths of about 1900 m and that can flow spontaneously for years.
- $HG' = 1.8$ above less-prolific Nisku biostrome reservoirs that are at depths of about 1800 m and most of which need to be pumped to produce oil.
- $HG' = 1.0$ above still less prolific Cretaceous clastic reservoirs that are at depths of 600 to 1500 m and almost all of which need to be pumped.
- $HG' = 0.7$ above the least productive and D&A wells. The nonzero HG' values imply that oil is there, but it is neither easily nor economically producible.

This monotonic decrease in HG' values with inferred reservoir pressure, as well as the *lognormal* distributions of HG' values, the *lognormal* distributions of HRGM anomaly intensities, and the *lognormal* distributions of free-gas anomalies, suggests that *reservoir pressure* ultimately controls the concentration and grain size of authigenic magnetic minerals in the near-surface magnetically enhanced zones, which are the source of our HRGM anomalies and of Foote's HRAM anomalies in Western Canada.

The observed correlation between the strongest HRGM anomalies above the most prolific (Leduc) reservoirs probably reflects both (1) the focusing of ascending hydrocarbon microbubbles by the more nearly point-source pinnacle reefs and along reef-bounding faults and fractures, and (2) the higher pore pressure in the Leduc reef reservoirs, because of their being in contact with Duvernay source rocks and in hydraulic continuity with a major Upper Devonian regional aquifer (Cooking Lake Formation) through which hydrocarbons probably migrated during the late stages of the Laramide orogeny. Beneath the Cooking Lake Formation but still within the Duvernay Petroleum System, authigenic magnetite was being precipitated in Beaverhill Lake Group/Swan Hills Formation reservoirs to record a reversed-polarity, early Tertiary chemical remanent magnetization (CRM). This reversed-polarity CRM, which formed during the early Tertiary reversed-polarity-bias interval (63 to 41 Ma), was being acquired near (and just beyond) the time of peak oil generation and near the time (55 to 38 Ma) of the closest approach of the Laramide fold-thrust belt to our study area.

This coincidence of peak organic maturation, maximum depth of burial, and maximum horizontal compression from the approaching Laramide fold-thrust belt acted to increase regional pore pressure, thereby lowering effective stresses and facilitating propagation of regional, vertical fractures in the Laramide foreland. Above reservoirs in which oil was trapped during early Tertiary migration, a first pulse of buoyant hydrocarbon microbubbles began to rise along these regional, vertical microfractures. At near-surface levels, these hydrocarbon gases caused magnetic mineral authigenesis (by inorganic and/or biogenic processes) in magnetically enhanced zones, which also record the early Tertiary, reversed-polarity CRM. Later in the Tertiary, another generation of magnetically enhanced zones was produced during a second pulse of microseepage driven by methane exsolution triggered by pressure reduction during isostatic uplift. Within the magnetically enhanced zones, vector sums of Tertiary reversed-polarity-biased CRM + modern normal-polarity-induced and viscous remanent magnetization (VRM) yield shallow-inclination, eastern-hemisphere resultant vectors that are detected as *dipolar* residual anomalies in HRGM surveys.

Ultimately, the reservoir pressure and gas composi-

tion determine the total concentration of authigenic magnetic minerals, the magnetic mineralogy (magnetite, maghemite, pyrrhotite, greigite), the magnetic grain-size distribution, the reversed/normal-polarity ratio, and hence the *intensity and azimuths* of HRGM and HRAM anomalies originating in the magnetically enhanced zones.

For hydrocarbon exploration, the most important practical application of results of this study is our ability, based on the combination of the HG' value and distinctive residual magnetic anomaly *azimuth*, to identify the microseeping reservoir that instigated a specific HRGM anomaly. This implies that HRGM surveys can be used to determine not only *where* to drill but also *how deep* to drill. This ability of HRGM surveys to determine the microseeping reservoir formation is a unique ability among the currently available surface exploration techniques.

The dipolar HRGM anomalies described in our six case histories are probably not unique to Western Canada but can be expected wherever reversed-polarity CRM is recorded in magnetically enhanced zones. Based on our discovery of reversed-polarity CRM in cores from hydrocarbon reservoirs in other regions, we expect that dipolar HRGM anomalies may be present on the North Slope of Alaska (Sadlerochit Mountains to Prudhoe Bay), in the Texas Gulf of Mexico coastal plain (Austin Chalk trend), and in the North Sea (above Rotliegende Sandstone and North Sea Chalk reservoirs), Gulf of Campeche (offshore Mexico), and Lake Maracaibo, Venezuela.

Statistical comparisons between ground-based HRGM and aeromagnetic HRAM anomalies, as well as direct ground verification of a specific HRAM anomaly, demonstrate how airborne and ground-magnetic surveys can be used together, advantageously and cost-effectively, for hydrocarbon exploration. For hydrocarbon exploration over a wide region, reconnaissance HRAM surveys can be conducted to target areas for higher-resolution, ground-based HRGM and radiometric surveys. Apparently, only ground-based surveys have sufficient resolution to detect magnetic anomalies over pinnacle reefs and to resolve microseepage-related magnetic anomalies into dipoles, from which distinctive anomaly azimuths can be calculated.

In our experience, HRGM surveys and concurrent radiometric surveys substantially reduce exploration costs at whatever point in the exploration cycle they are used. This conclusion is supported by others who have con-

ducted similar exploration in North America and elsewhere around the world. These ground-based surveys are particularly effective when integrated with geologic and seismic studies, because they provide independent confirmation or negation of specific prospects, and they ensure a higher probability of success than does geologic and seismic work alone. We have been highly successful in using HRGM and/or radiometric surveys for hydrocarbon exploration in Western Canada, and we have achieved 85% success in new field discoveries.

Although ground-based HRGM and radiometric surveys significantly increase the probability of finding hydrocarbons, these surveys, like seismic surveys or subsurface geologic mapping, do not necessarily indicate whether any given well will be an economic success. However, the total cost for a combined ground-based HRGM and radiometric survey, including permitting, surveying, data processing, and interpretation, is approximately 20% of the total cost for a 3-D seismic survey.

ACKNOWLEDGMENTS

We thank Gulf Canada Resources Limited for facilitating our surveys over the Rumsey reef, for providing the 3-D seismic survey for correlation, and for permission to publish the results. We also thank Donald F. Saunders for providing valuable guidance on survey strategy during the conduct of our fieldwork and for reviewing this paper. We thank Richard E. Wyman for reviewing this paper and for providing the Alberta HRAM data used for statistical comparison with our Alberta HRGM data. We also thank John M. Andrichuk, Kevin Brown, Peter Eick, Robert S. Foote, Natalie Marchand, and William A. Morris for reviewing earlier drafts of this paper and for providing many helpful suggestions. We acknowledge Ty Pfeifer, who early on recognized the potential of our surveys; he commissioned several surveys and facilitated the drilling that verified the anomalies in case histories 1 and 2. We especially thank the major Canadian oil company that sponsored the surveys in case histories 5 and 6 and that gave us permission to publish the results. We are grateful to Pamela E. Vipond, Kevin Wutherich, Joy Elliott, Topher Elliott, and John E. Lewis for extensive field support and Joseph E. Butterworth for paleomagnetic lab and fieldwork. The Canadian National Research Council/Alberta Research Council under IRAP 26220U provided partial financial support.

APPENDIX A

Glossary of Terms

ac	acre
ADW	apparent directional wander
APW	apparent polar wander
ATV	all-terrain vehicle
CRM	chemical remanent magnetization
D&A	dry and abandoned
D/I	declination/inclination = azimuth/dip
DRAD	difference between thorium-normalized uranium and thorium-normalized potassium
DRM	detrital remanent magnetization
GPS	global-positioning system
greigite	Fe ₃ S ₄ ; magnetic iron sulfide
ha	hectare
hematite	αFe ₂ O ₃ ; magnetic iron oxide
HG	horizontal gradient (first horizontal derivative) of residual magnetic anomaly
HG'	absolute value of second horizontal derivative of residual magnetic anomaly
HRAM	high-resolution aeromagnetic
HRGM	high-resolution ground-magnetic
κ	precision parameter (Fisher, 1953) for directional distributions on a sphere
Ma	million years (geologic age)
maghemite	γFe ₂ O ₃ ; magnetic iron oxide
magnetite	Fe ₃ O ₄ ; magnetic iron oxide
MD	multidomain (magnetic grain size; >10 μm for magnetite)
MeV	million electron volts
MEZ	magnetically enhanced zone
MN	magnetic north
m.y.	million years (duration of time)
NRM	natural remanent magnetization
nT	nanotesla = 10 ⁻⁹ tesla, unit of magnetization
PADF	present axial dipole field; points to true north (TN)
PADF VRM	VRM recording a time-average of the past 10 ⁴ to 10 ⁶ yr
PF	present magnetic field; points to magnetic north (MN)
PF VRM	VRM recording a time-average of the past <10 ² yr
PSD	pseudosingle-domain (magnetic grain size; 1–10 μm for magnetite)
pyrrhotite	Fe ₇ S ₈ (monoclinic) ; magnetic iron sulfide
RTM	reaction-transport-mechanical
SD	single-domain (magnetic grain size; 0.05–1 μm for magnetite)
S _{Hmax}	maximum horizontal principal stress
S _{Hmin}	minimum horizontal principal stress
S _V	vertical principal stress
TN	true north = geographic north
TRM	thermoremanent magnetization
VPTRM	viscous partial thermoremanent magnetization
VRM	viscous remanent magnetization

APPENDIX B

A Guide to Paleomagnetic Nomenclature and Basic Concepts

To aid in understanding the origin and significance of HRGM anomalies in Western Canada, we provide the following guide to the terminology and basic principles of the science of paleomagnetism.

Induced versus Remanent Magnetization

Ground-magnetic (HRGM) and aeromagnetic (HRAM) anomalies represent vector sums of induced magnetization + remanent magnetization. *Induced magnetization* is aligned with the present magnetic field (PF) direction. The induced magnetization (J_{Ind}) can be calculated if the magnetic susceptibility (χ) of a magnetically enhanced zone is known, using the following equation:

$$J_{\text{Ind}} = \chi \times H$$

where H is the strength of the earth's magnetic field (0.58 oersteds in central Alberta).

Unlike induced magnetization, *remanent magnetization* would still be recorded and measurable in a rock sample (or in a magnetically enhanced zone) even if the earth's magnetic field were suddenly switched off. Remanent magnetization (RM) can have many different origins, specified by the letter preceding the RM. In near-surface hydrocarbon microseepage environments as well as within the hydrocarbon reservoirs at depth, *chemical remanent magnetization* (CRM) is most common. CRM is acquired when a magnetic mineral, such as magnetite or pyrrhotite, grows in a magnetic field. Other forms of remanent magnetization include *detrital remanent magnetization* (DRM) in sedimentary rocks and *thermoremanent magnetization* (TRM) in igneous rocks.

One important type of RM is *viscous remanent magnetization* (VRM), which can be thought of as induced magnetization that does not disappear when a sample is removed from the earth's magnetic field. VRM is ubiquitous, both in surface-outcrop samples and in subsurface cores, and it is the basis for the "paleomagnetic core-orientation technique" (e.g., Bleakly et al., 1985a, b; Hamilton et al., 1995, 1996; Van Alstine et al., 1991; Van Alstine and Butterworth, 1993). When VRM time-averages the geomagnetic field for the past <100 yr, it records the present-field (PF) direction, just like induced magnetization. In our central Alberta study area, the PF direction has a declination (azimuth) of 18° and an inclination (dip) of +75°. When VRM time-averages the geomagnetic field for the past 10⁴ to 10⁶ yr, it records the present-axial-dipole-field (PADF) direction. In our central Alberta study area, the PADF direction has a declination (azimuth) of 0° and an inclination (dip) of +68°. The PADF

direction has a declination = 0° (i.e., points to true north) everywhere in the world in rocks of all ages.

The vector sum of *all* the different types of RM present in a rock is referred to as the *natural remanent magnetization* (NRM). In our paleomagnetic laboratory, we measure the NRM in a magnetically shielded room, so the total magnetization of a rock sample is only the NRM (i.e., no induced magnetization is present).

In HRGM and HRAM surveys, measurements are performed in the earth's magnetic field, so the total magnetization (J_{HRGM}) of a "residual" HRGM (or HRAM) anomaly actually represents the NRM + induced magnetization as follows:

$$J_{\text{HRGM}} = J_{\text{NRM}} + J_{\text{Ind}} = (J_{\text{CRM}} + J_{\text{VRM}}) + (\chi \times H)$$

where J_{CRM} is the CRM component of the NRM, J_{VRM} is the VRM component of the NRM, and other terms are as defined above. In some rock samples (or magnetically enhanced zones), the remanent component (J_{NRM}) may be much larger than the induced component (J_{Ind}), such that the induced component can be ignored. In other rock samples (or magnetically enhanced zones), the induced component (J_{Ind}) may be much larger than the remanent component (J_{NRM}), such that the remanent component can be ignored. Because most of the HRGM anomalies in Western Canada are nearly *perpendicular* to the present magnetic field (PF) direction, about half of the total magnetization in the magnetically enhanced zones (J_{HRGM}) must represent *remanent magnetization* (probably reversed-polarity CRM).

Magnetic Directions and Poles

In paleomagnetism, we make the distinction between directions and poles. Paleomagnetic *directions* and magnetic field *directions* are unit vectors specified by a paired set of declination (azimuth) and inclination (dip) values and are reported in this paper as "D/I = ." *Declination* is measured in a horizontal plane and is clockwise-positive (0° to 360°) from geographic north. *Inclination* is measured in a vertical plane, from +90° (vertically downward) to 0° (horizontal) to -90° (vertically upward).

Paleomagnetic *poles* are unit vectors specified by a paired set of longitude and latitude values, which can be plotted directly on a globe. Conversions of directions into poles and of poles into directions are based on the "geocentric axial dipole" hypothesis, which states that the time-averaged magnetic field is that of a dipole at the center of the earth and aligned with the earth's rotation axis. The actual conversion equations can be found in standard paleomagnetic textbooks (e.g., McElhinny, 1973; Tarling, 1983; Butler, 1992; Van der Voo, 1993).

In this paper, we refer mostly to magnetic and paleomagnetic *directions* (rather than *poles*), because this is the reference frame in which HRGM anomalies are measured.

Instantaneous Magnetic Directions and Poles

In paleomagnetism, we further make the distinction between whether a direction or pole represents an instantaneous “spot reading” of the geomagnetic field or a time-average of the geomagnetic field over thousands to millions of years.

An “*instantaneous magnetic pole*”, referred to as a *virtual geomagnetic pole (VGP)*, represents a spot reading of the geomagnetic field over a time span of less than ~100 yr. For example, a VGP would be recorded by a thin lava flow or by authigenic magnetite synthesized by a bacterial colony that lived entirely within a single 100-yr time span.

An “*instantaneous magnetic direction*” can be calculated from any given VGP, using the pole-to-direction conversion for a geocentric dipole. We refer to the present-day “instantaneous” magnetic-field direction as the “present-field” (PF) direction. For example, in 1999, near the Rumsey reef, the PF direction was $D/I = 18^\circ/+75^\circ$. If an HRGM anomaly merely reflected *induced* magnetization (i.e., had no contribution from remanent magnetization), the anomaly would merely record this PF direction.

Although the PF direction near the Rumsey reef is $D/I = 18^\circ/+75^\circ$, this direction is constantly changing because of geomagnetic secular variation. *Geomagnetic secular variation* causes the instantaneous magnetic north-pole position to migrate in a nearly random walk around the geographic north pole such that the time-averaged magnetic north pole coincides (within 2°) with the geographic north pole. It is generally thought to take about 10^4 yr for the time-averaged magnetic pole to coincide with the geographic pole.

The geomagnetic secular variation history is especially well known for western North America. Based on detailed paleomagnetic studies of Holocene lava flows from the western United States, Champion (1980) determined VGPs for the past 2000 yr at 100-yr intervals. This is the same VGP data set discussed in Butler (1992). Applying the pole-to-direction conversion to the western North America regional averages (Table 3 of Champion, 1980), we calculated the instantaneous magnetic field directions expected near the Rumsey reef at 100-yr intervals over the past 2000 yr (Figure 18a).

Time-averaged Magnetic Directions and Poles

A *time-averaged magnetic pole* is referred to as a *paleomagnetic pole*. A paleomagnetic pole derived by averaging VGPs from western North America for the past 2000 yr coincides with the present geographic north pole to within 2° , in accordance with the “geocentric axial dipole” hypothesis. Paleomagnetic poles derived from ancient rocks, therefore, are thought to approximate past

positions of the geographic poles, as viewed from a given tectonic plate.

A “*time-averaged magnetic direction*” can be calculated from any given paleomagnetic pole, using the same pole-to-direction conversion as for treating VGPs. We refer to the most recent time-averaged magnetic-field direction as the present-axial-dipole-field (PADF) direction. Near the Rumsey reef, the PADF direction is $D/I = 0^\circ/+68^\circ$.

Just as instantaneous VGPs migrate over 10^2 -yr time scales by the process of geomagnetic secular variation, time-averaged paleomagnetic poles migrate over 10^6 -yr time scales by the process of *apparent polar wandering*. The “apparent-polar-wander” phenomenon is thought to reflect contributions both from plate tectonics (motions of individual plates relative to the geographic pole) and from “true polar wander” (net motion of the entire lithosphere and mantle with respect to the earth’s spin axis). For 40 years, paleomagnetists have been establishing the “reference” *apparent-polar-wander (APW) paths* for the major tectonic plates. The reference APW path for North America is probably the best-determined APW path for any plate, and was the subject of author Van Alstine’s Ph.D. thesis (Van Alstine, 1979). The reference APW path used in this paper is derived following procedures discussed in Van Alstine (1979), but it has been updated with more recently published paleomagnetic poles through 1999. For most time intervals, this reference APW path agrees with other recently published compilations (e.g., Van der Voo, 1993) to within 5° .

In Figure 18b, we applied pole-to-direction conversions to the reference APW path for North America to derive what we call an *apparent-directional-wander (ADW) path* for a location at the center of our study area, near Rumsey reef, Alberta. The purpose of constructing the ADW path is to be able to determine the age of *remanent* magnetization recorded either in magnetically enhanced zones responsible for HRGM anomalies or in subsurface cores taken from within the hydrocarbon reservoirs. The reference ADW path is actually two separate paths, which differ by exactly 180° on a stereographic projection. Near the Rumsey reef, the “normal-polarity ADW path” is characterized by paleomagnetic directions with declinations (azimuths) in the northwest quadrant and with positive (downward-pointing) inclinations (dips). The “reversed-polarity ADW path” is characterized by paleomagnetic directions with declinations in the southeast quadrant and with negative (upward-pointing) inclinations.

The Magnetic-polarity Time Scale

In paleomagnetism, we refer to the *polarity* of a magnetic or paleomagnetic direction, as follows.

- 1) *Normal-polarity* directions have time-averaged declinations pointing toward the geographic north pole. From the Mississippian (335 Ma) to the present at the

Rumsey reef, normal-polarity directions have positive (+, downward-pointing) inclinations (Figure 18b).

- 2) *Reversed-polarity* directions have time-averaged declinations pointing toward the geographic south pole. From the Mississippian (335 Ma) to the present at the Rumsey reef, reversed-polarity directions have negative (–, upward-pointing) inclinations (Figure 18b).

The polarity of the earth's magnetic field has changed repeatedly in the past, as indicated by the *magnetic-polarity time scale* (Figure 18c). The most recent geomagnetic polarity reversal occurred at 0.78 Ma (Ogg, 1995). Intervals between polarity reversals are called *polarity chrons*. On the magnetic-polarity time scale, “normal-polarity chrons” are colored black, and “reversed-polarity chrons” are colored white. The time from the most recent reversal (0.78 Ma) to the present is called the *Brunhes normal-polarity chron*.

Figure 18c reveals that the polarity-reversal frequency is variable, probably reflecting long-term temperature changes at the core-mantle boundary (McFadden and Merrill, 1984). The highest reversal frequency (~5 reversals/m.y.) occurred at ~10 Ma (late Miocene time). However, for 35 m.y. during the Cretaceous (from 118 to 83 Ma), the geomagnetic field probably did not reverse at all; this interval is commonly referred to as the *Cretaceous normal-polarity superchron*.

From the end of the Cretaceous normal-polarity superchron to the present, the reversed/normal-polarity ratio has also varied. Intervals when the average length of reversed-polarity chrons is longer than the average length of normal-polarity chrons are referred to as *reversed-polarity-bias intervals*. Conversely, intervals when the average length of normal-polarity chrons is longer than the average length of reversed-polarity chrons are referred to as *normal-polarity-bias intervals*.

In Figure B-1a, we used a 10-m.y. sliding window to calculate the polarity bias for the past 100 m.y. In this paper, we refer to the early Tertiary interval from 63 to 41 Ma as the early Tertiary reversed-polarity-bias interval. This interval is probably when most Devonian and Mississippian hydrocarbon reservoir rocks in Western Canada (east of the McConnell thrust) were chemically remagnetized (Appendix C).

CRM in magnetically enhanced zones over microseeping hydrocarbon reservoirs probably time-averages the geomagnetic field over millions of years. If most authigenic magnetic minerals in a magnetically enhanced zone grew in a single 10-m.y. pulse of enhanced microseepage, the expected polarity bias of the CRM could be determined from Figure B-1a. If most authigenic magnetic minerals in a magnetically enhanced zone grew during constant-flux microseepage (linear acquisition of CRM from the initiation of microseepage to the present), the expected polarity bias of the CRM could be determined from Figure B-1c.

Figure B-1a reveals that if microseepage occurred in a 10-m.y. pulse centered any time between 63 and 5 Ma, there is an 88% probability that reversed-polarity-biased CRM would be recorded in a magnetically enhanced zone (capable of causing a dipolar HRGM anomaly). Figure B-1c reveals that if microseepage occurred at constant flux from the initiation of microseepage to the present, there is a 99.5% probability that reversed-polarity-biased CRM would be recorded in a magnetically enhanced zone, as long as microseepage began between 89.7 and 1.8 Ma.

Magnetic Grain Size

As emphasized in this study, magnetic grain size exerts the most important control on whether a magnetically enhanced zone records a normal-polarity, reversed-polarity, or intermediate direction.

Within a magnetically enhanced zone above a microseeping hydrocarbon reservoir, chemical remanent magnetization (CRM) is probably being acquired by the growth of magnetic minerals over millions of years. As each magnetic grain grows through its “blocking volume” (about 0.05 μm for equant grains of magnetite), it becomes *single domain* (SD) and can record the magnetic-field direction and polarity at that time. Single-domain magnetite grains 0.05–1 μm in diameter can retain a stable remanent magnetization for billions of years.

If an authigenic magnetic mineral grows to much larger sizes, it becomes *multidomain* (MD), becomes increasingly magnetically unstable, and can retain a remanent magnetization for much shorter times. Most viscous remanent magnetization (VRM) resides in these multidomain grains. Large multidomain grains ($\gg 10 \mu\text{m}$) are the most magnetically unstable and can retain remanent magnetization for only seconds to years; MD grains such as these record PF VRM, which is $<10^2$ years old. Smaller multidomain grains, slightly more than 10 μm , are somewhat more stable magnetically and can retain remanent magnetization for 10^4 to 10^6 yr; MD grains such as these record PADF VRM, which is between 10^4 and 8×10^5 years old. Thus, because of their short relaxation times, MD grains in magnetically enhanced zones can record only *normal-polarity* remanent magnetization (VRM).

Grains intermediate in size between single domain and multidomain are referred to as *pseudosingle domain* (PSD). PSD grains are the most important grains in paleomagnetism, and grain-size distributions of many sedimentary and igneous rocks peak in the PSD range, which for magnetite is 1–10 μm (Butler, 1992). PSD and SD grains are the only grains in a magnetically enhanced zone that can retain their remanent magnetization over geologic time scales of millions of years. In particular, only PSD and SD grains can be recording the *reversed-polarity remanent* magnetization that appears to be ubiquitous above microseeping reservoirs in Western Canada.

APPENDIX C

Insights into the Origin of Dipolar HRGM Anomalies in Western Canada

In this appendix, we demonstrate how paleomagnetic studies of hydrocarbon reservoir rocks of Western Canada can elucidate the age and origin of the dipolar HRGM anomalies we observe over microseeping reservoirs in this region. Both HRGM and HRAM surveys have the disadvantage that the magnetometers they employ, whether on the ground or in the air, can measure only the *vector sum* of a variety of magnetizations: induced and remanent, modern and ancient, normal and reversed polarity, in unknown relative proportions within a magnetically enhanced zone. This problem is compounded by the fact that no cores exist of the near-surface magnetically enhanced zones anywhere in Western Canada. Hence, it is impossible to predict the relative strength of induced versus remanent magnetization or to know whether remanent magnetization will be dominated by recently acquired viscous remanent magnetization (VRM in magnetic grains $>10\ \mu\text{m}$) or by ancient chemical remanent magnetization (CRM in magnetic grains $<10\ \mu\text{m}$).

As discussed below, paleomagnetic data from surface-outcrop and subsurface-core samples of reservoir rocks of the Alberta and Williston Basins provide valuable in-

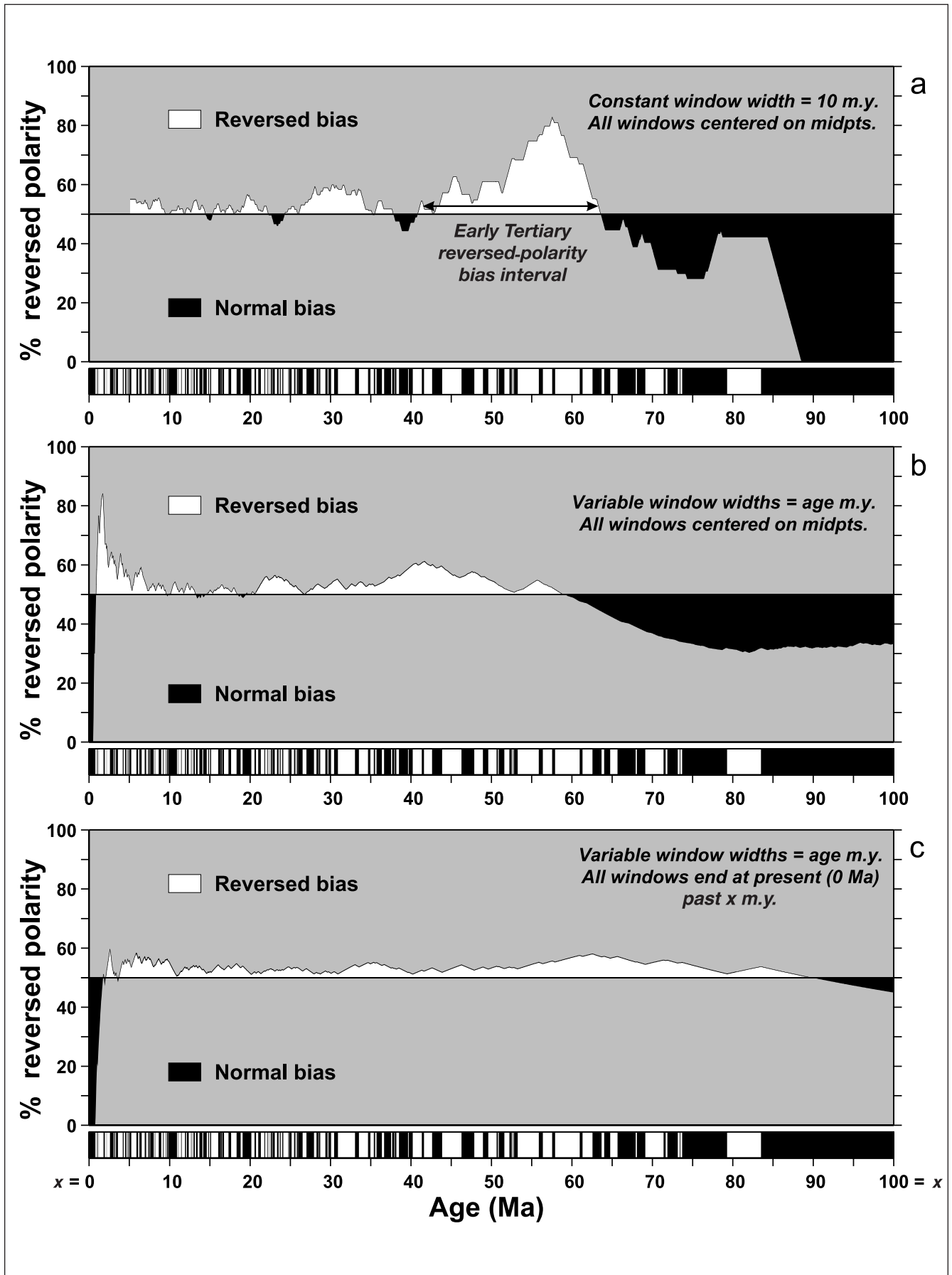
sights into the types, ages, and relative proportions of the various magnetizations that can be expected in magnetically enhanced zones above microseeping reservoirs of Western Canada. In particular, we have found that hydrocarbon reservoir rocks of Western Canada have been pervasively remagnetized chemically as a result of hydrocarbon generation and migration events, especially during the early Tertiary. It seems intuitively reasonable that the geochemical changes recorded by CRM in paleomagnetic samples from hydrocarbon reservoirs at depth are linked closely to the geochemical changes recorded by CRM in near-surface magnetically enhanced zones above microseeping reservoirs, perhaps in a “source”-and-“sink” relationship. We commonly find that the most oil-saturated reservoir rocks are the *least magnetic*, so perhaps hydrocarbon reservoirs can be thought of as magnetically *depleted* zones with a net transport of Fe to be reprecipitated in the magnetically *enhanced* zones detected by HRGM and HRAM surveys. For example, 46% of the Rundle Group (Mississippian) surface-outcrop paleomagnetic samples discussed below exhibit *negative magnetic susceptibility*. In subsurface cores from Rundle Group reservoirs farther to the east, 72% of the paleomagnetic samples exhibit *negative magnetic susceptibility*. Negative magnetic susceptibility means that a sample is so depleted in Fe that it is *diamagnetic*, such as quartz, calcite, water, and oil.

FIGURE B-1. Within a magnetically enhanced zone (MEZ) above a microseeping hydrocarbon reservoir, chemical remanent magnetization (CRM) is probably being acquired as new magnetic minerals grow over millions of years. Depending on whether microseepage occurs in 10-m.y. pulses (a) or at constant flux (c), the resultant vector of the billions of magnetic grains in an MEZ will exhibit the polarity bias (dominant polarity) indicated by the curves in this figure. During the past 100 million years, 188 reversals of the geomagnetic field have occurred, separating normal-polarity chrons (black) from reversed-polarity chrons (white) on the magnetic-polarity time scale (Ogg, 1995). For most of the time from the beginning of the Tertiary (65 Ma) to the present, reversed-polarity chrons have been slightly longer than normal-polarity chrons, so the reversed polarity bias has been $>50\%$. This is the major reason why all of the >100 HRGM anomalies we observed in Western Canada are inferred to record reversed-polarity-biased CRM.

(a) Polarity-bias time-averaging of the magnetic-polarity time scale if CRM in an MEZ is acquired during a single 10-m.y. pulse (as in Models 1A and 1B, Appendix D). Polarity bias has been calculated by sliding-window averages with a constant window width of 10 m.y. centered at 2000 equally spaced points between 100 Ma and the present. CRM acquired during a 10-m.y. microseepage pulse centered at any time between 63 and 5 Ma has an 88% probability of recording reversed polarity bias.

(b) Polarity bias time-averaging of the magnetic-polarity time scale if CRM is acquired during a single pulse but with variable duration. Polarity bias has been calculated by sliding-window averages with variable-width windows centered at 2000 equally spaced points between 100 Ma and the present. For example, CRM acquired during a 30-m.y. pulse from 15 to 45 Ma will exhibit reversed-polarity bias of 53.5%, and CRM acquired during a 7-m.y. pulse from 3.5 to 10.5 Ma will exhibit reversed-polarity bias of 53.9%.

(c) Polarity bias time-averaging of the magnetic-polarity time scale if CRM is acquired linearly during microseepage at constant flux, from the initiation of microseepage to the present (as in Models 2A and 2B, Appendix D). This is geologically reasonable in Western Canada, given that most reservoirs of this study are presently microseeping (based on radiometric, free-gas, and microbial surveys). Polarity bias has been calculated by sliding-window averages with variable-width windows at 2000 equally spaced points between 100 Ma and the present. Unlike in (a) and (b), these windows are *not* centered on their midpoints; instead, all windows end at the present (0 Ma). For example, CRM acquired during constant-flux microseepage from 30 Ma to the present will exhibit reversed-polarity bias of 51.5%, and CRM acquired during constant-flux microseepage from 7 Ma to the present will exhibit reversed-polarity bias of 56.3%. There is a 99.5% probability that reversed-polarity-biased CRM will be recorded in an MEZ as long as constant-flux microseepage begins between 89.7 and 1.8 Ma.



Next, we discuss the variety of sophisticated laboratory and mathematical procedures that are used routinely in paleomagnetism to isolate and separate superimposed normal- and reversed-polarity magnetizations. We then apply these procedures to show how we can infer a 57-Ma chemical remagnetization age for Rundle Group carbonates exposed at Moose Mountain, Alberta, and to infer a 45-Ma chemical remagnetization age in a subsurface core of Three Forks (Devonian) dolomite from the Williston Basin, North Dakota. These hydrocarbon reservoir rocks all record vector sums of reversed-polarity-biased CRM + normal-polarity VRM, perhaps in similar proportions to those in the magnetically enhanced zones that are the source of HRGM anomalies.

Paleomagnetic Laboratory and Mathematical Procedures for Separating Superimposed Normal- and Reversed-polarity Magnetizations

Paleomagnetic natural-remanent-magnetization (NRM) directions, as well as HRGM and HRAM anomalies, represent vector sums of *all* the magnetizations (modern and ancient, normal- and reversed-polarity) that may simultaneously be present in a single paleomagnetic sample or magnetically enhanced zone. In the paleomagnetic laboratory, we have the luxury of being able to separate the individual components of magnetization that contribute to the NRM resultant vector; these magnetic components can then be used for age-dating or paleomagnetic core-orientation purposes.

After samples arrive at our paleomagnetic laboratory, their NRM directions and intensities are first measured, using a three-axis, superconducting magnetometer at liquid helium temperatures. Magnetic susceptibility is also commonly measured, both (1) to permit calculation of the induced magnetization (for modeling HRAM and HRGM magnetic anomalies), and (2) to monitor any chemical changes in the magnetic mineralogy that may occur during the thermal demagnetization process discussed below.

After we measure their NRM, we subject paleomagnetic samples to either “progressive alternating-field” (AF) or “progressive thermal” demagnetization to separate the normal-polarity from the reversed-polarity components. During progressive thermal demagnetization, samples are heated in 25° to 50°C increments to as high as 580°C (for samples containing magnetite) or 680°C (for samples containing hematite). After being heated to each incremental temperature, the sample is cooled in a zero-magnetic-field environment, after which the remanence is again measured. After each demagnetization step, some of the less magnetically or less chemically stable part of the original NRM has been removed. We commonly observe a last-in, first-out principle, whereby the recently acquired magnetizations (e.g., PF or PADF

VRM residing in multidomain magnetite) are the first to be removed, and ancient secondary (e.g., CRM) or primary (e.g., DRM) magnetizations are the last to be removed.

When the endpoints of magnetic vectors at successive AF or thermal demagnetization steps are plotted on a stereographic projection, they are commonly coplanar or lie on great-circle arcs (remagnetization circles) in cases in which the sample contains two superimposed magnetizations. Application of “remagnetization-circle analysis” (Halls, 1976, 1978) and “principal-component analysis” (Kirschvink, 1980) yields good estimates of the superimposed magnetization directions, even in cases in which the normal- and reversed-polarity components cannot be fully separated by demagnetization treatments in the paleomagnetic laboratory.

Surface-outcrop Example of Remagnetization-circle and Principal-component Analysis

Figure C-1 illustrates typical examples of remagnetization circles we encountered during a paleomagnetic study of surface-outcrop samples of Rundle Group (Mississippian) carbonates at Moose Mountain, Alberta, in the Foothills structural province west of Calgary (Van Alstine et al., 1997). Each point on these stereographic projections represents a magnetization direction recorded in an individual paleomagnetic specimen, which is an 11-cm³ cylinder. The stereographic projections in Figure C-1a and b show paleomagnetic directions from 12 specimens from the southwestern limb of the anticline at Moose Mountain. The stereographic projections in Figure C-1c and d show paleomagnetic directions from 12 specimens from the northeastern limb of this fold.

Figure C-1b and d illustrates the NRM directions (red stars), which represent the vector sums of *all* the magnetizations present in each specimen. By comparison, the volume of a cylindrical magnetically enhanced zone 150 m thick, over a 150-m-diameter pinnacle reef, would contain billions of individual 11-cm³ paleomagnetic specimens. Thus, HRGM and HRAM anomalies probably integrate billions of the individual paleomagnetic directions shown in Figure C-1 *all at once*.

All 24 of the paleomagnetic specimens included in Figure C-1 contain two superimposed magnetizations: (1) modern, normal-polarity VRM aligned with the present-magnetic-field (PF) direction, and (2) ancient, reversed-polarity CRM acquired during hydrocarbon migration at ~57 Ma in the early Tertiary. Together, these two magnetizations add vectorially to produce the NRM directions (resultant vectors) indicated by the red stars in Figure C-1b and d.

The average NRM direction from the Moose Mountain northeastern limb (Figure C-1d) is a “real” example of a shallow-inclination (+4°), eastern-hemisphere (decli-

nation = 89°) NRM direction capable of causing a dipolar HRGM anomaly with an easterly azimuth. Good clustering of these NRM directions means that the grain-size distribution of the authigenic magnetite is nearly the same in all 12 Rundle specimens from the northeastern limb. Within each specimen, nearly equal proportions of the normal-polarity PF VRM and the reversed-polarity, ~57-Ma CRM yield intermediate NRM directions halfway between the normal- and reversed-polarity endpoints. This Moose Mountain northeastern-limb example illustrates one way in which eastern-hemisphere, shallow-inclination NRM directions (resultant vectors) could produce dipolar HRGM anomalies with easterly azimuths.

The NRM directions from the Moose Mountain southwestern limb (Figure C-1b) provide a good example of a “streaked” distribution, with NRM directions smeared over 140° of arc between the PF (normal-polarity) and 57-Ma (reversed-polarity) endpoints. The streaked distribution reflects differences in grain size (which controls the reversed/normal-polarity ratio) among the different Rundle samples from the southwestern limb. In this example, the streaked distribution trends toward the south-southwest, because the structural dip on this limb is 35° toward the southwest, and the reversed-polarity magnetization was acquired *prior to* the folding event. If these rocks were flat-lying (as in our central Alberta and Manitoba case-history areas) or if the reversed-polarity magnetization had been acquired *after* the folding event, the NRM distribution would be streaked toward the east-southeast (like Leduc HRGM anomalies). This Moose Mountain southwestern-limb example illustrates another way in which eastern-hemisphere, shallow-inclination NRM directions (resultant vectors) could produce dipolar HRGM anomalies with easterly azimuths.

Within a magnetically enhanced zone, which *integrates billions of these specimens all at once*, the vector sum of the streaked NRM distribution (such as Figure C-1b) and the intermediate NRM directions (such as Figure C-1d) would be a shallow-inclination, eastern-hemisphere magnetization direction capable of producing dipolar HRGM anomalies with eastern-hemisphere azimuths.

The streaked distribution of NRM directions in Figure C-1b forms a classic remagnetization circle between the normal-polarity PF direction and the reversed-polarity endpoint in the southwestern quadrant. From this NRM distribution alone, we can infer that Model 1B or 2B (Appendix D) is applicable in these surface-outcrop samples, because the remagnetization circle includes the PF direction but excludes the PADF direction.

Applying principal-component analysis to the thermal demagnetization data allows us to directly calculate the unbiased endpoint directions that would otherwise merely be inferred from the NRM distribution. In Figure C-1a and c, principal-component analysis has been used to isolate the present-field (PF) direction (indicated by green circles) and the ancient ~57-Ma magnetization

direction (indicated by blue triangles). The average of the normal-polarity directions (green circles) lies within 2° of the known present-magnetic-field (PF) direction at Moose Mountain. This PF VRM probably resides in multidomain magnetite grains coarser than 10 μm. In contrast, the early Tertiary ~57-Ma reversed-polarity magnetization is CRM residing in single-domain and pseudosingle-domain magnetite grains between 0.05 and 10 μm. VRM in surface-outcrop samples such as these typically records the PF direction, which represents a time-average of the geomagnetic field for the past <100 yr. In contrast, VRM in subsurface-core samples (discussed below) typically records the PADF direction, which represents a time-average of the geomagnetic field for the past 10⁴ to 10⁶ yr. We cannot predict whether magnetically enhanced zones at 150-m depths will record PF VRM or PADF VRM, which is why we consider both possibilities in Appendix D.

Applying a paleomagnetic “fold test” (Butler, 1992, p. 123–125) at Moose Mountain (Figure C-1e and f) reveals that these Mississippian carbonate reservoir rocks were completely chemically remagnetized during the Laramide orogeny in the early Tertiary. The ancient, reversed-polarity magnetization in these Rundle carbonates was acquired during the 63- to 41-Ma early Tertiary reversed-polarity-bias interval (Figure B-1a). We know that this reversed-polarity magnetization is older than this Laramide fold, because the reversed-polarity directions (blue triangles) from opposite limbs of the fold are more dispersed relative to the present-day horizontal (Figure C-1e) than relative to the Mississippian paleohorizontal (Figure C-1f). However, we also know that this reversed-polarity magnetization is an early Tertiary “secondary magnetization,” because the blue triangles cluster near the 57-Ma reference direction (57_R black star) derived from the North American APW path. If this magnetization were a “primary magnetization” acquired near the time of deposition in the Mississippian, the blue triangles would cluster near both the M_N (Mississippian, normal-polarity) and M_R (Mississippian, reversed-polarity) reference directions (black stars), because geomagnetic polarity reversals are known to have occurred in Mississippian time, when Moose Mountain was at a paleolatitude of 8°.

Strictly speaking, the Moose Mountain northeastern limb (Figure C-1d) is not a perfect analog for our observed eastern-hemisphere HRGM anomalies, because the easterly azimuths partly reflect the 15° eastward structural dip on the northeastern limb. Our remagnetization-circle hypothesis must be capable of explaining shallow-inclination, eastern-hemisphere HRGM anomalies without invoking the postremagnetization tectonic rotations that occurred at Moose Mountain. Below, we discuss two examples of eastern-hemisphere remagnetization circles from subsurface cores in hydrocarbon reservoirs of the Alberta and Williston Basins where the structural dip is <0.3°.

Subsurface-core Examples of Eastern-hemisphere Remagnetization Circles

All of the dipolar HRGM anomalies we measured in the Alberta and Williston Basins occur at locations where the structural dip is $<0.3^\circ$. Thus, the subsurface-core case histories illustrated in Figure C-2 provide better examples of how shallow-inclination, eastern-hemisphere NRM directions and HRGM anomalies can be produced without invoking structural tilting. These are typical examples of paleomagnetic data we routinely acquire east of the Laramide fold-thrust belt as a by-product of paleomagnetic core-orientation studies we have been conducting since 1980. The paleomagnetic directions illustrated in Figure C-2 represent endpoints of magnetic vectors observed during thermal demagnetization of subsurface-core samples from several hydrocarbon reservoirs in nearly flat-lying Devonian carbonates. These paleomagnetic directions are distributed along classic remagnetization circles formed by superimposing a modern, normal-polarity PADF VRM on an ancient, reversed-polarity CRM acquired during hydrocarbon generation and migration in the early Tertiary.

In Figure C-2, the “demagnetization path trajectories” (i.e., trends of remagnetization circles on the stereographic projections) are controlled by the precise angle between the modern normal-polarity PADF direction and the early Tertiary, reversed-polarity CRM direction. Each remagnetization circle is following the shortest path ($<180^\circ$ great-circle arc length) connecting the normal-polarity and reversed-polarity magnetizations within

each specimen. Remagnetization circles from a suite of paleomagnetic specimens from the same reservoir do not all coincide, because there is always some dispersion about the mean of the normal- and reversed-polarity directions (i.e., real paleomagnetic specimens do not perfectly record either the normal-polarity or the reversed-polarity endpoints). However, by calculating an average remagnetization-circle trajectory from a suite of specimens and by calculating the point at which they “converge” (Halls, 1978), we can reasonably infer the age of the reversed-polarity magnetization, by comparison with the “reference” remagnetization circles, as discussed in Appendix D.

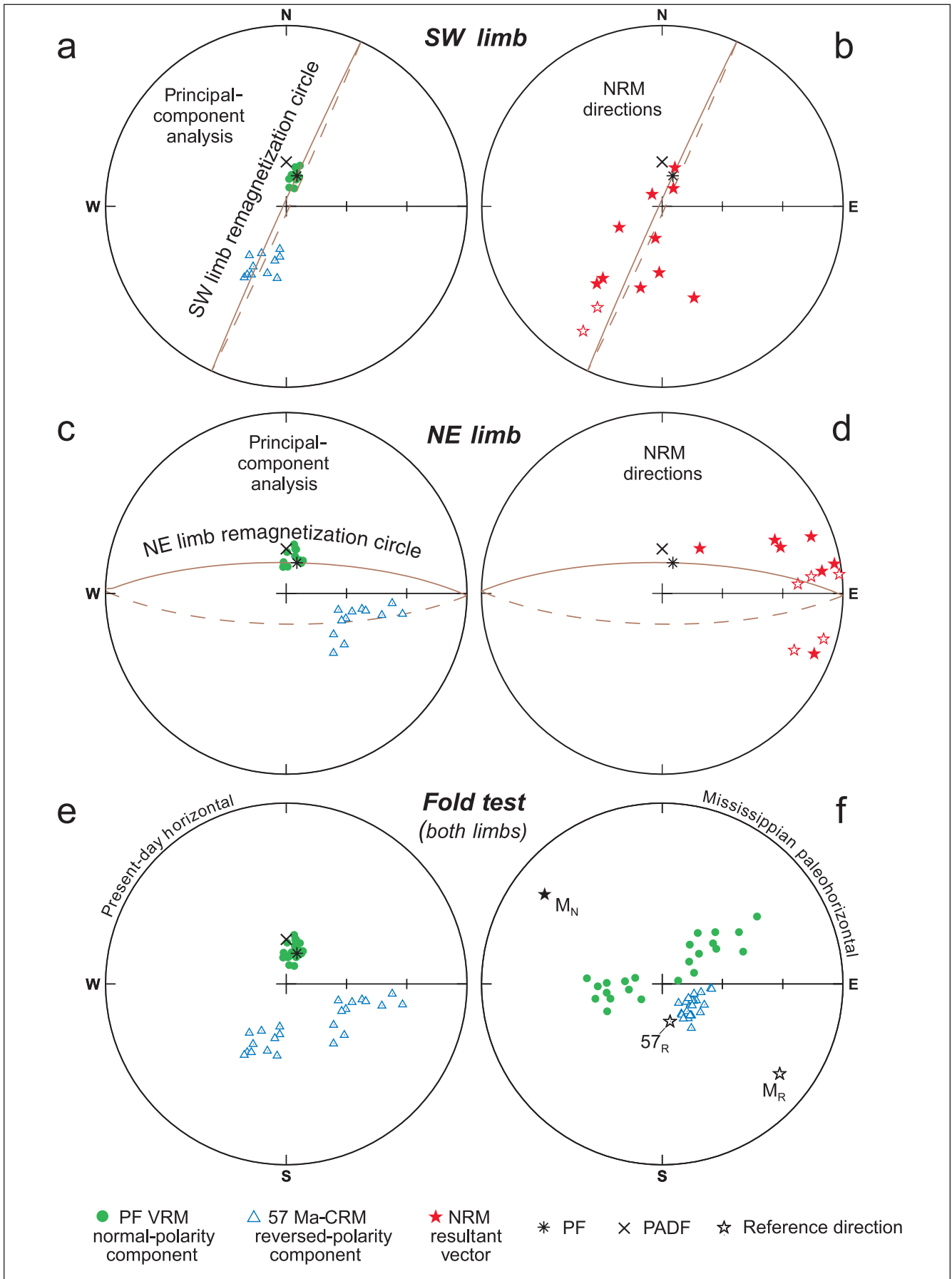
The most important observations about the remagnetization circles in Figure C-2 are as follows.

- 1) In both of these examples from the Alberta and Williston Basins, the remagnetization circles converge on the PADF direction rather than on the PF direction. This means that remagnetization circles *at reservoir depths* are following Models 1A or 2A (Appendix D) rather than Models 1B or 2B, as in surface outcrops. The paleomagnetic data from the Alberta Basin in Figure C-2a are from several reservoirs at depths of 1500–3050 m (5000–10,000 ft). The paleomagnetic data from the Williston Basin in Figure C-2b are from one reservoir at a depth of 3350 m (11,000 ft).
- 2) The average remagnetization-circle trajectory from the Alberta Basin best fits the 57-Ma reference-remagnetization circle in Appendix D, Figure D-2a. This is also the best-fit remagnetization age for the Moose

FIGURE C-1. Remagnetization circles from surface-outcrop samples in Rundle carbonates at Moose Mountain, Alberta. The shallow-inclination, eastern-hemisphere magnetization directions that form the distinctive HRGM anomaly clusters (Figure 17b) probably represent vector sums of reversed-polarity Tertiary chemical remanent magnetization (CRM) + modern normal-polarity viscous remanent magnetization (VRM), like the NRM directions (red stars) in this example. These NRM directions are distributed along great circles (brown) called “remagnetization circles,” which connect the normal-polarity (solid green circles on the lower hemisphere) and reversed-polarity (open blue triangles on the upper hemisphere) components. This figure illustrates remagnetization circles we encountered during a paleomagnetic study of surface-outcrop samples of Rundle Group (Mississippian) carbonates at Moose Mountain, Alberta, in the Foothills west of Calgary (Van Alstine et al., 1997).

Paleomagnetic lab analysis (thermal demagnetization followed by principal-component analysis) separated the NRM resultant vectors (b, d) into their individual normal- and reversed-polarity components (a, c). A paleomagnetic “fold test” (e, f) indicates that the reversed-polarity CRM was acquired prior to folding, at about 57 Ma in the early Tertiary. This steep-inclination Laramide “secondary” CRM has obliterated any shallow-inclination Mississippian “primary” DRM, which would cluster near the stars labeled M_N and M_R . The different structural attitudes on each limb of the fold have changed the angle between the normal-polarity PF VRM and the prefolding reversed-polarity CRM. This angle determines the trend of the remagnetization circles, the midpoints of which probably correspond to HRGM anomaly directions. Thus, the trends of remagnetization circles, and hence HRGM anomaly azimuths, provide powerful constraints on the direction (and hence the age) of the reversed-polarity component, even when the reversed-polarity component cannot be observed directly. In this Moose Mountain surface-outcrop example, the normal-polarity magnetization is VRM recording the present-magnetic-field (PF) direction. This PF direction has existed only for about the past 100 yr, so this normal-polarity VRM must be <100 years old.

Of the four models discussed in Appendix D, Models 1B and 2B assume that this same PF component contributes to HRGM anomalies above microseeping reservoirs. For HRGM anomalies, the PF component could reflect either PF VRM (as in these samples that were measured in a zero magnetic field) or induced magnetization (which would also be aligned with the PF direction).



Mountain surface-outcrop samples (Figure C-1f) and for the “Nisku” HRGM anomalies (as discussed in Appendix D). A remagnetization age of ~57 Ma lies near the middle of the early Tertiary reversed-polarity-bias interval (63 to 41 Ma), and all of these paleomagnetic specimens are probably time-averaging the geomagnetic field for at least 10 m.y. (Figure B-1a).

- 3) The average remagnetization-circle trajectory from the Williston Basin best fits an interpolated 45-Ma reference-remagnetization circle in Appendix D, Figure D-2b. (Note: the Williston Basin reference remag-

netization circles in Figure D-2 are calculated for a location at the Waskada field, Manitoba; our 45-Ma age estimate is based on similar remagnetization circles we calculated for the center of the Williston Basin in North Dakota.) A remagnetization age near 45 Ma lies near the end of the early Tertiary reversed-polarity-bias interval (63 to 41 Ma), and all of these paleomagnetic specimens are probably time-averaging the geomagnetic field for about 10 m.y. (Figure B-1a).

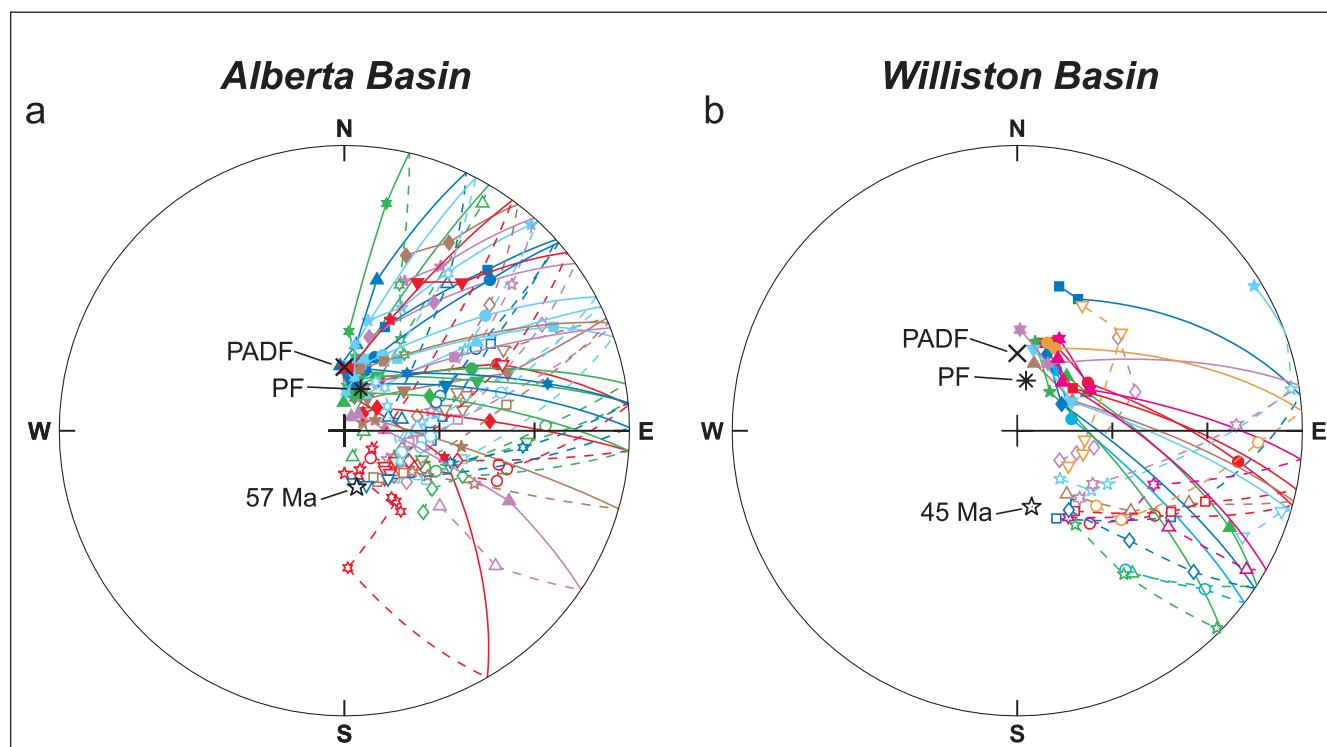


FIGURE C-2. Remagnetization circles observed during progressive thermal demagnetization of subsurface-core samples from nearly flat-lying Devonian carbonate reservoir rocks of Western Canada. Left = paleomagnetic directions from Beaverhill Lake Group and Swan Hills Formation cores from the Alberta Basin. Right = paleomagnetic directions from Three Forks Group cores from the Williston Basin, North Dakota. All of these Devonian samples were chemically remagnetized during the Laramide orogeny in the early Tertiary. Data are from Applied Paleomagnetism Inc.’s project files. Different symbols and colors are used for different samples. Each point represents a different thermal demagnetization step. Solid (open) symbols and solid (dashed) lines are on the lower (upper) hemispheres, respectively. All remagnetization circles are confined to the *eastern* hemisphere, because this is the shortest path (<180° angle) connecting the modern normal-polarity magnetization (PADF VRM) with the early Tertiary reversed-polarity reference directions (black stars). If the modern normal-polarity and the early Tertiary reversed-polarity magnetizations had near-equal intensity, their vector sum would produce a dipolar HRGM anomaly with an easterly azimuth. At *high* thermal-demagnetization steps, the remagnetization circles converge on the 57 Ma reversed-polarity reference direction for the Alberta Basin, and they converge on the 45 Ma reversed-polarity reference direction for the Williston Basin. At *low* thermal-demagnetization steps, the remagnetization circles in both basins converge on the PADF direction, which represents the time-average of the past 10^4 to 10^6 yr. Of the four models discussed in Appendix D, Models 1A and 2A assume that this same PADF VRM component contributes to HRGM anomalies above microseeping reservoirs.

APPENDIX D

Explanation of Nisku, Leduc, Cretaceous, and Alida HRGM Anomaly Azimuths

In this appendix, we discuss how paleomagnetism can be used to infer the timing of microseepage above Nisku, Leduc, and Cretaceous reservoirs of the Alberta Basin and above Alida (Mission Canyon) reservoirs of the Williston Basin. In this analysis, we are making the assumption that HRGM anomaly directions represent approximate midpoints of remagnetization circles connecting the normal-polarity PF or PADF direction with reversed-polarity directions calculated from the North American APW path.

Figure D-1 illustrates four possible models for explaining how shallow-inclination, eastern-hemisphere magnetization directions (red resultant vectors) can be produced by vector sums of reversed-polarity-bias chemical remanent magnetization (CRM), shown in blue, and normal-polarity magnetizations (VRM and induced), shown in green. In Models 1A and 1B, the reversed-polarity-bias CRM is acquired during a single, 10-m.y. pulse of enhanced microseepage. In Models 2A and 2B, the reversed-polarity-bias CRM is acquired at constant-flux microseepage, over the entire interval from the initiation of microseepage to the present. Figure D-1a and c illustrates a 10-m.y. pulse centered on 57 Ma. Figure D-1e and g illustrates constant-flux microseepage beginning at 57 Ma. We emphasize that the 57-Ma age illustrated in Figure D-1 is not intrinsic to the models, but was chosen merely to show how differences in the models (pulsed versus constant-flux microseepage; PADF VRM versus PF VRM + induced) can produce dipolar HRGM anomalies with different azimuths.

We will discuss these four models in greater detail. The microseepage ages inferred from each model are summarized in Table 3. Broadly speaking, as long as the remagnetization circles are anchored on the old end by Tertiary (65- to 1.8-Ma) reversed-polarity-bias CRM and on the young end by PADF (10^4 - to 10^6 -yr) or PF ($<10^2$ -yr) normal-polarity VRM or induced magnetization, then shallow-inclination, eastern-hemisphere vector sums (remagnetization-circle midpoints) provide reasonable explanations for dipolar HRGM anomalies with eastern-hemisphere azimuths.

Model 1A

According to Model 1A, dipolar HRGM anomalies in Western Canada reflect a vector sum (nearly equal balance) between a 10-m.y. pulse of reversed-polarity-bias CRM and normal-polarity magnetization aligned with the present axial-dipole field (PADF) direction. The normal-polarity component must reflect VRM acquired during the past 10^4 to 10^6 yr. The reversed-polarity component is modeled as reversed-polarity-bias CRM acquired during a 10-m.y. pulse of microseepage at a time of re-

versed-polarity bias in the Tertiary. When averaged over 10-m.y. windows, reversed-polarity bias has prevailed for 88% of the time for windows centered between 63 and 5 Ma (Figure B-1a).

Model 1A can be summarized by the equation:

$$J_{\text{HRGM}} = J_{\text{CRM-Rbias}} + J_{\text{VRM-PADF}}$$

where J_{HRGM} is the HRGM anomaly intensity, $J_{\text{CRM-Rbias}}$ is the intensity of the reversed-polarity-bias CRM, $J_{\text{VRM-PADF}}$ is the intensity of the viscous remanent magnetization pointing to the present-axial-dipole field direction ($D/I = 0^\circ/+68^\circ$), and with the following conditions:

$$\begin{aligned} J_{\text{CRM-Rbias}} &\cong J_{\text{VRM-PADF}} \\ J_{\text{Induced}} &\cong 0. \end{aligned}$$

This model is best illustrated by paleomagnetic data from subsurface cores in hydrocarbon reservoirs of the Alberta and Williston Basins (Figure C-2). In these subsurface cores, each paleomagnetic specimen is probably time-averaging the geomagnetic field for about 10 m.y., as in Figure B-1a. The best-fit 57-Ma reference remagnetization circle for the Beaverhill Lake/Swan Hills data in Figure C-2a implies that these reservoir rocks from the Duvernay Petroleum System were chemically remagnetized over the interval 62–52 Ma, when reversed-polarity bias was 80%. This is near the maximum reversed-polarity-bias value (83%) during the early Tertiary reversed-polarity-bias interval (Figure B-1a).

According to Model 1A, this Tertiary reversed-polarity-bias CRM is in nearly equal balance with normal-polarity viscous remanent magnetization (PADF VRM) acquired during the past 10^4 to 10^6 yr. On the magnetic-polarity time scale of Ogg (1995), the polarity bias changes from reversed to normal at 1.74 Ma, when time-averaged over the “past x m.y.” (Figure B-1c). Although a depth of about 150 m (i.e., the estimated average depth to source of HRGM anomalies in Western Canada) might seem too shallow to record PADF VRM (rather than the PF VRM recorded in surface-outcrop samples as in Figure C-1), we must keep in mind that our central Alberta study area probably experienced about 500 m of uplift during the past 2 m.y. (Figure 21). As a result of this uplift, the coarsest magnetic grains (multidomain grains $>10 \mu\text{m}$) within the magnetically enhanced zones might well have recorded a viscous partial thermoremanent magnetization (VPTRM). Acquisition of VPTRM, also known as thermoviscous remanent magnetization (TVRM; Butler, 1992) has been described by Pullaiah et al. (1975). VPTRM is VRM acquired at elevated temperatures during burial and subsequently “frozen in” upon cooling during uplift. As indicated in Figure B-1c, VPTRM acquired during the past 1.74 m.y. will exhibit normal polarity (i.e., reversed-polarity bias $<50\%$).

Model 1A represents growth of authigenic magnetic

minerals in a magnetically enhanced zone during a single 10-m.y. pulse of high microseepage flux. This pulse corresponds to a time of high fracture permeability in the seal of the petroleum system containing the microseeping reservoir. By analogy with the Piceance Basin (Figure 20a), the most likely times for HRGM anomalies in Western Canada would be during the early Tertiary (“Pulse 1 fractures” on the blue curve in Figure 20a) and during the middle Tertiary (“Pulse 2 fractures” on the blue curve in Figure 20a). Note that the magnetic grain-size distribution in Model 1A is unimodal (Figure D-1b), with about half the grains in the single-domain (0.05–1 μm) and pseudosingle-domain (1–10 μm) range and half the grains in the multidomain (>10 μm) range. Grains <10 μm record the reversed-polarity-bias CRM (blue arrows in Figure D-1a); grains >10 μm record the normal-polarity PADF VRM or VPTRM (green arrows). Their vector sum yields the resultant vector (red arrows), which represents the total magnetization recorded in the magnetically enhanced zone. The red arrow in Figure D-1a has an azimuth of 62°, like “Nisku” HRGM anomalies.

Model 1B

According to Model 1B, the dipolar HRGM anomalies in Western Canada reflect a vector sum (nearly equal balance) between a 10-m.y. pulse of reversed-polarity-bias CRM and a normal-polarity magnetization aligned with the present-magnetic-field (PF) direction. The normal-polarity component could reflect either induced magnetization or VRM acquired during the past <10² yr. As in Model 1A, the reversed-polarity component is modeled as reversed-polarity-bias CRM acquired during a 10-m.y. pulse of microseepage at a time of reversed-polarity bias during the Tertiary. The only difference between Models 1A and 1B is that in Model 1B, the average grain size of the magnetic minerals in the magnetically enhanced zones is slightly larger (recording PF VRM) than in Model 1A (recording PADF VRM).

Model 1B can be summarized by the equation

$$J_{\text{HRGM}} = J_{\text{CRM-Rbias}} + J_{\text{VRM-PF}} + J_{\text{Induced}}$$

where the notation is the same as in Model 1A, except that $J_{\text{VRM-PF}}$ is viscous remanent magnetization pointing to the present-field direction ($D/I = 18^\circ/+75^\circ$), and J_{Induced} is induced magnetization also pointing to the present-field direction ($D/I = 18^\circ/+75^\circ$) and with the following condition:

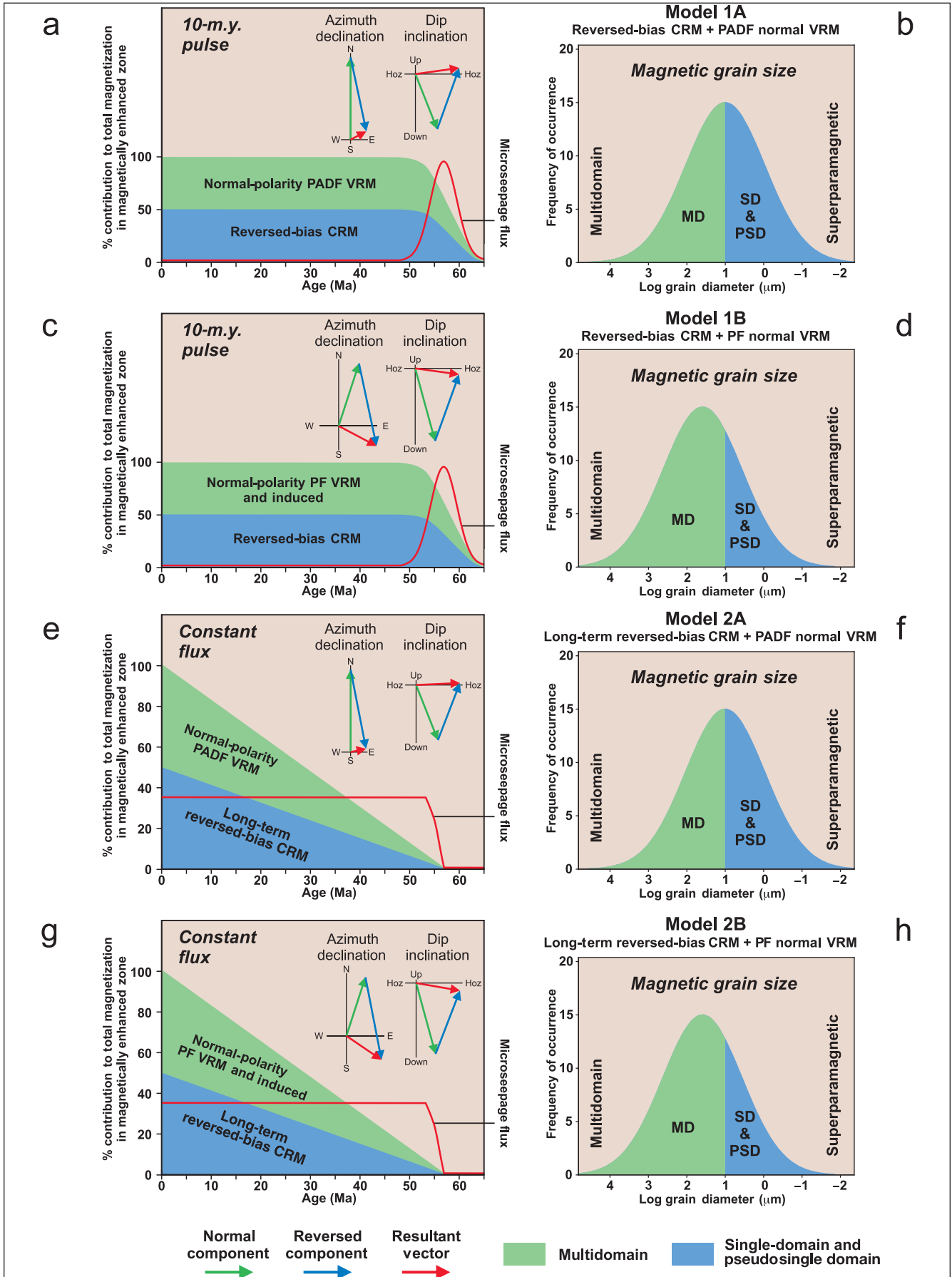
$$J_{\text{CRM-Rbias}} \cong J_{\text{VRM-PF}} + J_{\text{Induced}}$$

This model is best illustrated by paleomagnetic data from surface-outcrop samples in hydrocarbon reservoir rocks (Rundle Group) at Moose Mountain, Alberta; this is an actual example in which intermediate average NRM directions (i.e., vector sums halfway between normal and reversed polarity) were produced, either by nearly equal balances within individual 11-cm³ specimens (Figure C-1d) or by the average direction of a streaked distribution (Figure C-1b). According to Model 1B, requirements for the nearly equal balance between normal- and reversed-polarity components are relaxed somewhat (51 \pm 3% reversed component; Figure D-5a) compared with Model 1A (49.5 \pm 1.5% reversed component; Figure D-4a), so that this nearly equal balance could be achieved more easily.

In the Moose Mountain example, the reversed-polarity CRM recorded in each paleomagnetic specimen is probably time-averaging the geomagnetic field for about 10 m.y., as in Figure B-1a. These Mississippian reservoir rocks, like Devonian reservoir rocks of the underlying Duvernay Petroleum System (Figure C-2a) and Pulse 1 magnetically enhanced zones over Nisku reservoirs, were probably chemically remagnetized between 62 and 52 Ma, when the reversed-polarity bias was near its maximum during the early Tertiary reversed-polarity-bias interval (Figure 20).

Model 1B represents growth of authigenic magnetic

FIGURE D-1. Four possible models for the origin of shallow-inclination, eastern-hemisphere magnetization directions inferred from dipolar HRGM anomalies in Western Canada. CRM = chemical remanent magnetization; VRM = viscous remanent magnetization; PADF = present axial dipole field ($D/I = 0^\circ/+68^\circ$) = past 10⁴–10⁶ yr; PF = present magnetic field ($D/I = 18^\circ/+75^\circ$) = past <10² yr. The models differ as to whether the reversed-polarity component (blue) reflects acquisition of CRM in a single 10-m.y. pulse of enhanced microseepage (Models 1A and 1B) or reflects linear acquisition of CRM at constant flux from the initiation of microseepage to the present (Models 2A and 2B). The models also differ as to whether the normal-polarity component (green) represents PADF VRM (Models 1A and 2A, as in Figure C-2) or represents PF VRM (Models 1B and 2B, as in Figure C-1). The insets at the top right corner of a, c, e, and g show how the reversed component (blue arrows) and the normal component (green arrows) add vectorially to yield the resultant vector (red arrows). These red arrows represent the shallow-inclination, eastern-hemisphere magnetizations recorded in the magnetically enhanced zones responsible for the dipolar HRGM anomalies. Note that different models yield much different HRGM anomaly azimuths, even though the microseepage age is 57 Ma in all four examples. The reversed-polarity CRM resides in single-domain (0.05–1 μm) and pseudosingle-domain (1–10 μm) grains, whereas the normal-polarity VRM resides in multidomain grains (>10 μm).



minerals in a magnetically enhanced zone during the same 10-m.y. pulse of high microseepage flux described for Model 1A. The only difference in Model 1B is that more than half of the magnetic grains are multidomain ($>10\ \mu\text{m}$); the magnetic grain-size distribution peaks at about $50\ \mu\text{m}$ (Figure D-1d), compared with $10\ \mu\text{m}$ as in Model 1A (Figure D-1b). Although this grain-size difference may seem subtle, it produces a 56° change in the modeled HRGM anomaly azimuth (red resultant vectors in Figure D-1), from an east-northeast azimuth of 62° (like Nisku HRGM anomalies; Figure D-1a) to an east-southeast azimuth of 118° (like Leduc HRGM anomalies; Figure D-1c). This example demonstrates how the magnetic grain-size distribution within a magnetically enhanced zone can exert a profound influence on the HRGM anomaly azimuth.

Model 2A

According to Model 2A, dipolar HRGM anomalies in Western Canada reflect a vector sum (nearly equal balance) between long-term reversed-polarity-bias CRM and normal-polarity magnetization aligned with the present axial-dipole field (PADF) direction. As in Model 1A, the normal-polarity component must reflect PADF VRM or VPTRM acquired during the past 10^4 to 10^6 yr. The reversed-polarity component is modeled as reversed-polarity-bias CRM acquired during constant-flux microseepage into the magnetically enhanced zones, from the initiation of microseepage to the present.

Model 2A can be summarized by the same equation and conditions that apply to Model 1A. The only difference between Models 2A and 1A is that in Model 2A, the reversed-polarity component reflects long-term acquisition of CRM from the initiation of microseepage to the present, rather than in a single 10-m.y. pulse as in Model 1A. In both models, the reversed-polarity component resides in the pseudosingle-domain and single-domain half of a unimodal grain-size distribution.

Model 2A was inspired by Larson et al. (1982), who proposed long-term acquisition of CRM during “several tens of millions of years” as the explanation for the magnetization of most red beds. Although this represents one of the end-member models for the “red bed controversy” in paleomagnetism (Butler, 1992), long-term acquisition of CRM seems even more likely within magnetically enhanced zones above microseeping hydrocarbon reservoirs. In our Alberta Basin case-history areas, the hydrocarbon reservoirs of the Duvernay Petroleum System were almost certainly filled in the early Tertiary and fractured in the waning stages of the Laramide orogeny (55–38 Ma; Stockmal et al., 1997). These fractures would be expected to be held open in the present-day in-situ stress field (Bell et al., 1994), and microseepage is demonstrably occurring over these reservoirs at present. Thus, the constant microseepage flux required by Models 2A and 2B is geologi-

cally reasonable, especially for microseepage being driven by methane exsolution upon uplift (e.g., the horizontal red and dashed-red line labeled “exsolved methane in gas phase” in Figure 20a from 32 Ma to the present).

Model 2B

According to Model 2B, dipolar HRGM anomalies in Western Canada reflect a vector sum (nearly equal balance) between long-term reversed-polarity-bias CRM and normal-polarity magnetization aligned with the present-magnetic-field (PF) direction. As in Model 1B, the normal-polarity component could reflect either induced magnetization or viscous remanent magnetization (VRM) acquired during the past $<10^2$ yr. The reversed-polarity component is modeled as reversed-polarity-bias CRM acquired during constant-flux microseepage into the magnetically enhanced zones, from the initiation of microseepage to the present.

Model 2B can be summarized by the same equation and conditions that apply to Model 1B. The only difference between Models 2B and 1B is that in Model 2B, the reversed-polarity component reflects long-term acquisition of CRM, from the initiation of microseepage to the present, rather than in a single 10-m.y. pulse, as in Model 1B. In both models, the reversed-polarity component resides in the pseudosingle-domain and single-domain fraction of a unimodal grain-size distribution, with an average value at about $50\ \mu\text{m}$ (i.e., mostly multidomain grains).

Testing the Four Models for Explaining the Dipolar HRGM Anomalies in Western Canada

We now consider whether each of the four models can explain the specific HRGM anomaly azimuths we observe over Nisku, Leduc, Cretaceous, and Alida reservoirs in Western Canada. Results of this analysis are summarized earlier in this chapter in Table 3, which is a 4×4 matrix of the best-fit remagnetization circle ages according to each model. An “x” in Table 3 indicates that the model cannot explain the particular HRGM anomaly azimuth, for reasons discussed below. Although 16 figures would be needed to illustrate each model for each of the HRGM anomaly classes, to conserve space, we included figures showing three typical examples for Models 1A, 1B, and 2A.

In testing the four models, we calculated reference remagnetization circles for two locations: (1) in the central Alberta Basin at 51.6°N , 112.7°W , and (2) in the Waskada field (southwest Manitoba) at 49.1°N , 100.7°W . The following paleomagnetic reference poles were used, and other ages cited in the text are based on linear interpolation between reference directions calculated from these reference poles.

64 Ma	the Paleocene reference pole (81.5°N, 192.6°E) listed in Table 6 of Diehl et al. (1983), with the 64-Ma age based on weighted-average ages (by number of sites) in their Table 5
57 Ma	the bisector of reference directions calculated from the 64- and 49-Ma reference poles
49 Ma	the middle-early Eocene reference pole (82.8°N, 170.4°E) listed in Table 6 of Diehl et al. (1983), with the 49-Ma age based on weighted-average ages (by number of sites) in their Table 5
35 Ma	the 30- to 40-Ma middle Tertiary reference pole (80.5°N, 149.4°E) listed in Table 3 of Diehl et al. (1988)
30 Ma	the 20- to 40-Ma middle Tertiary reference pole (81.5°N, 147.3°E) listed in Table 3 of Diehl et al. (1988)
25 Ma	the 20- to 30-Ma middle Tertiary reference pole (82.0°N, 146.9°E) listed in Table 3 of Diehl et al. (1988)
17 Ma	the bisector of reference directions calculated from the 30- and 5-Ma reference poles
5 Ma	the 11-Ma reference pole (87.7°N, 73.6°E) listed in Table 4.2 of Van Alstine (1979). Of the 20 paleomagnetic poles included in this average pole, 80% have ages <7 Ma. For these 20 poles, 5 Ma is their average age.

The reference remagnetization circles we used to test the four models are shown in Figure D-2. For Models 1A and 1B (the 10-m.y. pulse models), calculating the reference remagnetization circles was straightforward, because we merely needed to connect the known PADF (Model 1A) or PF (Model 1B) direction with age-dated reversed-polarity “test points” calculated directly from the North American reference APW path (i.e., the red reversed-polarity directions shown in Figure 18b). For Models 2A and 2B (the long-term CRM models at constant flux), the normal-polarity components are the same PADF and PF normal-polarity magnetizations as in Models 1A and 1B. However, the reversed-polarity test points require more work to simulate accurately, as discussed below.

In this study, we simulated long-term acquisition of CRM during tens of millions of years by constructing a “polarity-bias-weighted reference ADW path.” This technique *combines* the North American reference APW path with the magnetic-polarity time scale to calculate the expected “long-term CRM” direction and polarity in magnetically enhanced zones with different microseepage initiation ages. This methodology assumes that CRM acquisition is linear (at constant microseepage flux), from the initiation of microseepage to the present. At each of 10,000 equally spaced time increments from the simulated microseepage initiation age to the present, we calculated a unit vector pointing toward the reference magnetization direction with the closest age. Each unit vector was assigned either normal polarity (if its age fell

within a normal-polarity chron on the magnetic-polarity time scale) or reversed polarity (if its age fell within a reversed-polarity chron on the magnetic-polarity time scale). At the end of the simulation, the vector sum of all 10,000 unit vectors was calculated to yield the resultant vector expected for long-term acquisition of CRM from the simulated microseepage initiation age to the present. As a check on the accuracy of the calculation, the resultant vectors yield R/N polarity ratios nearly identical to the “% reversed-polarity” values indicated in Figure B-1c. In particular, >99% of the long-term CRM simulations for microseepage initiation in the Tertiary (between 65 and 1.8 Ma) exhibit a reversed-polarity resultant vector, as expected from Figure B-1c and as required to form dipolar HRGM anomalies with eastern-hemisphere azimuths.

Figure D-2 reveals significant differences among the reference remagnetization circles (and inferred HRGM anomaly azimuths) predicted by each of the four models. For example, in Model 1A (10-m.y. pulse reversed-bias CRM + PADF normal VRM) in both the Alberta and Williston Basins, the remagnetization-circle midpoints (i.e., inferred HRGM anomaly directions) exhibit increasingly more clockwise azimuths with decreasing age: from northeast at 64 Ma, to east at ~40 Ma, to southeast at 17 Ma, to south at 5 Ma. In contrast, in Model 1B (10-m.y. pulse reversed-bias CRM + PF normal VRM) in both basins, the remagnetization-circle midpoints are confined entirely to the southeastern quadrant, although still with an increasing clockwise azimuth with decreasing age. Regardless of which of the four models is most likely to be correct, they all have the property that nearly equal balances of the reversed- and normal-polarity components will produce dipolar HRGM anomalies with shallow inclinations and eastern-hemisphere azimuths, as indicated by the shaded regions in Figure D-2.

Simulated Remagnetization Circles

In testing the four models, we are attempting to match observed HRGM anomaly directions with remagnetization circles connecting known normal-polarity (PADF or PF) and reversed-polarity (Tertiary reference directions) endpoints. Within magnetically enhanced zones, however, neither the normal- nor the reversed-polarity endpoints will ever be perfectly recorded, so there will always be some dispersion about the endpoints. In paleomagnetism, dispersion about mean directions is measured by the “precision parameter” κ (Fisher, 1953), which is related to the standard deviation in Gaussian statistics. Schmidt (1985) gives the equations for simulating a magnetization direction drawn at random from a distribution that has (1) a true mean direction that is vertically down and (2) a precision parameter κ .

In Figure D-3, we simulated families of remagnetization circles of different ages by (1) drawing 33 directions

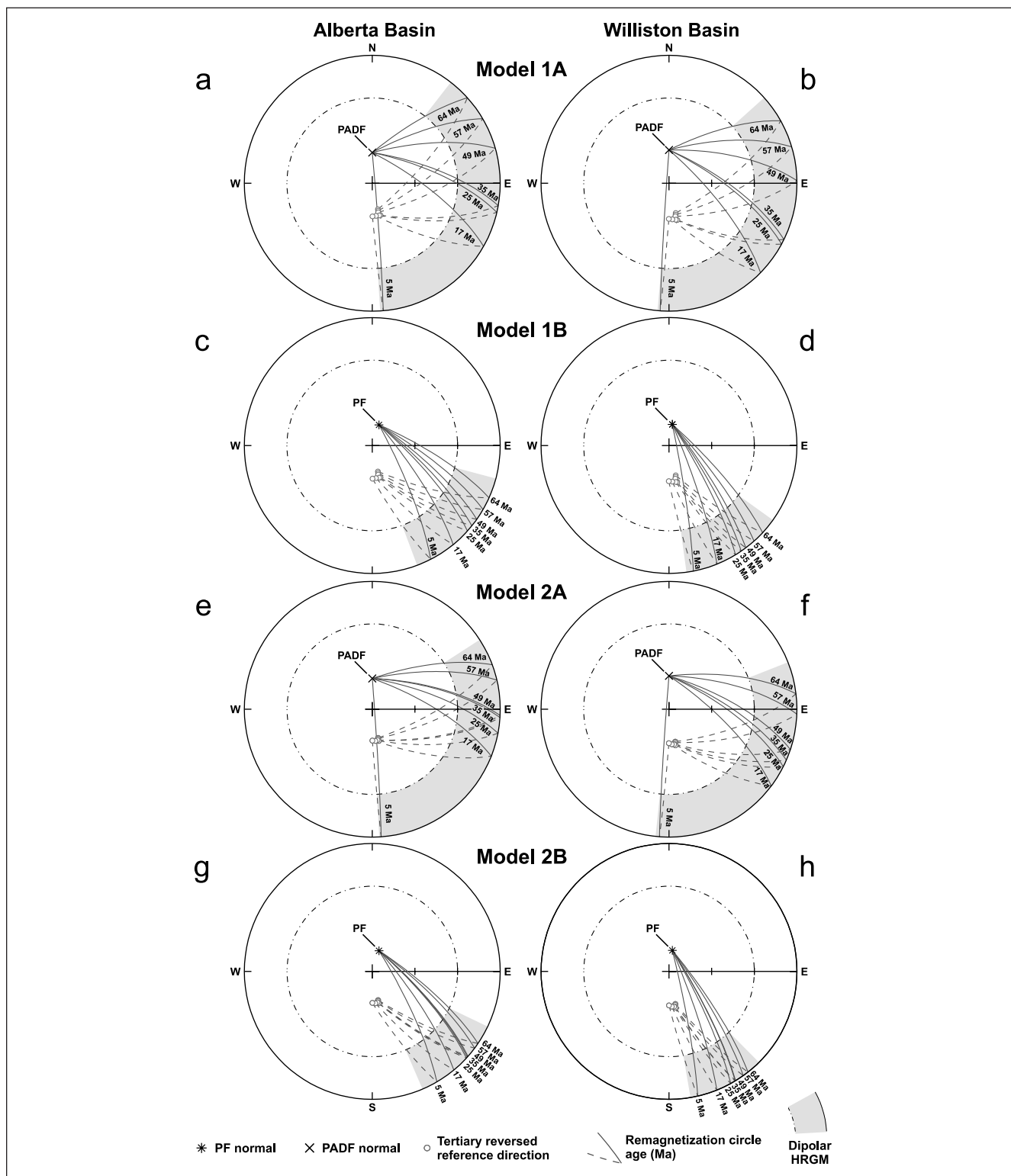


FIGURE D-2. Reference remagnetization circles connecting the known normal-polarity (PADF or PF) VRM directions with Tertiary reversed-polarity CRM directions expected for microseepage at 64, 57, 49, 35, 25, 17, and 5 Ma. For Models 1A and 1B, reversed-polarity directions are calculated directly from the reference North American APW path (i.e., the red circles in Figure 18b). For Models 2A and 2B, reversed-polarity directions are calculated from simulations of long-term CRM acquisition, as described in the text. For all four models, midpoints of the remagnetization circles are within the shaded region in the eastern hemisphere and with shallow inclinations (dips) between $\pm 30^\circ$. Depending on the model, these shaded regions include 83% of the Leduc, Nisku, and Alida HRGM anomaly directions shown in Figure 17b.

at random from one parent normal-polarity distribution with $\kappa = 600$ and with a mean pointing vertically down; (2) drawing 33 directions at random from a parent reversed-polarity distribution also with $\kappa = 600$ but with a mean pointing vertically up; (3) rotating the normal-polarity population so that the mean of its parent distribution coincides with the normal-polarity direction to be tested (i.e., PF or PADF); (4) rotating the reversed-polarity population so that the mean of its parent distribution coincides with the reversed-polarity direction to be tested (i.e., Tertiary reference directions); and (5) drawing alternately from the two rotated populations to connect one normal-polarity simulated direction with one reversed-polarity simulated direction. This yields populations of 33 remagnetization circles that can be used to predict HRGM anomaly directions (i.e., remagnetization-circle midpoints) based on each of the four models. We have no reason a priori to think that the normal- or reversed-polarity magnetizations would have different dispersions, which is why we assigned $\kappa = 600$ to both the parent normal- and reversed-polarity distributions. However, there is nothing magical about the $\kappa = 600$ value used in computing Figure D-3. For any given modeled age, increasing the κ value increases the clustering of midpoints (red stars), and decreasing the κ value increases the dispersion of midpoints.

In Figure D-3, we show examples of simulated remagnetization circles at 17, 30, and 57 Ma, according to Models 1A (Figure D-3e, f, g) and 1B (Figure D-3a, b, c). A red star marks the midpoint of each individual remagnetization circle, where the reversed/normal-polarity ratio is 50/50. For each stereographic projection, the average of the red stars (there would be billions of them in a real magnetically enhanced zone) would represent the observed HRGM anomaly direction for the simulated microseepage age, if our hypothesis is correct that HRGM anomalies record approximate midpoints of remagnetization circles.

As revealed in Figure D-3, the remagnetization circle trajectories and dispersion are controlled by the angle between the normal- and reversed-polarity endpoint directions. The “ Δ antiparallel angle” on the ordinate in Figure D-3d indicates the number of degrees by which the normal- and reversed-polarity reference directions differ from being “antiparallel” (i.e., from being 180° apart, or pointing in opposite directions). For Models 1B and 2B (both having PF normal-polarity components), the normal- and reversed-polarity reference directions are always between 8° and 13° from being antiparallel, so the remagnetization circles trend more consistently toward the southeastern quadrant. In contrast, for Models 1A and 2A (both having PADF normal-polarity components), the normal- and reversed-polarity reference directions are 4° to 6° from being antiparallel during the period 64 to 30 Ma, after which this Δ antiparallel angle then decreases almost linearly, to 0° at present. As the Δ antiparallel

angle decreases, the dispersion of remagnetization-circle azimuths increases.

Explanation of the Nisku HRGM Anomaly Direction

As indicated in Table 3, the HRGM anomalies above microseeping Nisku reservoirs are demonstrably the oldest, because only a 10-m.y. pulse centered on 57 Ma (Model 1A) or constant-flux microseepage from 64 Ma to the present (Model 2A) can explain the cluster of Nisku HRGM anomaly azimuths in the northeastern quadrant (Figure 17). Preservation of an ~ 60 Ma CRM in magnetically enhanced zones above Nisku reservoirs is the best paleomagnetic “proof” that magnetically enhanced zones of Western Canada probably represent eroded vertical geochemical chimneys, because at least 700 m of sediment has been removed by erosion since maximum burial at ~ 38 Ma (Figures 19, 20, and 21).

Figure D-4 illustrates details of how HRGM anomalies with east-northeast azimuths can be produced according to Model 1A. This model assumes a nearly equal balance between normal-polarity PADF VRM and reversed-polarity-bias CRM acquired in a single pulse of enhanced microseepage from 62 to 52 Ma. According to this model, the reversed-bias CRM was acquired during the Pulse 1 fracture event (Figure 20a, Piceance Basin analog), which probably corresponds to late Laramide thrusting in the Alberta Foothills (Figure 20b). Model 1A is exactly how we explain the ubiquitous early Tertiary reversed-polarity CRM we observe in subsurface cores from the Duvernay Petroleum System (e.g., Figure C-2a). Thus, explaining Nisku HRGM anomalies by Model 1A is appealing in that it links geochemical and paleomagnetic changes in the Devonian reservoirs to geochemical and paleomagnetic changes in the magnetically enhanced zones and in the geochemical chimneys detected by HRGM surveys.

In Figure D-4a, vector sums (red circle symbols) were calculated at 101 points corresponding to a mixing of the reversed-bias CRM with the normal-polarity PADF VRM in ratios between 0% R (= the PADF direction) and 100% R (= the reversed-polarity 57-Ma reference direction). The remagnetization circle (red) connecting the 101 calculated points matches the 57-Ma reference remagnetization circle in Figure D-2a. In Figure D-4a, the shaded region near the edge of the stereographic projection in the northeastern quadrant and with an inclination of $+30^\circ$ to -30° represents the region where dipolar HRGM anomalies with east-northeast azimuths can be expected. This shaded region corresponds to maximum/minimum ratios of 0.5 to 2.0; these ratios were observed for 87% of the 15 Nisku HRGM anomalies from the Alberta Basin case-history areas. This shaded region also corresponds to mixing of the N (normal-polarity PADF VRM) and R (reversed-polarity 57-Ma CRM) vectors in ratios of 48% to

51%, demonstrating the nearly equal balance required to explain Nisku HRGM anomalies according to Model 1A.

Figure D-4b illustrates, at five of these 101 points, how the PADF magnetization (green arrows pointing toward true north and down) and the 57-Ma reversed-polarity magnetization (blue arrows pointing toward the south-southeast and up) add vectorially (head-to-tail rule) to produce the resultant vector (red arrows). The 62° azimuth of the red arrow at 50% R closely matches the azimuth of the Nisku HRGM anomaly average (D/I = 61°/-5°) in Figure 17b.

Figure D-4c reveals that even with a 50/50 balance between normal- and reversed-polarity components, according to Model 1A, 4.0% of the remanent magnetization is *not* self-canceled by normal- and reversed-polarity magnetizations pointing in opposite directions. This implies that even with a Δ antiparallel angle as small as 4.6° (Figure D-3d), significant *remanent* magnetization (red resultant vectors in Figure D-4b) can be expected to be preserved in magnetically enhanced zones in Western Canada, a situation unlike the complete self-cancellation of remanent magnetization that Reynolds et al. (1990b) postulated at Cement field, Oklahoma. Moreover, as indicated in Figure 20c, a 10-m.y. microseepage pulse centered on 57 Ma occurs near the maximum reversed-bias value (83%) of the early Tertiary reversed-polarity-bias interval, so that remanent magnetization also is *not* self-canceled by geomagnetic polarity reversals.

Simulated remagnetization circles for Nisku HRGM anomalies according to Model 1A are shown in Figure D-3g. These circles closely resemble the actual remagnetization circles derived from paleomagnetic studies of subsurface cores of the Duvernay Petroleum System in the Alberta Basin (Figure C-2a). The similarity between Figure C-2a and Figure D-3g, the cluster of Nisku HRGM anomalies in Figure 17b, and the geologic plausibility of 57 Ma microseepage from Nisku reservoirs fractured during late Laramide thrusting (Figure 20b) increase our confidence that the HRGM anomalies are in fact recording midpoints on remagnetization circles and are not merely arti-

facts of our procedures. We emphasize again that the HRGM anomaly azimuths were picked by author LeSchack before he was aware of their paleomagnetic implications.

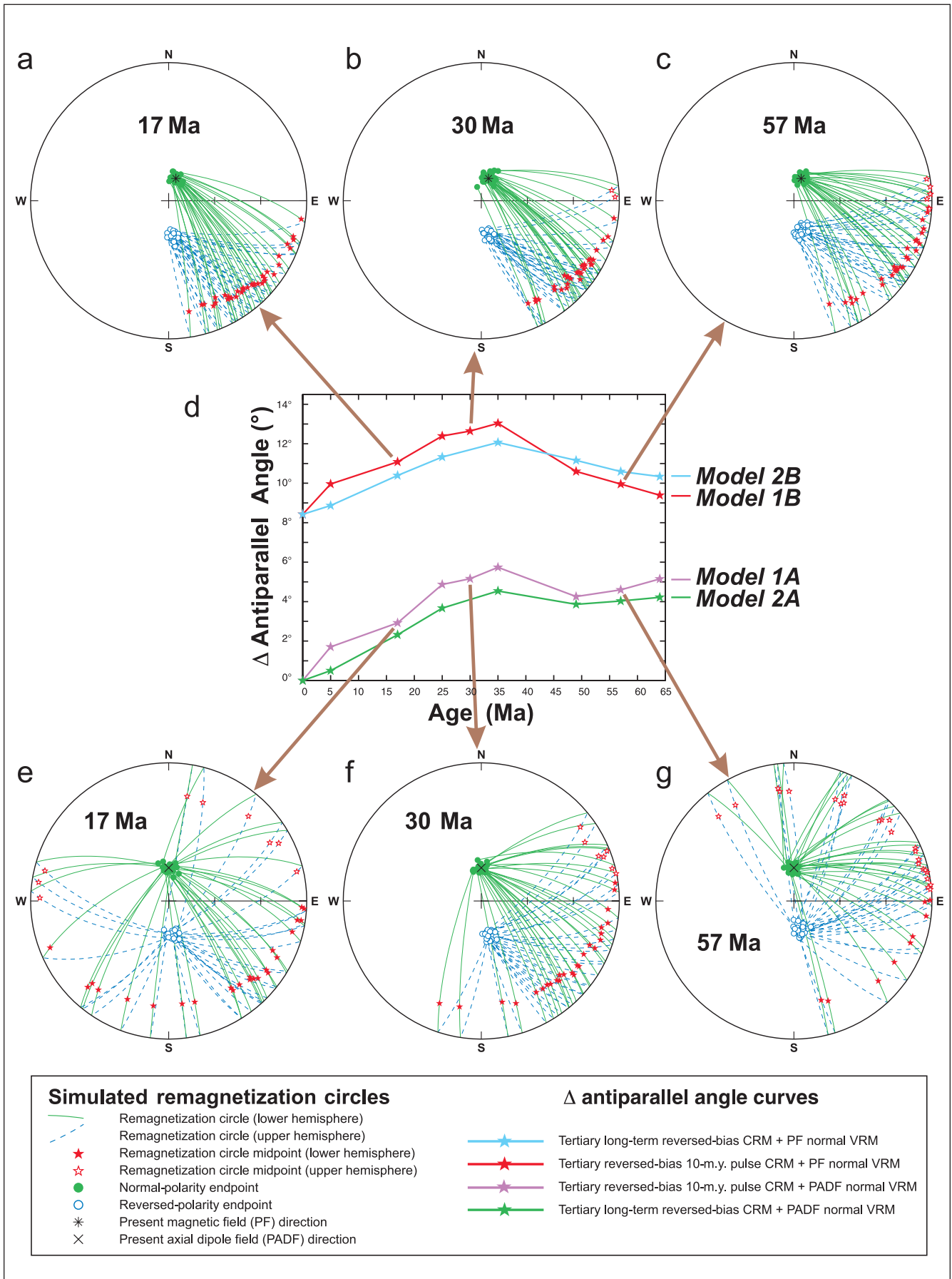
In Table 3, we also listed the 64-Ma Model 2A as an alternative explanation for Nisku HRGM anomalies. However, this option is less plausible than the 57-Ma Model 1A option discussed above. Constant-flux microseepage from 64 Ma to the present is geologically unlikely, considering the multistage fracture, subsidence, and uplift history for Tertiary time in the Alberta Basin (Figure 20). Moreover, the 64-Ma reference remagnetization circle for Model 2A in Figure D-2e is more clockwise than is the average Nisku HRGM anomaly azimuth, and any significantly older ages are precluded by the 63- to 67-Ma maximum age of the host rock (Paskapoo/Scollard Formations).

Explanation of the Leduc HRGM Anomaly Direction

HRGM anomalies above Leduc reservoirs are fundamentally different from HRGM anomalies above Nisku reservoirs in two ways: (1) Leduc HRGM anomalies are, on average, five times stronger than Nisku anomalies, and (2) Leduc HRGM anomalies exhibit east-southeast (120°) azimuths, whereas Nisku anomalies exhibit east-northeast (61°) azimuths. In evaluating which of the four models can explain the Leduc HRGM anomalies, we emphasize that Nisku reservoirs of this study are drape traps over Leduc pinnacle reefs, and oil in these Nisku reservoirs is thought to have migrated out of fractured Leduc pinnacle reefs (Podruski et al., 1987). Thus, if microseepage occurred above Nisku reservoirs at ~60 Ma, then it also probably occurred above Leduc reservoirs at ~60 Ma.

As indicated in Table 3, two possible explanations for Leduc HRGM anomalies are provided by Model 1B (10-m.y. pulse centered on 57 Ma) and Model 2B (constant-flux microseepage from 64 Ma to the present). As shown

FIGURE D-3. Simulated remagnetization circles for Model 1B (top) and Model 1A (bottom) reflecting reversed-polarity-bias CRM acquired in a single 10-m.y. microseepage pulse centered on 17, 30, or 57 Ma. The midpoints of the remagnetization circles (red stars) are the points where the normal-polarity (green) and reversed-polarity (blue) components are in equal balance, as inferred in magnetically enhanced zones responsible for dipolar HRGM anomalies. Dispersion about the mean normal- and reversed-polarity reference directions is simulated by $\kappa = 600$ (Fisher, 1953) for $N = 33$ modeled remagnetization circles. The scatter and trajectories of remagnetization circles are controlled by the “ Δ antiparallel angle” between the normal- and reversed-polarity components. The Δ antiparallel angle (graph at center) indicates the number of degrees by which the normal- and reversed-polarity components differ from being antiparallel (i.e., point in opposite directions, in which case they would self-cancel). For Models 1B and 2B, the Δ antiparallel angle is consistently $>8^\circ$, so good clustering of HRGM anomaly azimuths can be expected for microseepage occurring any time in the Tertiary. For Models 1A and 2A, microseepage ages >25 Ma will produce good clustering of HRGM anomalies (as observed above Nisku and Leduc reservoirs), because the Δ antiparallel angle is $>4^\circ$. For Models 1A and 2A, microseepage ages <25 Ma will produce scattered HRGM anomaly azimuths with a distinctive shadow zone in the northwest quadrant (as in Figure D-3e and as observed above Cretaceous reservoirs), because the Δ antiparallel angle is between 0° and 4° .



in Figure D-1d and h, these two models are coarser-grained versions of the two models (1A and 2A) discussed above for the Nisku. Of these two Leduc models, Model 1B provides the better match between the reference remagnetization circle and the average direction of the cluster of five Leduc anomalies in Figure 17b. Thus, we illustrate Model 1B at 57 Ma in greater detail in Figure D-5.

In Figure D-5a, vector sums (red circle symbols) were calculated at 101 points corresponding to mixing of the reversed-bias CRM with the normal-polarity PF VRM in ratios between 0% R (= the PF direction) and 100% R (= the reversed-polarity 57-Ma reference direction). The remagnetization circle (red) connecting the 101 calculated points matches the 57-Ma reference remagnetization circle in Figure D-2c. In Figure D-5a, the shaded region near the edge of the stereographic projection in the southeastern quadrant and with inclination of $\pm 30^\circ$ represents the region where dipolar HRGM anomalies with east-southeast azimuths can be expected. This shaded region corresponds to maximum/minimum ratios of 0.5 to 2.0; these ratios were observed for all five of the Leduc HRGM anomalies in the Alberta Basin case-history areas. This shaded region also corresponds to mixing of the N (normal-polarity PF VRM or induced) and R (reversed-polarity 57 Ma reference direction) vectors in ratios of 48% to 54%. These ratios would be easier to achieve than the 48% to 51% nearly equal balance required for Nisku HRGM anomalies according to Model 1A (Figure D-4a).

Figure D-5b illustrates, at five of these 101 points, how the PF magnetization (green arrows pointing toward magnetic north and down) and the 57 Ma reversed-polarity magnetization (blue arrows pointing toward the south-southeast and up) add vectorially to produce the resultant vector (red arrows). The 118° azimuth of the red

arrow at 50% R closely matches the azimuth of the Leduc HRGM anomaly average ($D/I = 120^\circ/+2^\circ$) in Figure 17b and also closely matches the 117° azimuth of the type example of a dipolar HRGM anomaly at the Rumsey reef (Figure 15).

Figure D-5c reveals that even with a 50/50 balance between normal- and reversed-polarity components according to Model 1B, 8.7% of the remanent magnetization is *not* self-canceled by normal- and reversed-polarity magnetizations pointing in opposite directions. This value is about twice the 4.0% value indicated for the Nisku in Figure D-4c. Thus, about half of the increase in intensity of Leduc HRGM anomalies compared with Nisku HRGM anomalies can be explained merely by the different amounts of vector self-cancellation predicted by Models 1A and 1B at 57 Ma. This difference reflects the greater Δ antiparallel angle for Model 1B (10.0°) compared with Model 1A (4.6°) at 57 Ma (Figure D-3d). Again, this example illustrates the profound control that magnetic grain size exerts on the azimuth and strength of HRGM anomalies, because the only difference between these two models is the coarser grain size of Model 1B (Figure D-1d).

The greater strength of Leduc HRGM anomalies compared with Nisku anomalies is also probably controlled by the *greater volume* of light-hydrocarbon gases that seeped from Leduc pinnacle-reef reservoirs compared with Nisku biostrome reservoirs. Greater volumes of microseepage from Leduc reservoirs would probably increase the average magnetic grain size in the magnetically enhanced zones. This may explain why authigenic magnetic minerals are mostly multidomain above Leduc reservoirs (average grain size $\sim 50 \mu\text{m}$, according to Model 1B). In contrast, only about half of the authigenic mag-

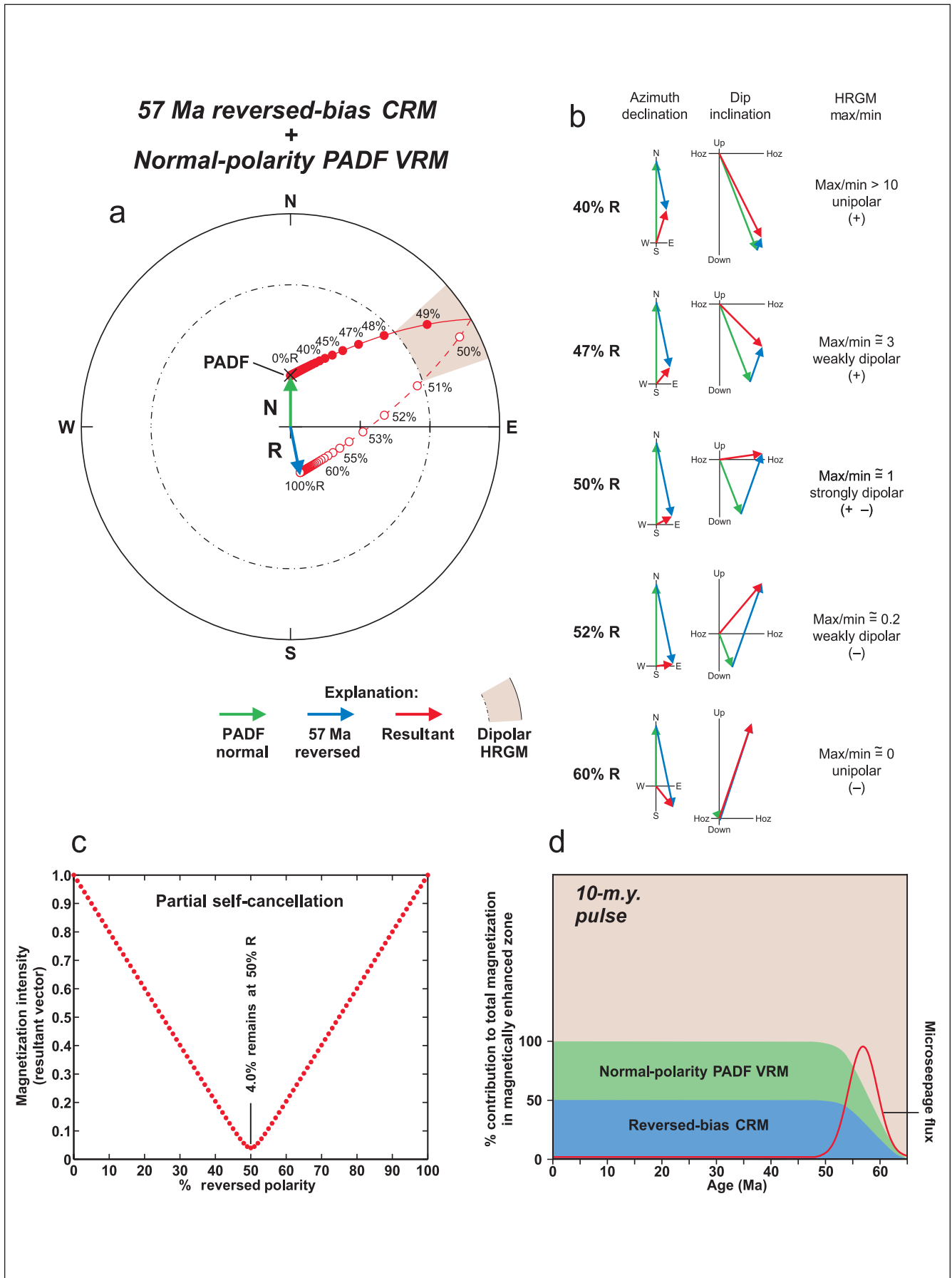
FIGURE D-4. Explanation of Nisku HRGM anomalies with east-northeast azimuths by Model 1A: a 10-m.y. pulse of enhanced microseepage centered on 57 Ma. The magnetically enhanced zones are inferred to record a nearly equal balance (vector sum) between reversed-polarity-bias CRM, acquired from 62 to 52 Ma, and normal-polarity PADF VRM.

(a) Stereographic projection on which endpoints of resultant vectors (red dots) are plotted for 101 points representing mixing of the normal-polarity (green) and reversed-polarity (blue) reference directions in ratios between 0%R (= PADF reference direction, $D/I = 0.0^\circ/+68.4^\circ$) and 100%R (= reversed-polarity 57 Ma reference direction, $D/I = 168.0^\circ/-70.2^\circ$). The shaded region in the northeast quadrant corresponds to inclinations (dips) of $\pm 30^\circ$, which is where dipolar HRGM anomalies can be expected.

(b) At five of the red points shown in (a), vector addition of the normal-polarity PADF component (green arrows) + the reversed-polarity 57 Ma reference direction (blue arrows) yields the resultant vector (red arrows) recorded in the magnetically enhanced zone. At 50% R, which represents the midpoint of the remagnetization circle shown in (a), the azimuth of the resultant vector is 62° , which closely matches the 61° average HRGM anomaly azimuth we observe over Nisku reservoirs in the Alberta Basin.

(c) For Model 1A, the normal-polarity PADF direction and the 57-Ma reversed-polarity reference direction differ by 4.6° from being antiparallel (Figure D-3d). When these two magnetizations are added vectorially in a 50/50 ratio, they do *not* completely self-cancel, and 4.0% of the intensity remains to be detected in HRGM surveys.

(d) According to Model 1A, the authigenic magnetic minerals in the magnetically enhanced zones grow chiefly during a 10-m.y. pulse of enhanced microseepage, centered on 57 Ma, as modeled here for the Nisku. The reversed-polarity CRM resides in grains $< 10 \mu\text{m}$, which can retain their remanent magnetization for billions of years. The normal-polarity PADF VRM resides in $\sim 10 \mu\text{m}$ multidomain grains that have retained their remanent magnetization only during the past 10^4 to 10^6 yr.



netic minerals are multidomain above Nisku reservoirs (average grain size $\sim 10\ \mu\text{m}$, according to Model 1A).

Although Model 1B provides an attractive explanation for the east-southeast azimuths of Leduc HRGM anomalies, Table 3 suggests yet another possibility—a 10-m.y. pulse of microseepage centered on 30 Ma, according to Model 1A. Leduc HRGM anomalies with east-southeast azimuths could have been produced by a vector sum of PADF VRM and 30-Ma reversed-bias CRM, as indicated by the east-southeast trends of the 25- and 35-Ma reference remagnetization circles in Figure D-2a. Given the small statistical sample size (only five Leduc anomalies) and the possible errors in the reference directions, the 120° average Leduc HRGM anomaly azimuth is sufficiently close to the 103° average midpoint of the 25- and 35-Ma reference remagnetization circles that Model 1A at 30 Ma must be seriously considered.

As illustrated in Figure 20, Model 1A for the Leduc can be imagined as a 10-m.y. pulse of microseepage triggered by uplift after maximum burial, when large volumes of light-hydrocarbon gases probably exsolved and when overpressure was near its maximum. This interval would correspond to the time of Pulse 2 fractures, indicated by the blue curve (Piceance Basin analog) in Figure 20a. Simulated remagnetization circles for Model 1A at 30 Ma are shown in Figure D-3f. At 30 Ma, the Δ antiparallel angle is 5.2° (Figure D-3d), about the same as the 4.6° angle for the Nisku at 57 Ma. Thus, Leduc (if we use Model 1A at 30 Ma) and Nisku (if we use Model 1A at 57 Ma) HRGM anomalies would be expected to achieve equally good clustering of anomaly directions. Also, at 30 Ma, reversed-polarity bias achieves its maximum value (58%) after the early Tertiary reversed-polarity-bias interval (Figure 20c).

Therefore, strong HRGM anomalies would not be precluded by self-cancellation by geomagnetic reversals.

We consider 25 Ma to be the youngest possible age for forming dipolar HRGM anomalies with good clustering of azimuths, according to Models 1A or 2A, because the Δ antiparallel angle quickly falls to $<3^\circ$ from 20 Ma to the present (Figure D-3d). For Δ antiparallel angles $<3^\circ$, extreme vector self-cancellation can be expected to cause scattered HRGM anomaly distributions, as we now discuss for Cretaceous reservoirs of the Alberta Basin.

Explanation of the Cretaceous HRGM Anomaly Directions

At first, interpreting the HRGM anomalies above Cretaceous reservoirs of the Alberta Basin seemed daunting, given their scattered distribution of azimuths (Figure 17b). Why would HRGM anomaly directions above Cretaceous reservoirs not form a unimodal cluster, like the distinctive HRGM anomaly directions above Nisku, Leduc, and Alida reservoirs?

On further analysis, we found that some key properties of the Cretaceous HRGM anomaly distribution are explained nicely by our hypothesis that HRGM anomalies in Western Canada represent midpoints of remagnetization circles connecting normal- and reversed-polarity magnetizations. Below, we show that the Cretaceous HRGM anomaly distribution exhibits three key characteristics expected for microseepage beginning at ~ 17 Ma, according to Models 1A and 2A (Table 3).

Figure D-6a simulates the effects of long-term acquisition of CRM, from 17 Ma to the present, according to Model 2A. Figure D-3e simulates the effects of a 10-m.y.

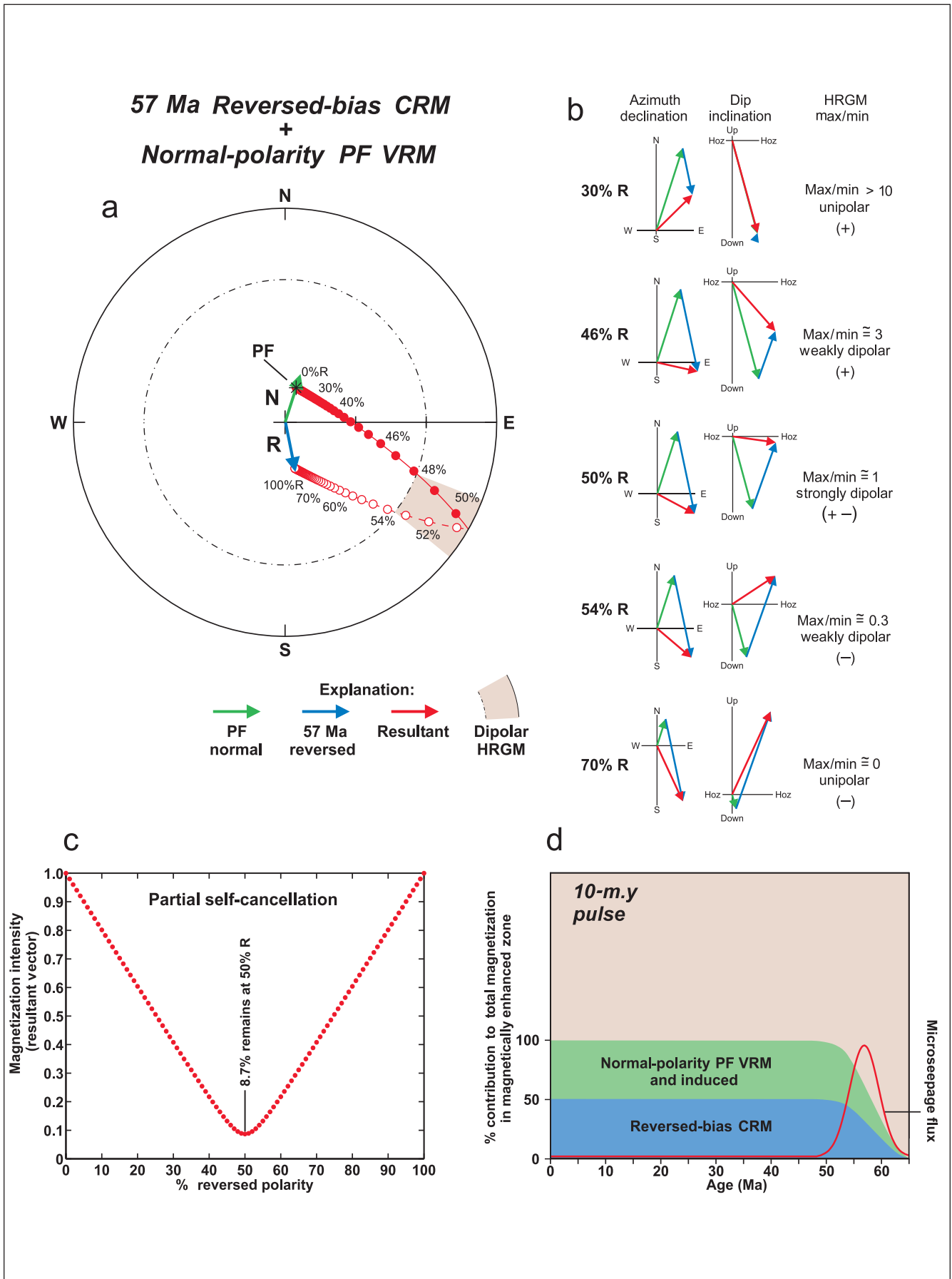
FIGURE D-5. Explanation of Leduc HRGM anomalies with east-southeast azimuths by Model 1B: a 10-m.y. pulse of enhanced microseepage centered on 57 Ma. The magnetically enhanced zones are inferred to record a nearly equal balance (vector sum) between reversed-polarity-bias CRM acquired between 62 to 52 Ma and normal-polarity PF VRM.

(a) Stereographic projection on which endpoints of resultant vectors (red dots) are plotted for 101 points representing mixing of the normal-polarity (green) and reversed-polarity (blue) reference directions in ratios between 0%R (= PF reference direction, $D/I = 18.0^\circ/+74.7^\circ$) and 100%R (= reversed-polarity 57-Ma reference direction, $D/I = 168.0^\circ/-70.2^\circ$). The shaded region in the southeast quadrant corresponds to inclinations (dips) between $\pm 30^\circ$, which is where dipolar HRGM anomalies can be expected.

(b) At five of the red points shown in (a), vector addition of the normal-polarity PF component (green arrows) + the reversed-polarity 57-Ma reference direction (blue arrows) yields the resultant vector (red arrows) recorded in the magnetically enhanced zone. At 50%R, which represents the midpoint of the remagnetization circle shown in (a), the azimuth of the resultant vector is 118° , which closely matches the 120° average azimuth we observe over Leduc reservoirs in the Alberta Basin, including the 117° azimuth at the Rumsey reef (Figure 15).

(c) For Model 1B, the normal-polarity PF direction and the 57-Ma reversed-polarity reference direction differ by 10° from being antiparallel (Figure D-3d). When these two magnetizations are added vectorially in a 50/50 ratio, they do *not* completely self-cancel, and 8.7% of the intensity remains to be detected in HRGM surveys.

(d) According to Model 1B, the authigenic magnetic minerals in the magnetically enhanced zones grow chiefly during a 10-m.y. pulse of enhanced microseepage, centered on 57 Ma, as modeled here for the Leduc. The reversed-polarity CRM resides in grains $<10\ \mu\text{m}$, which can retain their remanent magnetization for billions of years. The normal-polarity PF VRM resides in $>10\ \mu\text{m}$ multidomain grains that can retain remanent magnetization only during the past 10^2 yr.



microseepage pulse centered on 17 Ma, according to Model 1A. Figures D-6a and D-3e reveal three key characteristics of remagnetization-circle midpoints that are expected when the normal- and reversed-polarity endpoints are within 3° of being antiparallel (as occurs at 17 Ma in Western Canada). (1) The remagnetization-circle midpoints no longer form a unimodal distribution but begin to be aligned along a great circle (“girdle distribution”). (2) A remagnetization-circle “shadow zone” forms in the quadrant *opposite* the quadrant containing the 17-Ma reversed-polarity reference direction. (3) Remagnetization-circle midpoints with northeast azimuths are on the upper hemisphere (open red stars), whereas remagnetization-circle midpoints with southwest azimuths are on the lower hemisphere (filled red stars). Figure D-6b reveals that the actual distribution of HRGM anomaly directions above the 33 Cretaceous producers shown in Figure 17b from case-history 6 exhibits all three of these symptoms of a nearly equal balance between two magnetizations that are nearly (but not quite) antiparallel.

Distributions of paleomagnetic directions are commonly analyzed using “moment of inertia” statistics (Mardia, 1972), in which each direction is represented as a point mass on a unit sphere, and the principal moments of inertia of the distribution are computed. Statistical tests can then be made to determine whether an observed distribution of paleomagnetic directions forms a “symmetric bipolar distribution” (i.e., is symmetric about an axis) or whether it forms a “symmetric girdle distribution” (i.e., is symmetric along a great circle) (Mardia, 1972). The 33 simulated 17-Ma remagnetization circles (Figures D-6a and D-3e) pass the test for a symmetric girdle, whereas the observed distribution of 33 Cretaceous

HRGM anomalies (Figure D-6b) is intermediate between a symmetric-bipolar and a symmetric-girdle distribution.

Ideally, in Figure D-6b, we might have expected the minimum eigenvector (brown star) of the distribution of remagnetization-circle midpoints (red stars) to plot closer to the PADF direction, as it does in the simulation (Figure D-6a). This difference probably reflects the coarse interpolation we had to make in converting maximum/minimum HRGM anomaly ratios into dip (inclination) values, using Table 2 of Zietz and Andreasen (1967). The actual sense of the asymmetry (northeast and up versus southwest and down) cannot be an artifact of the interpolation, because *it is a direct outcome of the actual maximum and minimum residual anomaly nT values we measured on the ground.*

For reasons we do not fully understand, the observed Cretaceous HRGM anomalies with east-southeast azimuths (i.e., those more like Leduc azimuths) are underrepresented in Figure D-6b compared with the 17-Ma simulation (Figure D-6a). This might reflect more nearly complete vector self-cancellation (and hence our failure to detect) HRGM anomalies above Cretaceous reservoirs with east-southeast remagnetization-circle midpoints. For example, *after* partial self-cancellation at the midpoint of the 17-Ma Model 2A reference remagnetization circle, only 2.0% of the intensity remains (Figure D-6c). This reflects the 2.3° Δ antiparallel angle between the PADF normal-polarity and the 17-Ma reversed-polarity direction for Model 2A (Figure D-3d). Similarly, for Model 1A (10-m.y. pulse centered on 17 Ma), the Δ antiparallel angle is 2.9° , and 2.6% of the intensity remains after partial self-cancellation. By comparison, 4.0% to 8.7% of the intensity remains, respectively, for the Nisku and

FIGURE D-6. Explanation of Cretaceous HRGM anomalies by Model 2A: microseepage at constant flux from 17 Ma to the present. The magnetically enhanced zones are inferred to record a nearly equal balance (vector sum) between reversed-polarity-bias CRM linearly acquired from 17 Ma to the present and normal-polarity PADF VRM.

(a) Stereographic projection showing 33 simulated remagnetization circles for constant-flux microseepage from 17 Ma to the present. Solid green dots are on the lower hemisphere and simulate dispersion ($\kappa = 600$) about the PADF direction ($D/I = 0.0^\circ/+68.4^\circ$). Open blue circles are on the upper hemisphere and simulate dispersion ($\kappa = 600$) about the reversed-polarity 17-Ma long-term CRM reference direction ($D/I = 174.3^\circ/-67.5^\circ$). Red stars represent remagnetization-circle midpoints, which are the predicted HRGM anomaly directions according to this model. Note the shadow zone in the northwest quadrant, which is nearly devoid of remagnetization circles.

(b) Stereographic projection showing the observed distribution of 33 HRGM anomaly directions above Cretaceous reservoirs in case history 6 (Figure 17b). Note the shadow zone (no HRGM anomalies) in the northwest quadrant, as predicted in (a). Note also the asymmetry in HRGM anomaly dip values also predicted in (a): open stars (pointing up) are in the northeast quadrant, and filled stars (pointing down) are in the southwest quadrant.

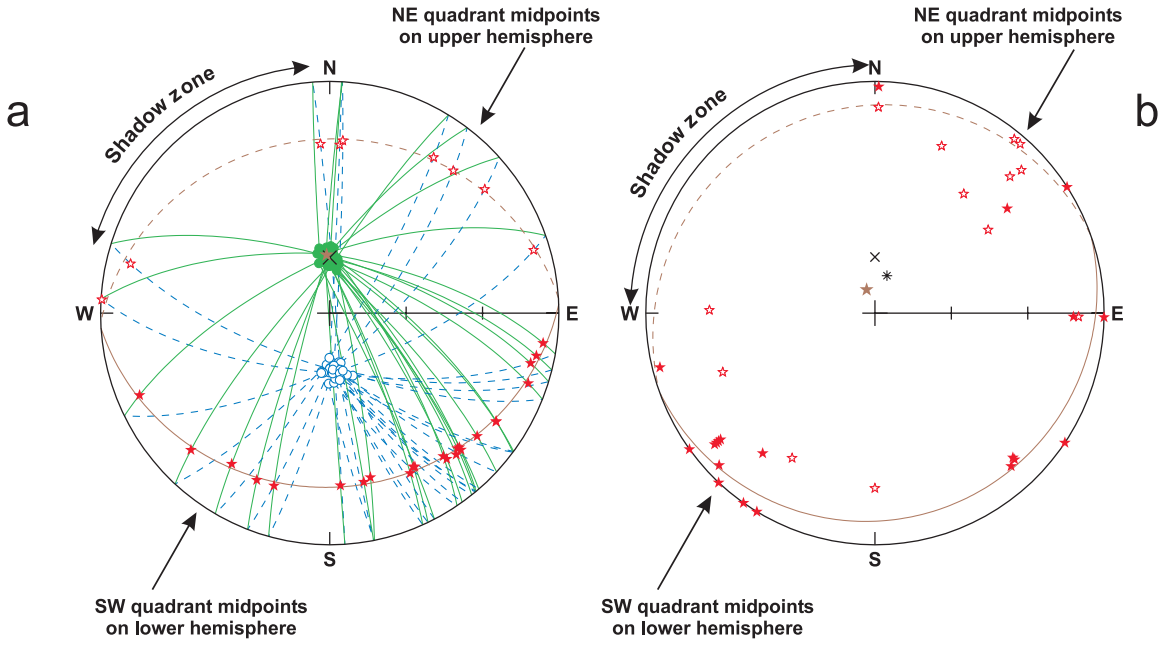
(c) For Model 2A, the normal-polarity PADF direction and the 17-Ma reversed-polarity long-term CRM reference direction differ by 2.3° from being antiparallel (Figure D-3d). When these two magnetizations are added vectorially in a 50/50 ratio, they do *not* completely self-cancel, and 2.0% of the intensity remains to be detected in HRGM surveys. Nearly complete vector self-cancellation probably contributes to the azimuthal scatter and weak intensity of Cretaceous HRGM anomalies.

(d) According to Model 2A, the authigenic magnetic minerals in the magnetically enhanced zones grow from the initiation of microseepage to the present, beginning at 17 Ma, as modeled here for the Cretaceous reservoirs. The linearly acquired, reversed-polarity CRM resides in grains $<10 \mu\text{m}$, which can retain their remanent magnetization for billions of years. The normal-polarity PADF VRM resides in $\sim 10 \mu\text{m}$ multidomain grains that have retained their remanent magnetization only during the past 10^4 to 10^6 yr.

**17-Ma long-term reversed-bias CRM
+
Normal-polarity PADF VRM**

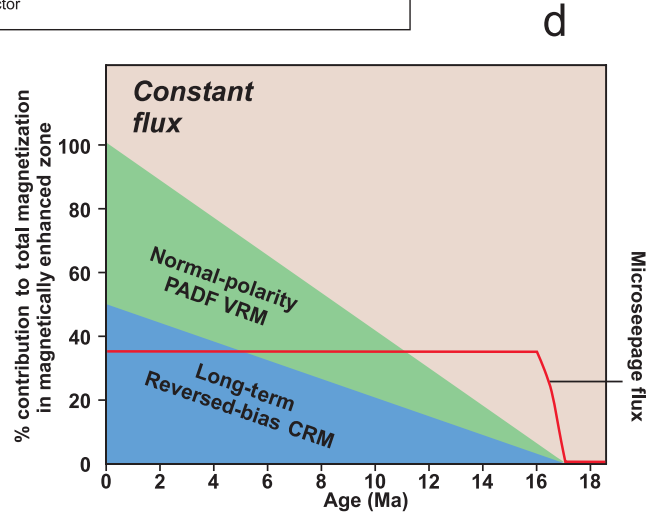
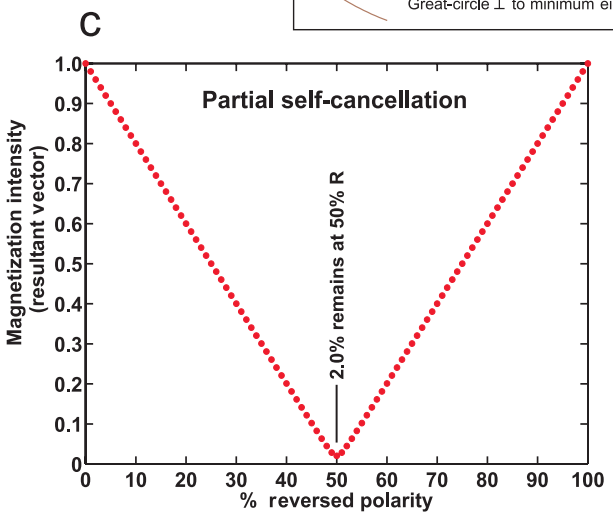
Simulated 17-Ma remagnetization circles

Observed HRGM anomalies above Cretaceous producers



Explanation of Symbols

- Remagnetization circle (lower hemisphere)
- - - Remagnetization circle (upper hemisphere)
- ★ HRGM residual anomaly = remagnetization circle midpoint (lower hemisphere)
- ★ HRGM residual anomaly = remagnetization circle midpoint (upper hemisphere)
- Normal-polarity PADF endpoint
- Reversed-polarity 17 Ma endpoint
- * Present-magnetic-field (PF)-direction
- × Present-axial-dipole-field (PADF) direction
- ★ Direction of minimum eigenvector of HRGM anomalies and remagnetization-circle midpoints
- Great-circle \perp to minimum eigenvector



Leduc models discussed above (Figures D-4c and D-5c). Thus, part of the weakness of HRGM anomalies above Cretaceous reservoirs in the Alberta Basin is probably attributable to more complete vector self-cancellation (a smaller Δ antiparallel angle) caused by micro-seepage ages younger than 25 Ma for the Cretaceous reservoirs.

Another possible cause of weaker HRGM anomalies above the Cretaceous reservoirs is the more nearly 50% reversed-polarity bias at 17 Ma (Figure 20c). For Model 1A (10-m.y. microseepage pulse), the reversed-polarity bias is only 51.3% if the pulse is centered on 17 Ma (Cretaceous reservoirs), which is much lower than the 58.2% reversed bias if it is centered on 30 Ma (Leduc reservoirs?), or the 79.8% reversed bias if it is centered on 57 Ma (Nisku reservoirs). Thus, the reference North American APW path (the ultimate source of the Δ antiparallel angles) and the magnetic-polarity time scale (Ogg, 1995) have both conspired to cause more complete vector self-cancellation in magnetically enhanced zones above microseeping Cretaceous reservoirs.

Part of the weakness of HRGM anomalies above the Cretaceous reservoirs is undoubtedly attributable to geologic causes—microseepage at lower pressures, from shallower depths, and in lesser volumes than for Leduc and Nisku reservoirs. The 17-Ma inferred microseepage age appears to correlate with the end of the Cypress Plain (i.e., beginning of the red dashed line in Figure 21), which probably increased the microseepage flux as a result of methane exsolution upon uplift. Most of the Cretaceous reservoirs in our case-history 5 and 6 areas are in the Erosional Rebound System (Tóth and Corbet, 1987), in which gas is known to have exsolved by this mechanism.

In summary, the strong similarity between the Model 1A and Model 2A simulated remagnetization circles at 17 Ma versus the observed distribution of 33 HRGM anomalies above the case-history 6 Cretaceous reservoirs further corroborates that our interpretation of HRGM anomalies as remagnetization-circle midpoints is valid. It is difficult to imagine how any artifact of our data-acquisition or gridding procedures could yield (1) *no* HRGM anomalies with northwest azimuths, (2) negative average dips when the azimuths are in the northeastern quadrant, and (3) positive average dips when the azimuths are in the southwestern quadrant. However, all three of these observed characteristics are predicted for remagnetization-circle midpoints at 17 Ma, according to Models 1A and 2A.

In Table 3, the “x” for the Cretaceous under Models 1B and 2B indicates that these two models are totally incapable of explaining the observed distribution of HRGM anomalies above the Cretaceous reservoirs. According to Models 1B and 2B, all 33 Cretaceous HRGM anomaly azimuths should have been in the southeastern quadrant, because the Δ antiparallel angles for these models are $>8^\circ$ at all ages from 64 Ma to the present (Figure D-3d). Even a Δ antiparallel angle of 4.6° yielded

good unimodal clustering of Nisku HRGM anomaly azimuths, so $>8^\circ$ Δ antiparallel angles implied by Models 1B and 2B would have yielded even more tightly clustered HRGM anomaly azimuths above Cretaceous reservoirs than we observed above Nisku reservoirs.

Explanation of the Alida HRGM Anomaly Direction

Our remagnetization-circle hypothesis is more difficult to test in the Williston Basin, because we have only five HRGM anomaly directions on which to base our interpretation (from the Mississippian Alida beds; Figure 16c). Moreover, of these five anomalies, two are unusual in that they have the lowest maximum/minimum ratios, which imply the steepest negative inclinations (-45°) of any of the HRGM anomalies we measured in Western Canada. Nevertheless, by analogy with the Alberta Basin, we can make some general inferences about hydrocarbon microseepage ages in the Williston Basin.

Our first observation, based on our paleomagnetic studies of subsurface cores (Figure C-2), is that the reversed-polarity CRM appears to be younger in the Williston Basin (45 Ma in Devonian reservoirs) compared with the Alberta Basin (57 Ma in Devonian and Mississippian reservoirs). The 45-Ma age indicated in Figure C-2b is from near the center of the Williston Basin in North Dakota, whereas our five Alida HRGM anomalies are from the North Pierson field in southwestern Manitoba, 300 km to the northeast. It may well have taken millions of years to fill all the traps between the center of the Williston Basin and the Alida (Mission Canyon) reservoirs on the northeastern basin margin.

The average south azimuth ($D/I = 172.8^\circ/-15.9^\circ$) of the five Alida HRGM anomalies precludes an origin according to Models 1A or 2A. In the Williston Basin, south azimuths could be produced by Models 1A or 2A (Figure D-2b and f) only if the microseepage age had been between 5 and 17 Ma, at which times the Δ antiparallel angle is $<3^\circ$ (Figure D-3d). Yet we have already seen how dispersed the remagnetization-circle midpoints (and HRGM anomaly azimuths) become when the Δ antiparallel angle is as low as 2° to 3° (Figures D-3e and D-6a, b). We regard 25 Ma as the youngest possible age for forming unimodal clusters of HRGM anomaly directions by Models 1A or 2A.

This means that Models 1B and 2B (both with Δ antiparallel angles $>8^\circ$) are the only viable models for explaining the cluster of five HRGM anomalies with south azimuths above Alida reservoirs of the Williston Basin. Microseepage-related CRM acquired at any time in the late Tertiary between about 17 Ma and 1.8 Ma could account for the south azimuths and reversed-polarity component of HRGM anomalies above Alida reservoirs. Interestingly, on the magnetic-polarity time scale, the past 10 m.y. exhibits an increase in reversed-polarity bias,

to values >55% (Figure B-1). The only other times in the Tertiary that reversed-polarity bias was >55% were at about 30 Ma (10-m.y. window) and during the early Tertiary reversed-polarity-bias interval, when Nisku and Leduc HRGM anomalies probably acquired their strong reversed-polarity-bias CRM (Figure 20c). Perhaps the comparatively steep negative inclination (-16° average) and the consistent south azimuth (173° average) of the Alida HRGM anomalies were produced by a CRM recording a fairly strong (>55%) reversed-polarity bias in the late Tertiary. As indicated in Table 3, this could have occurred either during a 10-m.y. pulse (Model 1B) centered on 7 Ma (Figure B-1a) or by constant-flux microseepage (Model 2B) from 7 Ma to the present (Figure B-1c).

In summary, the consistent south azimuth and the unusually strong reversed-polarity bias recorded by the Alida HRGM anomalies suggest that about 7 Ma is the most likely age of microseepage-related CRM above Alida reservoirs.

Implications of the Four Models on the Origin of HRGM Anomalies in Western Canada

Table 3 reveals that only two (Leduc and Alida) of the four reservoir classes have entries explainable by Model 1B or 2B, and Alida HRGM anomalies are explainable *only* by Model 1B or 2B. Moreover, these are the two models in which the magnetically enhanced zones are inferred to contain the *coarsest-grained* authigenic magnetic minerals (i.e., multidomain grains $\gg 10\ \mu\text{m}$, which record PF VRM during the past $<10^2$ yr). Interestingly, the Leduc and Alida HRGM anomalies also exhibit the *highest intensities*; on a histogram of HG' values, the average (geometric mean) Alida anomaly value (3.8) falls between average values associated with Leduc (9.4) and Nisku (1.8) reservoirs. Both the Leduc pinnacle-reef reservoirs and the Alida cuesta reservoirs probably have the thickest oil and gas columns, based on their reservoir geometries (i.e., compared with Nisku biostrome and Cretaceous and lower Amaranth blanket/channel-sand reservoirs). The Leduc and Alida reservoirs also have the *highest pressures*: Most Leduc pinnacle-reef reservoirs initially flow spontaneously, and the Alida reservoirs have a strong natural water drive.

These observations provide further evidence that reservoir pressure and height of the oil/gas column ultimately control the microseepage flux, the concentration and grain size of authigenic magnetic minerals in magnetically enhanced zones, and hence the intensity of HRGM anomalies. These inferences made from surface observations will be testable by direct sampling of cores obtained from magnetically enhanced zones above Leduc, Nisku, Cretaceous, and Mississippian reservoirs of Western Canada.

REFERENCES CITED

- Anderson, N. L., L. V. Hills, D. A. Cederwall, E. V. Greenwood, and B. J. Ulaszonek, 1989, Geophysical atlas of Western Canadian hydrocarbon pools: Calgary, Canadian Society of Exploration Geophysicists and Canadian Society of Petroleum Geologists, 344 p.
- Andrew, J. A., D. M. Edwards, R. J. Graf, and R. J. Wold, 1991, Empirical observations relating near-surface magnetic anomalies to high-frequency seismic data and Landsat data in eastern Sheridan County, Montana: *Geophysics*, v. 56, p. 1553–1570.
- Andrichuk, J. M., 1958, Stratigraphy and facies analysis of Upper Devonian reefs in Leduc, Stettler, and Redwater areas, Alberta: *AAPG Bulletin*, v. 42, p. 1–93.
- Banerjee, S., R. D. Elmore, and M. H. Engel, 1997, Chemical remagnetization and burial diagenesis: Testing the hypothesis in the Pennsylvanian Belden Formation, Colorado: *Journal of Geophysical Research*, v. 102, p. 24825–24842.
- Barchyn, D., 1984, The Waskada lower Amaranth (Spearfish) oil pool, southwestern Manitoba: A model for Spearfish exploration in Saskatchewan, in J. A. Lorsche and M. A. Wilson, eds., *Oil and gas in Saskatchewan*: Saskatchewan Geological Society, Special Publication No. 7, p. 103–111.
- Bell, J. S., P. R. Price, and P. J. McLellan, 1994, In-situ stress in the Western Canada Sedimentary Basin, in G. D. Mossop and I. Shetsen, comps., *Geological atlas of the Western Canada Sedimentary Basin*: Calgary, Canadian Society of Petroleum Geologists and Alberta Research Council, p. 439–446.
- Berg, R. R., and A. F. Gangi, 1999, Primary migration by oil-generation microfracturing in low-permeability source rocks: Application to the Austin Chalk, Texas: *AAPG Bulletin*, v. 83, p. 727–756.
- Bethke, C. M., and S. Marshak, 1990, Brine migration across North America—The plate tectonics of groundwater: *Annual Review of Earth and Planetary Science*, v. 18, p. 287–315.
- Bleakly, D. C., D. R. Van Alstine, and D. R. Packer, 1985a, Core orientation 1: Controlling errors minimizes risk and cost in core orientation: *Oil & Gas Journal*, December 2, v. 83, p. 103–109.
- Bleakly, D. C., D. R. Van Alstine, and D. R. Packer, 1985b, Core orientation 2: How to evaluate orientation data, quality control: *Oil & Gas Journal*, December 9, v. 83, p. 46–54.
- Brothers, L., M. H. Engel, and R. D. Elmore, 1996, The late diagenetic conversion of pyrite to magnetite by organically complexed ferric iron: *Chemical Geology*, v. 130, p. 1–14.
- Butler, R. F., 1992, *Paleomagnetism: Magnetic domains to geologic terranes*: Boston, Blackwell, 319 p.
- Champion, D. E., 1980, Holocene geomagnetic secular variation in the western United States: Implications for the global geomagnetic field: Ph.D. thesis, California Institute of Technology, Pasadena, 314 p.
- Cioppa, M. T., E. T. Karlstrom, E. Irving, and R. W. Barendregt, 1995, Paleomagnetism of tills and associated paleosols in southwestern Alberta and northern

- Montana: Evidence for Late Pliocene–Early Pleistocene glaciations: *Canadian Journal of Earth Sciences*, v. 32, p. 555–564.
- Corbett, K. P., D. R. Van Alstine, and J. D. Edman, 1997, Stratigraphic controls on fracture distribution in the Austin Chalk: An example from the First Shot field, Gonzales County, Texas: AAPG Hedberg Research Conference, June 22–28, Bryce, Utah.
- Creaney, S., J. Allan, K. S. Cole, M. G. Fowler, P. W. Brooks, K. G. Osadetz, R. W. Macqueen, L. R. Snowdon, and C. L. Riediger, 1994, Petroleum generation and migration in the Western Canada sedimentary basin, in G. D. Mossop and I. Shetsen, comps., *Geological atlas of the Western Canada sedimentary basin*: Calgary, Canadian Society of Petroleum Geologists and Alberta Research Council, p. 455–468.
- Dankers, P. H. M., 1978, Magnetic properties of dispersed natural iron-oxides of known grain-size: Ph.D. thesis, State University of Utrecht, 142 p.
- Davis, T. L., 1972, Velocity variations around Leduc reefs, Alberta: *Geophysics*, v. 37, p. 584–604.
- Dawson, F. M., C. G. Evans, R. Marsh, and R. Richardson, 1994, Uppermost Cretaceous and Tertiary strata of the Western Canada sedimentary basin, in G. D. Mossop and I. Shetsen, comps., *Geological atlas of the Western Canada sedimentary basin*: Calgary, Canadian Society of Petroleum Geologists and Alberta Research Council, p. 387–406.
- Dekkers, M. J., 1988, Magnetic properties of natural pyrrhotite Part I: Behaviour of initial susceptibility and saturation-magnetization-related rock-magnetic parameters in a grain-size dependent framework: *Physics of the Earth and Planetary Interiors*, v. 52, p. 376–393.
- von der Dick, H. H., K. R. Barrett, and D. A. Bosman, 2002, Numerically reconstructed methane-seep signal in soil gases over Devonian gas pools and prospects (northeast British Columbia), in D. Schumacher and L. A. LeSchack, eds., *Surface exploration case histories: AAPG Studies in Geology No. 48 and SEG Geophysical References Series No. 11*, this volume.
- Diehl, J. F., M. E. Beck Jr., S. Beske-Diehl, D. Jacobson, and B. C. Hearn Jr., 1983, Paleomagnetism of the Late Cretaceous–Early Tertiary north-central Montana alkalic province: *Journal of Geophysical Research*, v. 88, p. 10593–10609.
- Diehl, J. F., K. M. McClannahan, and T. J. Bornhorst, 1988, Paleomagnetic results from the Mogollon-Datil volcanic field, southwestern New Mexico, and a refined mid-Tertiary reference pole for North America: *Journal of Geophysical Research*, v. 93, p. 4869–4879.
- Donovan, T. J., R. J. Forgey, and A. A. Roberts, 1979, Aeromagnetic detection of diagenetic magnetite over oil fields: *AAPG Bulletin*, v. 63, p. 245–248.
- Donovan, T. J., J. D. Hendricks, A. A. Roberts, and P. T. Eliason, 1984, Low-altitude aeromagnetic reconnaissance for petroleum in the Arctic National Wildlife Refuge, Alaska: *Geophysics*, v. 49, p. 1338–1353.
- Dunlop, D. J., 1983, Viscous magnetization of 0.04–100 μm magnetites: *Geophysical Journal*, v. 74, p. 667–687.
- Edwards, D. E., J. E. Barclay, D. W. Gibson, G. E. Kville, and E. Halton, 1994, Triassic strata of the Western Canada Sedimentary Basin, in G. D. Mossop and I. Shetsen, comps., *Geological atlas of the Western Canada Sedimentary Basin*: Calgary, Canadian Society of Petroleum Geologists and Alberta Research Council, p. 259–275.
- Ellwood, B. B., and B. Burkart, 1996, Test of hydrocarbon-induced magnetic patterns in soils: The sanitary landfill as laboratory, in D. Schumacher and M. Abrams, eds., *Hydrocarbon migration and its near-surface expression: AAPG Memoir 66*, p. 91–98.
- Ellwood, B. B., and R. E. Crick, 1988, Paleomagnetism of Paleozoic asphaltic deposits in southern Oklahoma, USA: *Geophysical Research Letters*, v. 15, p. 436–439.
- Elmore, R. D., and M. C. Leach, 1990, Remagnetization of the Rush Springs Formation, Cement, Oklahoma: Implications for dating hydrocarbon migration and aeromagnetic exploration: *Geology*, v. 18, p. 124–127.
- Elmore, R. D., and L. Crawford, 1990, Remanence in authigenic magnetite: Testing the hydrocarbon-magnetite hypothesis: *Journal of Geophysical Research*, v. 95, p. 4539–4549.
- Elmore, R. D., M. H. Engel, L. Crawford, K. Nick, S. Imbus, and Z. Sofer, 1987, Evidence of a relationship between hydrocarbons and authigenic magnetite: *Nature*, v. 325, p. 428–430.
- Elmore, R. D., D. London, D. Bagley, D. Fruit, and G. Gao, 1993, Remagnetization by basinal fluids: Testing the hypothesis in the Viola limestone, southern Oklahoma: *Journal of Geophysical Research*, v. 98, p. 6237–6254.
- Erlich, R. N., S. F. Barret, and Guo Bai Ju, 1990, Seismic and geologic characteristics of drowning events on carbonate platforms: *AAPG Bulletin*, v. 74, p. 1523–1537.
- Fenton, M. M., B. T. Schreiner, E. Nielsen, and J. G. Paulowicz, 1994, Quaternary geology of the Western Plains, in G. D. Mossop and I. Shetsen, comps., *Geological atlas of the Western Canada Sedimentary Basin*: Calgary, Canadian Society of Petroleum Geologists and Alberta Research Council, p. 416.
- Fisher, R. A., 1953, Dispersion on a sphere: *Proceedings, Royal Society of London*, v. A217, p. 295–305.
- Fishman, N. S., R. L. Reynolds, M. R. Hudson, and V. F. Nuccio, 1989, Source of anomalous magnetization in area of hydrocarbon potential: Petrologic evidence from Jurassic Preuss Sandstone, Wyoming-Idaho thrust belt: *AAPG Bulletin*, v. 73, p. 182–194.
- Foote, R. S., 1986a, Horizontal gradient interpretation of low-altitude cesium vapour magnetometer data compared with measurement of rock magnetic susceptibility of drill cuttings, in M. J. Davidson, ed., *Unconventional methods in exploration for petroleum and natural gas 4*: Dallas, Southern Methodist University Press, Institute for the Study of Earth and Man, p. 107–112.
- Foote, R. S., 1986b, Integrating airborne and surface magnetic data: *Proceedings of the Fifth Thematic Conference, Remote Sensing for Exploration Geology*, Reno, Nevada, September 29–October 2, p. 233–247.

- Foote, R. S., 1992, Use of magnetic field aids oil search, *Oil & Gas Journal*, May 4, p. 137–142.
- Foote, R. S., 1996, Relationship of near-surface magnetic anomalies to oil- and gas-producing areas, *in* D. Schumacher and M. A. Abrams, eds., *Hydrocarbon migration and its near-surface expression: AAPG Memoir 66*, p. 111–126.
- Foote, R. S., R. Nowak, and J. Sobehrad, 1997, Aeromagnetic near-surface profiling as an exploration tool, *in* *Applications of emerging technologies: Unconventional methods in exploration for petroleum and natural gas 5: Dallas*, Southern Methodist University Press, Institute for the Study of Earth and Man, p. 183–193.
- Fruit, D., R. D. Elmore, and S. Halgedahl, 1995, Remagnetization of the folded Belden Formation, northwest Colorado: *Journal of Geophysical Research*, v. 100, p. 15009–15023.
- Garven, G., 1989, A hydrogeologic model for the formation of the giant oil sands deposits of the Western Canada sedimentary basin: *American Journal of Science*, v. 289, p. 105–166.
- Gillen, K. P., R. Van der Voo, and J. H. Thiessen, 1999, Late Cretaceous–early Tertiary remagnetization of the Devonian Swan Hills Formation recorded in carbonate cores from the Caroline gas field, Alberta, Canada: *AAPG Bulletin*, v. 83, p. 1223–1235.
- Gose, W. A., and J. R. Kyle, 1988, Paleomagnetic studies of salt domes: *AAPG Bulletin*, v. 72, p. 190.
- Halls, H. C., 1976, A least-squares method to find a remanence direction from converging remagnetization circles: *Geophysical Journal*, v. 45, p. 297–304.
- Halls, H. C., 1978, The use of converging remagnetization circles in paleomagnetism: *Physics of the Earth and Planetary Interiors*, v. 16, p. 1–11.
- Hamilton, W. D., D. R. Van Alstine, J. E. Butterworth, and G. Raham, 1995, Paleomagnetic orientation of fractures in Jean Marie Member cores from NE British Columbia/NW Alberta: *Calgary, Petroleum Society of CIM, Paper 95–56*.
- Hamilton, W. D., D. R. Van Alstine, and J. E. Butterworth, 1996, A fracture-orientation comparison between core-based and borehole-imaging techniques: Paleomagnetic, electronic multishot, and FMI (abs.): *AAPG Annual Meeting*, May 19–22, San Diego, p. 59–60.
- Hanks, C. L., J. Lorenz, L. Teufel, and A. P. Krumhardt, 1997, Lithologic and structural controls on natural fracture distribution and behavior within the Lisburne Group, northeastern Brooks Range and North Slope subsurface, Alaska: *AAPG Bulletin*, v. 81, p. 1700–1720.
- Harding, K. L., W. A. Morris, S. J. Balch, P. LaPointe, and A. G. Latham, 1988, A comparison of magnetic character and alteration in three granite drill cores from eastern Canada: *Canadian Journal of Earth Sciences*, v. 25, p. 1141–1150.
- Hart, M., and M. Fuller, 1988, Magnetization of a dolomite bed in the Monterey Formation: Implications for diagenesis: *Geophysical Research Letters*, v. 15, p. 491–494.
- Hennings, P. H., J. E. Olson, and L. B. Thompson, 2000, Combining outcrop data and three-dimensional structural models to characterize fractured reservoirs: An example from Wyoming: *AAPG Bulletin*, v. 84, p. 830–849.
- Hitzman, D., B. Rountree, J. Tucker, and S. Smith, 2002, Integrated microbial and 3-D seismic surveys discover Park Springs (Conglomerate) field and track microseepage reduction, *in* D. Schumacher and L. A. LeSchack, eds., *Surface exploration case histories: AAPG Studies in Geology No. 48 and SEG Geophysical References Series No. 11*, this volume.
- Hornafius, J. S., 1984, Origin of remanent magnetization in dolomite from the Monterey Formation, *in* R. E. Garrison et al., eds., *Dolomites of the Monterey Formation and other organic-rich units: SEPM Pacific Section*, Los Angeles, p. 195–212.
- Hudson, M. R., R. L. Reynolds, and N. S. Fishman, 1989, Synfolding magnetization in the Jurassic Preuss Sandstone, Wyoming-Idaho-Utah thrust belt: *Journal of Geophysical Research*, v. 94, p. 13681–13705.
- Kent, D. M., 1984, Depositional setting of Mississippian strata in southeastern Saskatchewan: A conceptual model for hydrocarbon accumulation, *in* J. A. Lorsche and M. A. Willson, eds., *Oil and gas in Saskatchewan: Saskatchewan Geological Society, Special Publication No. 7*, p. 19–30.
- Kilgore, B., and R. D. Elmore, 1989, A study of the relationship between hydrocarbon migration and the precipitation of authigenic magnetic minerals in the Triassic Chugwater Formation, southern Montana: *Geological Society of America Bulletin*, v. 101, p. 1280–1288.
- Kirschvink, J. L., 1980, The least-squares line and plane and the analysis of palaeomagnetic data: *Geophysical Journal*, v. 62, p. 699–718.
- Kyle, J. R., and W. A. Gose, 1991, Paleomagnetic dating of sulfide mineralization and cap rock formation in Gulf Coast salt domes: *AAPG Bulletin*, v. 75, p. 615.
- Kyle, J. R., M. R. Ulrich, and W. A. Gose, 1987, Textural and paleomagnetic evidence for mechanism and timing of anhydrite cap rock formation, Winnfield salt dome, Louisiana, *in* I. Lerche and J. J. O'Brian, eds., *Dynamical geology of salt and related structures: London*, Academic Press, p. 497–542.
- Larson, E. E., T. R. Walker, P. E. Patterson, R. P. Hoblitt, and J. G. Rosenbaum, 1982, Paleomagnetism of the Moenkopi Formation, Colorado Plateau: Basis for long-term model of acquisition of chemical remanent magnetism in red beds: *Journal of Geophysical Research*, v. 87, p. 1081–1106.
- Laubach, S. E., 1997, A method to detect natural fracture strike in sandstones: *AAPG Bulletin*, v. 81, p. 604–623.
- Lemon, T. and B. Taylor, 1993, The Rumsey Leduc pinnacle reef: Where are the rest?: 1993 Canadian Society of Exploration Geophysicists National Convention, May 4–6, CSEG Abstracts, p. 406.
- Lerbekmo, J. F., and A. R. Sweet, 2000, Magnetostratigraphy and biostratigraphy of the continental Paleocene in the Calgary area, southwestern Alberta: *Bulletin of Canadian Petroleum Geology*, v. 48, p. 285–306.
- Lerbekmo, J. F., A. R. Sweet, and D. R. Braman, 1995, Magnetobiostratigraphy of Late Maastriichtian to

- Early Paleocene strata of the Hand Hills, south central Alberta, Canada: *Bulletin of Canadian Petroleum Geology*, v. 43, p. 35–43.
- LeSchack, L. A., 1994, Ground-based magnetic horizontal gradient intensity and radiometric surveys, a cost-effective hydrocarbon exploration tool: Three case histories in Western Canada: *Canadian Society of Exploration Geophysicists Recorder*, v. 19, p. 7–13.
- LeSchack, L. A., 1997, Results of magnetic HGI and radiometric surveys in Western Canada: *Oil & Gas Journal*, May 19, p. 84–89, and May 26, p. 82–87.
- Lewchuk, M. T., I. S. Al-Aasm, D. T. A. Symons, and K. P. Gillen, 1998, Dolomitization of Mississippian carbonates in the Shell Waterton gas field, southwestern Alberta: Insights from paleomagnetism, petrology and geochemistry: *Bulletin of Canadian Petroleum Geology*, v. 46, p. 387–410.
- Limpert, E., W. A. Stahel, and M. Abbt, 2001, Log-normal distributions across the sciences: Keys and clues: *BioScience*, v. 51, p. 341–352.
- Lisle, R. J., 1994, Detection of zones of abnormal strains in structures using Gaussian curvature analysis: *AAPG Bulletin*, v. 78, p. 1811–1819.
- Lorenz, J. C., and S. J. Finley, 1991, Regional fractures II: Fracturing of Mesaverde reservoirs in the Piceance Basin, Colorado: *AAPG Bulletin*, v. 75, p. 1738–1757.
- Lorenz, J. C., L. W. Teufel, and N. R. Warpinski, 1991, Regional fractures I: A mechanism for the formation of regional fractures at depth in flat-lying reservoirs: *AAPG Bulletin*, v. 75, p. 1714–1737.
- Machel, H. G., 1995, Magnetic mineral assemblages and magnetic contrasts in diagenetic environments—with implications for studies of palaeomagnetism, hydrocarbon migration and exploration, in P. Turner and A. Turner, eds., *Palaeomagnetic applications in hydrocarbon exploration and production: Geological Society [of London] Special Publication No. 98*, p. 9–29.
- Machel, H. G., 1996, Magnetic contrasts as a result of hydrocarbon seepage and migration, in D. Schumacher and M. A. Abrams, eds., *Hydrocarbon migration and its near-surface expression: AAPG Memoir 66*, p. 99–109.
- Machel, H. G., and E. A. Burton, 1991a, Causes and spatial distribution of anomalous magnetization in hydrocarbon seepage environments: *AAPG Bulletin*, v. 75, p. 1864–1876.
- Machel, H. G., and E. A. Burton, 1991b, Chemical and microbial processes causing anomalous magnetization in environments affected by hydrocarbon seepage: *Geophysics*, v. 56, p. 598–605.
- Magoon, L. B., 1988, The petroleum system—A classification scheme for research, exploration, and resource assessment, in L. B. Magoon, ed., *Petroleum systems of the United States: United States Geological Survey Bulletin 1870*.
- Mardia, K. V., 1972, *Statistics of directional data*: London, Academic Press, 357 p.
- Márquez, X. M., and E. W. Mountjoy, 1996, Microfractures due to overpressures caused by thermal cracking in well-sealed Upper Devonian reservoirs, deep Alberta Basin: *AAPG Bulletin*, v. 80, p. 570–588.
- Martin, R., 1966, Paleogeomorphology and its application to exploration for oil and gas (with examples from Western Canada): *AAPG Bulletin*, v. 50, p. 2277–2311.
- McCabe, C., R. Sassen, and B. Saffer, 1987, Occurrence of secondary magnetite within biodegraded oil: *Geology*, v. 15, p. 7–10.
- McElhinny, M. W., 1973, *Palaeomagnetism and plate tectonics*: London, Cambridge University Press, 356 p.
- McFadden, P. L., and R. T. Merrill, 1984, Lower mantle convection and geomagnetism: *Journal of Geophysical Research*, v. 89, p. 3354–3362.
- Miller, E. G., 1972, Parkman Field, Williston Basin, Saskatchewan, in R. E. King, ed., *Stratigraphic oil and gas fields—Classification, exploration methods, and case histories: AAPG Memoir 16*, p. 502–510.
- Morse, J. G., 1989, Improving the quality of radiometric data: *Oil & Gas Journal*, October 16, p. 88–89.
- Narr, W., 1991, Fracture density in the deep subsurface: Techniques with applications to Point Arguello oil field: *AAPG Bulletin*, v. 75, p. 1300–1323.
- Nettleton, L. L., 1971, *Elementary gravity and magnetics for geologists and seismologists*: Tulsa, Society of Exploration Geophysicists, 121 p.
- Ogg, J. G., 1995, Magnetic polarity time scale of the Phanerozoic, in T. J. Ahrens, ed., *Global earth physics: A handbook of physical constants: American Geophysical Union Reference Shelf*, p. 240–270.
- Olea, R. A., 1992, Kriging: Understanding allays intimidation: *AAPG Geobyte*, v. 7, p. 12–17.
- Osborne, M. J., and R. E. Swarbrick, 1997, Mechanisms for generating overpressure in sedimentary basins: A reevaluation: *AAPG Bulletin*, v. 81, p. 1023–1041.
- Payne, D. F., K. Tuncay, A. Park, J. B. Comer, and P. Ortoleva, 2000, A reaction-transport-mechanical approach to modeling the interrelationships among gas generation, overpressuring, and fracturing: Implications for the Upper Cretaceous natural gas reservoirs of the Piceance Basin, Colorado: *AAPG Bulletin*, v. 84, p. 545–565.
- Pirson, S. J., 1969, Geological, geophysical, and chemical modifications of sediments in the environment of oil fields, in W. B. Heroy, ed., *Unconventional methods in exploration for petroleum and natural gas*: Dallas, Southern Methodist University, p. 159–186.
- Podruski, J. A., J. E. Barclay, A. P. Hamblin, P. J. Lee, K. G. Osadetz, R. M. Procter, and G. C. Taylor, 1987, Conventional oil resources of Western Canada (light and medium): *Geological Survey of Canada Paper 87-26*, 149 p.
- Pullaiah, G., E. Irving, K. L. Buchan, and D. J. Dunlop, 1975, Magnetization changes caused by burial and uplift: *Earth and Planetary Science Letters*, v. 28, p. 133–143.
- Reynolds, R. L., 1990, A polished view of remagnetization: *Nature*, v. 345, p. 579–580.
- Reynolds, R. L., N. S. Fishman, R. B. Wanty, and M. B. Goldhaber, 1990a, Iron sulfide minerals at Cement oil field, Oklahoma: Implications for magnetic detection of oil fields: *GSA Bulletin*, v. 102, p. 368–380.
- Reynolds, R. L., M. Webring, V. J. S. Grauch, and M. Tuttle, 1990b, Magnetic forward models of Cement oil

- field, Oklahoma, based on rock magnetic, geochemical, and petrologic constraints: *Geophysics*, v. 55, p. 344–353.
- Robinson, J. E., 1982, Computer applications in petroleum geology: New York, Hutchinson Ross/Van Nostrand, 164 p.
- Sahagian, D. L., and A. A. Proussevitch, 1992, Bubbles in volcanic systems: *Nature*, v. 359, p. 485.
- Sassen, R., 1987, Organic geochemistry of salt dome cap rocks, Gulf Coast Salt Basin, in I. Lerche and J. J. O'Brian, eds., *Dynamical geology of salt and related structures*: London, Academic Press, p. 497–542.
- Saunders, D. F., K. R. Burson, and C. K. Thompson, 1991, Observed relation of soil magnetic susceptibility and soil gas hydrocarbon analysis to subsurface petroleum accumulations: *AAPG Bulletin*, v. 75, p. 389–408.
- Saunders, D. F., K. R. Burson, and C. K. Thompson, 1999, Model for hydrocarbon microseepage and related near-surface alterations: *AAPG Bulletin*, v. 83, p. 170–185.
- Saunders, D. F., K. R. Burson, J. J. Brown, and C. K. Thompson, 1993a, Combined geological and surface geochemical methods discovered Agaritta and Brady Creek fields, Concho County, Texas: *AAPG Bulletin*, v. 77, p. 1219–1240.
- Saunders, D. F., K. R. Burson, J. F. Branch, and C. K. Thompson, 1993b, Relation of thorium normalized surface and aerial radiometric data to subsurface petroleum accumulations: *Geophysics*, v. 58, p. 1417–1427.
- Saunders, D. F., K. R. Burson, J. J. Brown, and C. K. Thompson, 2002, Combined geological and surface geochemical methods discover Agarrita, Brady Creek, Selden, and New Year '95 fields, Concho County, Texas, in D. Schumacher and L. A. LeSchack, eds., *Surface exploration case histories: AAPG Studies in Geology No. 48 and SEG Geophysical References Series No. 11*, this volume.
- Schmidt, P. W., 1985, Bias in converging great circle methods: *Earth and Planetary Science Letters*, v. 72, p. 427–432.
- Schumacher, D., and M. Abrams, eds., 1996, Hydrocarbon migration and its near-surface expression: *AAPG Memoir 66*, 446 p.
- Sheriff, R. E., 1973, *Encyclopedic dictionary of exploration geophysics*: Tulsa, Society of Exploration Geophysicists, 266 p.
- Shock, E. L., 1988, Organic acid metastability in sedimentary basins: *Geology*, v. 16, p. 886–890.
- Sikka, D. B., 1959, A radiometric survey of Redwater oilfield, Alberta, Canada: Ph.D. thesis, McGill University, Montreal, Quebec, Canada.
- Sikka, D. B., and R. B. K. Shives, 2002, Radiometric surveys of the Redwater oil field, Alberta: Early surface exploration case histories suggest mechanisms for the development of hydrocarbon-related geochemical anomalies, in D. Schumacher and L. LeSchack, eds., *Surface exploration case histories: AAPG Studies in Geology No. 48 and SEG Geophysical References Series No. 11*, this volume.
- Smith, G. G., A. R. Cameron, and R. M. Bustin, 1994, Coal resources of the Western Canada sedimentary basin, in G. D. Mossop and I. Shetsen, comps., *Geological atlas of the Western Canada sedimentary basin*: Calgary, Canadian Society of Petroleum Geologists and Alberta Research Council, p. 471–481.
- Sommer, S. E., and B. K. Jain, 1990, Utilization of micro-magnetic surveys in exploration: *AAPG Bulletin*, v. 74, p. 768.
- Spector, A., and F. S. Grant, 1970, Statistical models for interpreting aeromagnetic data: *Geophysics*, v. 35, p. 293–302.
- Spencer, C. W., 1987, Hydrocarbon generation as a mechanism for overpressuring in Rocky Mountain region: *AAPG Bulletin*, v. 71, p. 368–388.
- Stockmal, G., D. R. Issler, and D. Lebel, 1997, Early to Middle Eocene thrusting, outer Foothills belt, southern Alberta: Evidence from apatite fission track data: *CSPG-SEPM Joint Convention*, June 1–6, Calgary, p. 269.
- Suk, D., D. R. Peacor, and R. Van der Voo, 1990, Replacement of pyrite framboids by magnetite in limestone and implications for palaeomagnetism: *Nature*, v. 345, p. 611–613.
- Surdam, R. C., L. J. Crossey, E. S. Hagen, and H. P. Heasler, 1989, Organic-inorganic interactions and sandstone diagenesis: *AAPG Bulletin*, v. 73, p. 1–23.
- Surdam, R. C., Z. S. Jiao, and D. B. MacGowan, 1993, Redox reactions involving hydrocarbons and mineral oxidants: A mechanism for significant porosity enhancement in sandstones: *AAPG Bulletin*, v. 77, p. 1509–1518.
- Switzer, S. B., W. G. Holland, D. S. Christie, G. C. Graf, A. S. Hedinger, R. J. McAuley, R. A. Wierzbicki, and J. J. Packard, 1994, Devonian Woodbend-Winterburn strata of the Western Canada Sedimentary Basin, in G. D. Mossop and I. Shetsen, comps., *Geological atlas of the Western Canada Sedimentary Basin*: Calgary, Canadian Society of Petroleum Geologists and Alberta Research Council, p. 165–202.
- Symons, D. T. A., H. Pan, D. F. Sangster, and E. C. Jowett, 1993, Paleomagnetism of the Pine Point Zn-Pb deposits: *Canadian Journal of Earth Sciences*, v. 30, p. 1028–1036.
- Tarling, D. H., 1983, *Palaeomagnetism: Principles and applications in geology, geophysics, and archaeology*: New York, Chapman and Hall, 379 p.
- Telford, W. M., L. P. Geldart, and R. E. Sheriff, 1990, *Applied Geophysics*, 2nd ed.: New York, Cambridge University Press, 770 p.
- Thompson, C. K., D. F. Saunders, and K. R. Burson, 1994, Model advanced for hydrocarbon microseepage, related alterations: *Oil & Gas Journal*, November 14, v. 92, p. 95–99.
- Tissot, B. P., and D. H. Welte, 1984, *Petroleum Formation and Occurrence*, 2nd ed.: New York, Springer-Verlag, 699 p.
- Tompkins, R., 1990, Direct location technologies: A unified theory: *Oil & Gas Journal*, September 24, p. 126–134.
- Tóth, J., and T. Corbet, 1987, Post-Palaeocene evolution of regional groundwater flow systems and their relation to petroleum accumulations, Taber area, south-

- ern Alberta, Canada, *in* J. C. Goff and B. P. J. Williams, eds., Fluid flow in sedimentary basins and aquifers, Geological Society [of London] Special Publication 34, Blackwell Scientific, 230 p.
- Van Alstine, D. R., 1979, Apparent polar wandering with respect to North America since the late Precambrian: Ph.D. thesis, California Institute of Technology, Pasadena, 358 p.
- Van Alstine, D. R., 1986, Normal- and reversed-polarity synfolding CRM along the Brooks Range mountain front, northern Alaska: Transactions, American Geophysical Union (EOS), v. 67, p. 269–270.
- Van Alstine, D. R., 1987, Normal- and reversed-polarity synfolding CRM along the Brooks Range mountain front, northern Alaska, *in* I. Tailleux and P. Weimer, eds., Alaskan North Slope geology, v. 2: Pacific Section SEPM (Bakersfield) and Alaska Geological Society (Anchorage), p. 580.
- Van Alstine, D. R., and J. E. Butterworth, 1993, Paleomagnetic orientation of fractures and bedding in Rotliegende and Zechstein cores from the southern Permian Basin, North Sea (abs.): AAPG Bulletin, v. 77, p. 1672.
- Van Alstine, D. R., and J. E. Butterworth, 1994, Paleomagnetic dating of orogenic fluid migration events in carbonates from the Western Canada sedimentary basin and northern Alaska: CSEG and CSPG Joint National Convention, May 9–12, Calgary, p. 300.
- Van Alstine, D. R., J. E. Butterworth, E. J. M. Willemse, and W. J. E. van de Graaff, 1991, Paleomagnetic core-orientation for characterizing reservoir anisotropy: Case histories from fractured reservoirs in Abu Dhabi and Venezuela (abs.): AAPG Bulletin, v. 75, p. 687.
- Van Alstine, D. R., J. E. Butterworth, S. R. May, and M. C. Covey, 1997, Paleomagnetic constraints on fluid migration, tectonic, and thermal histories in triangle zones of southern Alberta and the Arkoma basin: CSPG-SEPM Joint Convention, June 1–6, Calgary, p. 282.
- Van der Voo, R., 1993, Paleomagnetism of the Atlantic, Tethys, and Iapetus Oceans: Cambridge University Press, 411 p.
- von der Dick, H. H., *see under* Dick [von der].
- Wendte, J. C., 1994, Cooking Lake platform evolution and its control on Late Devonian Leduc reef inception and localization, Redwater, Alberta: Bulletin of Canadian Petroleum Geology, v. 42, p. 499–528.
- Wisniowiecki, M. J., R. Van der Voo, C. McCabe, and W. C. Kelly, 1983, A Pennsylvanian paleomagnetic pole from the mineralized late Cambrian Bonnetterre Formation, southeast Missouri: Journal of Geophysical Research, v. 88, p. 6540–6548.
- Wolleben, J. A., and D. W. Greenlee, 2002, Successful application of micromagnetic data to focus hydrocarbon exploration, *in* D. Schumacher and L. A. LeSchack, eds., Surface exploration case histories: AAPG Studies in Geology No. 48 and SEG Geophysical References Series No. 11, this volume.
- Wright, G. N., M. E. McMechan, and D. E. Potter, 1994, Structure and architecture of the Western Canada sedimentary basin, *in* G. D. Mossop and I. Shetsen, comps., Geological atlas of the Western Canada sedimentary basin: Calgary, Canadian Society of Petroleum Geologists and Alberta Research Council, p. 25–40.
- Yassir, N. A., and J. S. Bell, 1994, Relationships between pore pressure, stresses, and present-day geodynamics in the Scotian Shelf, offshore eastern Canada: AAPG Bulletin, v. 78, p. 1863–1880.
- Yurkovich, R., and C. Sitzler, 1997, New discovery in the Yeoman Formation (Ordovician), Midale Field, southeastern Saskatchewan: Core Conference, June 5–6, CSPG-SEPM Joint Convention, Calgary, June 1–6, p. 41.
- Zietz, I., and G. F. Andreasen, 1967, Remanent magnetization and aeromagnetic interpretation, *in* D. A. Hansen, W. E. Heinrichs Jr., R. C. Holmer, R. E. MacDougall, G. R. Rogers, J. S. Sumner, and S. H. Ward, eds., SEG mining geophysics, v. 2, Theory: Society of Exploration Geophysicists, p. 569–590.